RSKy Business in the Mammary Gland

By

Katarzyna Anna Ludwik

Dissertation

Submitted to the Faculty of the

Graduate School of Vanderbilt University

in partial fulfillment of the requirements

for the degree of

DOCTOR OF PHILOSOPHY

in

Pathology

May 11 2018

Nashville, Tennessee

Approved:

Deborah Lannigan, Ph.D.
Ian Macara, Ph.D.
Thomas Stricker, M.D., Ph.D.
Alissa Weaver, M.D., Ph.D.
Christopher Wright, Ph.D.
Andries Zijlstra, Ph.D.

To my Parents and Grandparents

and

To Jacek

ACKNOWLEDGEMENTS

I would like to thank those who contributed to my training as a scientist and to my graduate experience. First, I would like to express my deepest appreciation for my mentor Deborah A. Lannigan PhD for her tireless efforts on my behalf. I would also like to thank my thesis advisory committee members, Ian G. Macara PhD for his continuous guidance and support and Alissa Weaver MD, PhD, Thomas Stricker, MD, PhD, Andries Zijlstra PhD, and Chris Wright PhD for critical inputs to my work.

I would like to thank my collaborators Oliver McDonald PhD, Kelli Boyd PhD, David Brenin MD, George O'Doherty PhD. Their contribution to my work has been invaluable. For the assistance in administrative issues, I would like to acknowledge Kristi Hargrove, Cellular and Molecular Pathology Program Coordinator, and Reddy Radhika at International Students and Scholars Services.

Finally, I would like to thank the members of the Lannigan lab and Macara labs, past and present for their help, kindness, friendship and continuous support. It has been a privilege to know and work with them. In particular, Zach Sandusky, Lejla Pasic, Frances Greathouse, Miranda Sowder, Roman Mrozowski PhD, David Clark, Amanda Halfond, Lindsey Seldin PhD, and Janusz Petkowski PhD have been incredible friends. I would also like to thank Karin Eisinger PhD, Angela Groehler PhD, Preston Campbell PhD, Marc Cantwell, Allison Isabelli, Shinji Fukuda PhD, Luiza Cruz for creating a challenging and enjoyable lab atmosphere.

TABLE OF CONTENTS

LIST OF FIGURES

Figure Page

LIST OF TABLES

Chapter 1 Introduction: Overview of RSK biology

Adapted from [1]: Ludwik K.A and Lannigan D.A. (2016) Ribosomal S6 kinase (RSK) modulators: a patent review. Expert Opin Ther Pat. 26(9):1061-78

Ribosomal S6 Kinases

The p90 ribosomal S6 kinases (RSK) are a family of Ser/Thr protein kinases, which are downstream effectors of the mitogen-activated protein kinase kinase 1/2 (MEK1/2) -extracellular signal-regulated kinase 1/2 (ERK1/2) signaling pathway [2]. RSK was initially identified by its ability to phosphorylate the 40S ribosomal protein subunit protein S6 (pS6) [3]. Subsequent cloning revealed that RSK is an unusual kinase that contains two un-related kinase domains [4] (Fig. 1A). Subsequent to the cloning of RSK, the p70 S6 kinases were discovered to phosphorylate pS6 [5]. Initially, it was thought that the p70 S6 kinases rather than RSK were responsible for translational regulation. However, it has since been determined that the physiological functions of RSK include phosphorylation of Ser-235 and Ser-236, which are necessary for cap-dependent translation [6].

There are 4 members of the RSK family (RSK1-4). By Northern blot analysis the RSK family members are expressed in numerous tissues and are frequently co-expressed [7, 8]. Therefore, to identify whether the individual RSK isoforms have unique functions we created a phylogenetic tree based on the protein sequences (Fig. 1B). Invertebrates have only one RSK isoform, which is not similar to their respective homologs in higher organisms but rather diverged from a common ancestor to form separate evolutionary branches. The vertebrates have four RSK isoforms and this expansion is consistent with the 2R hypothesis, which suggests that during speciation genomic duplication occurred twice [9]. The extra gene copies escaped the

constrains of selection, which allowed them to diverge and acquire novel functions [10]. The vast majority of duplicated genes were subsequently deleted but the few gene families that were preserved have possibly been major drivers to the increase in organism complexity [10]. The phylogenetic tree indicates that RSK2 and RSK4 are most closely related to each other than to RSK3, whereas RSK1 is the most distant relative. Human RSKs cluster together with other primate homologs with the exception of RSK3. Human RSK3 is more similar to the bovine and rodent homologs than to other primates. These observations suggest that evolutionary pressure existed to preserve an ancestral function of RSK3 in humans that is not present in other primates. We conclude based on the phylogenetic evidence that the RSK isoforms have distinct functions.

Figure 1 RSK structure and domain conservation.

(A) Domain conservation and structural schematic of the RSK family. (B) Phylogenetic tree of RSK1-4 homologs. Tree is rooted on *C.elegans* RSK1 as the earliest evolutionary sequence (green). Colors represent the isoform specific branches in vertebrates. Red branch indicates an exception; RSK1 in *D.rerio* is more closely related to RSK2 than to its respective homologs. Abbreviations: RSK1-R1; RSK2-R2; RSK3-R3; RSK4-R4.

Figure 1

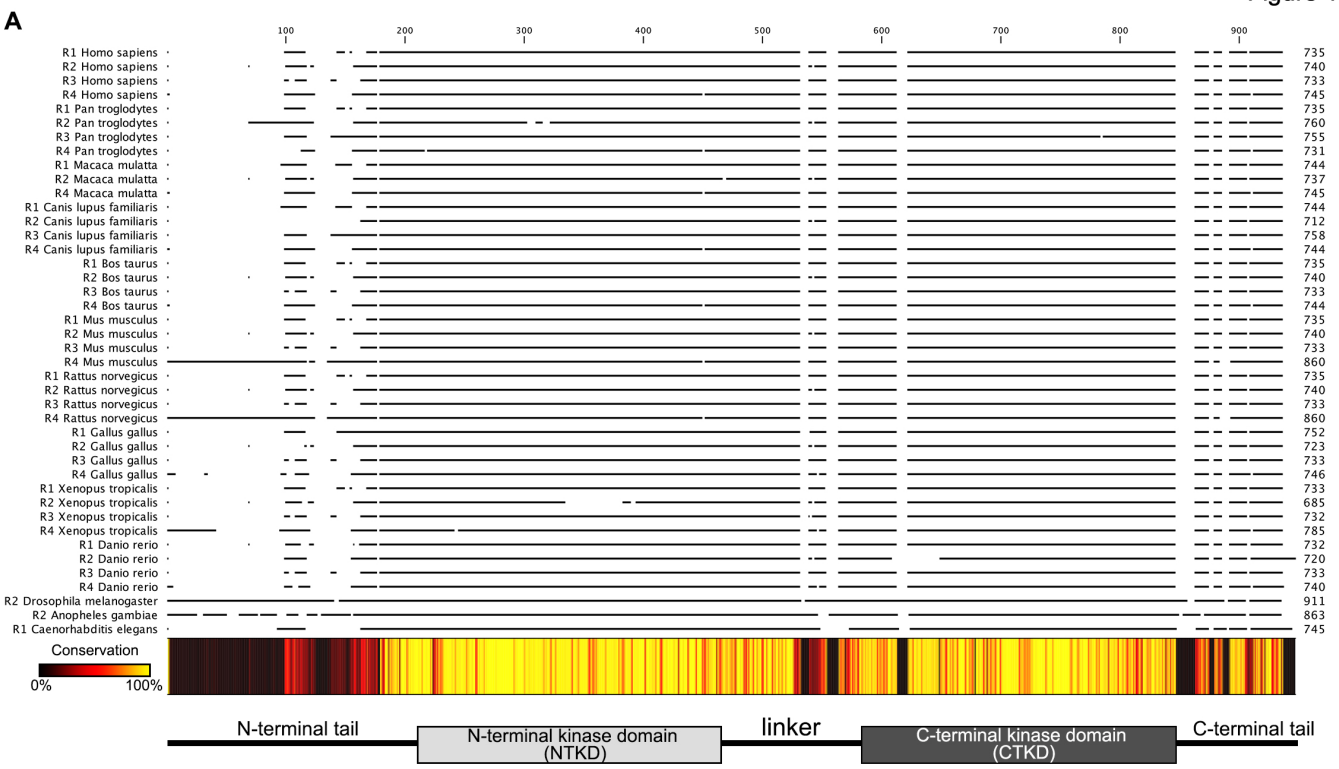
A
100
200
300
400
500
600
700
800
900
R1 Homo sapiens 735
R2 Homo sapiens 740
R3 Homo sapiens 733
R4 Homo sapiens 745
R1 Pan troglodytes 735
R2 Pan troglodytes 760
R3 Pan troglodytes 755
R4 Pan troglodytes 731
R1 Macaca mulatta 744
R2 Macaca mulatta 737
R4 Macaca mulatta 745
R1 Canis lupus familiaris 744
R2 Canis lupus familiaris 712
R3 Canis lupus familiaris 758
R4 Canis lupus familiaris 744
R1 Bos taurus 735
R2 Bos taurus 740
R3 Bos taurus 733
R4 Bos taurus 744
R1 Mus musculus 735
R2 Mus musculus 740
R3 Mus musculus 733
R4 Mus musculus 860
R1 Rattus norvegicus 735
R2 Rattus norvegicus 740
R3 Rattus norvegicus 733
R4 Rattus norvegicus 860
R1 Gallus gallus 752
R2 Gallus gallus 723
R3 Gallus gallus 733
R4 Gallus gallus 746
R1 Xenopus tropicalis 733
R2 Xenopus tropicalis 685
R3 Xenopus tropicalis 732
R4 Xenopus tropicalis 785
R1 Danio rerio 732
R2 Danio rerio 720
R3 Danio rerio 733
R4 Danio rerio 740
R2 Drosophila melanogaster 911
R2 Anopheles gambiae 863
R1 Caenorhabditis elegans 745
Conservation
0%
100%
N-terminal tail
N-terminal kinase domain (NTKD)
linker
C-terminal kinase domain (CTKD)
C-terminal tail

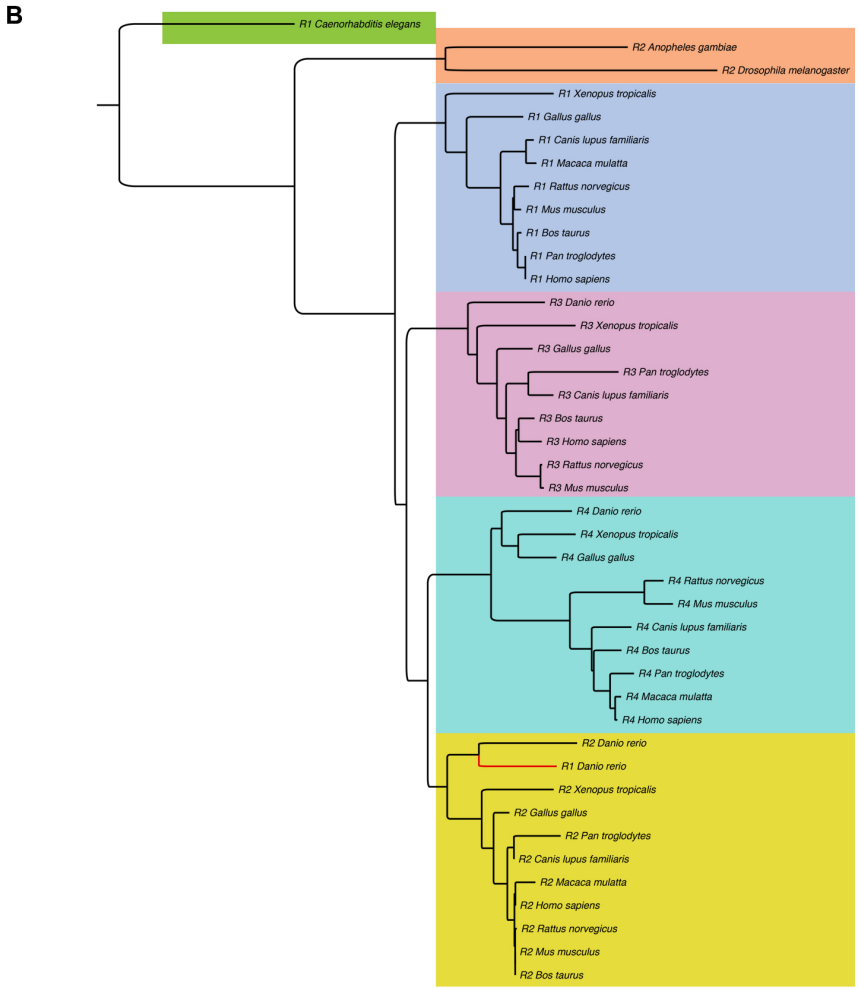
B
R1 Caenorhabditis elegans
R2 Anopheles gambiae
R2 Drosophila melanogaster
R1 Xenopus tropicalis
R1 Gallus gallus
R1 Canis lupus familiaris
R1 Macaca mulatta
R1 Rattus norvegicus
R1 Mus musculus
R1 Bos taurus
R1 Pan troglodytes
R1 Homo sapiens
R3 Danio rerio
R3 Xenopus tropicalis
R3 Gallus gallus
R3 Pan troglodytes
R3 Canis lupus familiaris
R3 Bos taurus
R3 Homo sapiens
R3 Rattus norvegicus
R3 Mus musculus
R4 Danio rerio
R4 Xenopus tropicalis
R4 Gallus gallus
R4 Rattus norvegicus
R4 Mus musculus
R4 Canis lupus familiaris
R4 Bos taurus
R4 Pan troglodytes
R4 Macaca mulatta
R4 Homo sapiens
R2 Danio rerio
R1 Danio rerio
R2 Xenopus tropicalis
R2 Gallus gallus
R2 Pan troglodytes
R2 Canis lupus familiaris
R2 Macaca mulatta
R2 Homo sapiens
R2 Rattus norvegicus
R2 Mus musculus
R2 Bos taurus

The kinase domains are highly conserved across all RSK isoforms (Fig. 1A). The N-terminal kinase domain (NTKD) belongs to the AGC subfamily of kinases, which includes protein kinases A, G and C. The C-terminal kinase domain (CTKD) belongs to the calcium/calmodulin-dependent protein kinase subfamily. The only known function of the CTKD is autophosphorylation whereas the NTKD is responsible for substrate phosphorylation [11]. RSK1, also referred to as p90RSK, RSK2 and RSK3 are activated in response to growth factor signaling whereas RSK4 is constitutively active even in serum-starved cells [12]. RSK activation is primarily dependent on the phosphorylation of four different residues, which are conserved [13]. In the canonical model inactive ERK1/2 interacts with a docking site located at the RSK extreme C-terminus (Fig. 2). This interaction is necessary for ERK1/2 activation of RSK [14] and this binding is regulated by phosphorylation and by physical association with other proteins to mediate the extent of RSK activation. Phosphorylation of Tyr 529 (human RSK2 numbering) by fibroblast growth factor receptor 3 [15] or Src tyrosine kinase [16] increases the interaction of inactive ERK1/2 with RSK2 to enhance RSK2 activation. The death effector domain protein, PEA-15, also interacts with RSK2, and facilitates the interaction of RSK2 with ERK1/2 to promote RSK2 activation [17]. Active ERK1/2 phosphorylates and activates the CTKD [18].

Figure 2 Schematic of RSK activation.

Schematic of RSK activation adapted from: Romeo et al. Regulation and function of the RSK family of protein kinases. *Biochem J.* 441:2:553-69. 2012. Portland Press. DOI:10.1042/BJ20110289 [8]. The phosphorylation site numbering as in human RSK1. NTKD – N-terminal kinase domain; CTKD – C-terminal kinase domain; ERK1/2 – extracellular-signal regulated kinase-1 and 2; PDK1 – phosphoinositide-dependent kinase-1; P-phosphorylation, at the given step – purple, at the previous steps – white.

Figure 2

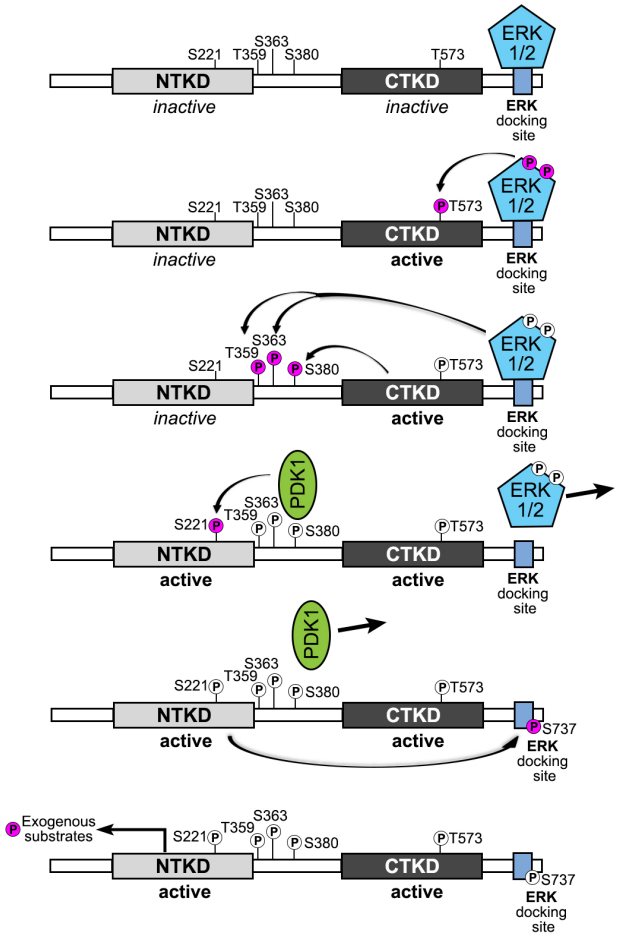
S221
T359
S363
S380
T573
NTKD
CTKD
inactive
active
ERK 1/2
ERK docking site
PDK1
Exogenous substrates
S737

Subsequently, the CTKD phosphorylates a hydrophobic motif in the linker between the kinase domains to create a docking site for 3'-phosphoinositide-dependent kinase 1 (PDK1) [19]. PDK1 binds to RSK to phosphorylate and activate the NTKD, which phosphorylates a residue in the PDZ-binding motif next to the ERK1/2 docking site [20]. This phosphorylation induces formation of a charge clamp that masks residues critical for ERK1/2 binding and results in disassociation of ERK1/2 [18, 20]. RSK4 is an exception and does not require PDK1 for its activation [12]. The requirement for CTKD activation can be bypassed in response to lipopolysaccharide (LPS) [21]. In dendritic cells LPS activates RSK through the p38-MAPK-activated protein kinases, MK2/3, and not via ERK1/2 [22, 23]. This mechanism has not been described for other cell types.

Analysis of the subcellular location of RSK2 has found that in response to growth factor activation RSK2 localizes to the nucleus by an unknown mechanism [24]. RSK2 does not contain an identifiable nuclear localization signal (NLS) and is too large to diffuse into the nucleus. Therefore, RSK2 most likely piggybacks onto an import factor to enter the nucleus. A putative NLS was identified in RSK1 but this sequence is identical in RSK2 and does not promote RSK2 nuclear translocation [24, 25]. An NLS has been identified in RSK3 but functional studies have not yet been performed [26]. RSK is known to regulate the activity of a number of different transcription factors by phosphorylation [8] and it is conceivable but not necessary that localization of RSK into the nucleus is important in this process.

In some circumstances interacting partners control RSK subcellular localization to facilitate the ability of RSK to interact with other signaling pathways. RSK2 was found to facilitate stress responses by interacting with TIA1, which sequesters RSK2 into sites of translational repression referred to as cytoplasmic stress granules [24]. The activity of RSK2 is necessary for the formation of stress granules, which promote cell survival. Another RSK member, RSK1, was found to interact with the protein kinase A (PKA) regulatory I subunit,

which sequesters inactive RSK1 in the cytoplasm [27]. However, active RSK1 is sequestered in the nucleus by its interaction with the PKA catalytic subunit, which results in inhibition of PKA signaling [25, 28]. These results demonstrate that RSK is able to interact as a scaffold and its interactions with other proteins influences its function as well as that of its binding partners.

The minimum consensus phosphorylation sequence for the NTKD was defined using synthetic peptide libraries and was found to consist of the motif Lys/Arg-X-Arg –X-X-pSer/Thr or Arg-Arg-X-pSer/Thr [29]. RSK prefers to phosphorylate Ser rather than Thr, which may explain why the majority of identified RSK substrates have a Ser residue as the phosphoacceptor site [8]. Based on the nature of these substrates, RSK has been implicated in cellular processes including cell survival [30] [31], transcriptional regulation [32-36], cell cycle [37-39], and motility[40]. Involvement of RSK isoforms in regulation of multiple cellular processes suggests that RSK is critical for normal development and homeostasis. In agreement with this hypothesis the gene encoding RSK2 (RPS6KA3) has been found to be associated with a human developmental disorder, Coffin-Lowry syndrome (CLS) [41]. This syndrome is associated with mental retardation, and skeletal and cardiac defects [42]. RSK2 knockout mice recapitulate some of these phenotypes [43-45]. In the mouse model, activating transcription factor 4 (ATF4) was identified as a RSK2 substrate in regulation of osteoblast differentiation and this axis is thought to be the major contributor to the skeletal phenotypes of CLS [45] [46]. In agreement with RSK2 importance for brain development [47], loss of the single Drosophila RSK isoform interferes with learning [48]. The genes encoding RSK1 (RPS6KA1), RSK3 (RPS6KA2) and RSK4 (RPS6KA6) are not associated with a genetic disorder and a RSK1/RSK2/RSK3 triple-knockout mouse has been generated and is reported to be viable. However, the characterization of these mice has not been published [49]. Thus, so far, only RSK2 appears to be important in development.

RSK and its association with human disease pathologies

RSK in cancer

RSK has been most intensively studied in the context of cancer and the majority of studies have focused on cancers with epithelial origins. The exceptions include osteosarcoma [50] and leukemia [51]. The evidence for RSK involvement in osteosarcoma is based only on mouse models and thus the relevance to human disease is unknown. The dependence on RSK2 in inducing leukemia varies according to the particular oncogenic tyrosine kinase. In FLT3-ITD induced leukemia knockout of RSK2 in a bone marrow transplant model resulted in a switch from a myeloproliferative neoplasm to T-cell acute lymphoblastic leukemia (T-ALL) [51]. Inhibition of RSK activity resulted in increased apoptosis in primary FLT3-ITD leukemia cells *in vitro*. The authors propose RSK inhibition as a possible treatment for FLT3-ITD induced leukemia but do not explain why T-ALL would be an acceptable consequence. The Kang group also demonstrated that TEL-FGFR3 expressing murine Ba/F3 leukemia cells and primary patient myeloma cells were dependent on RSK2 for survival *in vitro* [15] but that RSK2 did not alter BCR-ABL-induced myeloid leukemia. RSK2 is not required for normal myelopoiesis [52] but further investigations are needed to determine whether RSK2 would be suitable as a drug target for leukemia.

There is evidence that RSK is a possible target for two of the three major types of breast cancer, estrogen receptor/progesterone receptor positive (ER+/PR+) and triple negative breast cancer (TNBC), which lacks ER, PR and amplification of HER2. Approximately 70% of patients have active RSK in locally advanced breast cancers, which are mostly ER+/PR+ [53] and ~ 85% of TNBC tumors have active RSK [54]. Interestingly, the phosphorylation of ERα at Ser-167, a known RSK phosphorylation site [36, 55], was found to correlate with active RSK and responsiveness to endocrine-based therapies [56-58]. These results suggest that RSK is

involved in the etiology of ER+/PR+ breast cancer. There continues to be a need for novel therapeutic approaches for ER+/PR+ breast cancer as ~ 25% of patients will progress with endocrine-based therapies and only ~ 30% of those with metastatic disease will respond. Furthermore, there are no targeted therapies for TNBC. Total RSK1 and RSK2 were found to be overexpressed in breast cancer compared to normal breast tissue [59]. According to the TCGA database RSK1 and RSK2 mRNA levels are increased in ~ 4 and 5% of tumors, respectively. Taken together, these observations suggest that RSK would be an effective target for some types of breast cancer.

Prostate cancer is the second leading cause of cancer death in men [60]. Neuroendocrine prostate tumors are relatively rare at the time of initial diagnoses; however, these tumors are frequently found in patients who have received androgen ablation therapies. There are currently no targeted therapies for neuroendocrine prostate cancer. Strikingly, according to the TCGA database ~ 30% of neuroendocrine prostate tumors have increased expression of RSK2 at the mRNA level [61]. In agreement with these observations RSK2 levels were higher in prostate cancer than in benign prostatic hyperplasia and normal prostate tissue [62]. The importance of these observations to prostate cancer therapy has not yet been explored.

Melanomas frequently have mutations in BRAF that lead to activation of the MEK-ERK1/2 signaling pathway [63]. Therefore, it is not surprising that active RSK levels are higher in melanoma than normal skin. An anti- active RSK2 antibody was used to demonstrate that the increase in the levels of active RSK was due to RSK2 [64]. A previous study by the same group used an antibody to total RSK2 using the same tissue microarray to identify that total RSK2 levels were increased in melanoma [65]. These data are consistent with the TCGA database in which ~ 8% of melanomas have increased levels of RSK2 mRNA. A number of different BRAF and MEK1/2 inhibitors are currently in use for melanoma but drug resistance is frequently

observed [66]. A recent study using patient-derived melanoma cell lines with acquired resistance to combination of BRAF inhibitor vemurafenib and the MEK1/2 inhibitor selumetinib showed that inhibiting RSK decreases proliferation by blocking protein synthesis [67]. These results suggest that the addition of a RSK inhibitor to the therapeutic regimen could improve patient outcome.

Human head and neck cancer (HNCC) that has metastasized is frequently incurable [68]. An anti-RSK2 antibody that was extensively validated was used to demonstrate that there is an increase in RSK2 levels in metastatic tumors compared to their matched primary tumors [69]. In a xenograft model using the highly invasive M4e line, silencing RSK2 decreased metastasis to the lymph node. The Kang group followed up these observations using the RSK CTKD inhibitor, FMK-MEA, which resulted in a modest decrease in lymph node metastasis of M4e cells from 97% to 79% [70]. Silencing RSK2 or inhibiting RSK activity did not reduce primary tumor growth [70]. Importantly, metastasis is the major cause of cancer-related deaths and therefore, the ability to inhibit metastasis with a RSK inhibitor is of great interest.

Brain and nervous system cancers represent only 1.4% of new cancer cases every year and only half of those are glioblastomas (GBM). However, GBM patients have one of the lowest 5-year survival rate ranging from 5 to 19% [71] and no targeted therapies for GMB exist. A recent study identified EphA2, which is correlated with poor prognosis in GBM patients, as a target for RSK2-mediated phosphorylation. Inhibition and silencing of RSK2, reduced EphA2 phosphorylation and led to decreased proliferation of GBM cells [72]. RSK2 was also implicated in regulation of GBM motility through its ability to impair integrin-mediated matrix assembly [73] and by regulation of cytoskeleton dynamics by promoting activation of RhoA GTPase through phosphorylation of RhoGEF, LARG [74]. Further *in vivo* studies are needed to evaluate RSK as a target in GBM.

Most surprising are the observations in lung cancer that silencing RSK1 increased metastasis of the lung cancer line, A549, in a xenograft model using zebrafish [75]. In support of these studies a kinome-wide siRNA screen performed by Lara et al. identified RSK1 as a repressor of motility in a number of human lung cell lines. Total RSK1 expression was reported to be higher in 46% of primary lung tumors than in the metastatic sites although it is not possible to determine the relationship between total and activated RSK1 [75]. However, these studies are in contrast to Zhou et al [76] in which inhibition of RSK activity was associated with decreased motility in lung cancer lines. Observations by Lara et al. are also contradicted by reports showing that activated RSK in combination with phosphorylated EphA2 was associated with decreased probability of survival in lung cancer patients [77]. Thus, the discordance of RSK1 function between these studies in lung cancer indicates the need for further investigation.

Similarly, to lung cancer, there are conflicting reports of RSK functions in colorectal tumors. RSK2 was shown to inhibit colon cancer metastasis to the liver by phosphorylating transcription factor T-bet and activating an anti-tumor immune response [78]. In a RSK2 knock-out mouse model, loss of RSK2 was associated with decreased production of INFγ, a critical component of anti-metastatic immunity, allowing for uninhibited metastatic colonization of the liver. Importantly, these effects are due to RSK2 functions in microenvironment, as the implanted tumor cells expressed. In contrast with this report are in vitro studies showing that RSK is involved in colorectal cancer cells proliferation and motility [79], and inhibition of RSK-pathway diminishes multidrug resistance [80]. Therefore, further studies might be necessary to evaluate whether RSK is a desirable drug target in colorectal cancer.

In contrast to RSK1/2, which are generally thought to act as tumor promoters, RSK3/4 have been proposed to act as tumor suppressors. RSK3 was found to map to a region that was identified as containing a putative tumor suppressor in ovarian cancer [81] and in support of this observation ~3% of ovarian cancer tumors have a deletion in the RSK2 gene. However, loss of

RSK3 in combination with the EGFR inhibitor, erlotinib, was synergistically lethal to the pancreatic cancer cell line, BxPC-3, which argues against RSK3 being a tumor suppressor [82]. Active RSK3 was observed in pancreatic tumors by immunohistochemistry but it is likely that this antibody recognizes all active RSK isoforms and therefore, the function of RSK3 in pancreatic cancer needs to be further studied. A decrease in RSK4 mRNA expression has been reported for a number of different cancers including, ovarian, colon and renal cell and colon adenoma, endometrial and breast [83-87]. However, the decrease in RSK4 at the mRNA levels is not consistent with the information present in the TCGA database in which mRNA levels are available. For breast cancers there are additional conflicting observations, as some investigators have observed an increase in RSK4 at the mRNA level [88]. These results are consistent with the TCGA database in which an increase in RSK4 mRNA is observed in ~ 6% of breast cancers. Further evidence that RSK4 does not act as a tumor suppressor is shown by studies in which RSK4 mediates resistance to PI3 kinase inhibitors in breast cancer [89]. Serra et al. also reported that according to the Human Protein Atlas the levels of RSK4 and to a lesser extent RSK3 levels were elevated in numerous tumor types by immunohistochemistry. The observations in renal cell carcinoma are also conflicting as Fan et al. observed an increase in RSK4 by immunohistochemistry [90]. In agreement with these observations the TCGA database shows that ~ 2% of renal clear cell carcinomas have elevated levels of RSK4 at the mRNA level. Thus, the functions of RSK3/4 in cancer have not been clearly defined.

RSK in cardiovascular disease

RSK is activated in human hearts diagnosed with idiopathic dilated cardiomyopathy [91]. Additionally in animal models activated RSK is observed in vascular smooth muscle cells in spontaneously hypertensive rats [92] and in cardiomyopathies caused by ischemia/reperfusion (IR) injury [93, 94] and diabetes mellitus [95]. The proposed function of RSK in hypertension

does not appear to be fully resolved as differing effects are observed in response to angiotensin II [92, 96, 97]. Evidence supporting a function for RSK in cardiomyopathy is provided by observations that treatment with the CTKD RSK-inhibitor, FMK-MEA, reduced endothelial cell dysfunction and atherosclerosis formation in diabetic animal models [98]. Consistent with these results in an atherogenic mouse model targeting a dominant negative mutant of RSK1 decreased lesion formation and lipid deposition [99]. Furthermore, in an IR model of cardiac injury, expression of a dominant negative mutant of RSK1 targeted to the heart reduced infarct size, decreased cardiomyocyte apoptosis and improved cardiac function [100, 101]. A RSK inhibitor, BIX 02565, improved cardiac function in an IR model [102] but this inhibitor is reported to have off target effects on α-adrenergic receptors so the evidence that inhibition of RSK is responsible for the improved cardiac function is not clear [103]. It is proposed that RSK contributes to hypertension and cardiomyopathy by phosphorylation and activation of the Na+/H+ exchanger 1 (NHE1) [100, 104, 105], which is known to be important in cardiac dysfunction [106]. In multiple animal models, NHE1 inhibitors were found to protect against ischemic injuries but in clinical trials they showed limited or no protection [107]. The adverse side effects observed in the clinic were attributed to inhibition of NHE1 basal activity; however, it is hypothesized that specifically inhibiting NHE1 activation in periods of cardiovascular stress would be beneficial [106]. In addition to NHE1 RSK has been implicated in smooth muscle contraction [108], and inhibitors of this process have been proposed as a treatment for hypertension [109, 110]. Taken together, the evidence supports the development of RSK inhibitors for cardiovascular disease.

RSK3 has also been implicated in cardiomyopathies. Knockout of RSK3 led to a decrease in cardiomyocyte hypertrophy, which was induced by pressure overload and catecholamine infusion [111]. Furthermore, knockout of RSK3 improved cardiac function by reducing interstitial fibrosis, which was induced by mutant α-tropomyosin expression [112]. The

importance of RSK3 in cardiomyopathies is likely independent of those observed in diabetic hearts because the FMK-MEA inhibitor is unable to inhibit RSK3. Thus, RSK3 has distinct functions from the other RSKs in regulating the response to cardiac injury.

RSK in infectious disease

RSK has been implicated in regulating the virulence of Kaposi's sarcoma-associated herpes virus (KSHV), a common AIDS-associated pathogen and of Yersinia spp., which includes the plague bacterium. In both cases activation of RSK occurs by its association with a virulence factor. In KSHV RSK interacts with ORF45 and it is thought that RSK2 is the primary interaction partner [113, 114, 115{Avey, 2015 #1587, 116]. This interaction is critical for KSHV lytic gene expression and progeny virion production. In Yersinia spp. activation of RSK1 occurs by its interaction with YopM, which was shown to be important in regulating virulence in a mouse model [117]. Targeting a host protein, like RSK, that is required for infection is a very attractive strategy for therapeutics because the host proteins are unlikely to evolve as rapidly as the pathogens to circumvent the therapy.

RSK in fibrosis

Fibrosis occurs in nearly all tissues and very little is known at the mechanistic level. Excessive tissue repair in chronic liver disease results in phenotypic changes in hepatic stellate cells causing them to be hyper proliferative and to generate extracellular matrix proteins, which leads to fibrosis and cirrhosis [118, 119]. There are no available treatments for cirrhosis. As revealed by proteomic analysis using reverse phase protein microarrays, RSK is overexpressed and activated in hepatic fibrosis associated with chronic liver diseases, such as hepatitis C virus infections or non-alcoholic steatohepatitis, and alcoholic hepatitis [120]. In injured livers, RSK activation results in phosphorylation and activation of CCAAT-enhancer binding protein beta

(C/EBPβ) [121], which contributes to excessive fibrosis and cirrhosis [119, 122]. In a chemically-induced liver fibrosis mouse model a cell-permeable RSK-inhibitory peptide induced regression of liver fibrosis purportedly by inhibiting RSK-dependent phosphorylation of C/EBPβ [31, 119]. This peptide was based on the RSK phosphorylation site in which the RSK phosphorylation site was mutated. Consistent with the importance of RSK in chronic liver disease analysis of four patients with severe liver disease due to hepatitis C had increased levels of active RSK compared to control. These results are similar to those observed in patients with alcoholic hepatitis [120]. Taken together, the evidence suggests that inhibition of RSK in chronic liver diseases could have therapeutic benefits.

Fibrosis in the lung is thought to occur using a similar mechanism to that observed in the liver [123]. No therapies effectively target lung fibrosis and worldwide there is an increase in the incidence of idiopathic pulmonary fibrosis (IPF) [124]. In a chemically-induced lung fibrosis mouse model the RSK-inhibitory peptide used in the liver fibrosis studies was effective in reducing pulmonary fibrosis [123]. Analysis of two patient samples with IPF demonstrated high levels of active RSK staining in the lungs compared to the lungs of normal patients [123]. Taken together, these results suggest that RSK would be an attractive target for liver and lung fibrosis.

RSK in rheumatoid arthritis

There is a need for novel therapies for rheumatoid arthritis as current therapies targeting the immune cells are not always effective [125]. Activated RSK levels, which appears mainly due to RSK2, is higher in joints from patients with rheumatoid arthritis and inflamed osteoarthritis than non-inflamed osteoarthritis [126]. Surprisingly, loss of RSK2 in a mouse model of spontaneous arthritis led to a more aggressive behavior of fibroblasts. It will be important to investigate RSK2 using other mouse models of arthritis to identify whether treatment with a RSK inhibitor will have side effects on the bone.

Figure 3 RSK-inhibitors.

Structures of RSK inhibitors: (A) BIX 02565 and compound 15 (B) FMK (C) SL0101 and 5''-n-propyl-cyclitol-SL0101 (D) BI-D1870, LHJ685 and LHI308.

Figure 3

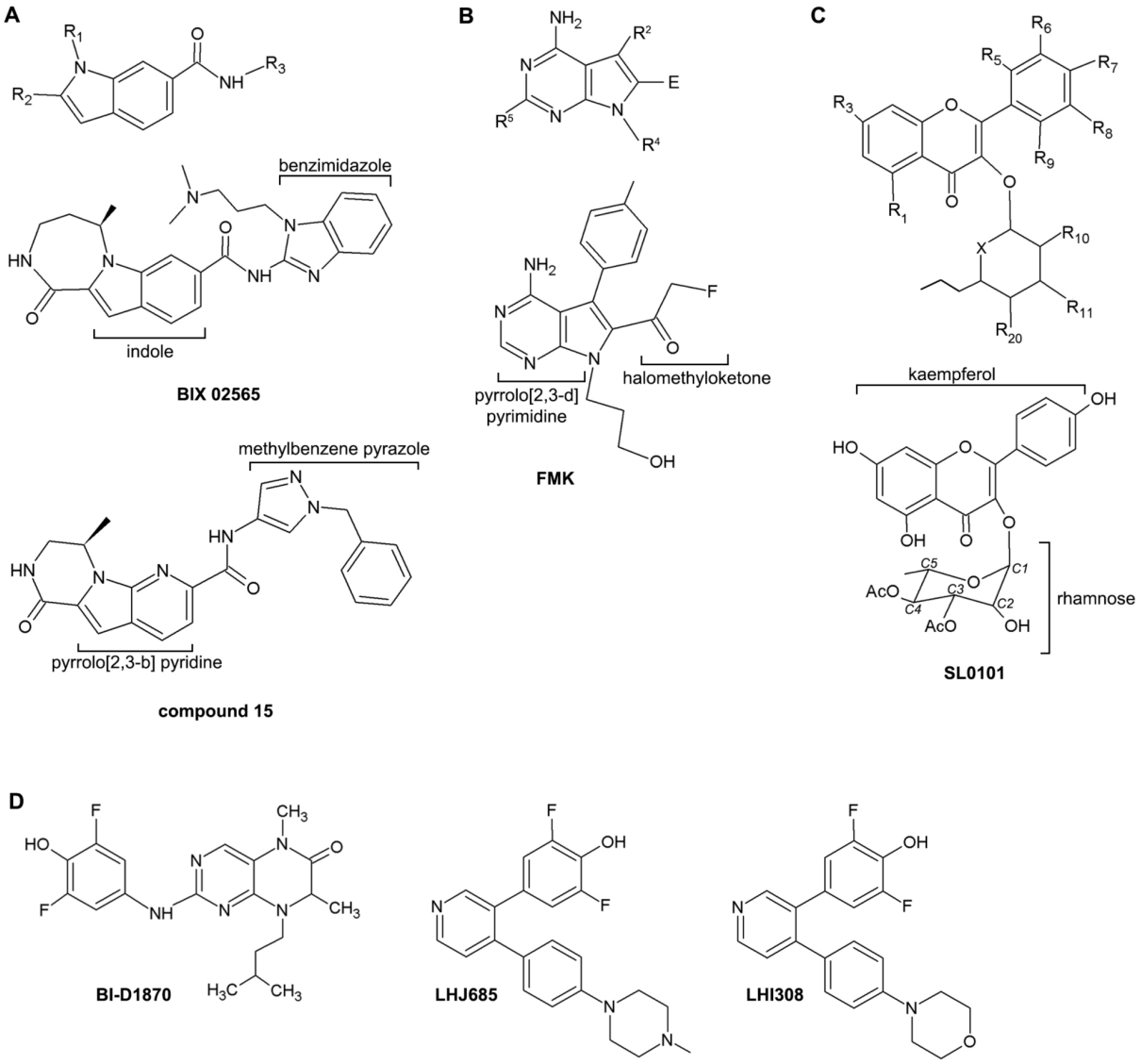
A
benzimidazole
indole
BIX 02565
methylbenzene pyrazole
pyrrolo[2,3-b] pyridine
compound 15
B
pyrrolo[2,3-d]
pyrimidine
halomethyloketone
FMK
C
kaempferol
rhamnose
SL0101
D
BI-D1870
LHJ685
LHI308

Overview of RSK inhibitors

In this overview RSK-specific inhibitors are defined as those compounds that have been extensively screened against a panel of kinases and have demonstrated preferential inhibition of RSK. Compounds that demonstrate equal potency in inhibiting kinases in addition to RSK are referred to as RSK inhibitors.

BIX 02565

In an effort to characterize RSK inhibitors for use in cardiovascular disorders, a family of compounds containing an indole corer was developed. One of the inhibitors from this family, compound 93, also known as BIX 02565 (Fig. 3A), has been characterized as a lead inhibitor for potential *in vitro* and *in vivo* use. In an *in vitro* kinase assay BIX 02565 inhibited RSK2 with an IC_{50} of 1.1 nM [103]. In a cell-based, luciferase reporter assay that tests the inhibition of phosphorylation of the transcription factor CREB, a known RSK2 target [127], BIX 02565 inhibited RSK with an IC_{50} of ~ 20 nM [103]. In a selectivity screen against a panel of 20 protein kinases BIX 02565 inhibited eight other kinases in addition to RSK2 with IC_{50}s < 1μM [128]. It has been reported that BIX 02565 prevents the decrease in the left-ventricular-developed pressure caused by I/R injury using a mouse model [102]. However, this report contradicts an earlier study in which BIX 02565 led to a dangerous decrease in both mean arterial pressure and heart rate in a mouse model [103]. To identify the mechanism for the cardiovascular effects BIX 02565 was screened against a panel of 68 receptors and ion channels using a competition radioligand binding assay. BIX 02565 was found to bind five adrenergic receptors (α1A, α1B, α1D, α2A, and β2) by >50% [103]. As adrenergic receptors are central regulators of sympathetic tone and control cardiac output and vasoconstriction of arteries, uncontrolled modulation of their activity can have deleterious effects [129]. To identify a RSK inhibitor that did not bind adrenergic receptors an additional screen of 30 compounds based on the BIX

02565 structure was performed. This resulted in compound 15 in which the BIX 02565 benzimidazole moiety and indole core were replaced with a methylbenzene substituted pyrazole and a pyrrolo pyridine, respectively. Compound 15 inhibits RSK2 with an IC_{50} of ~ 0.2 nM in an *in vitro* kinase assay and an IC_{50} of ~ 0.32 nM in a cell-based CREB-reporter assay. Furthermore, the compound did not exhibit off-target binding to the adrenergic receptors and *in vivo*, the new inhibitor did not decrease mean arterial pressure [103]. The benzimidazole moiety in BIX 02565 was identified as mediating the interaction with adrenergic receptors. However, further profiling against other kinases will be necessary to ensure specificity.

FMK

Protein kinases are attractive drug targets due to the presence of an ATP-binding pocket, which consists of a hydrophobic cleft at the interface of two conserved domains [130]. Many kinase inhibitors dock into that cleft and inhibit kinase activity by outcompeting ATP and are referred to as type I kinase inhibitors [131]. However, due to the high conservation of the ATP-binding pocket, the specificity of such compounds is limited [132]. A conserved residue in the ATP-binding pocket, called the 'gatekeeper' residue, can limit the number of kinases that bind to the inhibitor. The 'gatekeeper' is often a bulky amino-acid (Phe, Asp, Glu), which limits inhibitor access [133]. In ~20% of human kinases the "gatekeeper" is a Thr [131], which, due to its limited size, allows access of an inhibitor to the hydrophobic cleft. RSK1, 2 and 4 have a Thr in the 'gatekeeper' position, which is located in the CTKD [132]. Furthermore, including aromatic or heteroaromatic moieties, which interact with the 'gatekeeper' Thr, can enhance the affinity of the inhibitor for the kinase [133]. It is also possible to obtain additional inhibitor specificity by exploiting the presence of a reactive Cys residue, which is located in the ATP-binding pocket, but which is present in only a small number of protein kinases. These kinases include RSK1-4 and the closely related MSK1/2, as well as PLK1-3, MEKK1, and NEK2 [132].

The requirements for a Thr as the 'gatekeeper residue' and a reactive Cys in the ATP-binding pocket narrows down the types of compounds that can be used as potential inhibitors. Specifically, these compounds have heterocyclic cores comprising of two or more fused rings with at least one nitrogen ring-atom for gatekeeper interaction, and an electrophilic substituent that covalently binds the Cys residue [131]. One group of compounds that fulfills the above criteria can be collected under the general term of pyrrolo[2,3-d] pyrimidines with halomethyl ketone substitutions [134] (Fig. 3B). These compounds contain the halogen residue to covalently bind the Cys within the kinase ATP-binding pocket. Furthermore, a subset of the molecules contains multiple heteroaromatic rings that facilitate interaction with the gatekeeper Thr of RSK1, 2 and 4.

The key compound that was identified from this family of inhibitors is FMK (Fig. 3B), which is identified as a potent RSK2 CTKD inhibitor with an IC_{50} of 0.015±0.001 μM in an *in vitro* kinase assay [134]. To demonstrate that the structural selectivity features render the RSK2 CTKD a unique FMK target, mutations of the Cys or Thr within the ATP-binding pocket were generated. Basal kinase activity was not altered in the mutants, RSK2-C436V and RSK2-T493M, but inhibition by FMK was decreased by 600- and 200-fold, respectively, as compared to the wild type kinase. To demonstrate selectivity FMK was labeled with biotin and in a streptavidin pull down from epithelial cell lysates was found only to interact with RSK1 and RSK2 [134]. Further testing revealed off-target inhibition of protein tyrosine kinases, such as SRC, LCK, MNK1, and p70 S6 kinase 1 [135]. FMK is considered a fairly specific irreversible inhibitor of the RSK1/2 CTKD. *In vivo*, FMK reduced atherosclerosis in a diabetic mouse model [98] and to a modest extent inhibited HNCC metastasis [70]. FMK is a unique RSK inhibitor, in that it targets the RSK CTKD and the only known substrate of this kinase domain is a residue in the RSK linker region. In COS-7 cells stimulated with EGF, treatment with FMK inhibited this phosphorylation with an IC_{50} of ~ 200 nM, as detected by a phospho-specific antibody [134] [21].

However, because the CTKD is only required for activation of RSK, FMK is not effective at inhibiting the kinase after it is activated. Furthermore, the CTKD is not always required for RSK activation [21, 22] and therefore, despite relatively high specificity for RSK, application of FMK is limited.

SL0101

In a high-throughput luminescence-based ELISA screen 10,000 botanical extracts were tested for their ability to inhibit RSK2 phosphorylation of Ser-167 in ERα. Using bioassay-guided fractionation, SL0101, a kaempferol glycoside, obtained from the tropical plant, *Forsteronia refracta*, was identified as a RSK inhibitor (Fig. 3C) [59]. SL0101 was the first RSK-specific inhibitor reported, and had an IC_{50} of ~ 1 μM in an *in vitro* kinase assay, which measured substrate phosphorylation by luminescence [59]. In the initial characterization of SL0101 it did not inhibit p70 S6 kinase or MSK1, the most closely related kinases, or PKA, an archetypal Ser/Thr kinase. In further screening against 80 protein kinases SL0101 inhibited Aurora B, PIM1, and PIM3, but with a lower potency than for RSK1 and RSK2 [135]. The availability of SL0101 from natural sources is limited, and therefore, creation of a synthetic route was crucial.

The interaction of SL0101 with RSK is dependent on the presence of the sugar moiety, because kaempferol by itself has a 40-fold lower *in vitro* affinity for RSK than SL0101 [136]. Furthermore, the acetyl groups are necessary for high affinity binding as tri-hydroxy-SL0101 is ten-fold less potent than SL0101 [136]. The requirement of the acetyl groups for high affinity binding to RSK is unexpected as these groups do not appear to be required for interaction with the isolated NTKD [137, 138], which suggests that may interact with other regions within the full length kinase. In attempt to improve SL0101 efficacy the positions C3 and C4 of the rhamnose have been substituted in with butyryl groups (Bu-SL0101) or the position C2 was replaced with

an acetyl group (3Ac-SL0101) [139]. Both analogues inhibit RSK with similar potency in *in vitro* kinase assays, and 3Ac-SL0101 is marginally, ~2-fold, more potent than SL0101 at inhibiting MCF-7 proliferation [140]. However, using a phospho-specific antibody that recognizes the consensus site for RSK demonstrated that Bu-SL0101 was not as specific for RSK as SL0101 and 3Ac-SL0101 [140].

SL0101 binds to an allosteric pocket within the RSK NTKD [137]. The crystal structure of the RSK2 NTKD in complex with SL0101 indicates that a binding site for SL0101 is generated by structural rearrangement of the N-lobe of the NTKD [137]. The crystal structure also revealed that the 5''methyl moiety of the carbohydrate points into a hydrophobic pocket large enough to accommodate a longer aliphatic chain. To test whether longer aliphatic residue in this position could improve SL0101 efficacy, a series of analogues with varying aliphatic chain lengths at the C5" position was synthesized [141]. From the series the 5''-n-propyl-SL0101 derivative demonstrated a 50-fold improved IC_{50} for RSK in an *in vitro* kinase assay. However, the ability of 5''-n-propyl-SL0101 to inhibit MCF-7 proliferation was only two-fold better compared to SL0101, likely due to limited cell permeability [141]. To improve the *in vivo* pharmacokinetic properties of SL0101 [141], the rhamnose ring was replaced with a cyclitol, which eliminates the glycosidic bond susceptible to hydrolysis [142] (Fig. 3C). This modification did not significantly alter the *in vitro* affinity of the inhibitor for RSK, but the cyclitol analogues of SL0101 did not appear to be specific for RSK [142].

To combine improved IC_{50} of the 5''-n-propyl-SL0101 with the removal of the hydrolysable glycosidic bond, the series of 5''-n-substituted-cyclitol-SL0101 analogs was generated [143]. In an *in vitro* kinase assay the IC_{50} of 5''-n-propyl-cyclitol-SL0101 was 2-fold higher than IC_{50} of 5''-n-propyl-SL0101. Yet, the 5''-n-propyl-cyclitol-SL0101 inhibited MCF7 proliferation with 4-fold lower IC_{50} than 5''-n-propyl-SL0101 [141, 144], likely due to improved stability of the compound. The improved pharmacological properties of the 5''-n-propyl-cyclitol-

SL0101 allowed for testing of this compound in pre-clinical mouse model for TNBC [144]. This study is further described in Chapter 3.

BI-D1870

In an *in vitro* kinase selectivity screen of dihydropteridinones, BI-D1870 (Fig. 3D) was identified as potent inhibitor of the NTKD of RSK1 and RSK2 [145]. The IC_{50} values for RSK1 and RSK2 for inhibition with BI-D1870 were 31 and 24 nM respectively, and they were dependent on ATP concentrations. Further evaluation indicated that BI-D1870 lacks isoform specificity as it also inhibits RSK3 and RSK4 with IC_{50} values of 18 and 15 nM respectively. BI-D1870 is selective for RSK among other AGC kinases, but it also inhibits Polo Like Kinase 1 (PLK1), a key regulator of centrosome maturation and cell cycle. In addition, at concentrations 10-100-fold higher that necessary for RSK, BI-D1870 inhibits several other kinases including Aurora B, MELK, MST2 and PIM3 [135, 145]. These multiple off-target effects of BI-D1870 are likely the reason why its use remains limited to *in vitro* applications. There is only one report of BI-D1870 use *in vivo*. The inhibitor was used to test the effect of RSK inhibition on peptide induced autoimmune encephalomyelitis in mice, a model for multiple sclerosis [146]. BI-D1870 administered every other day at 0.5 mg/kg by intraperitoneal (IP) injection ameliorated paralytic symptoms and decreased inflammatory cell infiltration in the spinal cord. However, it is unclear whether these promising results can be attributed to RSK inhibition.

Two difluorophenol pyridines, BI-D170 derivatives, LJH685 and LJI1308, (Fig. 3D) have been identified as RSK inhibitors with LJH685 demonstrating fewer off target effects that LJI1308 [147]. The IC_{50} values against all RSK isoforms ranged from 4-13nM in *in vitro* kinase assays. However, these compounds demonstrated poor pharmacokinetics, with short plasma half-life (t1/2=13 min) and moderate tissue drug distribution [148]. Therefore, the utility of these derivatives is limited.

Synopsis of Chapters 2-6

Numerous studies provide evidence that RSK controls proliferation, viability and motility and, therefore, has accordingly been implicated in the etiology of numerous cancers. In breast cancer, increased levels of active RSK have been reported in two out of three clinically relevant subtypes. However, the contribution of individual RSK isoforms to breast cancer are not well understood partly due to the lack of RSK-specific inhibitors suitable for *in vivo* use, but also our limited understanding of RSK-dependent cellular processes in normal homeostasis. Therefore, the goal of my work described in this thesis was to integrate *in vitro* and *in vivo* models to develop an understanding of RSK in normal mammary gland biology and the etiology of breast cancer.

It has been previously known that one of the RSK isoforms, RSK2, can regulate transcriptional activity of ERα by phosphorylation and physical interaction [36, 55]. Surprisingly, in ER+ breast cancer active RSK correlates with disease-free survival and response to anti-estrogen treatment. The contents of the next chapter (Chapter 2) of this thesis details the mechanistic rationale that underpins this correlation and presents evidence that nuclear RSK2 in an obligate participant in ER+ driven tumorigenesis.

Despite the growing evidence of the importance of RSK in the etiology of breast cancer, very little is known about RSK-dependent functions in the normal mammary gland. As understanding molecular mechanisms regulating normal biological processes is a powerful strategy for identification of cancer vulnerabilities, we investigated how RSK2 contributes to mammary gland development and homeostasis. It is well established that ER+ cells are critical for maintenance of normal mammary gland development and [149, 150], yet it is poorly understood how ERα is regulated in a normal homeostasis. Given that, in response to estrogens, ERα is degraded through 26S proteasome pathway, it is especially puzzling how ER-

protein levels are maintained in the constant presence of estrogens prior to menopause. In the third Chapter of this thesis I will present our discovery of a negative feedback mechanism between estrogen signaling and the ERK1/2-RSK2 axis that is critical for maintaining ERα protein levels in the adult. In response to estrogens, ERα positively regulates growth factor signaling and activates ERK1/2-RSK2 signaling cascade, which in turn limits ER-mediated transcription and reduces ERα-degradation. I will provide evidence that RSK2 controls mammary gland function by regulating homeostasis of ER+ epithelial cells.

In addition to studies showing that RSK is a key contributor to ER+ breast cancer, ample evidence exists suggesting that RSK is a target in TNBC. This observation may seem counter-intuitive as TNBCs lack expression of ERα. However, it is likely that RSK-regulated processes involved in tumorigenesis differ between these two cancer subtypes. In support of this hypothesis, our work presented in Chapter 2 suggests that in ER+ disease RSK2 participates in initiation, whereas in TNBC both, RSK1 and RSK2, have been shown to control proliferation and migration [54, 151]. Despite evidence that RSK participates in metastatic process and the reports that ~80% of TNBCs have elevated active RSK [54], targeting RSK *in vivo* was not realistic mostly due to the lack of RSK-specific inhibitors with suitable pharmacokinetic properties. Therefore, in collaboration with Dr. O'Doherty, a medicinal chemist, our laboratory developed a RSK inhibitor, a derivative of SL0101, that is suitable for *in vivo* experiments. The contents of Chapter 4 of this thesis describes proof-of-concept *in vivo* studies showing the use of 5''-n-substituted-cyclitol-SL0101 to target TNBC metastasis.

One of the biggest challenges in developing targeted therapies in breast cancer is a lack of relevant model systems. Brest cancer is very heterogeneous with three subtypes distinguished clinically based on the hormone receptor status. In addition to the differences between subtypes, intra-tumor phenotypic and genetic heterogeneity exists and has been

shown to contribute to therapy resistance and patient outcomes [152]. Two-dimensional cultures of dissociated human tumors do not recapitulate the structural complexity, cellular phenotypes, or gene expression profiles of the intact tumor tissue. Patient-derived xenografts (PDX) have demonstrated an ability to predict patient response to treatment [153], but the establishment of them takes many months, precluding their use for personalized medicine. In Chapter 5 of this thesis I delineate our efforts in identifying robust *in vitro* conditions for growth of breast cancer organoids that would recapitulate the *in situ* inter- and intra- tumor heterogeneity.

In the last chapter, Chapter 6, I will discuss the key findings of our work in the context of the literature and I will define emerging questions and areas to be studied in the future.

Chapter 2 ERα-mediated nuclear sequestration of RSK2 is required for ER+ breast cancer tumorigenesis

Adapted from [154]: Ludwik K.A. McDonald O.G., Brenin D.R., Lannigan D.A. (2018) ERα-mediated nuclear sequestration of RSK2 is required for ER+ breast cancer tumorigenesis. Cancer Res. doi: 10.1158/0008-5472.CAN-17-2063.

Summary

Although ribosomal protein S6 kinase A3 (RSK2) activation status positively correlates with patient responses to anti-estrogen hormonal therapies, the mechanistic basis for these observations is unknown. Using multiple in vitro and in vivo models of ER+ breast cancer, we report that ERα sequesters active RSK2 into the nucleus to promote neoplastic transformation and facilitate metastatic tumor growth. RSK2 physically interacted with ERα through its N-terminus to activate a pro-neoplastic transcriptional network critical to the ER+ lineage in the mammary gland, thereby providing a gene signature that effectively stratified patient tumors according to ERα status. ER+ tumor growth was strongly dependent on nuclear RSK2, and transgenic mice engineered to stably express nuclear RSK2 in the mammary gland developed high grade ductal carcinoma in situ. Mammary cells isolated from the transgenic model and introduced systemically successfully disseminated and established metastatic lesions. Anti-estrogens disrupted the interaction between RSK2 and ERα, driving RSK2 into the cytoplasm and impairing tumor formation. These findings establish RSK2 as an obligate participant of ERα-mediated transcriptional programs, tumorigenesis, and divergent patient responses to anti-estrogen therapies.

Introduction

Intrinsic or therapy-induced resistance to endocrine-targeted therapy for estrogen receptor positive (ER+) breast cancer is a major obstacle to improving patient outcomes [155]. Therefore, there is an ongoing effort to identify predictive biomarkers that will indicate responsiveness to therapy. ERK1/2 in response to growth factor and cytokine signaling initiates a phosphorylation cascade that results in the activation of the Ser/Thr protein kinase, p90RSK (RSK) [13, 19]. Interestingly, active RSK correlates with disease-free survival and response to chemotherapy in ER+ breast cancer [53, 58]. The kinase domains of the four members that comprise the RSK family are very similar but family members appear to have both redundant and separate contributions to development, homeostasis and disease etiologies [1, 8]. RSK controls several oncogenic processes, including proliferation, viability and motility and, therefore, has accordingly been implicated in the etiology of numerous cancers including breast [50, 59, 62, 69, 75, 76, 144, 156, 157]. However, despite detailed knowledge on RSK oncogenic functions, the mechanistic rationale that underpins the correlation of active RSK with endocrine-based responsiveness in ER+ breast cancer remains an enigma.

Here we report that ERα physically interacts with RSK2, resulting in accumulation of RSK2 in the nucleus. This interaction activates a transcriptional network that is critical for ER+ tumor growth and provides a gene signature that stratifies patient tumors according to ER+ status. Anti-estrogens disrupt the association of ERα and RSK2 and drive RSK2 into the cytoplasm, which results in severely impaired tumorigenic capacity. Furthermore, forced nuclear RSK2 in a novel transgenic mouse model triggers neoplastic transformation of ER+ epithelial cells within the native mammary gland. Taken together, our results reveal that the nuclear sequestration of RSK2 by ERα activates a pro-neoplastic transcription program that is susceptible to disruption by anti-estrogen therapy. These data provide a mechanistic

explanation for the clinical observations that RSK2 correlates with responsiveness to endocrine-based therapies.

Materials and Methods

Antibodies, oligonucleotides and other key reagents are listed in Table 1.

Animals

All procedures involving animals were done in accordance with current federal (NIH Guide for Care and Use of Laboratory Animals) and university guidelines and were approved by the University of Virginia and Vanderbilt University Institutional Animal Care and Use Committee.

C57BL/6J mice carrying a transgene composed of the mouse mammary tumor virus-long terminal repeat (MMTV-LTR) linked to sequences encoding the hemagglutin (HA) tag, the NLS from SV40 (PKKKRKV) and murine RSK2 (MMTV-HA-NLS-RSK2) were generated by the University of Virginia Gene Targeting and Transgenic Facility (C57BL/6J$^{\text{MMTV-HA-NLS-RSK2}}$). Ten backcrosses were performed to wild type C57BL/6J. At 12 wk, 6m, or 16m virgin female MMTV-NLS-RSK2 or wild type mice were euthanized and the mammary glands analyzed.

Mice carrying a transgene composed of the MMTV-LTR linked to sequences encoding the tetracycline responsive reverse transactivator (rtTA: tet-on gene regulation) and a transgene composed of the tetracycline responsive promoter (tet-op) linked to sequences encoding murine ERα (C57BL/6J$^{\text{MMTV-rtTA/tet/op-ER}\alpha}$; CERM) were obtained from Priscilla Furth, M. D. (Georgetown University) [158]. Doxycycline was administered in diet (0.625 g/kg) for 16 weeks starting at weaning. Double transgenic (MMTV-rtTA/tet-op-ERα) and control single transgenic (tet-op-ERα) virgin females were euthanized at 19 weeks and the mammary glands analyzed.

Female NOD.Cg-*Prkdc*^{scid} *Il2rg*^{tm1Wjl}/SzJ (NSG; The Jackson Laboratory) mice (8 to 12 weeks) received a 17β-estradiol pellet (0.36-mg 60-day release) implanted subcutaneously in the shoulder region. Mice were injected (50 μl, 20% Matrigel) into both right and left 4th

mammary fat pads with 1.2 x 10^6 previously transduced MCF-7 cells. Tumor dimensions was measured using manual calipers twice per week and the tumor volume was calculated: $V = L^2 x H$ (V-volume; L-length; H-depth). At the end of the study tumors were extracted and either fixed in 10% buffered formalin for paraffin embedding, sectioning and immunofluorescence analysis or frozen for lysis as described [36].

Female NCG-Prkdc^{em26Cd52}Il2rg^{em26Cd22}/NjuCrl (NCG; Charles River) mice (8 wks) were injected in the left cardiac ventricle with 1x10^5 cells/100 ul PBS. Bioluminescence was detected as described in [144].

Cell culture and treatment

Mycoplasma free MCF-7, BT-474 and ZR-75-1 cells were obtained, cultured and authenticated as directed by American Type Culture Collection (ATCC). Cell lines were maintained in a log-phase of cell growth and screened for *Mycoplasma* by PCR. Cells were serum starved for 12-15 h before addition of phorbol 12-myristate 13-acetate (PMA) (0.5 μM), E_2 (1 or 10 nM), EGF (25 nM), FGF7 (10nM), CXCL1 (10 nM), prolactin (10 nM) or leptin (5 nM). PMA, E_2, FGF7 or EGF was added for 6-8 h and other growth factors for 24 h. In experiments with 4-OHT (2 μM) and ICI 182,780 (1 μM), cells were pre-treated for 12 h with each inhibitor before PMA treatment. Alternatively, 4-OHT (2 μM) was added for 8h after 2h pre-treatment with PMA. For kinase inhibitor screen cells were pretreated with individual compounds from the Screen-Well Kinase Inhibitor library for 2 h and then treated with PMA for 6 h. All compounds were tested at a final concentration of 10 μM. Proliferation assays were performed as described [144].

Single epithelial cells were isolated from the mammary glands of sixteen month old mice and spheres cultured as described [159]. For 2 passages (every 9 days) spheres were dissociated with 1x trypsin and equal number of cells from WT and NLS-RSK2 spheres were re-

plated. Alternatively, p0 spheres (day 9) were transduced with GFP-luciferase and after three days the linearity of the bioluminescence signal was tested [144].

Clinical Samples

The Cooperative Human Tissue Network (CHTN) provided the human breast cancer tissue and clinical data. Every CHTN institution has obtained human subjects assurance from the Office of Human Research Protections, DHHS. The Assurance document provides agreement that the institution will comply with federal human subjects regulations (The "Common Rule;" 45 CFR part 46). Each Division of the CHTN is approved by its local Institutional Review Board (IRB) to collect and distribute biospecimens. The IRBs review the procedures in place to ensure adequate protection of human subjects and protection of patient privacy and confidentiality. The approvals are reviewed by the IRB yearly. Samples are described in (Table 2). Assessment for ERα and progesterone receptor (PR) was determined by immunohistochemistry on formalin-fixed paraffin-embedded (FFPE) sections and scoring performed according to [160] by board certified pathologists at the University of Virginia.

HER2 amplification relative to chromosome 17 copy number was determined on FFPE sections by chromogenic in situ hybridization using Ventana/Roche Medical Systems INFORM HER2 Dual ISH DNA probe cocktail. Staining was performed on VENTANA Benchmark XT automated slide stainer (using NexES software) by light microscopy. Scoring was performed according to [161] by board certified pathologists at the University of Virginia. In some cases organoids were prepared from the tissue [162].

Immunoprecipitation

MCF-7 cells treated with the dimethyl-3,3'-dithiobispropionimidate (5mM in PBS (30 min)) were quenched in 50mM Tris pH8.0, 150mM NaCl (10min). The insoluble fraction was obtained [163]. Lysates were incubated with 2μg rabbit anti-ERα, rabbit IgG (1h, 4°C) followed

by MagnaBind goat anti-rabbit IgG magnetic beads (50μl, 1h, 4°C) or anti-GFP mAb-magnetic beads (50μl, 1h, 4°C). Alternatively, lysates were incubated with GFP-Trap®_M (ChromoTek GmbH) (18μl, 1h, 4°C) pre-bound with GFP-GST protein (150ng, 1h, 4°C). The immunoprecipitate was washed 2x with buffer (50mM Tris pH8.0, 150mM NaCl, 5mM EDTA, 1% Triton X-100, 0.1% deoxycholate) and 3x with the same buffer without detergents. The beads were boiled [163]. GST-fusion proteins were purified using glutathione sepharose 4B (300μl;) and stored (-20°C) in storage buffer (20mM HEPES pH 7.4, 300mM NaCl, 1mM EGTA, 1mM DTT, 50% glycerol).

Immunostaining and immunodetection

Tissue and organoids were fixed in buffered 10% formalin for 2 d and then placed in 70% ethanol. The fixed samples were paraffin-embedded, and 5-μm sections were prepared by the University of Virginia Research Histology Core or by the Translational Pathology Shared Resource at Vanderbilt University. The sections were deparaffinized, blocked in 10% bovine serum albumin (BSA) in PBS and incubated with primary antibody in 3% BSA in PBS o/n at 4°C. The sections were washed three times and incubated with secondary antibody for 1h at room temperature. The sections were washed and DNA was stained with Hoechst for 10 min. For mouse tissues Western Blot Blocking Reagent (Roche Life Science) in PBS was used for blocking and to dilute antibodies and all the washes were performed with PBS. The coverslips were mounted using Fluoro-Gel (Electron Microscopy Sciences).

For detection of Venus-tagged proteins or ERα cells were washed twice with PBS, fixed for 15 min with 4% PFA in PBS at room temperature (RT), washed twice with PBS and permeabilized for 15 min with 0.1% Triton-X100 in PBS prior to blocking. For detection of cyclin D1, cells were washed twice with ice-cold PBS, fixed for 10 min with ice-cold 90% methanol in

MES buffer (100 mM MeS, pH 6.9, 1 mM EGTA, 1 mM MgCl2) in -20°C. Fixed cells were blocked overnight in 10% BSA in PBS before incubation with primary antibodies.

Indirect and direct fluorescent images were obtained at room temperature with a laser-scanning microscope (510/Meta/FCS or LSM880 Airy Scan; Carl Zeiss, Inc.). Images of immunostained tissue sections were obtained with a 40× Plan-Neofluar oil objective NA 1.3 using a zoom of 0.7×. Images of cells were obtained using 63× Plan-Apochromat oil objective NA 1.4, zoom 1×. Images were acquired using LSM-FCS or ZEN software and quantitated using Openlab 5.5.0 or ImageJ64 software. Images were processed in Photoshop version CS6 version 13.0. For imaging of xenograft tumor sections expressing Venus-tagged RSK2 chimeras, six 1 μm Z-stacks were acquired and the 3D projections were assembled using Volocity 6.2.1. Imaging of live cells expressing RSK2-Venus and histoneH3-mCherry for the kinase inhibitor screen was performed using the ImageXpress Micro XL System (Molecular Devices). The RSK2-Venus nuclear to cytoplasmic fluorescence intensity ratio was quantified using MetaXpress software. For immunodetection cells were lysed as described [36]. The list of inhibitors is provided in Table 4.

Quantitative real time PCR (qRT-PCR)

WT and RSK2-KO MCF-7 were serum starved for 12-15 h and treated with EGF (25nM)/E_2(1nM) for 8 h before total RNA was extracted (RNeasy Kit). 1μg of RNA was reversely transcribed using High Capacity cDNA Reverse Transcription Kit. QRT-PCR was performed using IQ RealTime SybrGreen PCR Supermix on C1000Thermal Cycler CFX96 Real-Time System (BioRad Laboratoreis) and $\Delta\Delta C_t$ was calculated using GAPDH as a control. qRT-PCR primers are listed in Table 1.

RNASeq

Total RNA extraction (RNeasy Kit) was performed on serum starved cells treated with EGF ((10nM)/E_2(1nM) for 8h) and quality controlled using Agilent 2100 Bioanalyzer (RIN 8). Libraries were constructed (TruSeq RNA Library Prep Kit), and sequenced (Illumina HiSeq 2500 at the Vanderbilt VANTAGE Core). Raw reads were aligned to the human reference genome hg38 (Genome Reference Consortium GRCh38) and differential gene expression analyzed using CLC Workbench 10.0. Genes with absolute fold change>2.5 and false discovery rate (FDR) <0.05 were considered to be significantly DE. RNA-Seq data is available at Gene Expression Omnibus under accession: GSE99707.

Gene expression data from patients with invasive breast carcinoma (TCGA version 1/11/2015) were analyzed using Morpheus. Samples were filtered to include primary tumors from patients with infiltrating ductal carcinoma. Z-scores were calculated for each ER+ patient by adding z-scores of genes down regulated in RSK2-KO cells and subtracting z-scores of genes up-regulated in RSK2-KO cells. RSK2-low tumors have RSK2 z-score <0, and RSK2-high tumors RSK2 z-score>0. Hierarchical clustering of patient samples using one minus the Spearman's rank correlation and total linkage was performed using the RSK2_529 set. iRegulon1.3 (Cytoscape 3.5.0) was used for transcription factor prediction. STRING10.5 (confidence 0.7) was used to predict-and identify functional nodes of protein networks. GSEA was performed with javaGSEA software (Broad Institute) using expression of all detected genes (16,394) in RSK2-KO versus WT cells against gene signatures from the Molecular Signature Database v6.0 [164].

Statistical Analysis

Statistical analyses were performed using GraphPad Prism 6.0a.

Transfection and transduction

Transient transfections were performed with Lipofectamine 2000 (Invitrogen). Gene silencing was performed using non-targeting siRNA #1 and siRNA SMARTpools human ERα. Transient transfections were performed using pKH3 Venus-GST, pKH3 Venus-NLS-GST, pKH3 Venus-RSK2(1-67)-GST. Constructs used to generate lentivirus, including pSPAX2, pLVTHM, and pMD2G, were provided by D. Trono, Ph.D. (Swiss Federal Institute of Technology, Lausanne, Switzerland) [165]. The pLV-Venus lentivirus construct was provided by I.G. Macara , Ph.D. (Vanderbilt University, Nashville, TN) and lentiviral production was performed as described [166]. RSK2-Venus and RSK1-Venus were amplified using the polymerase chain reaction using the appropriate primers, and cloned into pLV-Venus in frame at the 5' end of Venus. The RSK1(1-401)RSK2(406-740) was generated by amplifying RSK1 from 1 to 1205 base pairs (bp) with an MfeI site added at the 3'-terminus, and inserting it upstream of the RSK2 C-terminal portion using an internal MfeI site (mouse RSK2 bp 1216). The RSK2(1-407)RSK1(404-735) was generated by amplifying RSK1 from 1212 to 2205 bp with an MfeI site added at the 5'-terminus, and inserting it downstream of the RSK2 N-terminal portion using an internal MfeI site (RSK2 bp 1216). To generate RSK2(1-67)RSK1(62-735), RSK2 was amplified from 1 to 234 bp, with a silent mutation introduced at bp 234 (A to C) to generate a BamH1 site. The 1-234 bp fragment was then inserted into RSK1 using an internal BamH1 site (rat RSK1 bp 211). To generate RSK1(1-61)RSK2(68-740), RSK2 was amplified from 229 to 2220 bp, and a silent mutation introduced at 234 bp (A to C) to generate a BamH1 site. The 229-2220 bp fragment was then inserted into RSK1 using an internal BamH1 site (RSK1 bp 211). RSK2(1-375)RSK1(370-402)RSK2(407-740) was generated by amplifying RSK1(370-401)RSK2(400-740) from RSK1(1-401)RSK2(406-740), using a primer with a DraIII site introduced at the 5' end. The RSK1(370-401)RSK2(400-740) fragment was then inserted into full-length RSK2 using internal DraIII sites. RSK2(S17A/S19A) and RSK2(S17D/S19D) were generated using QuickChange II site directed mutagenesis. To generate RSK2(Δ27-32), base pairs from 78 to

96 were deleted from RSK2 using Q5 site-directed mutagenesis. GST-Venus-RSK1(1-62), GST-Venus-RSK2(1-67) and GST-Venus-RSK2(1-67_Δ27-32) constructs were generated by PCR amplification using the appropriate template and insertion into pGEX-GST-Venus at the 3' end of Venus. To generate Venus-NLS-GST the NLS from SV40 (PKKKRKV) was inserted into pKR7 Venus-GST. Venus-RSK2(1-67)-GST was generated by amplification and insertion of RSK2(1-67) into pKR7 Venus-GST.

Refer to the Table 1 for short hairpin sequences targeting RSK2 and the scramble. The short hairpin sequence for luciferase was previously described [167]. To generate shRNA resistant RSK2 (rRSK2) QuickChange II Site-Directed Mutagenesis was used to introduce silent mutations in the shRNA targeting region: GGAACG(T/A)GATATC(T/C)TGGTA.

RSK2-KO MCF-7 cells were generated by co-transfection with guide RNA 1 (ACTTCATTAGAGCCCTTTAGGGG) and guide RNA 2 (ACTACATTATTGAGTATGCCAGG) inserted into Cas9 containing plasmid (pX330-U6-Chimeric_BB-CBh-hSpCas9). Single-cell clones were isolated and genomic DNA screened using PCR to identify clones with homozygous RSK2 deletion. For homozygous clones the DNA and RNA were sequenced. All sequences were verified by the Biomolecular Research Core (University of Virginia, Charlottesville, VA) or GenHunter Corporation (Nashville, TN).

Table 1 Reagents used in Chapter 1

REAGENT or RESOURCE	SOURCE	IDENTIFIER
Antibodies		
chicken anti-GFP (IF; IB)	Abcam	ab13970
chicken anti-keratin14 (IF)	BioLegend	SIG-3476
goat anti-RSK2 (IF)	Santa Cruz Biotechnology, Inc.	sc-1430
mouse anti-RSK2 (E-1) (IB)	Santa Cruz Biotechnology, Inc.	sc-9986
rabbit anti-pRSK (Thr359/Ser363) (IF)	Santa Cruz Biotechnology, Inc.	sc-12898-R
goat anti-Ki67 (IF)	Santa Cruz Biotechnology, Inc.	sc-7846
rabbit anti-cyclin D1 (IF)	Thermo Fisher Scientific Inc.	MA139546
rabbit anti- ERα (IF; IB)	Thermo Fisher Scientific Inc.	RM9101S0
rabbit anti-pSer-167 ERα	SignalWay Antibody	11073
rat anti-keratin 8 (IF)	University of Iowa	TROMA-I
mouse anti-ZO-1 (IF)	Thermo Fisher Scientific Inc.	33-9100
mouse anti-E-cadherin (IF)	BD Biosciences	BDB 610181
rabbit anti-pRSK (Thr359/Ser363) (IF)	EMD Millipore	04-419
rabbit anti- ERα (IP)	EMD Millipore	06-935
normal rabbit IgG (IP)	EMD Millipore	12-370
mouse anti-cyclin D1 (IF)	Cell Signaling Technology	2926S
rabbit anti-Ran (IB)	Cell Signaling Technology	4462
rabbit anti-pRSK (Thr359/Ser363, Ser380) (IB)	Cell Signaling Technology	9344S
rabbit anti-pSer-167 ERα	Cell Signaling Technology	5587S
rabbit anti-RSK2 (IF)	Bethyl Laboratories Inc.	IHC-00683
rat anti-HA (IF; IB)	provided by I.G. Macara, Vanderbilt University	NA
AlexaFluor goat anti-mouse 488 IgG (H+L) *highly cross-adsorbed*	Thermo Fisher Scientific Inc.	A-11029
AlexaFluor rabbit anti-mouse 488 IgG (H+L)	Thermo Fisher Scientific Inc.	A-11059
AlexaFluor donkey anti-goat 488 IgG (H+L)	Thermo Fisher Scientific Inc.	A-11055
AlexaFluor goat anti-rabbit 488 IgG (H+L)	Thermo Fisher Scientific Inc.	A-11034

AlexaFluor goat anti-mouse 546 IgG (H+L) *highly cross-adsorbed*	Thermo Fisher Scientific Inc.	A-11030
AlexaFluor goat anti-chicken IgG 546 (H+L)	Thermo Fisher Scientific Inc.	A-11040
AlexaFluor donkey anti-rabbit IgG 546 (H+L)	Thermo Fisher Scientific Inc.	A-10040
AlexaFluor donkey anti-goat IgG 647 (H+L),	Thermo Fisher Scientific Inc.	A-21447
AlexaFluor goat anti-rat 647 IgG (H+L)	Thermo Fisher Scientific Inc.	A-21247
Cy3-labeled donkey anti-chicken	Jackson ImmunoResearch Laboratories, Inc.	703-165-155
Cy3-labeled donkey anti-goat	Jackson ImmunoResearch Laboratories, Inc.	705-166-147
donkey anti-rabbit HRP	Jackson ImmunoResearch Laboratories, Inc.	711-035-152
goat anti-mouse HRP	Jackson ImmunoResearch Laboratories, Inc.	115-035-062
donkey anti-chicken HRP	Jackson ImmunoResearch Laboratories, Inc.	703-035-155
MagnaBind goat anti-rabbit IgG magnetic beads	Thermo Fisher Scientific Inc.	PI-21356
anti-GFP mAb-magnetic beads	Medical and Biological Laboratories	D153-9
Chemicals, Peptides, and Recombinant Proteins		
phorbol 12-myristate 13-acetate (PMA)	Sigma	P1585-1MG
17-β estradiol (E_2)	Sigma	E2758
EGF	Calbiochem	324831-200UG
AREG	R&D Systems	262AR100CF
FGF7	R&D Systems	251KG010CF
CXCL1	R&D Systems	275GR010
IL-6	EMD Millipore	IL006
prolactin	PeproTech	100-07
leptin	Thermo Fisher Scientific	398LP01M
4-hydroxytamoxifen 4-OHT	Sigma	H7904
Fulvestrant (ICI 182,780)	Sigma	I4409
hydrocortisone	Sigma	H0888
insulin- transferrin–selenium	Invitrogen	51500056
Amphotericin B	Sigma	A2942
dimethyl-3,3'-dithiobispropionimidate	Thermo Fisher Scientific Inc.	PI-20665

17-β-estradiol pellet; 0.36-mg 60-day release	Innovative Research of America	NE-121
Doxycycline; 0.625 g/kg	Harlan	TD.120769
Critical Commercial Assays		
QuickChange II Site-Directed Mutagenesis	Agilent Technologies	200521
Screen-Well Kinase Inhibitor library	Enzo Life Sciences	BML-2832-0100
RNeasy Mini Kit	Qiagen	74107
TruSeq RNA Library Prep Kit	Illumina	RS-122-2001
Deposited Data		
Raw and analyzed sequencing data	This paper	GEO:GSE63473
Human reference genome NCBI build 38	Genome Reference Consortium	https://www.ncbi.nlm.nih.gov/grc/human
Experimental Models: Cell Lines		
MCF-7	American Type Culture Collection	HTB-22
BT-474	American Type Culture Collection	HTB-20
ZR-75-1	American Type Culture Collection	CRL-1500
Experimental Models: Organisms/Strains		
Mouse: C57BL/6J$^{MMTV\text{-}HA\text{-}NLS\text{-}RSK2}$ (NLS-RSK2)	This paper	University of Virginia Gene Targeting and Transgenic Facility
Mouse: C57BL/6J$^{MMTV\text{-}rtTA/tet/op\text{-}ER}$ (CERM)	[158]	Priscilla Furth, PhD (Georgetown University)
Mouse: NOD.Cg-*Prkdc^{scid} Il2Rg^{tm1Wjl}*/SzJ (NSG)	The Jackson Laboratory	005557
Oligonucleotides		
non-targeting siRNA #1	Thermo Fisher Scientific Inc.	D-001210-01-05
ERα siRNA SMARTpool	Thermo Fisher Scientific Inc.	M-003401-04-0005
RSK2 shRNA: GATCCCC**GGAACGTGATATCTTGGTA**TTCAAGAGA**TACCAAGATATCACGTTCC**TTTTTGGAAA	This paper	N/A
Scrbl shRNA: CGCGTCC**TCGCGACTAAACACATCAA**TTCAAGA**TTGATGTGTTTAGTCGCGA**TTTTTGGAAA	This paper	N/A
Luciferase shRNA	[167]	N/A
RSK2 guide RNA 1: ACTTCATTAGAGCCCTTTAGGGG	This paper	N/A
RSK2 guide RNA 2: ACTACATTATTGAGTATGCCAGG	This paper	N/A
Recombinant DNA		

pX330-U6-Chimeric_BB-CBh-hSpCas9	[168]	Addgene;42230
pSPAX2	[165]	Addgene; 12260
pLVTHM	[165]	Addgene; 12247
pMD2.G	[165]	Addgene; 12259
Software and Algorithms		
LSM-FCS	Carl Zeiss, Inc.	N/A
ZEN	Carl Zeiss, Inc.	N/A
MetaXpress	Molecular Devices	N/A
Openlab 5.5.0	PerkinElmer Inc.	N/A
Volocity 6.2.1	PerkinElmer Inc.	N/A
GraphPad Prism 6.0a	GraphPad Software Inc.	N/A
CLC Workbench 10.0	Qiagen	N/A
Cytoscape 3.5.0	[169]	http://www.cytoscape.org/
iRegulon 1.3	[170]	http://iregulon.aertslab.org/index.html
Morpheus	Broad Institute	https://software.broadinstitute.org/morpheus/
STRING 10.5	[171]	https://string-db.org/
Gene Ontology Consortium	[172]	http://www.geneontology.org/)
Other		
510/Meta/FCS	Carl Zeiss, Inc.	N/A
LSM880 Airy Scan	Carl Zeiss, Inc.	N/A
ImageXpress Micro XL System	Molecular Devices	N/A

Results

Nuclear active RSK2 in invasive ER+ breast cancer

We first addressed activation and localization of RSK by immunofluorescence (IF) across a panel of 25 invasive ER+ breast cancer patient samples. Active nuclear RSK was observed in ~ 70% of these samples (Fig. 4A, Table 2) and, within these samples, the intensity of nuclear RSK was strongly correlated with the intensity of ERα (Fig. 4B). Cyclin D1 levels and ERα were also correlated (Fig. 4A, B), consistent with observations that cyclin D1 is frequently over-expressed in ER+ cancers [173]. Because IF provides a quantitative readout, we conclude that there is a positive linear relationship between the levels of active nuclear RSK and ERα in ER+ breast cancer.

Antibodies against active RSK cannot distinguish between different RSK isoforms, since the phosphorylation sites responsible for activation are identical [8]. An anti-RSK2 antibody identified that RSK2 was localized to the nucleus in those ER+ tumor samples containing active nuclear RSK (Fig. 4C). A specific anti-RSK1 antibody suitable for IF was not available and therefore, we used human ER+ cell lines to examine RSK1 and RSK2 nuclear translocation. In response to growth factors and cytokines, endogenous activated RSK2 accumulated in the nucleus (Fig. 5A-D), as did C-terminally fluorescently tagged RSK2 (Fig. 5E). In contrast, nuclear accumulation was not observed for RSK1 (Fig. 5E) despite both isoforms being active (Fig. 5F) and reports of RSK1 nuclear translocation [25]. Taken together, we conclude that RSK2 is the active isoform present in the nucleus in invasive ER+ breast cancer tumor samples.

Table 2 Patient histopathological information

Age; race; tumor: grade, size, and type; lymph node involvement; %ER+; %PR+; HER2 status; and pRSK localization in patient samples used in Figures 4A-C, 10A-B. Samples with nuclear pRSK are highlighted in blue.

Table 2

Lab ID	Age	Race	Grade	Size of Largest Invasive Carcinoma	Type					# of lymph nodes (LN) with tumor cells of all LN tested	ER: % positive nuclei	PR: % positive nuclei	HER2 Amplified	pRSK	
					IDC	**ILC**	**DCIS**	**LCIS**	**Other**					**Nuclear**	**Cytoplasmic**
002	76	Hispanic	2	3.5 cm	Yes	No	No	No	No	1 of 2	95	0	No	No	Yes
004	55	White	1	1.8 cm	Yes	No	No	No	No	0 of 2	95	95	No	No	Yes
236	58	White	2	0.3cm	Yes	No	Yes	No	No	NA	100	0	No	No	Yes
243	64	White	3	2 cm	Yes	Yes	Yes	No	No	1 of 2	80	10	No	Yes	No
245	>80	White	2	0.7 cm	Yes	No	Yes	No	No	0 of 1	100	100	No	Yes	No
250	66	Black	1	4 cm	No	No	No	No	Yes	0 of 9	95	20	No	Yes	Yes
253	>80	White	2	2.5 cm	Yes	No	Yes	No	No	0 of 2	100	0	Yes	Yes	No
286	>80	White	2	1.7 cm	Yes	No	No	No	No	NA	100	100	No	Yes	Yes
289	47	White	2	7 cm	Yes	No	No	No	No	1 of 2	95	0	No	No	Yes
315	63	White	3	2.1 cm	Yes	No	No	No	No	0 of 4	20	0	No	Yes	No
347	49	White	2	3.5 cm	Yes	No	Yes	No	No	0 of 2	90	90	No	Yes	No
360	59	Black	1	0.3 cm	Yes	No	Yes	No	No	0 of 2	100	0	No	No	Yes
369	58	Black	2	1.5 cm	Yes	No	No	No	No	0 of 1	80	0	Yes	Yes	No
373	46	White	1	0.2 cm	Yes	No	Yes	No	No	2 of 10	70	100	No	No	Yes
419	42	White	2	0.5 cm	Yes	No	Yes	No	No	1 of 3	100	100	NA	Yes	No
427	78	White	2	1.7 cm	Yes	No	No	No	No	NA	100	100	No	Yes	No
435	58	White	2	0.5 cm	Yes	No	Yes	No	No	NA	100	100	No	Yes	Yes
437	40	other	2	0.5 cm	Yes	No	Yes	No	No	NA	95	95	No	Yes	No
443	61	White	2	0.5 cm	No	Yes	No	No	No	NA	100	50	No	No	Yes
450	72	White	1	1.5 cm	Yes	No	No	No	No	5 of 14	90	60	No	Yes	Yes
461	50	White	1	0.5 cm	Yes	No	No	Yes	No	NA	100	100	No	Yes	No
486	30	White	2	1.9 cm	Yes	No	Yes	No	No	1 of 3	100	100	No	Yes	No
495	42	White	1	1.5 cm	Yes	No	Yes	No	No	1 of 15	90	90	No	Yes	No
499	44	White	3	1.5 cm	Yes	No	No	No	No	2 of 24	90	80	No	Yes	Yes
503	62	White	2	1.7 cm	Yes	No	Yes	No	No	2 of 18	100	50	No	Yes	No

Figure 4 RSK2 in ER+ breast cancer

(A) Serial sections of ER+ breast cancer tissue. Scale bar=20μm. (B) Correlation of ERα nuclear fluorescence intensity (Fn) with nuclear active (pRSK) and cyclin D1. (n=14 patients, ≥3 sections/patient). (C) RSK2 is nuclear in ER+ breast cancer tissue.

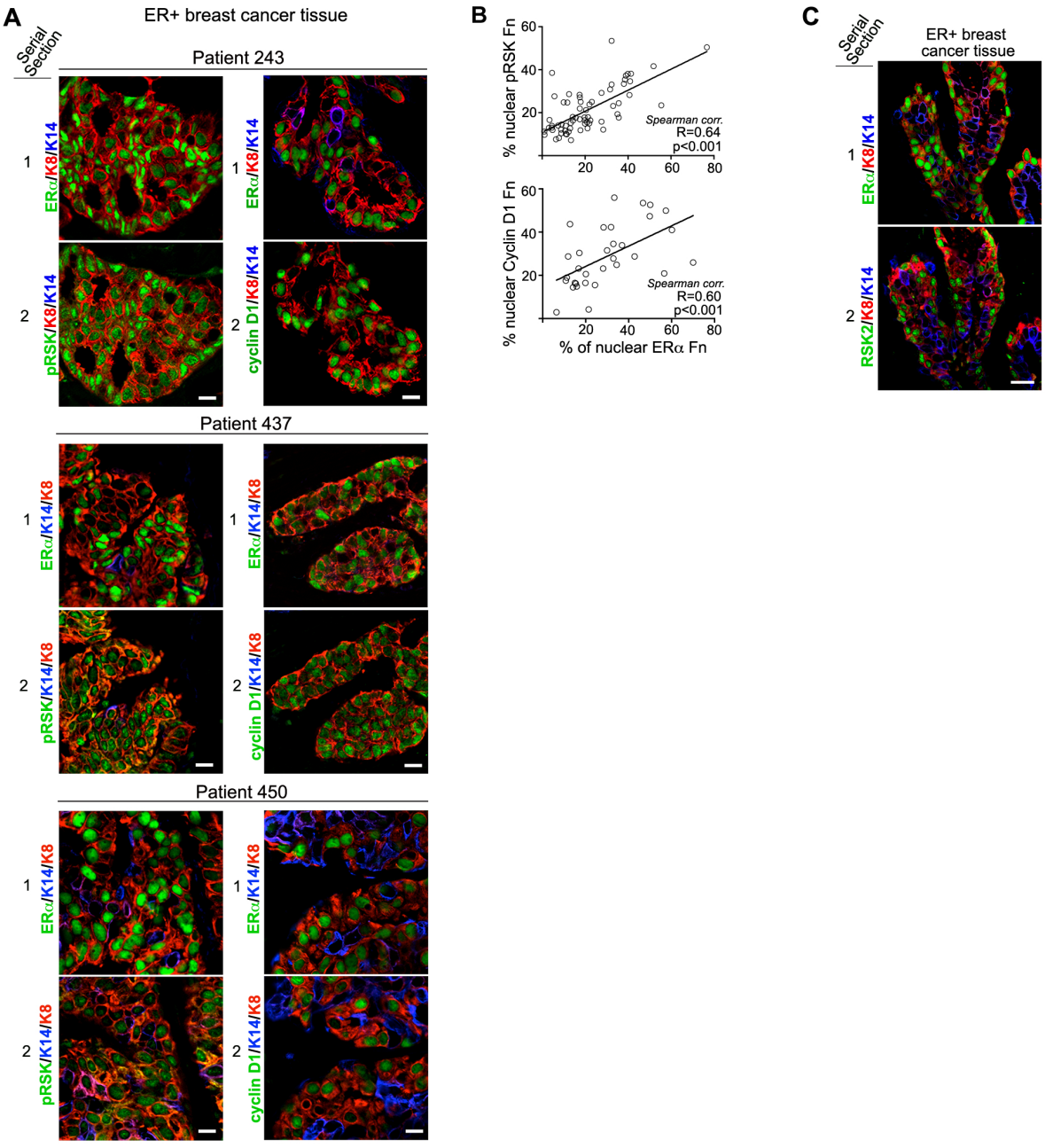
A
ER+ breast cancer tissue
Serial Section
Patient 243
1 ERα/K8/K14
2 pRSK/K8/K14
1 ERα/K8/K14
2 cyclin D1/K8/K14
Patient 437
1 ERα/K14/K8
2 pRSK/K14/K8
1 ERα/K14/K8
2 cyclin D1/K14/K8
Patient 450
1 ERα/K14/K8
2 pRSK/K14/K8
1 ERα/K14/K8
2 cyclin D1/K14/K8
B
% nuclear pRSK Fn
Spearman corr.
R=0.64
p<0.001
% nuclear Cyclin D1 Fn
Spearman corr.
R=0.60
p<0.001
% of nuclear ERα Fn
C
Serial Section
ER+ breast cancer tissue
1 ERα/K8/K14
2 RSK2/K8/K14

Figure 5 RSK2 accumulates in the nucleus in response to growth factors

(A) 4-OHT decreases EGF-induced RSK2 nuclear accumulation as measured by Fn to cytoplasmic fluorescence (Fc). MCF-7 and ZR-75-1 were treated with 2 or 10μM 4-OHT, respectively. DNA stained with Draq5. Scale bar=10μm. (Bar, median±quartile, n=3, ≥90 cells/treatment). **p<0.01, ***p<0.001; Student's t-test. (B) 4-OHT decreases FGF-induced RSK2 nuclear accumulation in MCF-7 and ZR-75-1 cells. MCF-7 and ZR-75-1 cells treated with 2 or 10 μM 4-OHT, respectively. Scale bar = 10μm. DNA stained with Draq5. (Bar, median ± quartile, n ≥ 3, ≥ 30 cells/condition) **p<0.01, ***p<0.001; Student's t-test. (C) RSK2 accumulates in the nucleus in response to growth factor/cytokine signaling. Scale bar = 10 μm. (D) Growth factors and cytokines activate ERK1/2 and RSK. MCF-7 cells were treated with the indicated agents and the lysates analyzed. (E) RSK2 but not RSK1 accumulates in the nucleus. Direct fluorescence of MCF-7 cells overexpressing RSK1-Venus or RSK2-Venus with or without activation of ERK1/2 signaling. Scale bar = 10μm. (Bar, median ± quartile; n ≥ 3, ≥ 145 cells/treatment) ***p<0.001; Student's t-test. (F) Analysis of lysates from experimental cells described in (E).

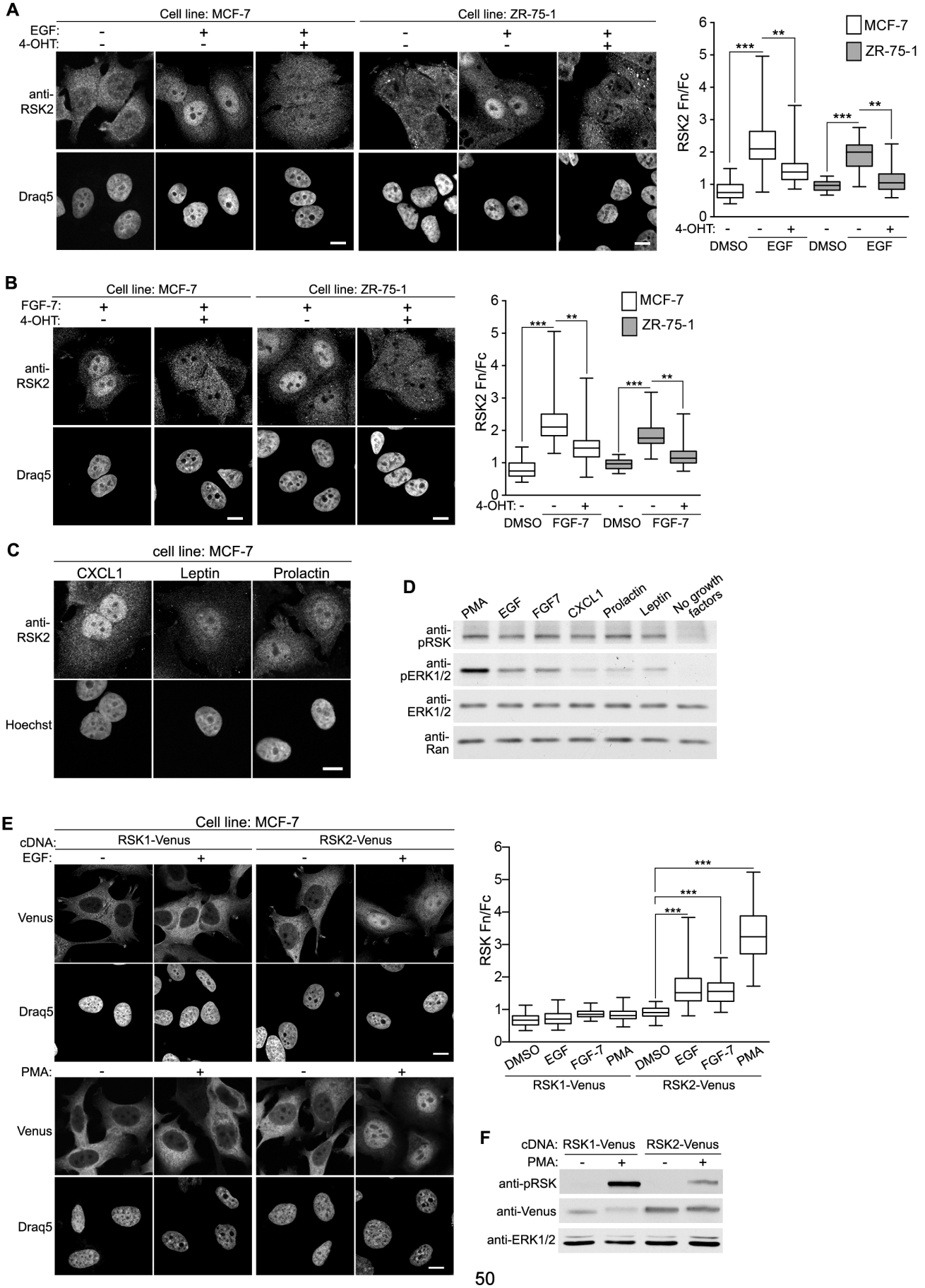
A
Cell line: MCF-7
Cell line: ZR-75-1
EGF:
4-OHT:
anti-RSK2
Draq5
RSK2 Fn/Fc
MCF-7
ZR-75-1
4-OHT:
DMSO
EGF
B
Cell line: MCF-7
Cell line: ZR-75-1
FGF-7:
4-OHT:
anti-RSK2
Draq5
RSK2 Fn/Fc
MCF-7
ZR-75-1
4-OHT:
DMSO
FGF-7
C
cell line: MCF-7
CXCL1
Leptin
Prolactin
anti-RSK2
Hoechst
D
PMA
EGF
FGF7
CXCL1
Prolactin
Leptin
No growth factors
anti-pRSK
anti-pERK1/2
anti-ERK1/2
anti-Ran
E
Cell line: MCF-7
cDNA:
RSK1-Venus
RSK2-Venus
EGF:
Venus
Draq5
PMA:
Venus
Draq5
RSK Fn/Fc
DMSO
EGF
FGF-7
PMA
RSK1-Venus
RSK2-Venus
F
cDNA:
RSK1-Venus
RSK2-Venus
PMA:
anti-pRSK
anti-Venus
anti-ERK1/2

RSK2-regulated gene signature correlates with invasive ER+ breast cancer

RNAi knockdown experiments revealed that RSK2 was essential for ER+ tumor growth and expression of cyclin D1 in an MCF-7 orthotopic model (Fig. 6A-C). To identify the mechanistic basis of these findings, we employed CRISPR/Cas9 gRNA targeting to genetically delete RSK2 in MCF-7 cells (RSK2-KO; Fig. 6D). RSK2-KO MCF-7 cells showed reduced proliferation relative to wild type (WT) controls, which could be rescued by ectopic expression of RSK2 (Fig. 6E). Addition of the ERα degrader, fulvestrant, reduced proliferation to the same extent in WT and RSK2-KO MCF-7 cells (Fig. 6F). These results indicated that ERα-dependent proliferation is partly controlled by RSK2, since knockout of RSK2 did not result in a further reduction of proliferation at high concentrations of fulvestrant. Next, we performed RNA sequencing (RNA-seq) on RSK2-KO and WT MCF-7 cells that were treated with a cocktail containing estradiol (E_2) and EGF, in order to explore transcriptomic changes under conditions where both ERα and RSK2 are active. This analysis identified 529 differentially expressed (DE) genes in the RSK2-KO cells relative to WT (RSK2_529; GEO99707, Fig. 6G). We confirmed the specificity of the DE by quantitative RT-PCR of selected genes, which was further validated with rescue by overexpression of RSK2 in the RSK2-KO cells (Fig. 6H). Gene set enrichment analysis (GSEA) demonstrated that genes up regulated in invasive ductal breast cancer versus ductal carcinoma in situ (DCIS) were significantly enriched in WT versus RSK-KO (FDR q-value < 0.05) (Fig. 7A) [174-176]. To test whether the directionality of changes of the RSK2_529 set were reflected in ER+ breast cancer patients, we calculated z-scores in ER+ patients with high and low RSK2 mRNA expression. Patient Z-scores were higher in RSK2-high compared to RSK2-low patients demonstrating that in ER+ breast cancer patients expression of the RSK2_529 set is correlated with RSK2 mRNA levels and that the direction of the effect of expression is concordant with that of the RSK2_529 set (Fig. 7B). Unsupervised hierarchical clustering of the RSK2_529 set across 782 breast cancer gene expression sets in the TCGA

dataset revealed that patients were stratified into two major clusters, based on their positivity for ERα (Fig. 7C). Hypergeometric enrichment probability analyses further showed that the RSK2_529 set separated the ER+ patients with a probability of $5.8*10^{-69}$ and the ER- patients with a probability of $1.0*10^{-75}$ (two tailed Fisher's exact test $p< 0.0001$; Table 3) [177]. These hypergeometric probabilities are in a similar range to those obtained with PAM50, a 50-gene intrinsic subtype classifier [178], and the luminal versus basal signature [179] (Table 3). There is <1% overlap between the RSK2_529 set and PAM50 ($p>0.05$ two-tailed Fisher's exact test) indicating that the RSK2_529 set is distinct from PAM50. The RSK2_529 set shares ~ 10% of the genes with those found in the luminal versus basal signatures, which indicates the importance of RSK2 to the luminal lineage (Fig. 7D). In contrast to results obtained with the RSK2_529 set, the signatures obtained from tissue homeostasis [180, 181], ductal versus lobular invasive carcinoma [182], or estrogen receptor related 1- gene set [183] failed to distinguish between ER+ and ER- patients (Table 3). Proliferation and cell cycle genes [180, 181] did not significantly contribute to the RSK2_529 set as shown by GSEA (FDR q-value>0.05) (Fig. 7F) and their removal did not substantially reduce the high enrichment probabilities for separating ER+ from ER- patients (Fig. 7G and Table 3).

Figure 6 Loss of RSK2 reduces orthotopic ER+ tumor growth

(A) RSK2 silencing reduces ER+ tumor growth. Transduced MCF-7 cells were injected into the 4th mammary fat pad of NSG mice implanted with an E_2 pellet. (Symbol, mean±SD, n≥5 mice/group) *p<0.05, ***p<0.001 Scramble (Scrbl) versus RSK2 shRNA; #<0.001 Scrbl (day 0) versus Scrbl (at each time point); two-way ANOVA. (Inset) Analysis of RSK2 levels after tumor isolation. Samples were normalized to ERK1/2. ns=non-specific. (B) Representative ex vivo images of resected tumors. Scale bar = 3 mm. (C) Loss of RSK2 decreases the percentage of cyclin D1+ cells in xenografts. Scale bar=20μm. (Bar, median±quartile, n=4 tumors; ≥5 fields/tumor). **p<0.01 Student's t-test. (D) Lysates of MCF-7 cells showing successful knockout of RSK2 using CRISPR/Cas9 technology. (E) Ectopic expression of RSK2 rescues the decreased proliferation in MCF-7 RSK2-KO cells. (Bar, mean + SD, n=3, quadruplicate) ***p<0.001; two-way ANOVA. (F) RSK2 and ERα regulate MCF-7 proliferation via the same pathway. RSK2 was genetically deleted (RSK2-KO) in MCF-7 cells and proliferation measured ± fulvestrant. (Bar, mean±SD, n=3, sextuplicate) ***p<0.001 WT versus RSK2-KO at each concentration; $^{\#}$p<0.001 WT (vehicle) versus WT (fulvestrant), ‡p<0.001 RSK2-KO (vehicle) versus RSK2-KO (Fulvestrant); two-way ANOVA. (G) Volcano plot in which each gene is represented as a circle. Grey circles represent genes whose levels are not changed whereas purple circles represent genes in which the absolute fold-change ≥ 2.5 and FDR corrected p-value ≤ 0.05 (529 genes). (F) Quantitative RT-PCR validation of selected transcripts from the RNA-seq data set demonstrating rescue of expression by re-introduction of RSK2 in RSK-KO MCF-7 cells. RPL13A was used as a negative control. (Bar, mean + SD, n=3, triplicate) ***p<0.001; Student's t-test.

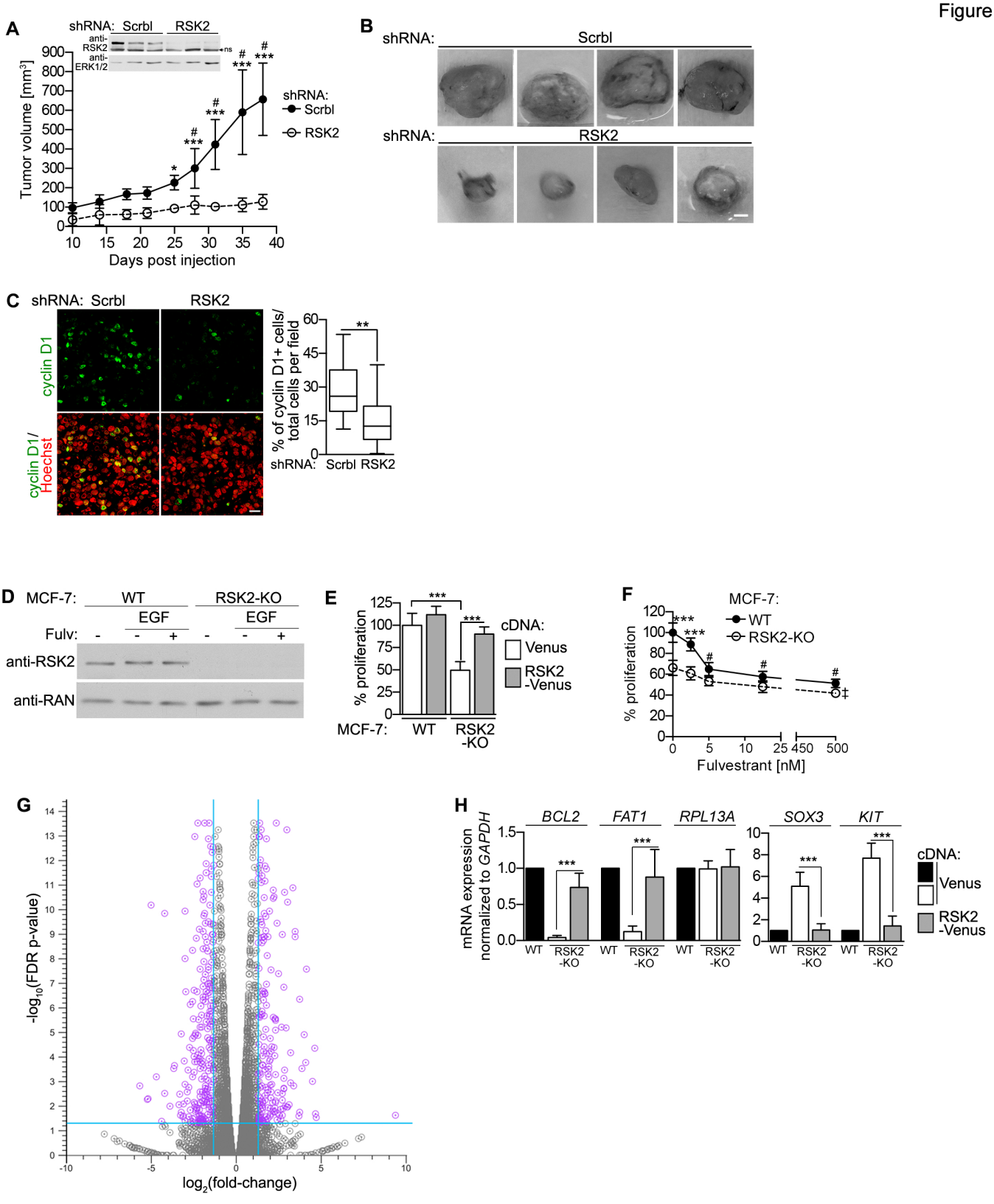
A
shRNA: Scrbl RSK2
anti-RSK2
anti-ERK1/2
ns
Tumor volume [mm3]
Days post injection
shRNA: Scrbl RSK2
B
shRNA: Scrbl
shRNA: RSK2
C
shRNA: Scrbl RSK2
cyclin D1
cyclin D1/ Hoechst
% of cyclin D1+ cells/ total cells per field
shRNA: Scrbl RSK2
D
MCF-7: WT RSK2-KO
EGF
Fulv:
anti-RSK2
anti-RAN
E
% proliferation
cDNA: Venus RSK2 -Venus
MCF-7: WT RSK2 -KO
F
MCF-7: WT RSK2-KO
% proliferation
Fulvestrant [nM]
G
-log10(FDR p-value)
log2(fold-change)
H
mRNA expression normalized to GAPDH
BCL2
FAT1
RPL13A
SOX3
KIT
cDNA: Venus RSK2 -Venus
WT RSK2 -KO

Figure 7 RSK2 gene signature stratifies patients based on ERα status

(A) GSEA plot showing a positive correlation between genes up regulated in invasive ductal carcinoma versus DCIS and genes up regulated in WT versus RSK2-KO cells. (B) Cumulative patient Z-scores were generated for each ER+ patient (TCGA) by adding individual z-scores of genes down regulated in RSK2-KO cells and subtracting individual z-scores of genes up regulated in RSK2-KO cells. Patients were divided into RSK2-low (RSK2 expression z-score<0) (n=254) and RSK2-high (RSK2 expression z-score>0) (n=287) and cumulative patient z-scores plotted. (Bar, median±quartile) ***p<0.001; Student's t-test. (C) Hierarchical clustering of TCGA gene expression data from 782 invasive breast tumors reveals that the RSK2_529 gene signature stratifies patients according to ERα. Horizontal axis: individual patients; vertical axis: individual genes. White bar separates columns at the first dendrogram split. (D) Venn diagram showing overlap of RSK2_529 gene set with the genes present in PAM50 or present in luminal versus basal. (E) Venn diagram showing overlap with cell cycle and proliferation gene set and the lack of enrichment of these genes in the RSK2_529 set as shown by GSEA (F). (G) Hierarchical clustering of TCGA gene expression data from 782 invasive breast tumors reveals that the RSK2_529 set minus proliferation and cell cycle genes stratifies patients according to the presence of ERα. Horizontal axis: individual patients; vertical axis: individual genes. White bar separates columns at the first dendrogram split.

Figure 7

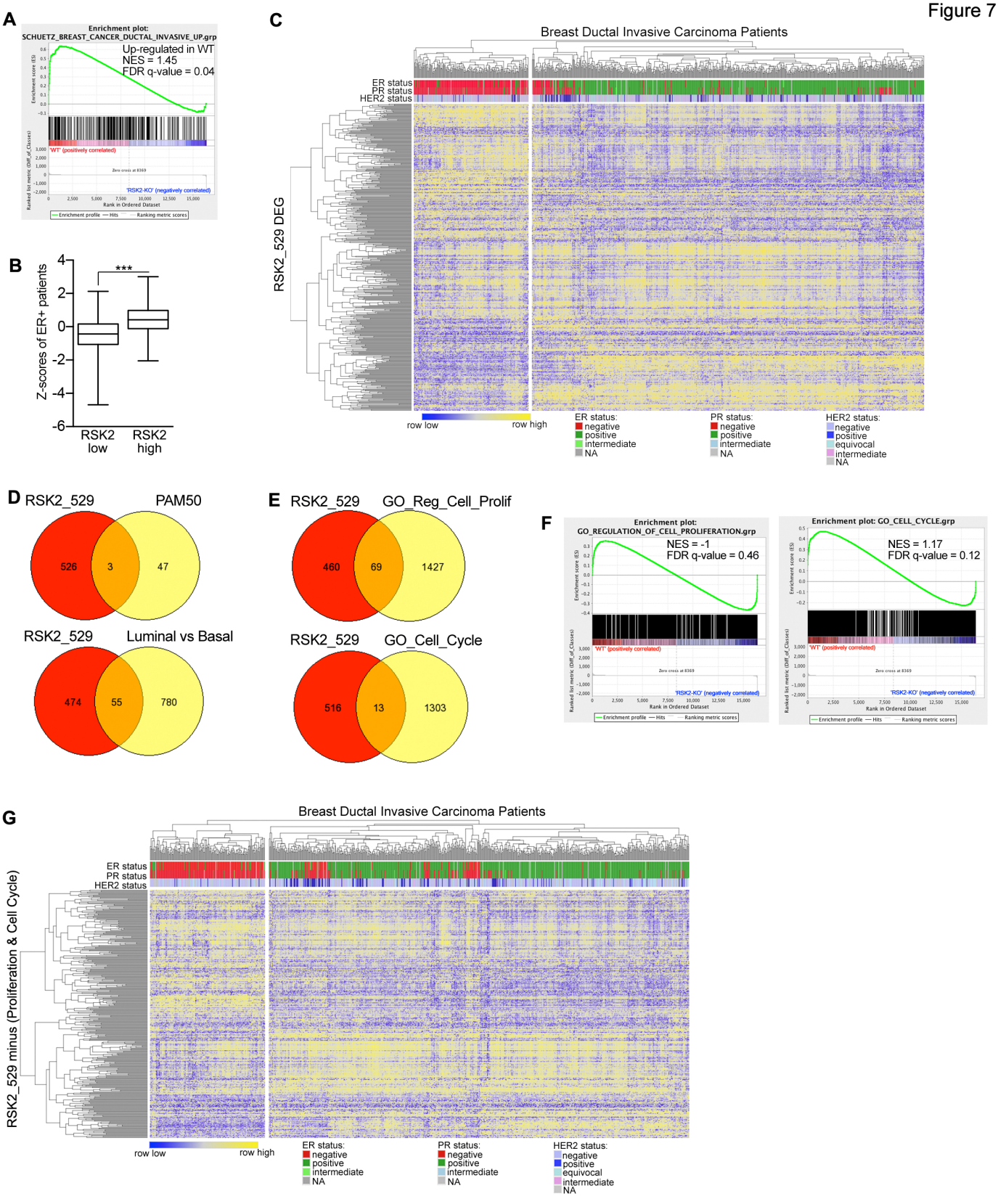
A
Enrichment plot:
SCHUETZ_BREAST_CANCER_DUCTAL_INVASIVE_UP.grp
Up-regulated in WT
NES = 1.45
FDR q-value = 0.04
B
Z-scores of ER+ patients
***
RSK2 low
RSK2 high
C
Breast Ductal Invasive Carcinoma Patients
ER status
PR status
HER2 status
RSK2_529 DEG
row low
row high
ER status:
negative
positive
intermediate
NA
PR status:
negative
positive
intermediate
NA
HER2 status:
negative
positive
equivocal
intermediate
NA
D
RSK2_529
PAM50
526
3
47
RSK2_529
Luminal vs Basal
474
55
780
E
RSK2_529
GO_Reg_Cell_Prolif
460
69
1427
RSK2_529
GO_Cell_Cycle
516
13
1303
F
Enrichment plot:
GO_REGULATION_OF_CELL_PROLIFERATION.grp
NES = -1
FDR q-value = 0.46
Enrichment plot: GO_CELL_CYCLE.grp
NES = 1.17
FDR q-value = 0.12
G
Breast Ductal Invasive Carcinoma Patients
RSK2_529 minus (Proliferation & Cell Cycle)
ER status
PR status
HER2 status
row low
row high
ER status:
negative
positive
intermediate
NA
PR status:
negative
positive
intermediate
NA
HER2 status:
negative
positive
equivocal
intermediate
NA

Table 3 Analysis of ER+ and ER- clustering of invasive ductal carcinoma samples using different gene sets

Hypergeometric probabilities and Fisher's exact test p-values for enrichment of ER+ and ER- samples in clusters generated by unsupervised hierarchical clustering using the indicated gene sets. In blue are gene sets that generated significant enrichment; in dark-blue are RSK2-regulated gene sets.

Table 3

Geneset	Source	# of genes	cluster 1 enrichment		cluster 2 enrichment		Fisher's exact test	Name in Molecular Signatures Database v6.0	Notes
			ER+	ER-	ER+	ER-	p-values		
PAM50	Patients	50	8.22E-74	1	1	8.70E-81	<0.0001		
Luminal vs Basal	Patients	801	7.61E-87	1	1	1.21E-96	<0.0001	CHARAFE_BREAST_CANCER:_LUMINAL_VS_BASAL_UP;_LUMINAL_VS_BASAL_DN	
RSK2_529	MCF-7	529	5.75E-69	1	1	1.02E-75	<0.0001		
RSK2_212	MCF-7	212	6.91E-70	1	1	5.40E-78	<0.0001		
RSK2_127	MCF-7	127	3.63E-72	1	1	8.70E-81	<0.0001		
Gene Ontology (GO) Tissue Homeostasis	GO Terms	160	0.31	0.72	0.75	0.34	0.63	GO_TISSUE_HOMEOSTASIS	
Invasive Carcinoma Ductal vs Lobular	Patients	67	0.93	0.2	0.1	0.85	0.33	BERTUCCI_INVASIVE_CARCINOMA_DUCTAL_VS_LOBULAR_UP	
Estrogen receptor related-1 (ESRRA) targets	MCF-7	524	0.097	0.007	0.0065	1	0.1	STEIN_ESRRA_TARGETS	
GO Regulation of Cell Proliferation	GO Terms	1402					0.1	GO_REGULATION_OF_CELL_PROLIFERATION	Failed to generate 2 clusters
GO Cell cycle	GO Terms	1256	0.14	0.96	0.9	0.06	0.14	GO_CELL_CYCLE	
RSK2_529 minus (Proliferation & Cell Cycle)	MCF-7	447	7.13E-62	1	1	4.82E-76	<0.0001		
RSK2_127 minus (Proliferation & Cell Cycle)	MCF-7	103	4.68E-95	1	1	1.10E-84	<0.0001		

The RSK2 signature was further reduced to 212 DE genes (RSK2_212) by taking into account transcript level abundance. Analysis of the RSK2_212 set by iRegulon [170] and the STRING 10.0 database identified a network of genes consisting of 127 DE genes (RSK2_127) that were regulated by GATA3, FOXA1, EP300 and ESR1 (ERα gene). These results are in agreement with GSEA analysis, which identified that E_2-responsive genes are enriched in WT versus RSK2-KO (FDR q-value < 0.05) (Fig. 8A) [184]. GATA3, FOX1 and EP300 are regulators of ERα function [150, 185-190] and high mRNA and protein expression of GATA3 and FOXA1 are associated with ER+ breast cancer [191]. The RSK2_127 set separated patients based on their ERα status with a greater probability that the RSK2_529 set (Fig. 8B and Table 3). Removal of the 23 genes related to cell cycle and proliferation that were present in the RSK2_127 set improved the hypergeometric probability of distinguishing between ER+ and ER- breast cancer samples (Fig. 8C, D). We conclude that RSK2 contributes to ER+ breast cancer through regulation of a subset of the ERα transcriptome.

ERK1/2 and ERα cooperatively control RSK2 nuclear sequestration

RSK2 activates ERα-mediated transcription through physical association and by phosphorylating ERα at Ser-167 (pSer-167) [55]. To distinguish whether physical association or pSer-167 was responsible for our transcriptomic findings, we treated MCF-7 cells with the anti-estrogen, 4-hydroxytamoxifen (4-OHT). 4-OHT disrupted the association of RSK2 and ERα without altering pSer-167 (Fig. 9A, B), strongly suggesting that the interaction of RSK2 with ERα (rather than pSer-167) is critical to the regulation of the ERα transcriptome. This conclusion was further supported in vivo, as inducible overexpression of ERα with doxycycline in the mammary gland, resulted in increased levels of active nuclear RSK, as predicted based on

Figure 8 A**nalysis of RSK2 gene signature**

(A) GSEA plot showing a positive correlation between genes up regulated by estradiol treatment and genes up regulated in WT versus RSK2-KO cells. (B) Hierarchical clustering of TCGA gene expression data from 782 invasive breast tumors reveals that the RSK2_127 gene signature stratifies patients according to the presence of ERα. Horizontal axis: individual patients; vertical axis: individual genes. White bar separates columns at the first dendrogram split. (Inset) The RSK2 regulatory network that is essential to the ER+ lineage. (C) Venn diagram showing overlap with cell cycle and proliferation of gene set controlled by GATA3, FOXA1, ESR1 and EP300 (RSK2_127). (D) Hierarchical clustering of TCGA gene expression data from 782 invasive breast tumors reveals that the gene set RSK2_127 minus the proliferation and cell cycle genes stratifies patients according to the presence of ERα. Horizontal axis: individual patients; vertical axis: individual genes. White bar separates columns at the first dendrogram split.

Figure 8

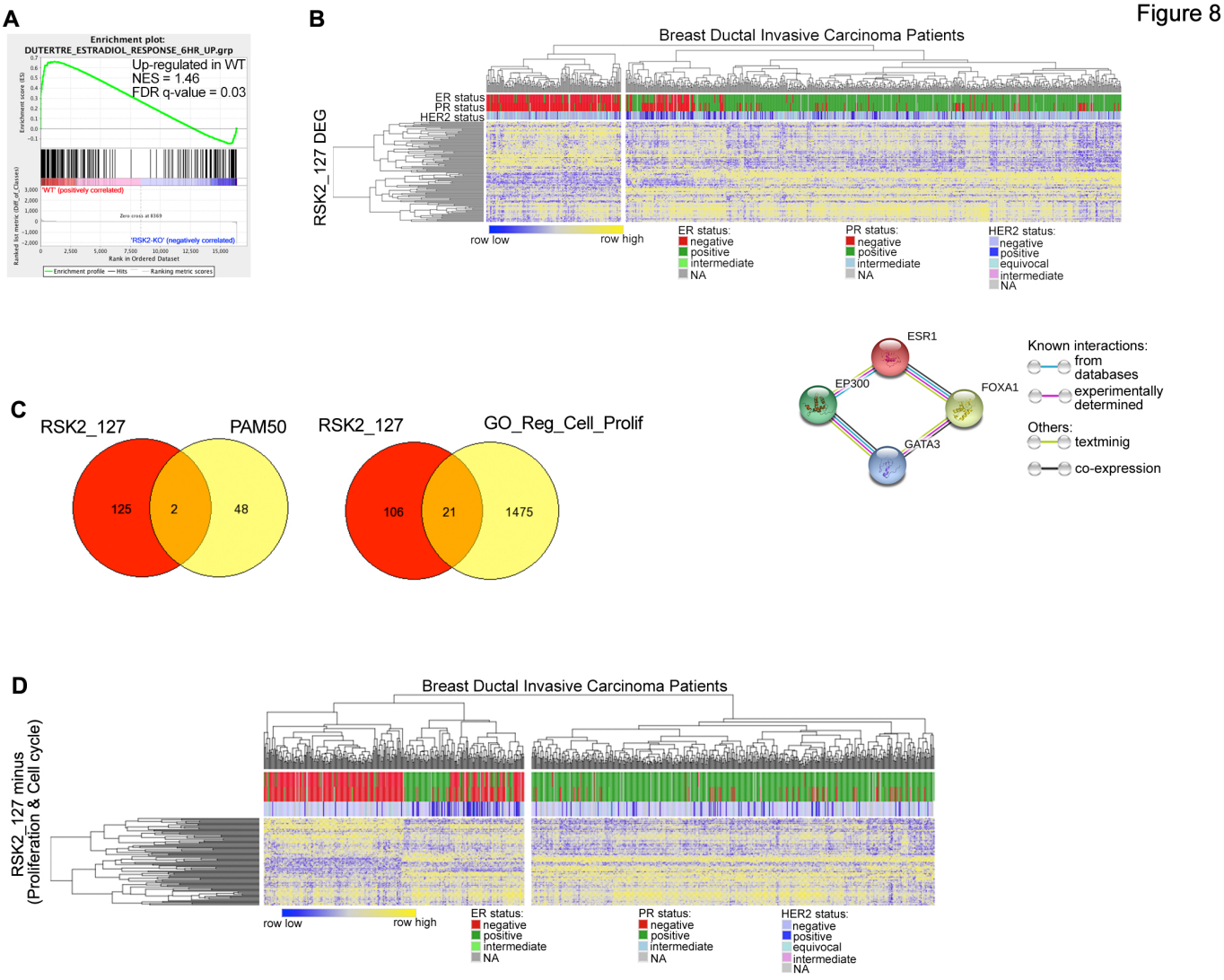
A
Enrichment plot:
DUTERTRE_ESTRADIOL_RESPONSE_6HR_UP.grp
Up-regulated in WT
NES = 1.46
FDR q-value = 0.03
'WT' (positively correlated)
'RSK2-KO' (negatively correlated)
Rank in Ordered Dataset
Enrichment profile
Hits
Ranking metric scores
B
Breast Ductal Invasive Carcinoma Patients
RSK2_127 DEG
ER status
PR status
HER2 status
row low
row high
ER status:
negative
positive
intermediate
NA
PR status:
negative
positive
intermediate
NA
HER2 status:
negative
positive
equivocal
intermediate
NA
C
RSK2_127
PAM50
125
2
48
RSK2_127
GO_Reg_Cell_Prolif
106
21
1475
ESR1
EP300
FOXA1
GATA3
Known interactions:
from databases
experimentally determined
Others:
textminig
co-expression
D
Breast Ductal Invasive Carcinoma Patients
RSK2_127 minus (Proliferation & Cell cycle)
row low
row high
ER status:
negative
positive
intermediate
NA
PR status:
negative
positive
intermediate
NA
HER2 status:
negative
positive
equivocal
intermediate
NA

Figure 9 ERα regulates RSK2 nuclear localization in breast cancer cell lines

(A) 4-OHT disrupts the association of ERα and RSK2. ERK1/2 signaling was activated in MCF-7 cells pre-treated ± 4-OHT and ERα and co-associated proteins immunoprecipitated with IgG (control) or anti- ERα. (Bar, mean ± SD, n=3) **p<0.01; Student's t-test. (B) 4-OHT does not decrease pSer- 167 ERα levels in ERK1/2 activated MCF-7 cells. (C) Forced expression of ERα increases nuclear RSK2 levels (Fn) in ER+ cells in mammary gland as measured by fluorescence in the CERM (rtTA+) compared to the control littermates (rtTA-). (Bar, median ± quartile, n≥3 ~ 4 months old/ ≥ 3 fields/mouse) **p<0.01; Student's t-test. (D) Anti-estrogens reduce RSK2 nuclear accumulation in ERK1/2 activated MCF-7 cells. MCF-7 cells treated with 4-OHT (2 μM) or ICI 182,780 (1 μM) and ZR-75-1 cells treated with 4-OHT (10 μM) before activation of ERK1/2 signaling. Scale bar = 10 μm. The data were normalized to the control. (Bar, median ± quartile, n=3, ≥ 80 cells/treatment) **p<0.01, ***p<0.001; Student's t-test. (E) 4-OHT (2 μM) reduces RSK2 nuclear accumulation in ERK1/2 activated BT-474 cells transduced with RSK2-Venus. Scale bar = 10 μm. (F) Inhibition of MCF-7 and ZR-75-1 proliferation after a 48 h treatment with various concentrations of 4-OHT. (Symbol, mean ± SD, n=2, quadruplicate) ***p<0.001, between the two cell lines at a given concentration; #p<0.001, within a cell line between the vehicle and each 4-OHT concentration; two-way ANOVA. (G) Anti-estrogens are able to drive RSK2 into the cytoplasm. ERK1/2 signaling was activated and RSK2 allowed to accumulate in the nucleus before treatment with 4-OHT (1μM). (Bar, median ± quartile, n=3, ≥ 80 cells/treatment). ***p<0.001; Student's t-test. (H) Treatment of MCF-7 cells with 4-OHT does not alter RSK or ERK1/2 activation or RSK2 levels. (I) Silencing ERα reduces RSK2 nuclear accumulation. MCF-7 cells transfected with control (Ctrl) or ERα-specific siRNA and treated ± growth factors. Scale bar=10μm. (Bar, median±quartile (n≥3, ≥100 cells/treatment). *p<0.05, **p<0.01, ***p<0.001; Student's t-test. (J) RSK2 does not regulate ERα nuclear localization. ERK1/2 was activated in MCF-7 cells transduced with a control (Ctrl) or RSK2 shRNA. Scale bar = 10 μm. (Bar, median ± quartile, n=2, ≥90 cells/treatment)

Figure 9

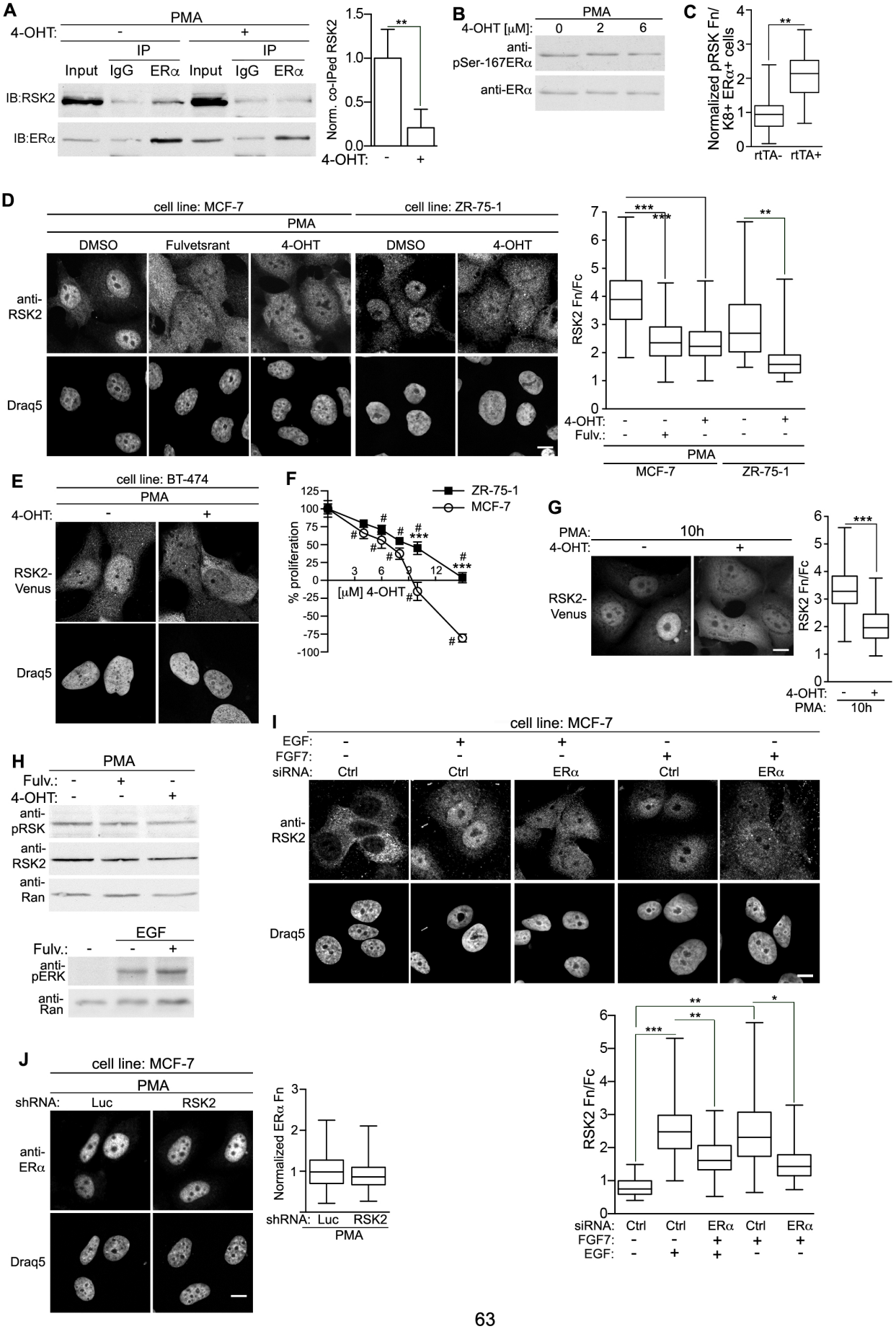
A
PMA
4-OHT: - +
IP
Input IgG ERα Input IgG ERα
IB:RSK2
IB:ERα
Norm. co-IPed RSK2
4-OHT: - +
B
PMA
4-OHT [μM]: 0 2 6
anti-pSer-167ERα
anti-ERα
C
Normalized pRSK Fn/K8+ ERα+ cells
rtTA- rtTA+
D
cell line: MCF-7
cell line: ZR-75-1
PMA
DMSO Fulvetsrant 4-OHT DMSO 4-OHT
anti-RSK2
Draq5
RSK2 Fn/Fc
4-OHT: - - + - +
Fulv.: - + - - -
PMA
MCF-7 ZR-75-1
E
cell line: BT-474
PMA
4-OHT: - +
RSK2-Venus
Draq5
F
ZR-75-1
MCF-7
% proliferation
[μM] 4-OHT
G
PMA: 10h
4-OHT: - +
RSK2-Venus
RSK2 Fn/Fc
4-OHT: - +
PMA: 10h
H
PMA
Fulv.: - + -
4-OHT: - - +
anti-pRSK
anti-RSK2
anti-Ran
EGF
Fulv.: - - +
anti-pERK
anti-Ran
I
cell line: MCF-7
EGF: - + + - -
FGF7: - - - + +
siRNA: Ctrl Ctrl ERα Ctrl ERα
anti-RSK2
Draq5
RSK2 Fn/Fc
siRNA: Ctrl Ctrl ERα Ctrl ERα
FGF7: - - + + +
EGF: - + + - -
J
cell line: MCF-7
PMA
shRNA: Luc RSK2
anti-ERα
Draq5
Normalized ERα Fn
shRNA: Luc RSK2
PMA

previous observations that proteins in a complex frequently regulate each other's protein levels (Fig. 9C). Based on these observations we tested whether association of ERα with RSK2 regulated RSK2 nuclear accumulation. Indeed 4-OHT inhibited RSK2 nuclear accumulation by ~ 50-80% across multiple different ER+ breast cancer cell lines, which were sensitive to 4-OHT (Figs. 5A-B, 9D-F). Fulvestrant also reduced RSK2 nuclear accumulation (Fig. 9D). In addition to preventing RSK2 nuclear accumulation anti-estrogen treatment was able to drive RSK2 into the cytoplasm after it had accumulated (Fig. 9G). Changes in RSK2 localization did not appear to arise secondary to altered expression levels or activity of RSK2 or ERK1/2 (Fig. 9H). Consistent with the anti-estrogen treatments, silencing ERα also reduced RSK2 nuclear accumulation in response to growth factors (Fig. 9I). Silencing RSK2 did not affect ERα nuclear localization (Fig. 9J), indicating that ERα nuclear accumulation occurs independently of RSK2. To more rigorously test whether ERα controls RSK2 nuclear accumulation we developed a 3D organoid culture system and generated organoids from primary human ER+ breast cancer tissue. Importantly, the levels of ERα, cyclin D1 and activated nuclear RSK were similar to those observed in the patient tissues from which they were derived. Similar to 2D cultures, 4-OHT treatments in 3D resulted in loss of nuclear RSK2 coupled to cytoplasmic accumulation of RSK2 and reduced cyclin D1 levels (Fig. 10A, B). We conclude that endocrine-based therapies result in dissociation of a complex consisting of RSK2 and ERα and that loss of this interaction reduces RSK2 nuclear accumulation.

Although our data clearly demonstrated that ERα is required for RSK2 nuclear accumulation, E_2 stimulation alone was insufficient (Fig. 10C) and required additional growth factor and cytokine signaling (Figs. 5A-D). A panel of 80 kinase inhibitors was therefore screened to identify signaling inputs that contribute to RSK2 nuclear localization. Of these, only compounds that inhibited ERK1/2 decreased the levels of nuclear RSK2, which is consistent with the known role of RSK2 in ERK1/2 signaling (Fig. 10D, Table 4). We conclude that ERK1/2

activation allows RSK2 to translocate into the nucleus while ERα interacts and sequesters RSK2 in the nucleus.

Figure 10 ERα regulates RSK2 nuclear localization in primary human breast cancer organoids

Anti-estrogens decrease nuclear active RSK (A) and cyclin D1 (B) levels in ER+ breast cancer organoids. Serial sections of starting tissues and ER+ breast cancer organoids treated ± 4-OHT. Scale bar=20 μm. Arrows indicate nuclear RSK2 in control versus cytoplasmic RSK2 with 4-OHT. (Bar, median±quartile, n=2 patients, ≥15organoids/condition) and cyclin D1 (Bar, median±quartile, n=2 patients, ≥8 organoids/condition). The data were normalized to the control. ***p<0.001; Student's t-test. (C) E_2 does not activate RSK2 nuclear accumulation in MCF-7 cells. (D) Small molecule inhibitor screen of RSK2-Venus nuclear accumulation. *p<0.05; Student's t-test.

Figure 10

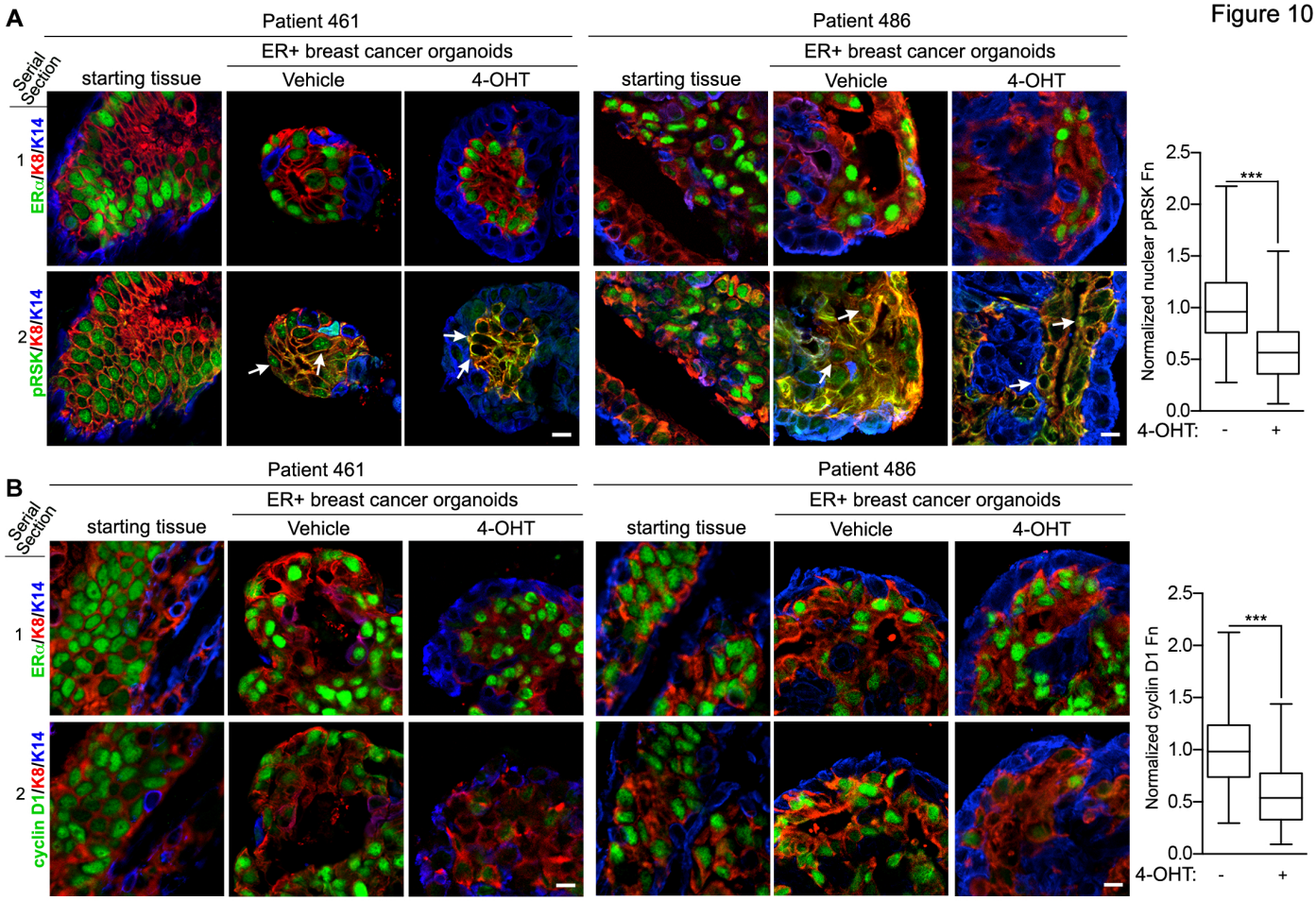
A
Patient 461
Patient 486
ER+ breast cancer organoids
Serial Section
starting tissue
Vehicle
4-OHT
1
ERα/K8/K14
2
pRSK/K8/K14
Normalized nuclear pRSK Fn
4-OHT:
B
cyclin D1/K8/K14
Normalized cyclin D1 Fn

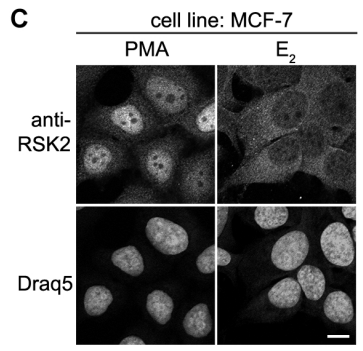
C
cell line: MCF-7
PMA
E2
anti-RSK2
Draq5

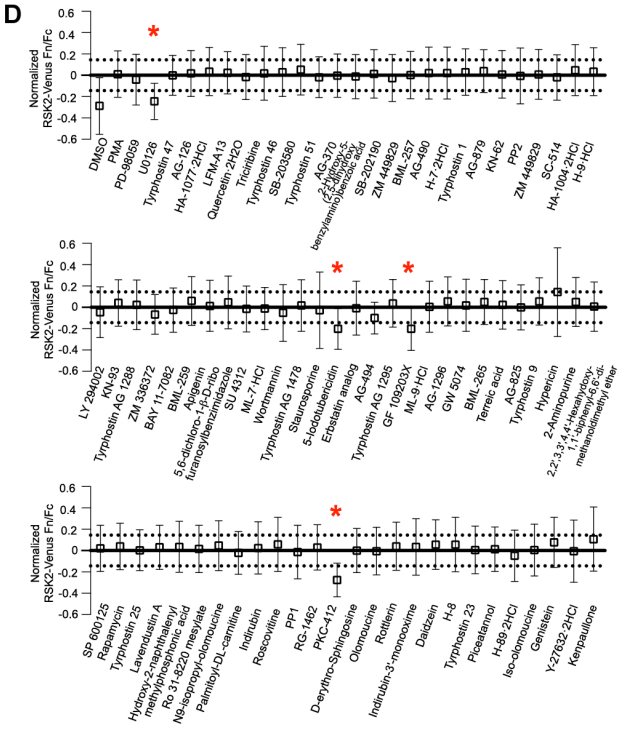
D
Normalized RSK2-Venus Fn/Fc
DMSO
PMA
PD-98059
U0126
Tyrphostin 47
AG-126
HA-1077-2HCl
LFM-A13
Quercetin 2H2O
Tricirbine
Tyrphostin 46
SB-203580
Tyrphostin 51
AG-370
SB-202190
ZM 449829
BML-257
AG-490
H-7-2HCl
Tyrphostin 1
AG-879
KN-62
PP2
ZM 449829
SC-514
HA-1004-2HCl
H-9-HCl
LY 294002
KN-93
Tyrphostin AG 1288
ZM 336372
BAY 11-7082
BML-259
Apigenin
5,6-dichloro-1-β-D-ribofuranosylbenzimidazole
SU 4312
ML-7-HCl
Wortmannin
Tyrphostin AG 1478
Staurosporine
5-Iodotubericidin
Erbstatin analog
AG-494
Tyrphostin AG 1295
GF 109203X
ML-9-HCl
AG-1296
GW 5074
BML-265
Tarreic acid
AG-825
Tyrphostin 9
Hypericin
2-Aminopurine
SP 600125
Rapamycin
Tyrphostin 25
Lavendustin A
Hydroxy-2-naphthalenyl methylphosphonic acid
Ro 31-8220 mesylate
N9-isopropyl-olomoucine
Palmitoyl-DL-carnitine
Indirubin
Roscovitine
PP1
RG-1462
PKC-412
D-erythro-Sphingosine
Olomoucine
Rottlerin
Indirubin-3'-monooxime
Daidzein
H-8
Tyrphostin 23
Piceatannol
H-89-2HCl
Iso-olomoucine
Genistein
Y-27632-2HCl
Kenpaullone

Table 4 Small molecule inhibitors screened for inhibition of RSK2 nuclear localization

List of inhibitors (and their known target kinase) used in Figure 10D.

Compound	Known target(s)
PD-98059	MEK
U-0126	MEK
Tyrophostin 47	EGFRK
AG-126	IRAK
HA-1077·2HCl	PKA, PKG
LFM-A13	BTK
Quercetin·2H_2O	PI 3-K
Triciribine	Akt signaling pathway
Tyrophostin 46	EGFRK, PDGFRK
SB-203580	p38 MAPK
Tyrophostin 51	EGFRK
AG-370	PDGFRK
2-Hydroxy-5-(2,5-dihydroxybenzylamino)benzoic acid	EGFRK, CaMK II
SB-202190	p38 MAPK
SU1498	Flk1
BML-257	Akt
AG-490	JAK-2
H-7·2HCl	PKA, PKG, MLCK, and PKC
Tyrophostin 1	Negative control for tyrosine kinase inhibitors
AG-879	NGFRK
KN-62	CaMK II
PP2	Src family
ZM 449829	JAK-3
SC-514	IKK2
HA-1004·2HCl	PKA, PKG
H-9·HCl	PKA, PKG, MLCK, and PKC
Tyrophostin AG 1288	Tyrosine kinases
LY 294002	PI 3-K
KN-93	CaMK II
ZM 336372	cRAF
BAY 11-7082	IKK pathway
BML-259	Cdk5/p25
Apigenin	CK II
5,6-dichloro-1-β-D ribofuranosylbenzimidazole	CK II

SU 4312	Flk1
ML-7·HCl	MLCK
Wortmannin	PI 3-K
Tyrophostin AG 1478	EGFRK
Staurosporine	Pan-specific
5-Iodotubericidin	ERK2, adenosine kinase, CK1, CK2
Erbstatin analog	EGFRK
AG-494	EGFRK, PDGFRK
Tyrophostin AG 1295	Tyrosine kinases
GF 109203X	PKC
ML-9·HCl	MLCK
AG-1296	PDGFRK
2,2',3,3',4,4'-Hexahydroxy-1,1'-biphenyl-6,6'-dimethanol dimethyl ether	PKC alpha, PKC gamma
BML-265	EGFRK
Terreic acid	BTK
AG-825	HER1-2
Tyrophostin 9	PDGFRK
Hypericin	PKC
2-Aminopurine	p58 PITSLRE beta1
GW 5074	cRAF
SP 600125	JNK
Rapamycin	mTOR
Tyrophostin 25	EGFRK
Lavendustin A	EGFRK
Hydroxy-2-naphthalenylmethyl-phosphonic acid	IRK
Ro 31-8220 mesylate	PKC
N9-isopropyl-olomoucine	CDK
Palmitoyl-DL-carnitine	PKC
Indirubin	GSK-3beta, CDK5
Roscovitine	CDK
PP1	Src family
RG-1462	EGFRK
PKC-412	PKC inhibitor
D-erythro-Sphingosine	PKC
Olomoucine	CDK
Rottlerin	PKC delta
Indirubin-3'-monooxime	GSK-3beta
Daidzein	Negative control for Genistein
H-8	PKA, PKG

Tyrophostin 23	EGFRK
Piceatannol	Syk
H-89·2HCl	PKA
Iso-olomoucine	Negative control for olomoucine
Genistein	Tyrosine Kinases
Y-27632·2HCl	ROCK
Kenpaullone	GSK-3beta

The extreme N-terminus of RSK2 is required for interaction with ERα

Because physical association with ERα was required for RSK2 nuclear accumulation, we next wished to identify the region of RSK2 responsible for nuclear accumulation and ERα binding. To this end we took advantage of the observations that the RSK1 isoform does not accumulate in the nucleus, and created chimeras of RSK1 and RSK2, which were fluorescently tagged at their C-terminus (Fig. 11A). A chimera in which the RSK2 C-terminal kinase domain (CTKD) was swapped with that of RSK1 (RSK2(1-407)RSK1(404-735)) retained its ability to accumulate, while a chimera with the reverse swap (RSK1(1-401)RSK2(406-740)) did not accumulate (Fig. 11B, C), despite the fact that both chimeras were active (Fig. 11D). Thus the RSK2 residues from 1 to 407 were necessary for RSK2 accumulation. Within this region, the RSK2 residues at the extreme N-terminus (1-67) and in the linker (329-424) diverge the most from those of RSK1 (54% and 68% identity, respectively, compared to 80% overall identity). We therefore hypothesized that either the linker domain or the N-terminus were most likely responsible for nuclear translocation. Replacing the RSK2 linker with that of RSK1 ((RSK2(1-375) RSK1(370-401)RSK2(406-740)) did not alter activity or nuclear accumulation (Fig. 11B-D), suggesting that the linker region did not play a role. Because a deletion mutant of residues from 1 to 67 of RSK2 was highly unstable, we replaced the extreme N-terminal region of RSK1 with that of RSK2 ((RSK2(1-67)RSK1(62-735)). This chimera was both active (Fig. 11D) and accumulated in the nucleus (Fig. 11B,C). In contrast, replacing the extreme N-terminal region of RSK2 with that of RSK1 to create RSK1(1-61)RSK2(68-740) resulted in a chimera that was active (Fig. 11D) yet lost its ability to accumulate in the nucleus (Fig. 11E). We conclude that residues from 1 to 67 are required for RSK2 nuclear accumulation. The RSK2 residues from 1 to 67 on their own could not facilitate accumulation of a heterologous protein in comparison to the nuclear localization signal (NLS) of SV40 (PKKKRKV) (Fig. 12A). Thus the extreme N-terminus is necessary but not sufficient for RSK2 accumulation.

We hypothesized that the RSK2 residues from 1 to 67 are important for RSK2 nuclear accumulation because they are responsible for interaction with ERα. Consistent with this, both RSK2 and the chimera, RSK2(1-67)RSK1(62-735), but not RSK1, co-immunoprecipitated with ERα (Fig. 12B). Additionally, silencing ERα reduced nuclear accumulation of the chimera, similar to the WT (Fig. 12C). The RSK2 region from 1 to 67 is highly conserved within the class Mammalia, as is the analogous region in RSK1 (Fig. 13A). There are two notable differences in the extreme N-terminus between RSK1 and RSK2, which include a Ser-Pro-Ser motif and a five amino acid insert that are present only in RSK2. A Ser-Pro-Ser motif regulates ERK2 nuclear translocation [192] but mutation of residues within this motif did not alter RSK2 nuclear accumulation (Fig. 13B, C). However, deletion of the five amino acid insert (RSK2Δ27-32) prevented nuclear accumulation (Fig. 13D), without affecting RSK2 activation (Fig. 13E). Moreover, ERα specifically co-associated with a purified, recombinant protein containing the RSK2 residues from 1 to 67 (Fig. 13F). We conclude that the extreme N-terminus interacts with ERα to sequester RSK2 in the nucleus.

Figure 11 Mapping the region responsible for RSK2 nuclear accumulation

(A) Schematic of RSK constructs. The N-terminal (NTKD) and C-terminal (CTKD) kinase domains are indicated. (B) Nuclear accumulation (Fn/Fc) of RSK constructs. (Bar, median±quartile, n≥3, ≥50 cells/treatment). ***p<0.001 Student's t-test. (C) The N-terminal region of RSK2 is required for RSK2 nuclear accumulation. Direct fluorescence of MCF-7 cells transduced with a C-terminal Venus-tagged WT RSK2 or RSK chimeras. Scale bar = 10 μm. (D) Expression and activation levels of the indicated constructs. ERK1/2 was activated in MCF-7 cells and lysates analyzed. The strip indicates that samples were electrophoresed on a separate gel with RSK1-Venus and RSK2-Venus controls included. (E) Replacement of the extreme N-terminus of RSK2 with that of RSK1 prevents nuclear accumulation. (Bar, median±quartile, n≥3, ≥50 cells/treatment). ***p<0.001; Student's t-test.

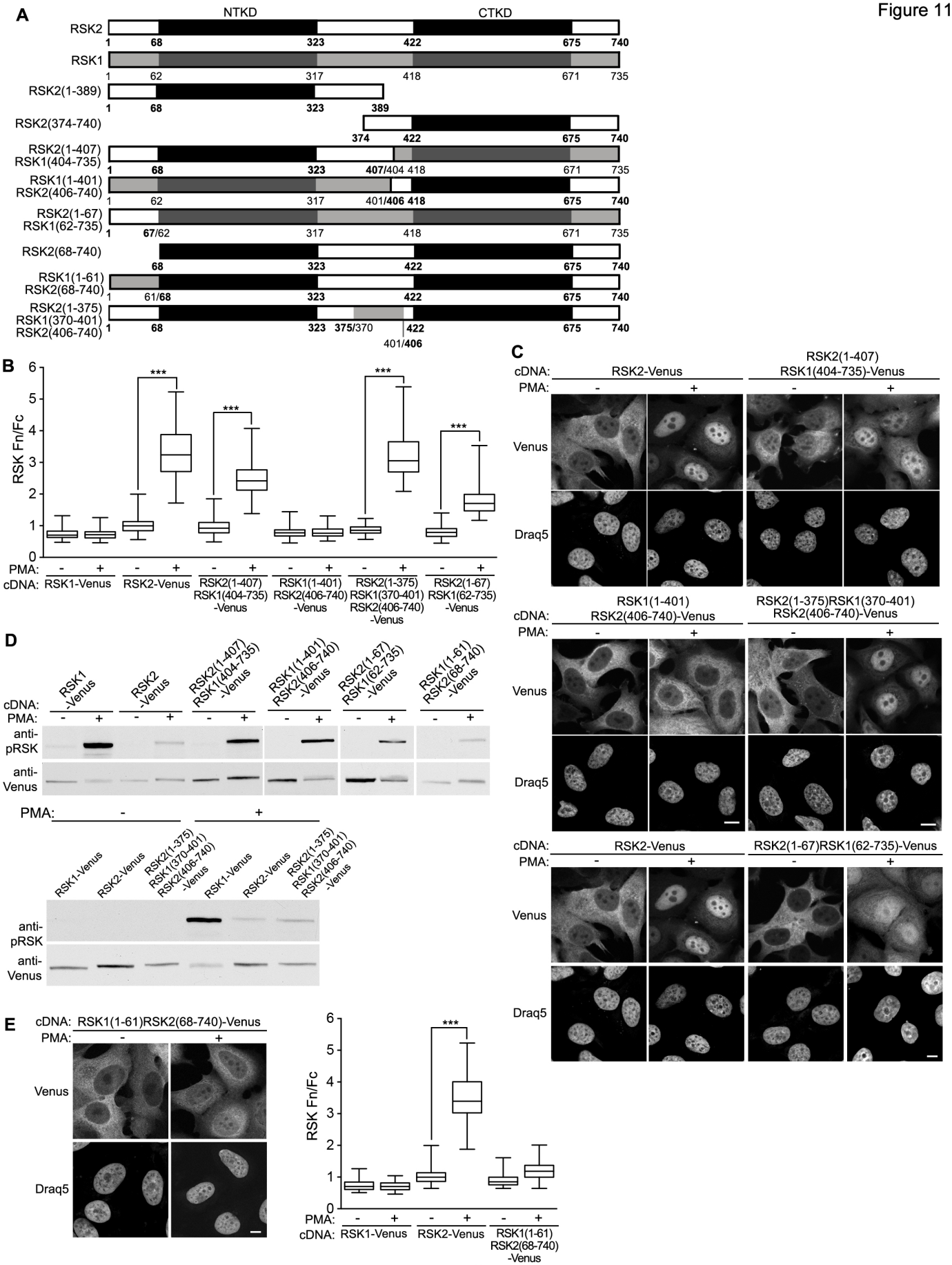
A
NTKD
CTKD
RSK2
RSK1
RSK2(1-389)
RSK2(374-740)
RSK2(1-407) RSK1(404-735)
RSK1(1-401) RSK2(406-740)
RSK2(1-67) RSK1(62-735)
RSK2(68-740)
RSK1(1-61) RSK2(68-740)
RSK2(1-375) RSK1(370-401) RSK2(406-740)
B
RSK Fn/Fc
PMA:
cDNA:
RSK1-Venus
RSK2-Venus
RSK2(1-407) RSK1(404-735) -Venus
RSK1(1-401) RSK2(406-740) -Venus
RSK2(1-375) RSK1(370-401) RSK2(406-740) -Venus
RSK2(1-67) RSK1(62-735) -Venus
C
cDNA:
RSK2-Venus
RSK2(1-407) RSK1(404-735)-Venus
PMA:
Venus
Draq5
RSK1(1-401) RSK2(406-740)-Venus
RSK2(1-375)RSK1(370-401) RSK2(406-740)-Venus
RSK2(1-67)RSK1(62-735)-Venus
D
RSK1 -Venus
RSK2 -Venus
RSK2(1-407) RSK1(404-735) -Venus
RSK1(1-401) RSK2(406-740) -Venus
RSK2(1-67) RSK1(62-735) -Venus
RSK1(1-61) RSK2(68-740) -Venus
anti-pRSK
anti-Venus
RSK2(1-375) RSK1(370-401) RSK2(406-740) -Venus
E
cDNA: RSK1(1-61)RSK2(68-740)-Venus
PMA:
Venus
Draq5
RSK Fn/Fc
RSK1(1-61) RSK2(68-740) -Venus

Figure 12 1-67aa of RSK2 control RSK2 nuclear accumulation through interaction with ERα

(A) RSK2(1-67) does not confer nuclear localization of a heterologous protein. Direct fluorescence of MCF-7 cells overexpressing Venus-NLS (SV40)-GST, Venus-RSK2(1-67)-GST or the control (Venus-GST). Scale bar = 10 μm. (Bar, mean ± SD, n=3, ≥20cells/treatment). (B) ERα physically associates with the extreme N-terminus of RSK2. MCF-7 cells were transduced, ERK1/2 signaling activated and Venus-tagged and co-associated proteins immunoprecipitated with an anti-Venus antibody. ns=nonspecific. (C) ERα regulates RSK2 nuclear accumulation through residues 1 to 67 of RSK2. MCF-7 cells over-expressing RSK2-Venus or RSK2(1-67)RSK1(62-735)-Venus were transfected with control or ERα-specific siRNA. Scale bar=10 μm. (Bar, median±quartile, n=3, 50 cells/treatment). ***p<0.001; Student's t-test.

Figure 12

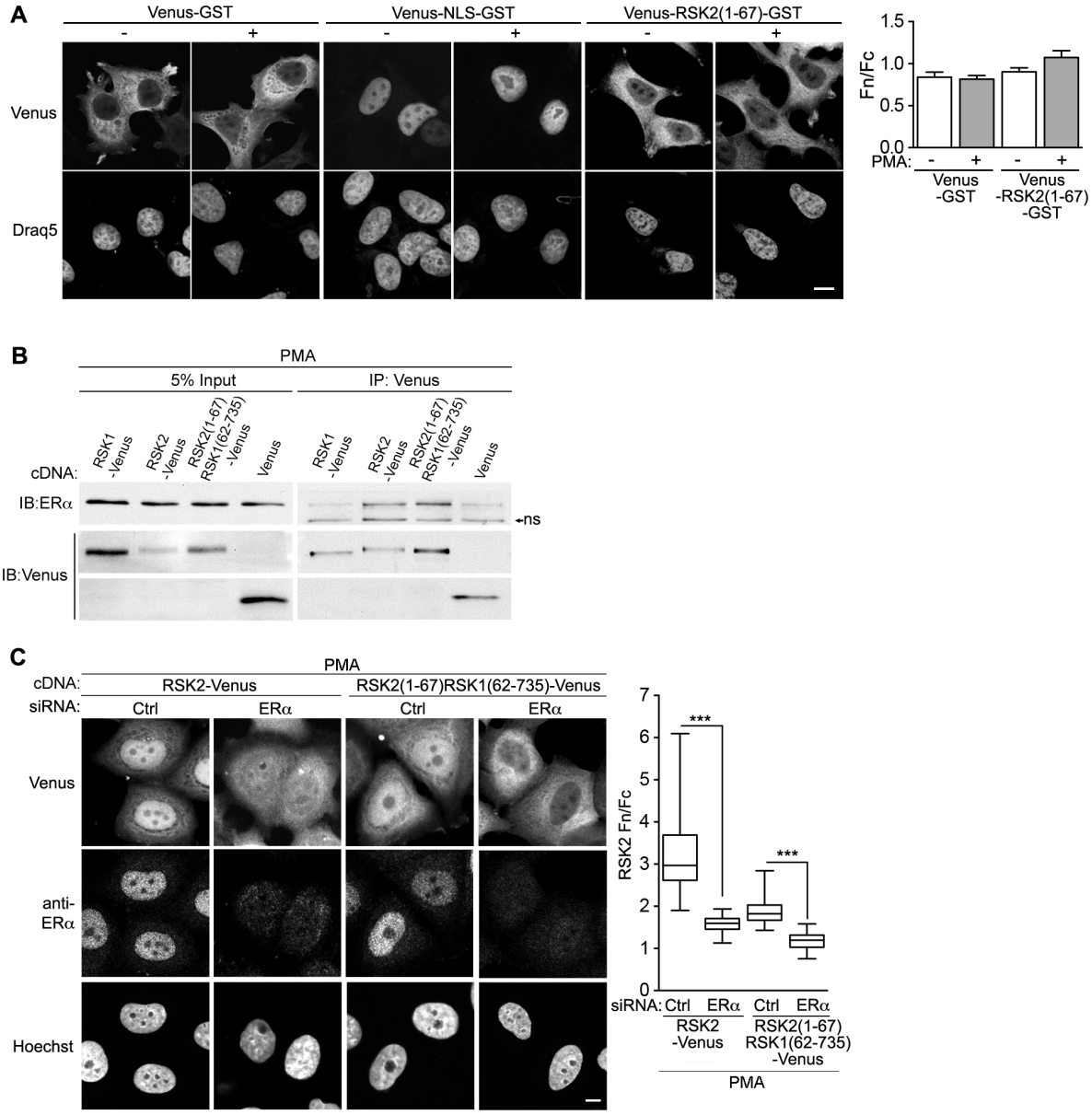
A
Venus-GST
Venus-NLS-GST
Venus-RSK2(1-67)-GST
Venus
Draq5
Fn/Fc
PMA:
Venus -GST
Venus -RSK2(1-67) -GST
B
PMA
5% Input
IP: Venus
cDNA:
RSK1 -Venus
RSK2 -Venus
RSK2(1-67) RSK1(62-735) -Venus
Venus
IB:ERα
ns
IB:Venus
C
PMA
cDNA:
RSK2-Venus
RSK2(1-67)RSK1(62-735)-Venus
siRNA:
Ctrl
ERα
Venus
anti-ERα
Hoechst
RSK2 Fn/Fc
***
siRNA:
RSK2 -Venus
RSK2(1-67) RSK1(62-735) -Venus
PMA

Figure 13 Identification of the RSK2 motif that interacts with ERα

(A) Amino acid sequences in representative examples from the class Mammalia of the extreme N-terminus of RSK2 and RSK1, which is located just prior to the NTKD. (B) The Ser-Pro-Ser motif of RSK2 does not regulate RSK2 nuclear accumulation. ERK1/2 was activated in transduced cells, which were analyzed by direct fluorescence at various time points. Scale bar = 10 μm. (Bar, median ± quartile, n=2, ≥30cells/treatment) **p<0.01, ***p<0.001; Student's t-test. (C) Analysis of lysates from (B). (D) RSK2 residues from 27 to 32 regulate RSK2 nuclear accumulation. Scale bar=10μm. (Bar, median±quartile, n=3, ≥50 cells/treatment) ***p<0.001; Student's t-test. (E) Analysis of lysates from (D). (F) ERα associates with purified, recombinant RSK2(1-67), but not with RSK1(1-62) or RSK2(1-67_Δ27-32).

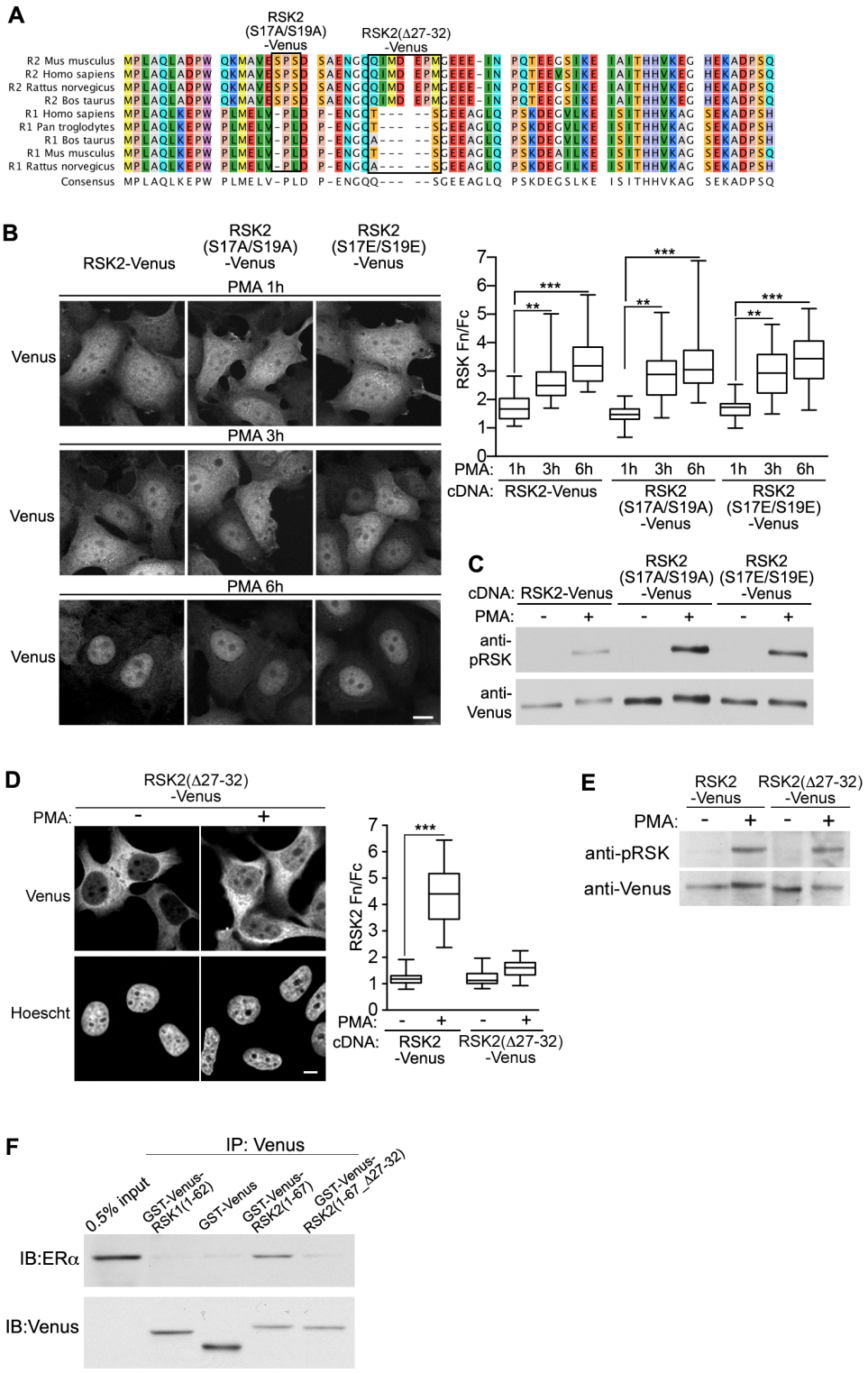
A
RSK2 (S17A/S19A) -Venus
RSK2(Δ27-32) -Venus
R2 Mus musculus
R2 Homo sapiens
R2 Rattus norvegicus
R2 Bos taurus
R1 Homo sapiens
R1 Pan troglodytes
R1 Bos taurus
R1 Mus musculus
R1 Rattus norvegicus
Consensus
B
RSK2-Venus
RSK2 (S17A/S19A) -Venus
RSK2 (S17E/S19E) -Venus
PMA 1h
PMA 3h
PMA 6h
Venus
RSK Fn/Fc
PMA: 1h 3h 6h 1h 3h 6h 1h 3h 6h
cDNA: RSK2-Venus
RSK2 (S17A/S19A) -Venus
RSK2 (S17E/S19E) -Venus
C
cDNA: RSK2-Venus
RSK2 (S17A/S19A) -Venus
RSK2 (S17E/S19E) -Venus
PMA: - + - + - +
anti-pRSK
anti-Venus
D
RSK2(Δ27-32) -Venus
PMA: - +
Venus
Hoescht
RSK2 Fn/Fc
cDNA: RSK2 -Venus
RSK2(Δ27-32) -Venus
E
RSK2 -Venus
RSK2(Δ27-32) -Venus
PMA: - + - +
anti-pRSK
anti-Venus
F
IP: Venus
0.5% input
GST-Venus-RSK1(1-62)
GST-Venus
GST-Venus-RSK2(1-67)
GST-Venus-RSK2(1-67_Δ27-32)
IB:ERα
IB:Venus

Nuclear accumulation of RSK2 promotes ER+ breast cancer growth

Silencing endogenous RSK2 with co-expression of a shRNA-resistant mutant that does not accumulate in the nucleus (rRSK1(1-61)RSK2(68-740)) failed to increase cyclin D1 levels compared to a mutant that localizes to the nucleus (rRSK2(1-67)RSK1(62-735)) (Fig. 14A, B). To further verify that RSK2 nuclear accumulation is required to support ER+ breast cancer growth we employed the RSK2 chimeras that did or did not accumulate in the nucleus, which reflects their ability to interact with ERα. As expected, silencing RSK2 in MCF-7 cells strongly impaired tumor growth, and this inhibition was rescued with ectopic expression of WT shRNA-resistant RSK2 (Fig. 14C, D). Importantly, restoration of tumor growth was also observed by ectopic expression of the nuclear accumulating chimera but not with the non-accumulating chimera (Fig. 14C, D). Nuclear accumulation of the various ectopically expressed fusion proteins (Fig. 14E) was consistent with our *in vitro* data (Figs. 11C, E) and their levels were similar (Fig. 14F). As expected, cyclin D1 levels mirrored the ability of the constructs to accumulate in the nucleus, while levels of pSer-167 ERα did not (Fig. 14G). These data are consistent with a RSK2-dependent activation of a gene program that facilitates ER+ breast cancer by physical association rather than ERα phosphorylation at Ser- 167. Collectively, these observations clearly demonstrate that RSK2 nuclear accumulation is required for tumor growth in ER+ breast cancer.

Nuclear accumulation of RSK2 triggers neoplastic transformation

Because nuclear RSK2 was required for ER+ tumor growth, we next asked whether forced expression of RSK2 in the nucleus of non-transformed ER+ mammary epithelia could facilitate neoplastic transformation *in vivo*. To this end a novel transgenic mouse with mammary gland-restricted, nuclear RSK2 expression (MMTV-NLS-RSK2) was generated. The transgene was expressed specifically in the mammary gland and localized to the nucleus (Fig. 15A, B).

Because mouse models of ER+ breast cancer have a long latency [193], we examined mammary glands at early (six months) and later (sixteen months) time points. At six months, ductal hyperplasia was observed (Fig. 15C, D) with expansion of the ER+ mammary population (Fig. 15E). By sixteen months, ducts and lobules were markedly expanded in NLS-RSK2 mice compared to controls (Fig. 16A, B). Microscopic examination of expanded ducts revealed clear evidence of neoplastic transformation, which was manifested as DCIS. DCIS can be histologically evaluated into a three tiered grading system that is largely based on increasing severity in nuclear morphology. NLS-RSK2 mice showed clearly evidence of high grade DCIS, including solid growth within ducts that obliterated the lumen (Fig. 16C), prominent apoptosis and mitosis including atypical mitotic forms (Fig. 16D, E), severe nuclear atypia including nuclear enlargement (16F, G), pleomorphism, loss of polarity and stratification (16F). Consistent with these observations IF experiments detected elevated levels of the S-phase marker, PCNA (Fig. 17A), and the DNA damage marker, γH2AX (Fig. 17B). Approximately 50% of the mice developed high grade ER+ DCIS (Fig. 17C, D). To functionally confirm neoplastic transformation we isolated the mammary cells from the sixteen month old NLS-RSK2 and assayed their *in vitro* and *in vivo* tumorigenic capacity. Sphere cultures generated from the NLS-RSK2 mice were more efficient at forming spheres over multiple passages than those obtained from WT mice (Fig. 17E). For the *in vivo* assays spheres generated from WT and NLS-RSK2 mammary glands from passage 0 were transduced with luciferase (Fig. 17F). Intra-cardiac (IC) injection of equal numbers of the transduced spheres into NCG mice resulted in 100% of the mice injected with NLS-RSK2 spheres developing metastatic tumors; whereas, WT spheres failed to form tumors (Fig. 17G-I). We conclude that forced nuclear expression of RSK2 triggers in situ transformation of ER+ mammary epithelial cells, and that these cells are capable of tumorigenic growth if removed from the mammary gland.

Figure 14 RSK2 nuclear accumulation is required for ER+ tumor growth

(A) Nuclear localization of RSK2 is required for increased cyclin D1 levels. MCF-7 cells were transduced with a control (Luc) or RSK2 shRNA in combination with resistant mutant RSK constructs before stimulation. Scale bar=10μm. (Bar, median±quartile, n=3, ≥78 cells/treatment). ***p<0.001; Student's t-test. (B) Expression levels of various RSK2 constructs. MCF-7 cells were transduced with a control or RSK2-specific shRNA and the indicated construct. ERK1/2 was activated in MCF-7 cells and lysates analyzed. (C) ER+ tumor growth is dependent on RSK2 nuclear accumulation. MCF-7 cells transduced with Scrbl or RSK2 shRNA were also transduced with Venus or resistant WT or mutant RSK constructs. Transduced MCF-7 cells were injected into the 4th mammary fat pad of NSG mice implanted with an E_2 pellet. (Symbol, mean±SD, n≥4 mice/group, 2 tumors/mouse) *p<0.05, ***p<0.001; two-way-ANOVA for the last time point. (D) Representative ex vivo images of resected tumors from (C). Scale bar =3 mm. (E) Nuclear accumulation of RSK constructs shown by 3D projections of 6 1μm Z-stack images. Arrows indicate nuclei. (F) Tumors (B) were lysed and expression levels of the constructs analyzed. (G) RSK2 nuclear accumulation correlates with cyclin D1 but not pSer-167 levels. The samples were normalized to RAN. The data were normalized to the control. (Bar, mean±SD, n=3 tumors (triplicate)). *p<0.05, **p<0.01, ***p<0.001; Student's t-test.

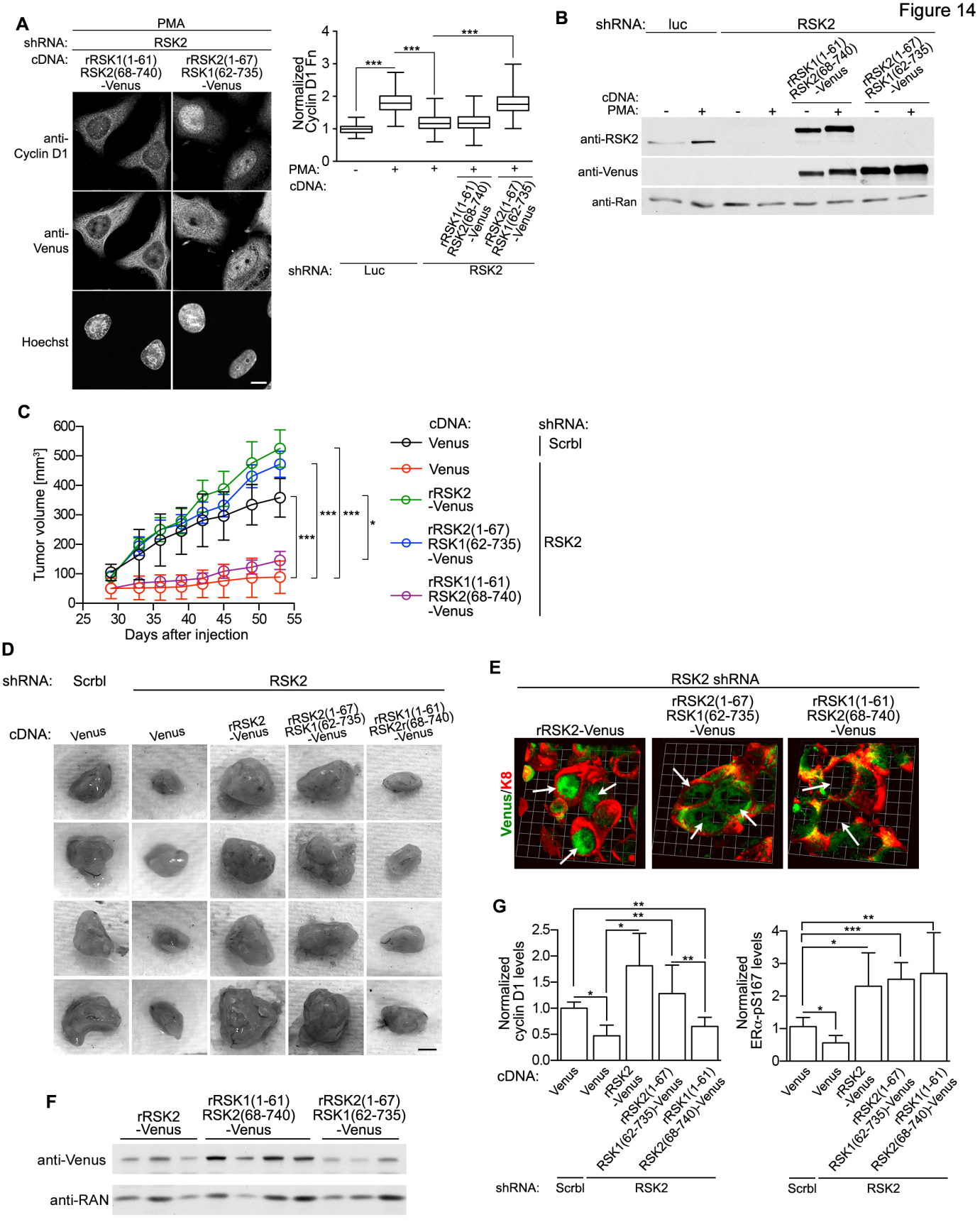
A
PMA
shRNA:
RSK2
cDNA:
rRSK1(1-61) RSK2(68-740) -Venus
rRSK2(1-67) RSK1(62-735) -Venus
anti-Cyclin D1
anti-Venus
Hoechst
Normalized Cyclin D1 Fn
PMA:
cDNA:
shRNA:
Luc
RSK2
B
shRNA:
luc
RSK2
cDNA:
PMA:
anti-RSK2
anti-Venus
anti-Ran
C
Tumor volume [mm³]
Days after injection
cDNA:
shRNA:
Venus
ScrbI
Venus
rRSK2 -Venus
rRSK2(1-67) RSK1(62-735) -Venus
rRSK1(1-61) RSK2(68-740) -Venus
RSK2
D
shRNA:
ScrbI
RSK2
cDNA:
Venus
Venus
rRSK2 -Venus
rRSK2(1-67) RSK1(62-735) -Venus
rRSK1(1-61) RSK2r(68-740) -Venus
E
RSK2 shRNA
rRSK2-Venus
rRSK2(1-67) RSK1(62-735) -Venus
rRSK1(1-61) RSK2(68-740) -Venus
Venus/K8
F
rRSK2 -Venus
rRSK1(1-61) RSK2(68-740) -Venus
rRSK2(1-67) RSK1(62-735) -Venus
anti-Venus
anti-RAN
G
Normalized cyclin D1 levels
Normalized ERα-pS167 levels
cDNA:
Venus
Venus
rRSK2 -Venus
rRSK2(1-67) RSK1(62-735)-Venus
rRSK1(1-61) RSK2(68-740)-Venus
shRNA:
ScrbI
RSK2

Figure 15 Analysis of NLS-RSK2 mouse model

(A*) NLS-RSK2 is expressed in the nucleus of transgenic animals. Section of mammary gland obtained from MMTV-NLS-RSK2 virgin female mice (10 weeks). Scale bar = 10 μm. (B) Mammary cells from (A) were isolated, lysed and analyzed. ns=non-specific. (C) Carmine stained whole mount images of the 4th mammary gland isolated from six month WT and NLS-RSK2 mice. Scale Bar = 200 μm. (D) H&E sections demonstrate hyperplasia in the mammary glands of the NLS-RSK2 transgenic mice at six months. Scale Bar = 10 μm. (E) Forced nuclear expression of RSK2 expands the ER+ population. Mammary gland sections from NLS-RSK2 or WT virgin female mice (6 months). Scale bar = 20 μm. (Bar, median ± quartile, n= 6 mice/genotype, ≥5 fields/mouse) ***p<0.001; Student's t-test.

* Lejla Pasic contributed panels A and B

Figure 15

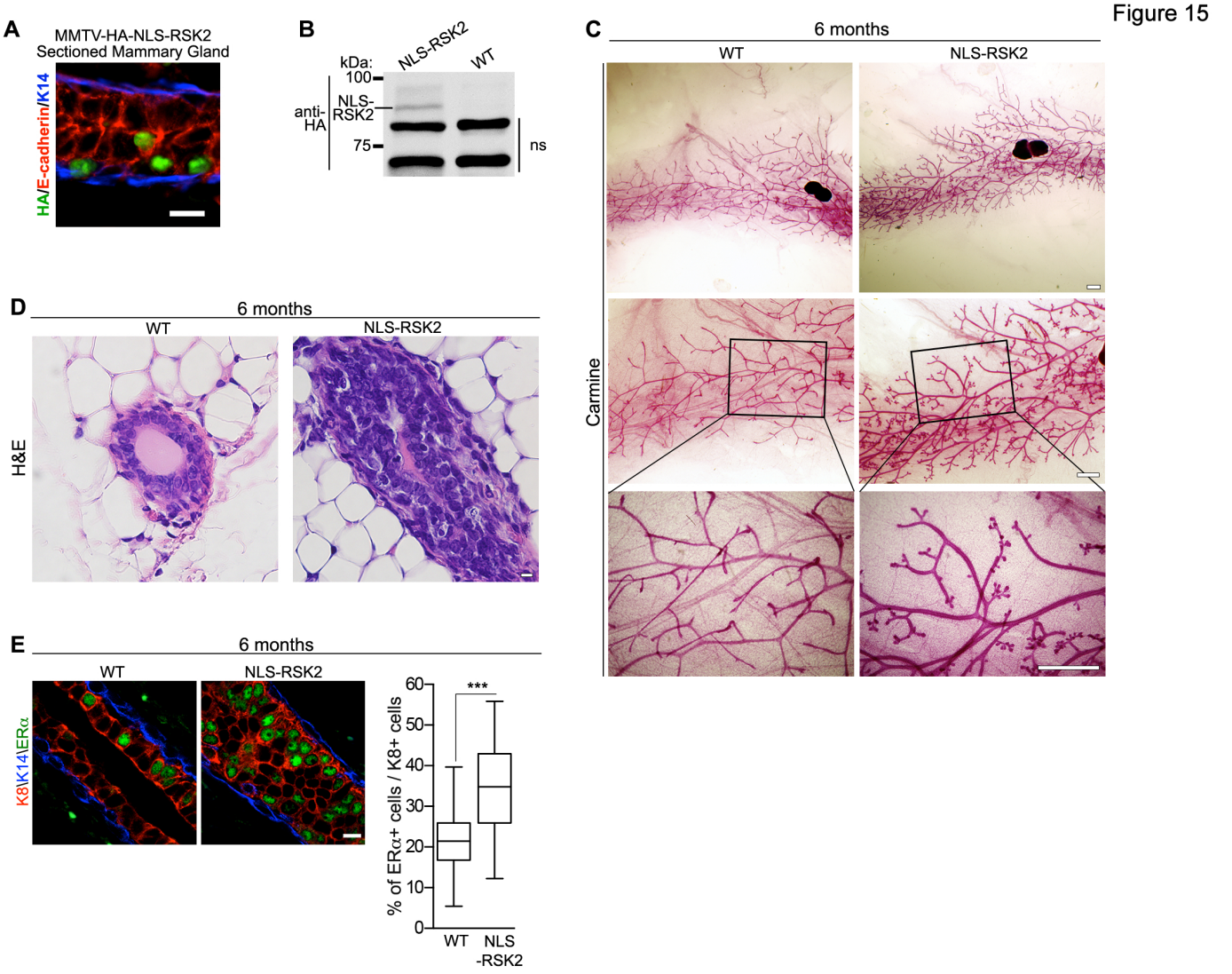
A
MMTV-HA-NLS-RSK2
Sectioned Mammary Gland
HA/E-cadherin/K14
B
kDa:
NLS-RSK2
WT
100
anti-HA
NLS-RSK2
75
ns
C
6 months
WT
NLS-RSK2
Carmine
D
6 months
WT
NLS-RSK2
H&E
E
6 months
WT
NLS-RSK2
K8\K14\ERα
% of ERα+ cells / K8+ cells
***
WT
NLS -RSK2

Figure 16 Nuclear RSK2 induces neoplastic transformation of the mammary gland

(A) Carmine stained whole mount images of the 4th mammary gland isolated from sixteen month WT and NLS-RSK2 mice. Scale Bar = 200 μm. (B) Carmine stained whole mount images of the 4th mammary gland isolated from sixteen month WT and NLS-RSK2 transgenic mice. Scale Bar=200μm. (C) H&E sections demonstrate ductal filling (red arrows) in the mammary glands of NLS-RSK2 versus normal ducts (white arrows) in WT mice. Scale Bar=100μm. (D) Increased mitosis and apoptosis are observed in the ducts of NLS-RSK2 mice. Scale Bar=10μm (Bar, mean±SD, n ≥4 mice/genotype). **p<0.01; Student's t-test. (E) Examples of mitotic defects in ducts of NLS-RSK2 mice. Scale Bar=10μm. (F) H&E sections of mammary glands from the NLS-RSK2 mice show numerous indications consistent with neoplastic transformation (red arrows). Scale Bar=10μm. (G) Nuclear size increases in cells within DCIS lesions from NLS-RSK2 mice relative to nuclei from ducts within WT mice. (Bar, median±quartile, n=4 mice/genotype, ≥4 fields/mouse) ***p<0.001; Student's t-test.

Figure 16

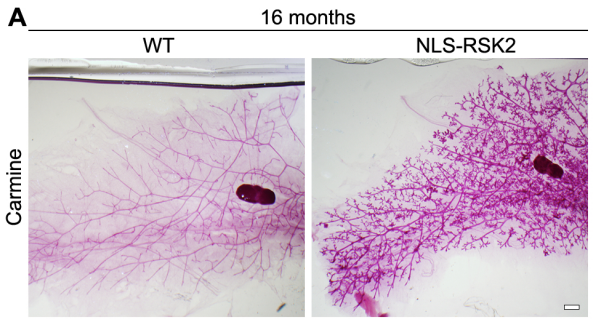
A
16 months
WT
NLS-RSK2
Carmine

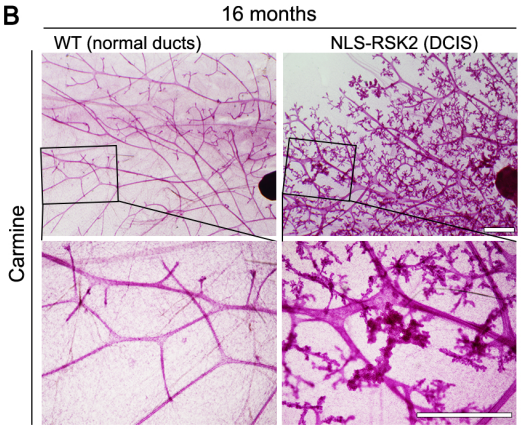
B
16 months
WT (normal ducts)
NLS-RSK2 (DCIS)
Carmine

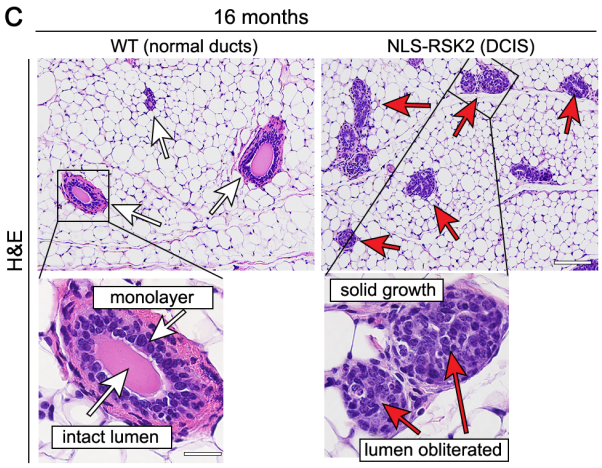
C
16 months
WT (normal ducts)
NLS-RSK2 (DCIS)
H&E
monolayer
intact lumen
solid growth
lumen obliterated

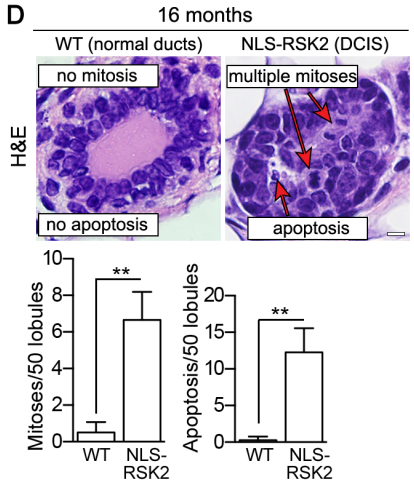
D
16 months
WT (normal ducts)
NLS-RSK2 (DCIS)
H&E
no mitosis
multiple mitoses
no apoptosis
apoptosis
Mitoses/50 lobules
Apoptosis/50 lobules
**
**
WT
NLS-RSK2
WT
NLS-RSK2

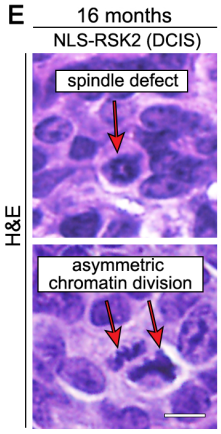
E
16 months
NLS-RSK2 (DCIS)
H&E
spindle defect
asymmetric chromatin division

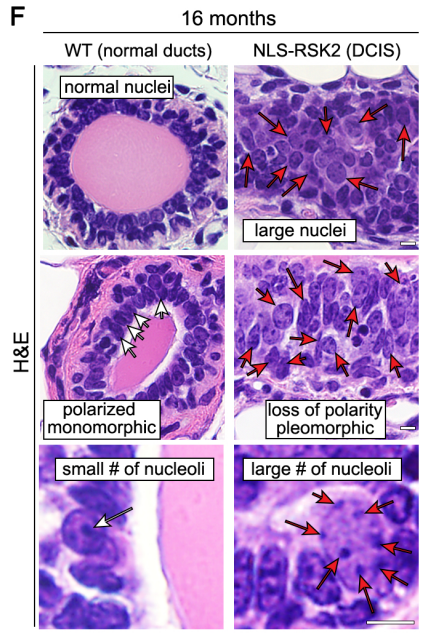
F
16 months
WT (normal ducts)
NLS-RSK2 (DCIS)
H&E
normal nuclei
large nuclei
polarized monomorphic
loss of polarity pleomorphic
small # of nucleoli
large # of nucleoli

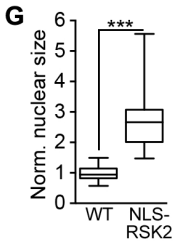
G
Norm. nuclear size
***
WT
NLS-RSK2

Figure 17 Analysis of DCIS in NLS-RSK2 mice

(A) Increased mitosis within the ducts of the NLS-RSK2 mice, as observed by PCNA staining. Scale Bar=20μm. (Bar, median±quartile, n=4 mice/genotype, ≥5 fields/mouse). **p<0.01; Student's t-test. (B) Increased DNA damage was observed by γH2AX staining within the ducts of the NLS-RSK2 mice. Arrow indicates γH2AX+ cell. Scale Bar=20μm (Bar, mean±SD, n=4 mice/genotype, ≥5 fields/mouse). *p<0.05; Student's t-test. (C) DCIS lesions in NLS-RSK2 mice are ER+. Scale Bar=20μm. (D) High grade DCIS incidence in sixteen month old NLS-RSK2 and WT mice. (E) Cells from isolated NLS-RSK2 mice demonstrate higher tumor potential than WT. Sphere cultures generated from mammary cells isolated from WT or NLS-RSK2 mice were cultured and passaged (p). Differential interference contrast (DIC) images are shown. Sphere forming capacity was normalized to WT. Scale Bar=50μm (Bar, median±quartile, n=4 mice/genotype, triplicate) *p<0.05, **p<0.01, Student's t-test. (F) *In vitro* bioluminescence analysis of luciferase transduced spheres demonstrating the linear response with varying cell number for both genotypes. (G) Mammary cells expressing NLS-RSK2 generate metastatic lesions when introduced by IC injection. Equal sphere numbers from (J: p0)) were transduced with luciferase and introduced into NCG mice with bioluminescence imaging performed at the indicated time. (H) Representative *ex vivo* images of the gross anatomy and bioluminescence of lungs from NCG mouse inoculated with spheres generated from sixteen-month old NLS-RSK2 mice. Arrows indicate metastatic lesions. Scale Bar = 1 cm. (I) H&E sections of the lungs from mice injected with NLS-RSK2 spheres show numerous metastatic lesions (outlined). Scale Bar=200μm. (n=3 mice with WT spheres; =4 mice with NLS-RSK2 spheres). p<0.05, Fisher's exact test.

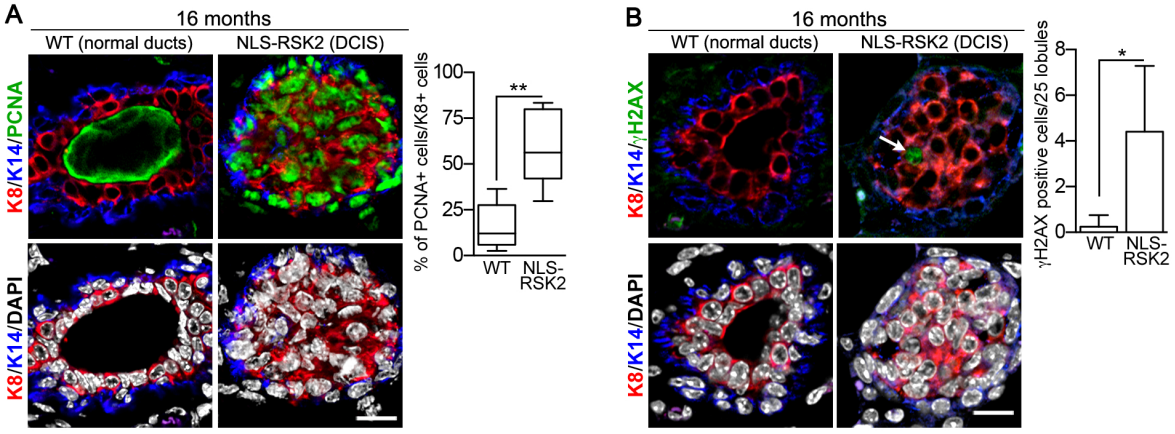

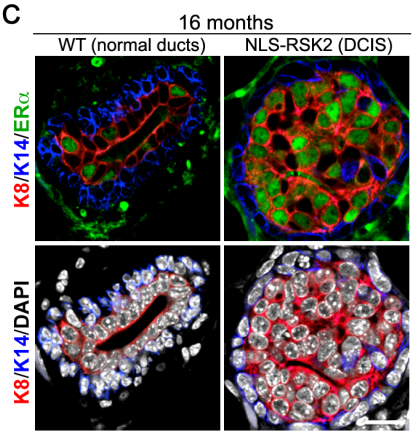

D

16 months

	Normal	High grade DCIS
WT	6	0
NLS-RSK2	5	6

Fisher's exact test: p=0.0427

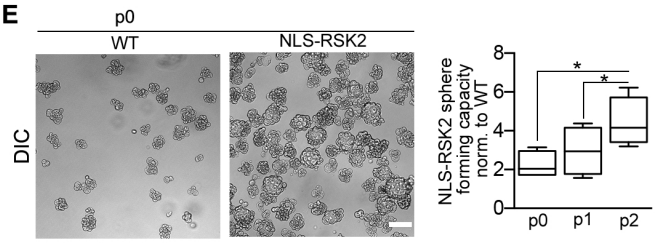

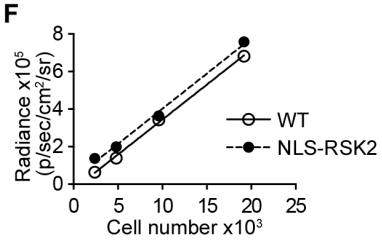

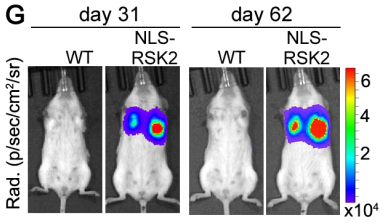

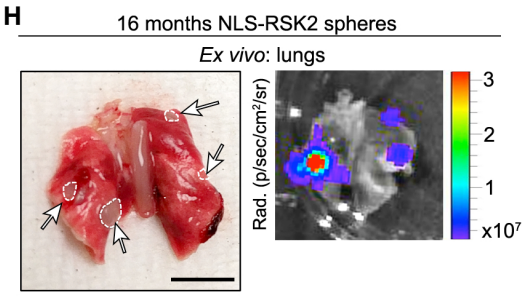

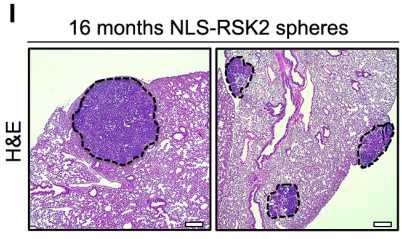

Discussion

Our studies provide a mechanistic basis for the clinical observations that active RSK correlates, with endocrine-therapy responsiveness and increased overall survival in patients with ER+ breast cancer. ERα interacts with residues from 27 to 32 located in the N-terminus of RSK2 to sequester RSK2 in the nucleus. This motif is highly conserved from Mammalia to Aves, which is a hallmark of residues that are important as functional domains. The interaction of RSK2 with ERα, which is disrupted by mutagenesis of RSK2, anti-estrogens, or silencing ERα, allows ERK1/2-activated RSK2 to accumulate to high levels in the nucleus. Loss of RSK2 from the nucleus results in reduced ER+ tumor formation, which is due to the inactivation of the pro-neoplastic transcriptional network comprised of ESR1, EP300, GATA3 and FOXA1 that is critical to maintain ER+ breast cancer [191, 194]. This conclusion is further supported by the ability of the RSK2 gene signature to stratify breast cancer patients according to their ERα status.

RSK2 influences ERα-mediated transcriptional activity via phosphorylation or physical association [24, 55]. The residue, Ser-167, within ERα is a RSK phosphorylation site [55] but a correlation between the phosphorylation of Ser-167 and tumor formation was not observed. However, tumor formation was absolutely dependent on RSK2 nuclear accumulation. Similar to the observations with active RSK, the phosphorylation of Ser-167 is correlated with responsiveness to endocrine-based therapies and overall survival [56, 58, 195] but we propose that this phosphorylation is an indirect biomarker for active RSK2 and therefore, is correlated but not causally related to ER+ breast cancer.

Remarkably, forced expression of RSK2 in normal mammary glands triggered the development of high grade DCIS. In this model transformation occurs with a long latency, which is similar to both human breast cancer and many other transgenic mouse models [193, 196].

We note that although mice developed high grade DCIS, no invasive tumors were identified, perhaps due to a need for additional time or because further genetic or epigenetic events beyond RSK2 are needed for initial invasion of neoplastic cells through the basement membrane into the surrounding stroma. Interestingly, bypassing the intravasation step, demonstrated that nuclear RSK2 supported metastatic tumor growth, indicating that RSK2-dependence is likely selected as an early *in situ* event that helps promote neoplastic transformation and remains essential thereafter to support tumorigenesis once invasive tumor growth has been established.

Chapter 3 ERK1/2-RSK2 signaling is a developmental switch required for estrogen homeostasis

Summary

Estrogen receptor alpha (ERα) is a critical regulator of adult homeostasis. In response to estrogens, ERα is degraded; however, despite the continued presence of estrogen prior to menopause, ERα protein levels are maintained in the adult by an unidentified mechanism. We discovered a negative feedback pathway in which estrogens increase the activity of ERK1/2-RSK2 in the adult mammary gland. Subsequently, activated RSK2 limits ERα -mediated transcription and reduces degradation of ERα through the 26S proteasome pathway. The ERK1/2-RSK2 pathway is temporally activated at the estrus phase during the estrous cycle in the adult. RSK2 is not required to maintain ERα protein levels in juvenile animals. Mammary gland regeneration demonstrated that the reduction in ERα in the RSK2 knockout (RSK2-KO) mice was intrinsic to the epithelium. Oophorectomy or inhibition of the 26S proteasome pathway restored ERα protein levels in the RSK2-KO. Transcriptomic analysis of the mature ER+ population in the mammary gland revealed enrichment for estrogen-responsive genes in the RSK2-KO compared to the wild type. This inappropriate estrogen response resulted in a reduction in alveolar expansion during pregnancy and decreased fertility. These findings establish RSK2 as an essential regulator of estrogen homeostasis in the pre-menopausal adult.

Introduction

Estrogen receptor alpha (ERα) is essential for development and maintenance of the reproductive system but it is now appreciated that ERα-mediated signaling is associated with numerous cancers as well as with metabolic syndrome and type 2 diabetes [150, 197-200]. Estrogen levels are highest at estrus and decrease approximately after ovulation at metestrus with this cycle being repeated until the onset of menopause [201, 202]. *In vitro* or *in vivo* exposure to estrogens results in rapid degradation of ERα by the 26S proteasome pathway, which is required for ERα-mediated transcription [203-207]. Based on these observations it would seem that the constant exposure to estrogens prior to menopause would result in ongoing ERα degradation and result in very low levels of ERα. However, ERα protein levels are maintained during chronic exposure to estrogens [208]. The mechanism that is responsible for maintaining ERα levels in the normal adult female is not known and therefore is a critical gap in our knowledge [209].

Estrogen through ERα positively regulates the expression levels of various growth factors and in turn growth factors are able to increase ERα-mediated transcriptional activity [210, 211]. These results suggest that a negative feedback loop must exist to maintain homeostasis, which is necessary for various metabolic functions and to prepare and to sustain reproduction and lactation [212]. These observations led us to investigate regulatory inputs into the feedback loop between estrogens and growth factors.

We focused on RSK2, a downstream effector of ERK1/2, as RSK2 generates a gene signature that stratifies patients with invasive breast cancer according to the presence of ERα [154]. Furthermore RSK2 regulates a transcriptional network critical to the ER+ lineage in the mammary gland and in a transgenic mouse model forced expression of RSK2 resulted in expansion of the ER+ lineage and high grade ductal carcinoma in situ. As molecular

mechanisms that are important in development are frequently hijacked in cancer, we investigated the contributions of RSK2 to the normal function of the mammary gland.

Unexpectedly, we identified that ERK1/2-RSK2 signaling acts as a developmentally regulated switch that is required for maintaining ERα protein levels in the adult. ERK1/2-RSK2 is temporally activated during the estrous cycle to constrain estrogen responsiveness by inhibiting the transcriptional activity and degradation of ERα. Mammary gland regeneration experiments demonstrated that the requirement for RSK2 was intrinsic to the epithelium. Release of the RSK2-mediated repression lead to enhanced ERα-mediated transcription, which surprisingly, resulted in decreased lactation and fertility. These results are the first to identify a mechanism that identifies how ERα protein levels are maintained in pre-menopausal women.

Materials and Methods

Antibodies, qRT-PCR primers and other critical reagents used in Chapter 3 are listed in Table 5.

Animals

All procedures involving animals were done in accordance with current federal (NIH Guide for Care and Use of Laboratory Animals) and university guidelines and were approved by the University of Virginia and Vanderbilt University Institutional Animal Care and Use Committee.

RSK2 KO mice were obtained from André Hanauer, PhD (Institut de Genetique et Biologie Moleculaire et Cellulaire, C.U. de Strasbourg) [45]. At 6, 8, 10, and 12 weeks virgin female C57BL6/J wild type (WT) or RSK2 KO mice were euthanized and the mammary glands or indicated organs analyzed.

Estrous cycle stages were determined by vaginal swabs as described [213, 214]. Briefly, estrous cycling in female mice was promoted by the addition of bedding from a male cage beginning two weeks prior to the experiment. The vaginal opening was flushed with 20μL of sterile PBS three to five times and the final flush was spotted onto a microscope slide. Cytology was determined using a light microscope. For all experiments requiring matched estrous stages, the cycles were monitored for 2 weeks prior to end point to ensure continuous cycling. Estrous stage was determined at 7-9AM and animals were euthanized at 9-11AM.

For pup swap experiments, virgin female mice were introduced into a male cage for breeding and the cages were monitored daily for new litters. On postnatal day 1, half the pups in a litter from RSK2 WT and RSK2 KO dams were cross fostered. The half of the litter that were not cross fostered served as control mice and were handled identically to experimental mice but were returned to their own parents. On postnatal day 21 the litters were weighed, photo-documented, tagged, and genotyped. For fertility assessment, adult virgin female mice

were introduced to a male cage. The number of female mice that gave birth within 4 weeks and the number of pups birthed per litter was recorded.

For timed collection of lactating glands, virgin female mice were introduced into a male cage for breeding and the cages were monitored daily for new litters. On postnatal day 1, dams were euthanized and mammary glands were fixed and analyzed. Epithelial area was quantified by measuring the percentage of fat pad area that was occupied by epithelium using ImageJ software.

For assessment of ductal branching during development, the 4th mammary gland from female mice at indicated age were fixed overnight in Carnoy's fixative o/n. The fixative was replaced with 70% EtOH, gradually rinsed in water, and stained o/n in Carmine Alum solution. Stained glands were dehydrated in increasing ethanol concentrations and cleared using SafeClear prior to mounting with Permount. For ductal distance the length from the nipple to the tip of the longest duct was measured. For branching the number of secondary branches along the longest primary branch were counted.

For oophorectomies, 6 wk female mice were anesthetized and a bilateral incision along the back was used to remove the ovaries and oviduct. For sham operations, the mice were treated identically to oophorectomy animals except the ovaries were not removed. At 12 weeks the mammary glands were collected in estrus stage and mammary glands analyzed.

For in vivo inhibition of 26S proteasome, 12wk female mice in estrus were injected intraperitoneally with vehicle or the proteasome inhibitor PS-341 at 5 mg/kg in 2% DMSO, 30% PEG, and 68% saline and 4h later the animals were euthanized and organscollected and analyzed.

For mammary gland regenerations, mammary epithelial cells were isolated as described before [162]with modifications. Briefly, mammary glands isolated from donor mice were minced,

and digested in DMEM/F12 supplemented with 2mg/ml Collagenase A and 100U/ml Pen/Strep for 2.5h in 37°C 5% CO_2 incubator. Digested material was pelleted at 180g for 5 min and the pellet was resuspended in DNAse I (1000U/ml) for 3-5 min in 37°C 5% CO_2 incubator. Fetal bovine serum (FBS) was added and the digested tissue was pelleted at 180g for 10 min. The pellet was washed with phosphate-buffer saline, pelleted, resuspended in Accumax and placed in Thermomixer at 37°C for 10 min. Digested material was pelleted at 180g for 3 min, resuspended in 5x trypsin for 5 min at 37°C. Trypsin was quenched with FBS and cells were pelleted and resuspended in PBS or DMEM/F12. The cell preparation was filtered through 70-mm mesh to obtain single cell suspension. For mammary gland regenerations, $4x10^7$ cells/ml of single cells in DMEM/F12 were mixed 1:1 with matrigel. 10 μL of cell suspension in matrigel was injected into the cleared 4th mammary fat pad of a recipient 3wk old mouse as described before [215]. Mouse estrous cycle was monitored and the regenerated mammary glands were collected and analyzed at estrus 20wks post injection. Alternatively, mice were mated and glands from pregnant animals analyzed at lactation d1

Fluorescence Activated Cell Sorting (FACS)

For FACS, single epithelial cells (10^6 cells/ml) obtained from mammary glands in PBS were incubated with Cell Trace Violet (1μM) and Zombie Yellow (1:250) for 20 min at room temperature. Cells were washed and resuspended in 5% FBS in PBS. Cells were blocked with 10% normal rat serum in 5%FBS for 10 min at 4°C, followed by incubation with biotin-conjugated primary antibodies against lineage markers for 10 min at 4°C. The cells were incubated with primary antibodies for 20 min at 4oC, washed and resuspended in 5%FBS. Cells were analyzed using FACSCantoII or sorted using FACSAriaII. Flow cytometry data were analyzed using Cytobank version 6.2.

EdU labeling was performed as described [216]. Birefly, mice in proestrus were injected intraperitoneally with 10mg/ml 5-ethynyl-2'-deoxyuridine (EdU) in PBS (100mg/kg) and then

administered EdU via the drinking water (1mg/ml). The estrus stage was monitored and mammary glands were isolated in metestrus (2 days after EdU injection). Alternatively, EdU labeling in pregnancy was performed as described [217] with modifications. The onset pregnancy was determined by vaginal plugs and mice were injected with EdU (10mg/ml; 100mg/kg) on day 3 of pregnancy and 48h later mammary glands were isolated and analyzed. Mammary cells were isolated as described above and analyzed for EdU incorporation using the Click-iT Edu Flow Cytometry Assay Kit according to manufacturer's instructions, followed by the antibody staining as described above carried out in 1xClick-iT saponin based permeabilization buffer.

Immunostaining

Mouse organs were fixed in buffered 10% formalin for 2d and then placed in 70% ethanol. The fixed samples were paraffin-embedded, and 5-μm sections were prepared by the Translational Pathology Shared Resource at Vanderbilt University. The sections were deparaffinized and subject to antigen retrieval in citrate buffer pH 6.0 or pH 7.0. The sections were blocked in 10% bovine serum albumin (BSA) in PBS and incubated with primary antibody in 3% BSA in PBS o/n at 4^{o}C. The sections were washed three times and incubated with secondary antibody for 1h in room temperature.

For immunofluorescence staining, the sections were washed and DNA stained with Hoechst in PBS for 10 min. The coverslips were mounted using Fluoro-Gel (Electron Microscopy Sciences).

For immunohistochemistry, the sections were washed once with 50mM Tris pH 7.6 and incubated for 15-60s with 6mg/ml 3,3'-diaminobenzidine in 0.05% H_2O_2 in 50mM Tris pH 7.6 at room temperature. The sections were washed with double deionized (dd) water for 5 min, stained with hematoxylin for 10s, briefly washed with water and placed in 0.5% NH_4OH for 10s.

The sections were washed with dd water, dehydrated by increasing ethanol concentrations and placed in SafeClear for 2min prior to coverslip mounting with Cytoseal XYL.

RNAseq

For RNA isolation, $5x10^4$ $EpCAM^{hi}CD49f^{+}Sca1^{+}Cd49b^{-}$ cells were FACS sorted and total RNA extraction (RNeasy Micro Kit) was performed. The RNA quality was tested using Agilent 100 Bioanalyzer (RIN 8). Libraries were constructed and sequenced by Genewiz LLC. Reads were aligned to the mm10 mouse genome with STAR, the transcripts were assembled using Gencode version 15 as gene models. Genes and transcripts were quantified with HTSeq. Two samples were clear outliers and were discarded. Batch correction was done with SVA, and differential gene expression analysis was performed with DESeq2. Gene set enrichment was done with GSEA using MSigDB and GSVA using GSKB mouse gene sets.

Quantitative real time PCR (qRT-PCR)

QRT-PCR was performed as previously described [154]. 1μg of RNA isolated as for RNAseq was reversely transcribed using High Capacity cDNA Reverse Transcription Kit. QRT-PCR was performed using IQ RealTime SyberGreen PCR Supermix on C1000Thermal Cycler CFX96 Real-Time System (BioRad Laboratories) and $\Delta\Delta C_t$ was calculated using GAPDH as a control. QRT-PCR primers are listed in the Table 5.

Table 5 Reagents used in Chapter 3

REAGENT or RESOURCE	SOURCE	IDENTIFIER
Antibodies		
Rat anti-keratin 8 (IF)	University of Iowa	TROMA-I
Chicken anti-keratin14 (IF)	BioLegend	SIG-3476
Rabbit anti-pRSK (Thr359/Ser363) (IF)	Santa Cruz Biotechnology, Inc.	sc-12898-R
Mouse anti-ERα 6F11 (IF)	Thermo Fisher Scientific Inc.	MA5-13304
Normal rabbit IgG (IP)	EMD Millipore	12-370
Rabbit anit-pERK1/2 (pTEpY)	Promega	V803A
Mouse anti-GATA3	Thermo Fisher Scientific Inc.	1A12-1D9
Donkey anti-rabbit 647	Invitrogen	A31573
Donkey anti-mouse 647	Invitrogen	A31571
Goat anti-rat 546	Invitrogen	A11081
Goat anti-chicken 488	Invitrogen	A11039
Biotin anti-CD140	Biolegend	APA5
Biotin anti-CD31	Biolegend	MEC13.3
Biotin anti-Ter-119	Biolegend	TER-119
Biotin anti-CD45	Biolegend	30-F11
Brilliant Violet 510 Streptavidin	Biolegend	405233
Anti-Sca1-PerCP	Biolegend	405233
Anti-Sca1-FITC	Biolegend	D7
Anti-CD49b-APC/Cy7	Biolegend	DX5
Anti-EpCAM-APC	Biolegend	G8.8
Anti-CD49f-PE/Cy7	Biolegend	GoH3
Chemicals, Peptides, and Recombinant Proteins		
Cell Trace Violet	Life Technologies Corp.	C34557
Zombie Yellow	Biolegend	423104
EdU (5-Ethynyl-2'-deoxyuridine)	Life Technologies Corp.	NEO87011604
Bortezomib (PS-341)	Calbiochem	50-431-40001
Experimental Models: Organisms/Strains		
Mouse: C57BL/6J$^{RSK2-/-}$ (RSK2-KO)	[45]	Andre Hanauer, PhD.
Commercial Assays		
Click-iT™ Plus EdU Alexa Fluor™ 488 Flow Cytometry Assay Kit	Thermo Fisher Scientific Inc.	C10632
RNeasy Micro Kit	Qiagen	74004

qRT-PCR primers		
f-GAPDHm	AGAACATCATCCCTGCATCCA	
r-GAPDHm	CAGATCCACGACGGACACATT	
f-GATA3m	GATGTAAGTCGAGGCCCAAG	
r-GATA3m	GCAGGCATTGCAAAGGTAGT	
f-ESR1m	TTACGAAGTGGGCATGATGA	
r-ESR1m	CCTGAAGCACCCATTTCATT	
Software and Algorithms		
LSM-FCS/ ZEN	Carl Zeiss, Inc.	N/A
Openlab 5.5.0 / Volocity 6.2.1	PerkinElmer Inc.	N/A
GraphPad Prism 6.0a	GraphPad Spftware Inc.	N/A
Morpheus	Broad Institute	https://software.broadinstitute.org/morpheus/

Results

RSK2 regulates alveolar expansion via a mammary epithelium intrinsic mechanism

Reduced pup size was observed in homozygous RSK2 knockout (RSK2-KO) crosses compared to wild type B57BL/6 (WT) (Fig. 18A). Importantly, decreased pup size could be rescued by fostering RSK2-KO pups to WT dams, which argues for reduced lactation in the RSK2-KO dams rather than a developmental defect in the offspring. In response to pregnancy, alveolar expansion occurs [218] and, consistent with a defect in lactation, decreased expansion was observed in the whole animal RSK2-KO (Fig. 18B). To evaluate whether this defect was intrinsic to the mammary gland, regenerated glands were analyzed in which mammary epithelial cells (MECs) from WT and RSK2-KO mice were separately introduced into the cleared 4th mammary fat pads of a WT recipient. The glands from either transplanted cells regenerated to similar extents (Fig. 18C); however, in response to pregnancy the glands regenerated from the RSK2-KO epithelium demonstrated reduced expansion (Fig. 18D).

To identify the mechanism that resulted in decreased alveolar expansion we analyzed adult mammary glands by fluorescence-activated cell sorting (FACS). Staging of the estrous cycle was determined by analysis of vaginal cytology and uterine wet weight [202] (Fig. 18E). WT and RSK2-KO mice moved through the four stages of the estrous cycle in a similar manner (Fig. 18F). A novel FACS protocol that allowing the simultaneous analysis of WT and RSK2-KO MECs (Fig. 18G) was developed in which one of the genotypes was permanently marked and equal numbers of cells from the marked and unmarked genotypes were mixed. The marked genotype was varied, and live cells and lineage-negative MECs determined (Fig. 18H). The luminal and basal populations were clearly separated using epithelial cell adhesion molecule (EpCAM) and integrin alpha 6 (CD49f) (Fig. 19B) and the distributions were similar in adult WT and RSK2-KO mice at each stage of the estrous cycle

Figure 18 RSK2 is necessary for alveolar expansion*

(A) Pups nursed by RSK2-KO dams are smaller than those nursed by WT dams. Weanling weight at 21 days nursed by a dam with the indicated genotype. (Bar, median ± quartile, n=3 litters/dam genotype). (B) Alveolar expansion is reduced in RSK2-KO dams as shown by H&E stains of mammary glands isolated from dams 1 d after birth (Bar, median ± quartile, n ≥ 3 mice/genotype). Scale bar = 1 cm. (D) Alveolar expansion is reduced in mammary glands regenerated from RSK2-KO mammary epithelial cells as shown by the H&E stains of mammary glands isolated from the same WT dam 1 d after birth. Scale bar = 1 cm. (E) Uterine wet weight is similar in WT and RSK2-KO. (Bar, median ± quartile, n≥8 mice/genotype). (F) Cycling through the estrous cycle is similar in WT and RSK2-KO mice. Left graph: (Bar, mean ± stdev, n≥10 mice/genotype); Right graph: Representative cycle. (G) Schematic of FACS protocol. (H) Gating strategy for flow cytometry analysis and sorting of mouse mammary epithelial. Cells were gated for forward (FCS-A) and side (SSC-A) scatter to remove debris. Single cells (p2) gated by FSC-H and SSC-H were then gated for live cells (ZombieYellow negative). Lineage$^+$ (Cd140a$^+$; CD31$^+$; Ter-119$^+$; and CD45$^+$) cells were gated out.

*Zach Sandusky contributed panels A-F

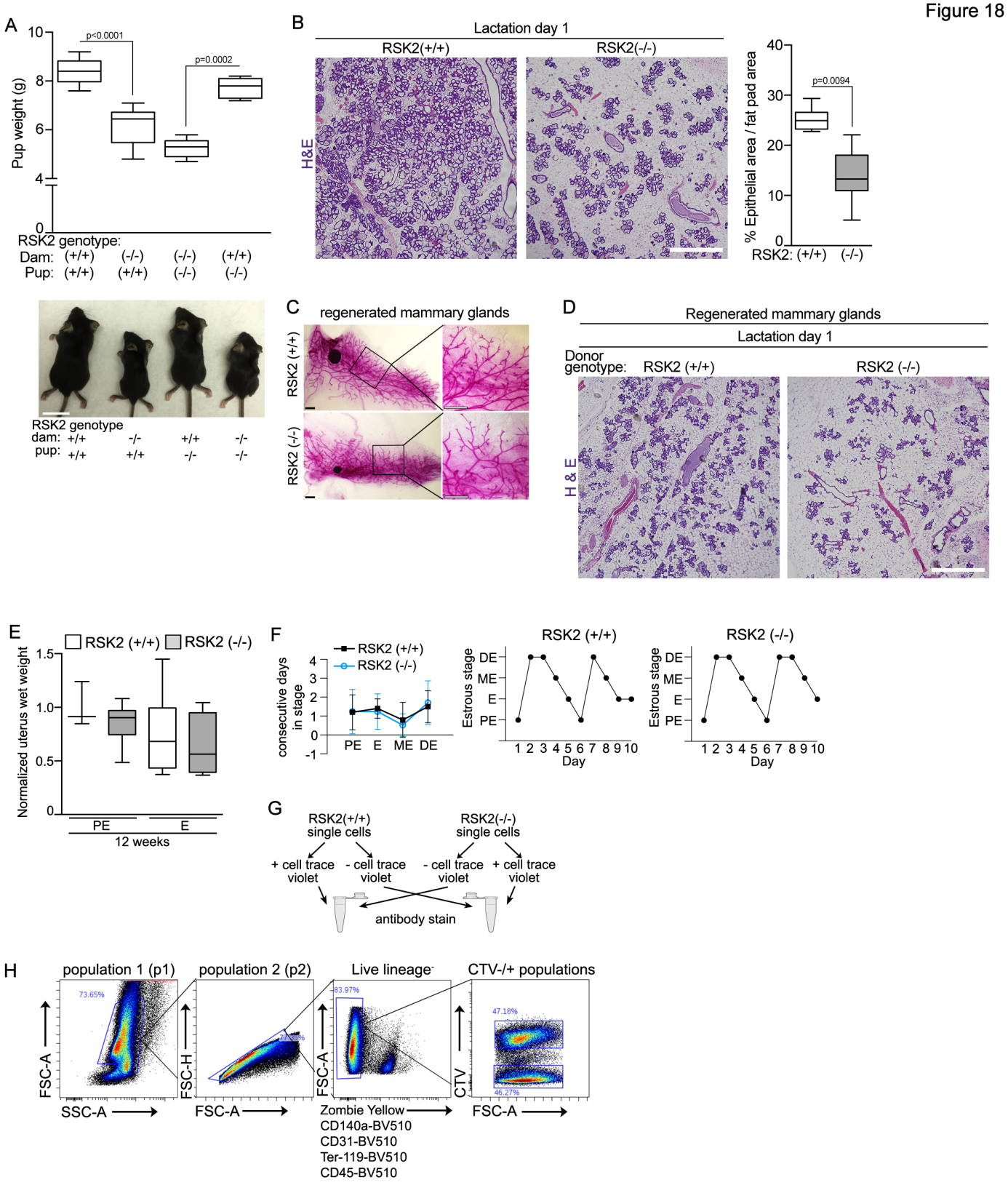
A
Pup weight (g)
p<0.0001
p=0.0002
RSK2 genotype:
Dam: (+/+) (-/-) (-/-) (+/+)
Pup: (+/+) (+/+) (-/-) (-/-)
B
Lactation day 1
RSK2(+/+)
RSK2(-/-)
H&E
% Epithelial area / fat pad area
p=0.0094
RSK2: (+/+) (-/-)
RSK2 genotype
dam: +/+ -/- +/+ -/-
pup: +/+ +/+ -/- -/-
C
regenerated mammary glands
RSK2 (+/+)
RSK2 (-/-)
D
Regenerated mammary glands
Lactation day 1
Donor genotype: RSK2 (+/+)
RSK2 (-/-)
H & E
E
RSK2 (+/+) RSK2 (-/-)
Normalized uterus wet weight
PE
E
12 weeks
F
RSK2 (+/+)
RSK2 (-/-)
consecutive days in stage
PE E ME DE
Estrous stage
DE
ME
E
PE
1 2 3 4 5 6 7 8 9 10
Day
G
RSK2(+/+) single cells
RSK2(-/-) single cells
+ cell trace violet
- cell trace violet
- cell trace violet
+ cell trace violet
antibody stain
H
population 1 (p1)
population 2 (p2)
Live lineage-
CTV-/+ populations
73.65%
83.97%
47.18%
46.27%
FSC-A
SSC-A
FSC-H
CTV
Zombie Yellow
CD140a-BV510
CD31-BV510
Ter-119-BV510
CD45-BV510

Figure 19 RSK2 maintains the EpCAM^{hi}CD49f^{+}Sca1^{+}CD49b^{-} (NCL) population within the adult mammary gland throughout the estrous cycle

(A) FACS analysis of luminal and basal epithelial populations in the mammary gland. (Bar, median ± quartile, n≥4 mice/genotype and stage). (B) FACS analysis of adult mammary glands isolated from females during estrus. Gating strategy of luminal cells by further subdivision using Sca-1 and CD49b. The percentage of NCL cells within the luminal population at estrus decreases in adult RSK2-KO mice (Bar, median ± quartile, n ≥ 6 mice/genotype). (C) Fluorescence minus one strategy for determining the gates for Sca1 and CD49b. (D) Loss of RSK2 results in a reduction in the percentage of NCL cells at all stages of the estrous cycle in adult mammary glands (Bar, median ± quartile, n≥3 mice/genotype and stage). (E) FACS analysis of luminal progenitor and undefined epithelial populations. (Bar, median ± quartile, n≥3 mice/genotype and stage). (F) The percentage of the NCL population within the luminal population also decreases in regenerated glands. (Bar, median ± quartile, n=3 mice). (G) In RSK2-KO mice the ERα protein levels are decreased in cells isolated from the NCL population (Bar, median ± quartile, n=3 mice/genotype, > 20 cells/mouse). Scale bar = 10 μm. (H) Loss of RSK2 decreases the percentage of ER+ cells in the NCL population. (n=3 mice/genotype, > 20 cells/mouse).

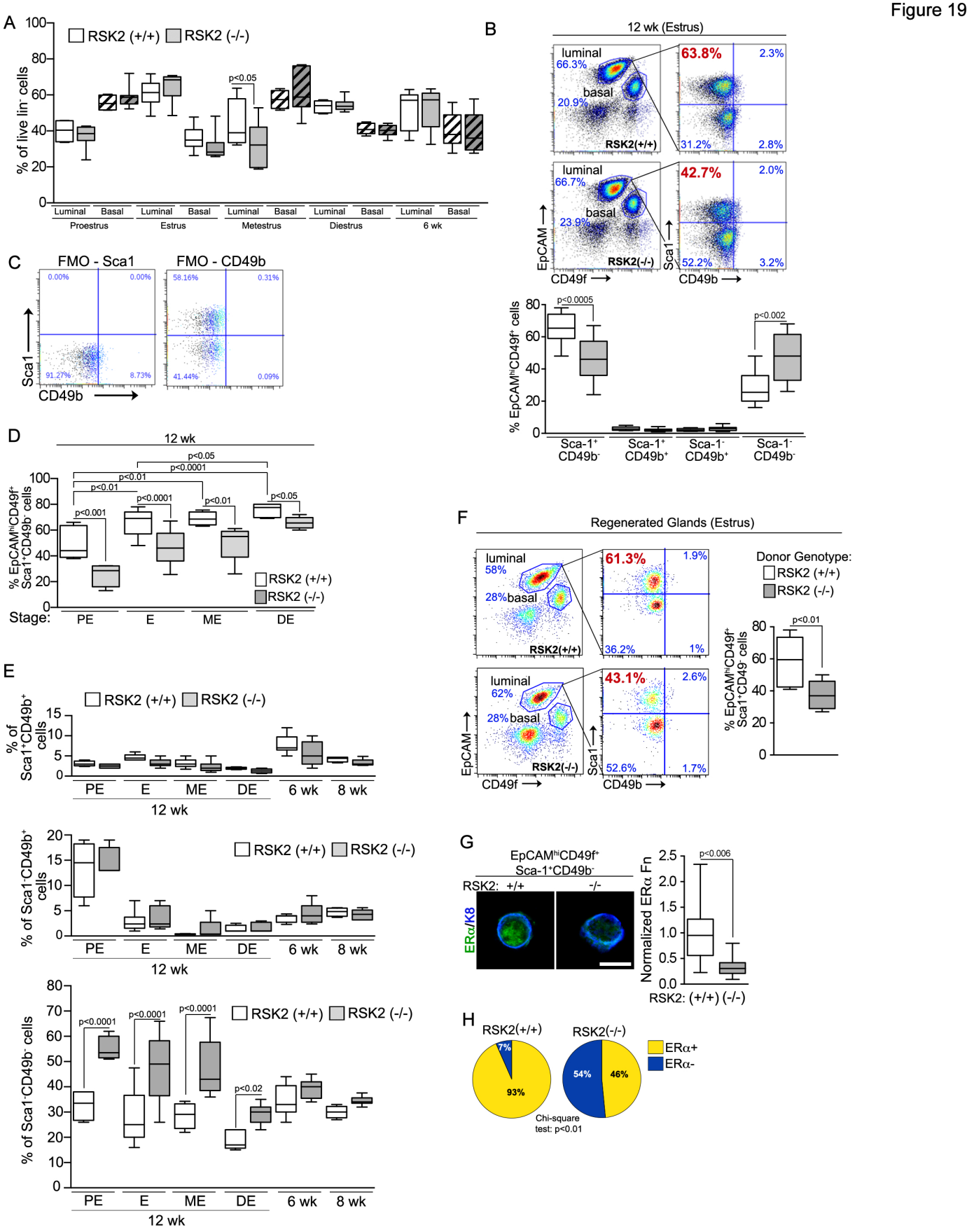
A
RSK2 (+/+) RSK2 (-/-)
% of live lin- cells
p<0.05
Luminal Basal Luminal Basal Luminal Basal Luminal Basal Luminal Basal
Proestrus Estrus Metestrus Diestrus 6 wk
B
12 wk (Estrus)
luminal
66.3%
basal
20.9%
RSK2(+/+)
63.8%
2.3%
31.2%
2.8%
luminal
66.7%
basal
23.9%
RSK2(-/-)
42.7%
2.0%
52.2%
3.2%
EpCAM
CD49f
Sca1
CD49b
% EpCAMhiCD49f+ cells
p<0.0005
p<0.002
Sca-1+ CD49b-
Sca-1+ CD49b+
Sca-1- CD49b+
Sca-1- CD49b-
C
FMO - Sca1
FMO - CD49b
0.00%
0.00%
91.27%
8.73%
58.16%
0.31%
41.44%
0.09%
Sca1
CD49b
D
12 wk
% EpCAMhiCD49f+ Sca1+CD49b- cells
p<0.05
p<0.0001
p<0.01
p<0.01
p<0.0001
p<0.01
p<0.05
p<0.001
RSK2 (+/+)
RSK2 (-/-)
Stage:
PE E ME DE
E
RSK2 (+/+) RSK2 (-/-)
% of Sca1+CD49b+ cells
PE E ME DE 6 wk 8 wk
12 wk
% of Sca1-CD49b+ cells
% of Sca1-CD49b- cells
p<0.0001
p<0.0001
p<0.0001
p<0.02
F
Regenerated Glands (Estrus)
luminal
58%
28%basal
RSK2(+/+)
61.3%
1.9%
36.2%
1%
luminal
62%
28%basal
RSK2(-/-)
43.1%
2.6%
52.6%
1.7%
EpCAM
CD49f
Sca1
CD49b
Donor Genotype:
RSK2 (+/+)
RSK2 (-/-)
% EpCAMhiCD49f+ Sca1+CD49- cells
p<0.01
G
EpCAMhiCD49f+
Sca-1+CD49b-
RSK2: +/+ -/-
ERα/K8
Normalized ERα Fn
p<0.006
RSK2: (+/+) (-/-)
H
RSK2(+/+)
RSK2(-/-)
7%
93%
54%
46%
ERα+
ERα-
Chi-square
test: p<0.01

(Fig. 19A). Further fractionation of the luminal cells by stem cells antigen-1 (Sca1) and integrin alpha 2 (CD49b) [219] resulted in four populations with the gates for each experiment established using fluorescence minus one strategy (Fig. 19C). The non-clonogenic luminal (NCL) population, defined by its lack of colony-forming potential in vitro and engrafting ability in vivo, is $EpCAM^{hi}CD49f^{+}Sca1^{+}CD49b^{-}$. The $EpCAM^{hi}CD49f^{+}Sca^{-}CD49b^{+}$ and $EpCAM^{hi}CD49f^{+}Sca^{+}CD49b^{+}$ are luminal progenitors, which express low or high levels of luminal differentiation markers, respectively [216]. The $EpCAM^{hi}CD49f^{+}Sca^{-}Cd49b^{-}$ population is currently undefined. At estrus the NCL population was decreased in the RSK2-KO with a concomitant increase in the undefined population but no change in either luminal progenitor population (Fig. 19B). These results were consistent across the estrous cycle (Fig. 19D, E). In regenerated glands loss of RSK2 also resulted in a decrease in the NCL population (Fig. 19F). Based on these results we hypothesized that the ER+ population was reduced in the RSK2-KO glands, which would be consistent with previous observations that the NCL population primarily consists of ER+ cells [216] and that the ER+ population act as sensor cells to induce alveolar expansion during pregnancy [210].

RSK2 maintains the ER+ population in the adult mammary gland

By quantitative immunofluorescence (IF) we found decreased ERα protein levels and a reduction in the number of ER+ cells in the FACS sorted NCL population of RSK2-KO mammary glands (Fig. 19G, H). Analysis of the mammary gland in situ revealed that in the WT the protein levels of ERα varied during the estrous cycle with low levels at proestrus and estrus and the highest at diestrus (Fig. 20A, B). The ERα protein levels and the number of ER+ cells were reduced at all stages of the estrous cycle in the RSK2-KO compared to the WT (Fig. 20A-C), which is consistent with the FACS data showing a reduction in the RSK2-KO NCL

Figure 20 RSK2 regulates ERα protein levels in the adult mammary gland throughout the estrous cycle

(A*) The levels of ERα protein expression are reduced in RSK2-KO at all stages of the estrous cycle in adult mammary glands. ERα protein levels were normalized to those observed in the W.T. mice at proestrous (n≥3 mice/genotype and stage). Scale bar = 20 μm. (B) Summary of ERα protein levels summarized by individual mice. ERα protein levels were normalized to those observed in the W.T. mice at proestrous (Bar, median ± quartile, n≥3 mice/genotype and stage). (C) Loss of RSK2 results in a decrease in the number of ER+ cells relative to K8+ cells at all stages of the estrous cycle in adult mammary glands (Bar, median ± quartile, n ≥ 4).
*Zach Sandusky assisted with panels A and C

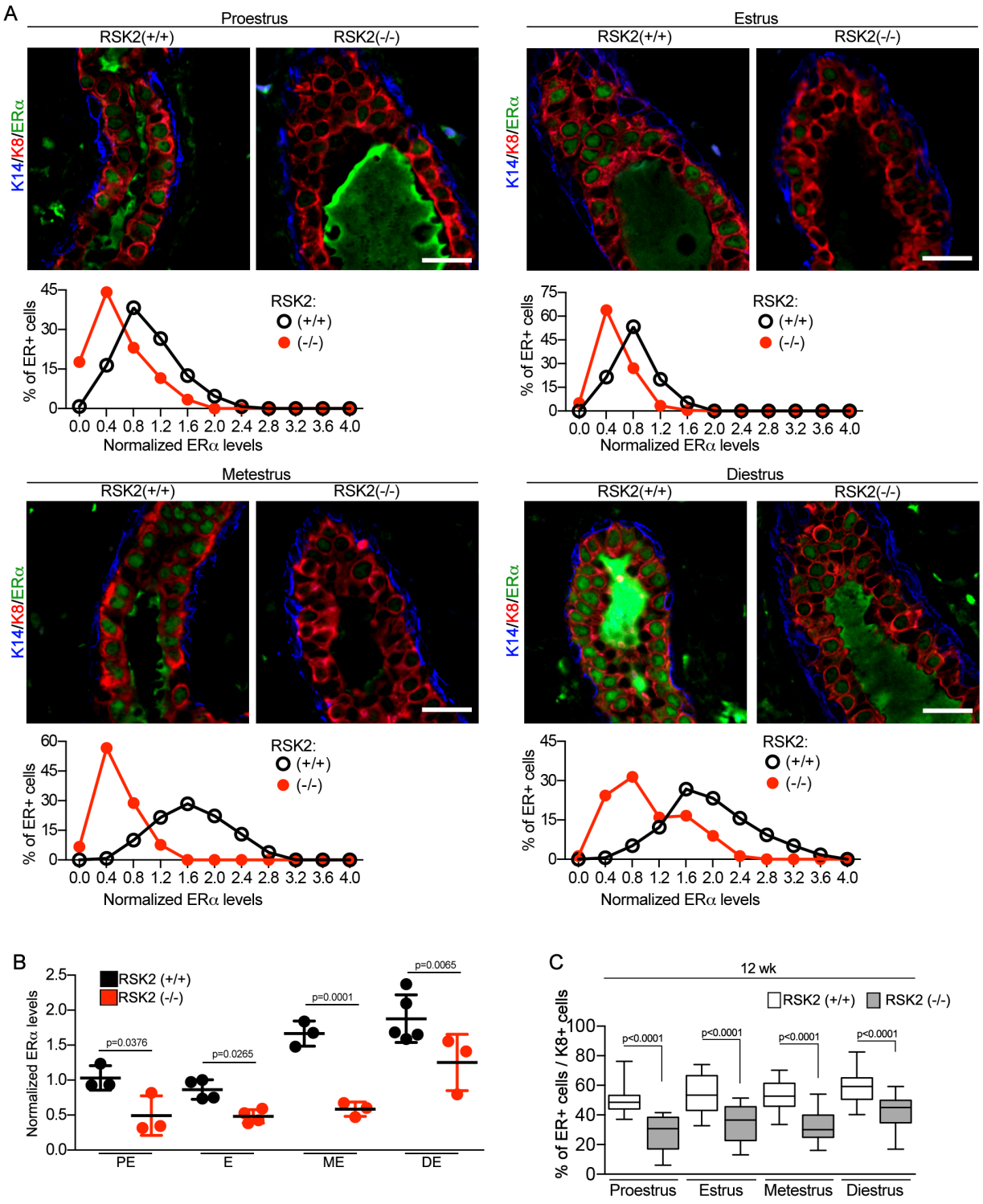
A
Proestrus
RSK2(+/+)
RSK2(-/-)
K14/K8/ERα
% of ER+ cells
Normalized ERα levels
RSK2:
(+/+)
(-/-)
Estrus
Metestrus
Diestrus
B
RSK2 (+/+)
RSK2 (-/-)
Normalized ERα levels
p=0.0376
p=0.0265
p=0.0001
p=0.0065
PE
E
ME
DE
C
12 wk
% of ER+ cells / K8+ cells
p<0.0001
Proestrus
Estrus
Metestrus
Diestrus

population. As ERα is absolutely required for mammary gland development [149] we analyzed gland development at the macroscopic level. No detectable difference in the expansion of the mammary gland into the fat pad or branching during development was observed (Fig. 21A). Analysis by FACS showed that the NCL populations as well as the luminal progenitor and undefined populations were similar between RSK2-KO and WT in juveniles (Fig. 21B, 19A, 19E). Consistent with these data, in situ analysis of the juvenile mammary glands showed similar protein levels of ERα and number of ER+ cells were present in the RSK2-KO and WT (Fig. 21C). Thus, the absence of a developmental defect is explained by the observations that RSK2 regulates the NCL population only in the adult.

ERK1/2-RSK2 signaling is dependent on estrogens

At the onset of puberty estradiol (E_2) increases the levels of growth factors [210], which will result in RSK activation through its upstream activator, ERK1/2 [220]. C57BL/6J mice initiate cycling by ~ six weeks [221], although we observed that cycling was irregular until ten weeks of age. Interestingly, ERK1/2 was not significantly active until the animals were ten to twelve weeks old and the levels of active ERK1/2 were similar between the WT and RSK2-KO at the same age (Figs. 22A-C). A causal relationship between E_2 and ERK1/2 activity was demonstrated by the observations that oophorectomy prevented ERK1/2 activation (Fig. 22D). Thus the ability of E_2 to activate ERK1/2 appears as the mice mature and then ERK1/2 activity levels parallel changes in E_2 levels during the estrous cycle (Fig. 22E) [222]. Active ERK1/2 was primarily confined to the luminal compartment and was present in ER+ cells (Fig. 22F). To confirm that RSK was activated in response to ERK1/2 in the WT mammary gland an anti-active RSK antibody was used (Fig. 22G). This antibody detects all members of the RSK family; however, active RSK was almost not detectable in the adult RSK2-KO mammary glands indicating that RSK2 is the predominant active RSK isoform. These results demonstrate that E_2

is required to activate ERK1/2-RSK2 signaling and this activation corresponds with the ability of RSK2 to regulate ERα protein levels (Figs. 21C, 22C).

Figure 21 RSK2 regulation of ERα is specific to the adult

(A*) Mammary gland development is similar in WT and RSK2-KO. (Bar, median ± quartile, n≥2 mice/genotype). Scale bar = 2mm. (B) The percentage of NCL cells within the luminal population is similar between WT and RSK2-KO juvenile females (Bar, median ± quartile, n ≥ 3 mice/genotype and age group). (C) The number of ERα cells are similar in WT and RSK2-KO juvenile females (Bar, median ± quartile, n=3 mice/genotype).

*Zach Sandusky contributed to panel A and assisted with panel C

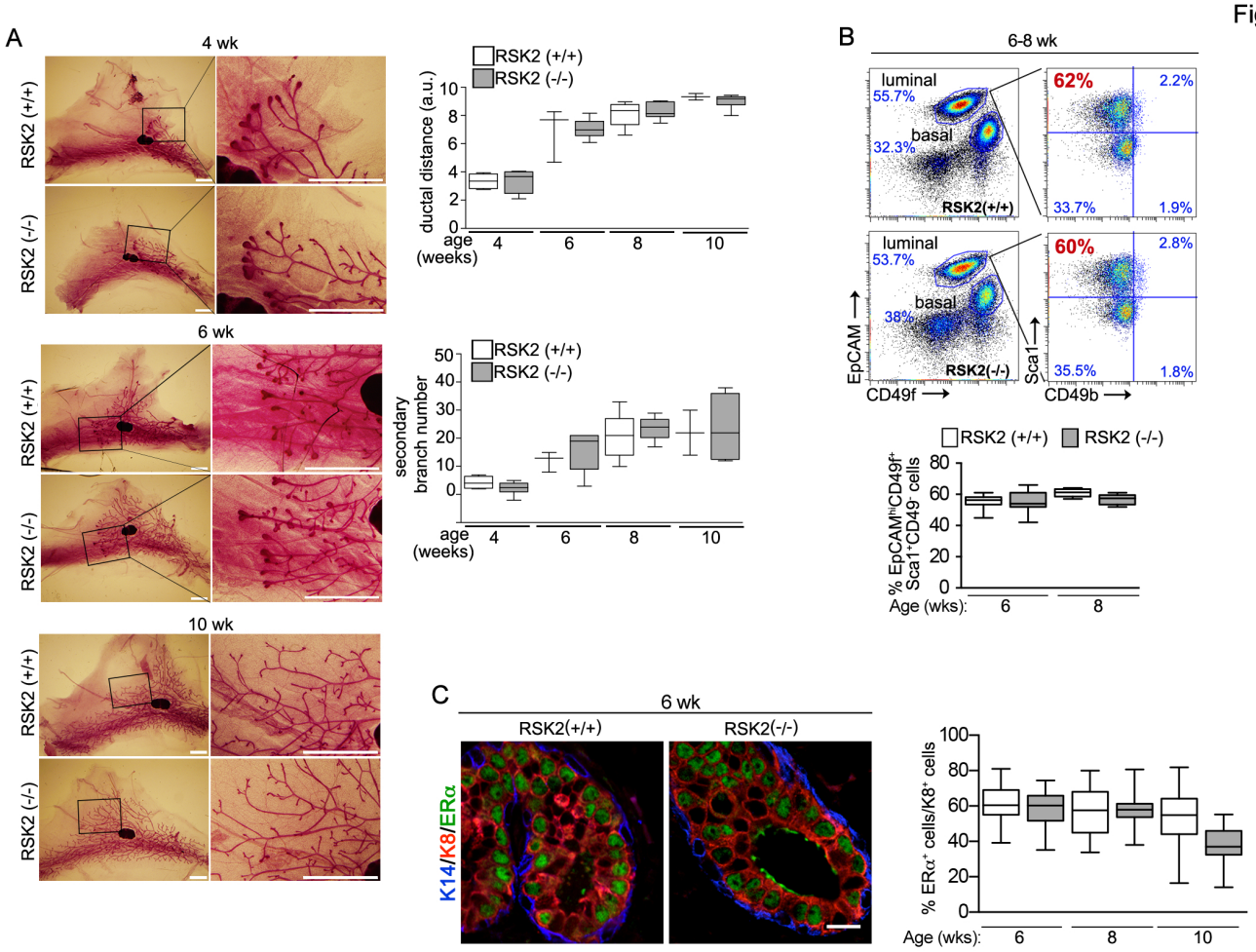
A
4 wk
RSK2 (+/+)
RSK2 (-/-)
6 wk
10 wk
RSK2 (+/+)
RSK2 (-/-)
ductal distance (a.u.)
age (weeks)
secondary branch number
B
6-8 wk
luminal
basal
55.7%
32.3%
62%
2.2%
33.7%
1.9%
RSK2(+/+)
53.7%
38%
60%
2.8%
35.5%
1.8%
RSK2(-/-)
EpCAM
CD49f
Sca1
CD49b
% EpCAM^hCD49f^+ Sca1^+CD49^- cells
Age (wks):
C
6 wk
RSK2(+/+)
RSK2(-/-)
K14/K8/ERα
% ERα^+ cells/K8^+ cells

Figure 22 ERK1/2-RSK2 signaling is activated only in the adult mammary gland*

(A) Activation of ERK1/2 occurs in the adult mammary gland. (B) Loss of RSK2 does not alter ERK1/2 activity in the adult mammary gland. (C) ERK1/2 activity is increased in the adult compared to juvenile animals (Bar, median ± quartile, n ≥2 mice/genotype and age). (D) ERK1/2 activity is highest in the adult mammary gland in females during estrus compared to diestrus (Bar, median ± quartile, n=4 mice/genotype). (E) ERK1/2 activity is dependent on ovarian function. (F) The image on the right is shown without K8 to facilitate the visualization of ER+ and pERK1/2. Serial sections were necessary to avoid antibody interference. Scale bar = 20 μm. (G) Active nuclear RSK2 is the predominant RSK in adult mammary glands.

*Zach Sandusky contributed Figure 22.

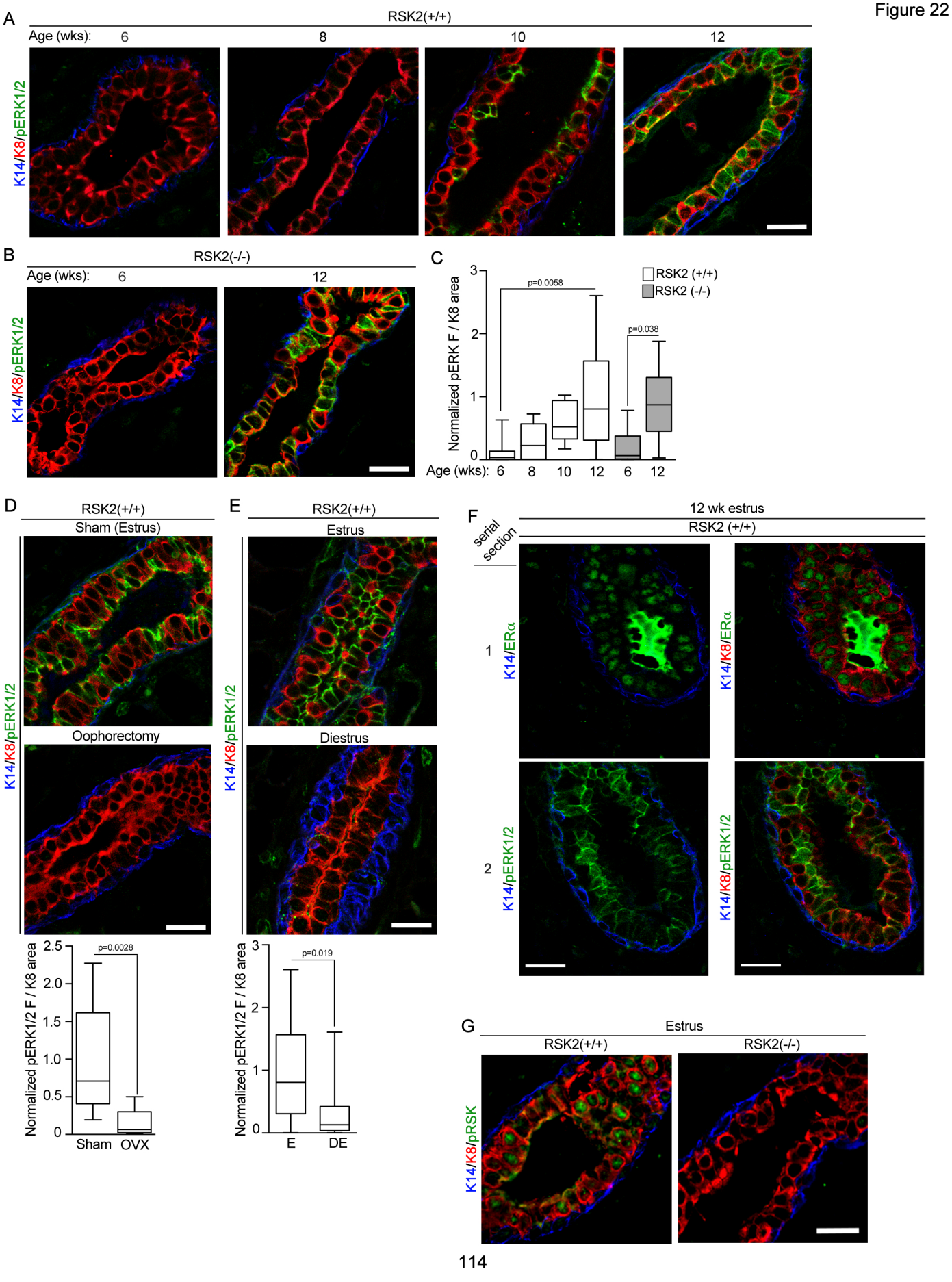
A
RSK2(+/+)
Age (wks): 6 8 10 12
K14/K8/pERK1/2
B
RSK2(-/-)
Age (wks): 6 12
K14/K8/pERK1/2
C
RSK2 (+/+)
RSK2 (-/-)
p=0.0058
p=0.038
Normalized pERK F / K8 area
Age (wks): 6 8 10 12 6 12
D
RSK2(+/+)
Sham (Estrus)
Oophorectomy
K14/K8/pERK1/2
p=0.0028
Normalized pERK1/2 F / K8 area
Sham OVX
E
RSK2(+/+)
Estrus
Diestrus
K14/K8/pERK1/2
p=0.019
Normalized pERK1/2 F / K8 area
E DE
F
12 wk estrus
RSK2 (+/+)
serial section
1
K14/ERα
K14/K8/ERα
2
K14/pERK1/2
K14/K8/pERK1/2
G
Estrus
RSK2(+/+)
RSK2(-/-)
K14/K8/pRSK

RSK2 maintains ERα protein levels in the adult reproductive tract

We next investigated whether RSK2 preserved ERα protein levels in other hormone-responsive tissues. We focused on the female reproductive tract, as we observed a 50% reduction in the fertility rate with crosses between RSK2-KO females and males (Fig. 23A). RSK2-KO males crossed with heterozygote females had similar fertility rates to that of the WT crosses, indicating that the reduced fertility is associated with the RSK2-KO females. Ovaries in the RSK2-KO and WT mice showed all stages of follicular development and the presence of the corpora luteum (Fig. 23B), demonstrating that hormonal signaling through the hypothalamic-pituitary-ovarian axis is not impaired in RSK2-KO mice [223]. The uterus endometrium expresses high levels of ERα, which is present in stromal cells as well as glandular and luminal epithelium (Fig. 23D). In comparison to the WT, the ERα protein levels were substantially decreased in the epithelial but not in the stromal cells in RSK2-KO mice. Interestingly, ERK1/2 activity was detected in the uterine epithelium but not in the stroma cells, providing further evidence of the connection between ERK1/2-RSK2 signaling and ERα protein levels (Fig. 23E). Uterine wet weight and total uterine width was similar in the WT and KO, as stromal cells are thought to primarily mediate uterine expansion [202, 224](Figs. 22A, 23C). The fertility defect is most likely explained by the decrease in ERα protein levels in the glandular epithelium, as the glandular secretions are known to be important for implantation [225].

Figure 23 RSK2 maintains ERα protein levels in the uterine epithelium*

(A) RSK2-KO mice show a fertility defect (n ≥ 15 dams/genotype). (B) The hypothalamic-pituitary-ovarian is not disrupted in RSK2-KO females. H&E sections of ovaries isolated from adult mice in estrous. PF=primary follicle; SF=secondary follicle; TF=tertiary follicle CL=corpus luteum. (C) Luminal height in the uterus in the WT and RSK2-KO are similar. Measurements from ≥30 randomly selected regions from each animal (Bar, median ± quartile, n≥3 mice/genotype). (D) RSK2-KO have reduced ERα protein levels in the glandular and luminal epithelium of the uterus (Bar, median ± quartile, n=3 mice/genotype, > 120 cells/mouse). (E) In the uterus, pERK1/2 is expressed in epithelial, but not in stromal cells. Scale bar = 20 μm. (F) GATA3 is expressed at very low levels in the uterus compared to the mammary gland.

*Zach Sandusky contributed Figure 23; Dr. Kelli Boyd assisted with panel B.

A Mouse Fertility

Genotype		Fertile females	# of pups
Female	Male		
RSK2(+/+)	RSK2(+/o)	71.40%	7.40±1.68
RSK2(+/-)	RSK2(-/o)	77.78%	6.93±2.42
RSK2(-/-)	RSK2(-/o)	43.33%	3.72±3.22

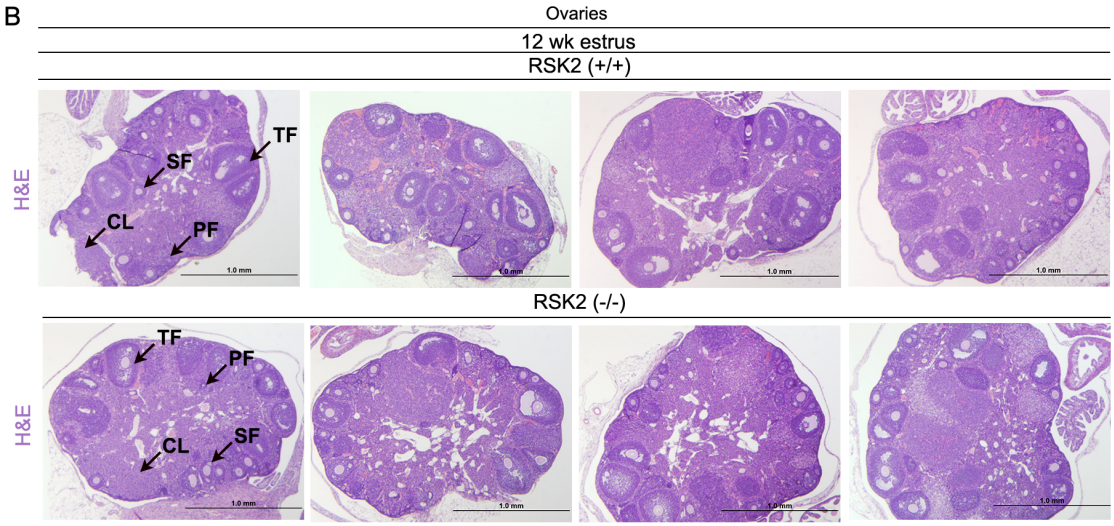

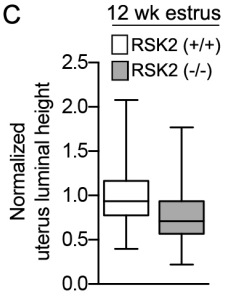

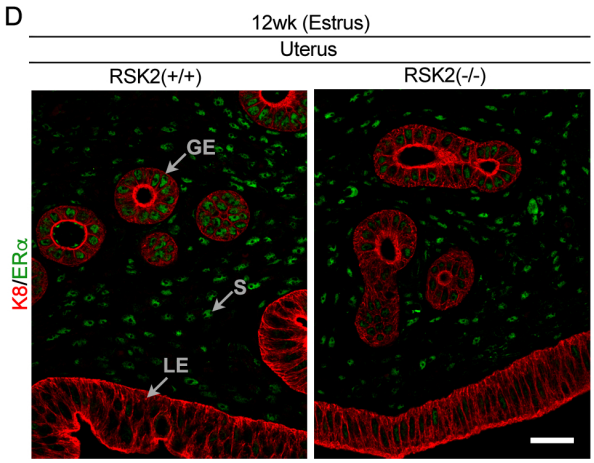

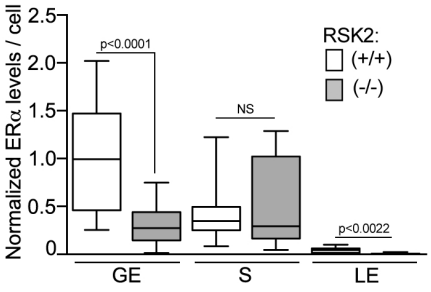

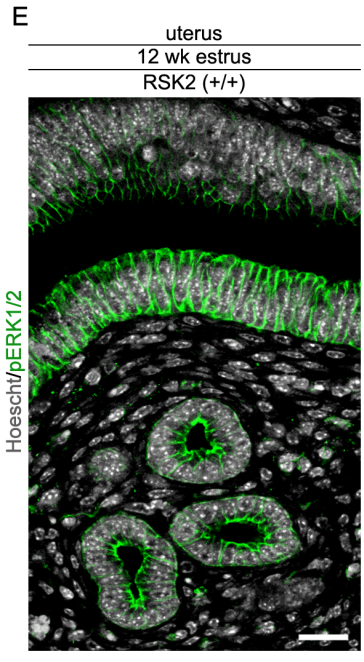

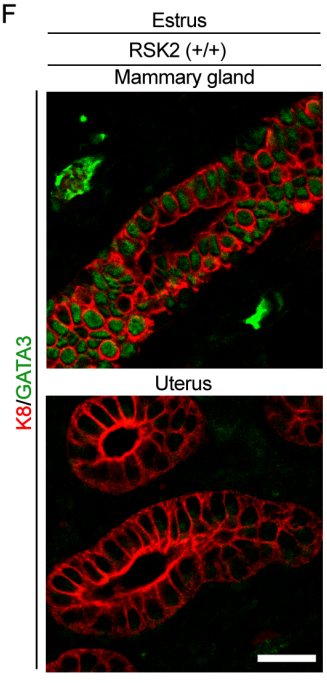

RSK2 reduction of ERα protein levels is independent of GATA3

To address the mechanism by which RSK2 regulates ERα protein levels we initially focused on GATA3, as GATA3 and ERα regulate each other's expression via a positive feedback mechanism in breast cancer cells [226]. Therefore, it is conceivable that RSK2 decreases GATA3 protein levels, which subsequently leads to a reduction in ERα protein levels. However, GATA3 levels are extremely low and ERα levels are very high in the glandular epithelium of the uterus. These data indicate that a positive feedback loop between GATA3 and ERα does not exist in the uterus (www.proteinatlas.org)[227] (Fig. 23F). Importantly, loss of RSK2 results in reduction of ERα protein levels in the glandular epithelium, which argues that the primary target of RSK2 is ERα and not GATA3.

RSK2 negatively regulates estrogen signaling in the adult mammary gland by inhibition of ERα protein turnover

To investigate the significance of the relationship between E_2 and active RSK2 we analyzed transcriptomic changes (RNAseq) that occurred in NCL cells isolated from RSK2-KO and WT at estrus or diestrus. Principal component analysis indicated that the signature obtained from RSK2-KO at estrus diverged the most from the other samples (Fig. 24A, B). These analyses identified 3670 differentially expressed (DE) genes in the RSK2-KO at estrus compared to diestrus (Fig. 24C). In contrast, there were only 40 DE genes between estrus and diestrus in the WT with ~ 50% of these genes also differentially regulated in the KO (Fig. 24C). Unexpectedly, we identified that the DE genes in the RSK2-KO at estrus were enriched for a gene signature for E_2-regulated genes identified in MCF-7 cells (Fig. 24D) [184]. We found that the ERα-signature z-scores were significantly higher in estrus RSK2-KO mice than in any other

condition, indicating that directionality of ERα-regulated gene expression in these mice is concordant with that observed in MCF-7 cells treated with E_2 (Fig. 24E).

The increase in estrogen-responsiveness in RSK2-KO mice suggested the hypothesis that the reduced ERα protein levels were linked to increased ERα degradation, as ERα degradation via the 26S proteasome pathway is required for ERα-mediated transcription [203, 204, 206, 207]. As support for this hypothesis no difference was observed in ESR1 (gene encoding ERα) and GATA3 mRNA levels between WT and RSK2-KO (Fig. 25A) indicating that transcription of these genes was not reduced in the RSK2-KO. To investigate whether RSK2 regulated ERα turnover we inhibited degradation through the 26S proteasome with PS-341 [205]. ERα levels in the WT did not substantially change in response to PS-341; however, in the RSK2-KO mouse, ERα protein levels increased by ~ five-fold (Fig. 25B). This degradation is dependent on E_2 and is not a general increase in degradation in the RSK2-KO mice as oophorectomy resulted in an increase in ERα protein levels (Fig. 25C).

Figure 24 RSK2 is a negative regulator of ERα-mediated signaling

Principal component analysis (A*) and similarity matrix (B) of RNAseq analysis showing, that RSK2-KO mice in estrus are most divergent from all the other samples. (C) RSK2-KO mice show greater DGE between estrus and diestrus than WT. Genes in which the fold-change > 1.5 and FDR adjusted p-value < 0.05 are plotted. (D) Heat map illustrating that the major chances in DE genes between RSK2-KO and WT occurs during estrus. (E) Z-scores demonstrate that RSK2-KO mice in estrus are enriched for ERα-regulated genes. Z- scores were identified for ERα-regulated genes that were in E_2 treated MCF-7 cells [184]

*Kimberly Stauffer contributed, and Dr. Thomas Stricker assisted with panels A, B and D

Figure 24

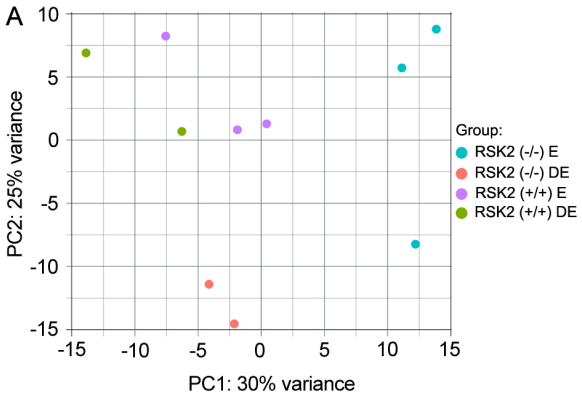
A
PC2: 25% variance
PC1: 30% variance
Group:
RSK2 (-/-) E
RSK2 (-/-) DE
RSK2 (+/+) E
RSK2 (+/+) DE

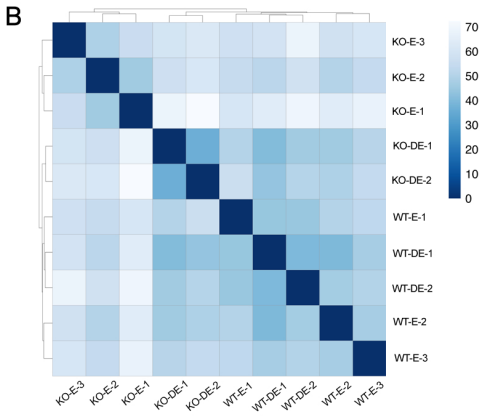
B
KO-E-3
KO-E-2
KO-E-1
KO-DE-1
KO-DE-2
WT-E-1
WT-DE-1
WT-DE-2
WT-E-2
WT-E-3

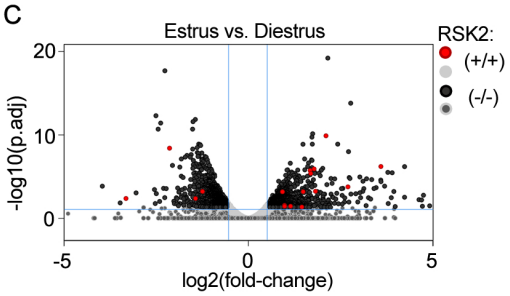
C
Estrus vs. Diestrus
-log10(p.adj)
log2(fold-change)
RSK2:
(+/+)
(-/-)

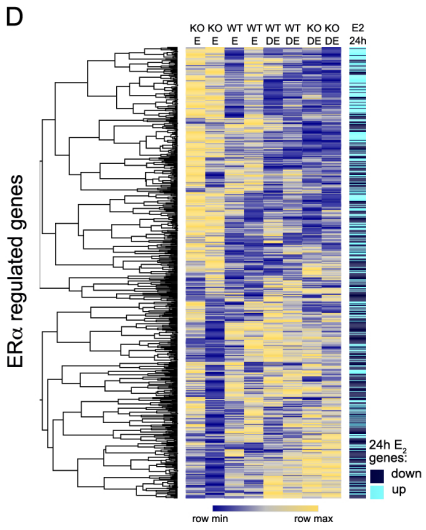
D
ERα regulated genes
24h E2 genes:
down
up
row min
row max

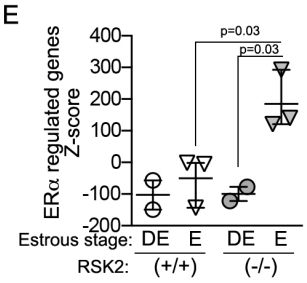
E
ERα regulated genes Z-score
p=0.03
p=0.03
Estrous stage: DE E DE E
RSK2: (+/+) (-/-)

Figure 25 RSK2 preserves estrogen homeostasis in the adult*

(A) ESR1 and GATA3 mRNA levels are similar in the NCL population of RSK2-KO and WT mice. (Bar, mean ± S.D., n=3 mice/genotype in triplicate) (B) Loss of RSK2 increases ERα turnover (Bar, median ± quartile, n=3 mice/genotype and condition, ≥ 200 cells/mouse). Adult mice staged at estrus were treated with vehicle or PS-341 or 2 h before euthanasia and isolation of the mammary gland isolated. Number of ER+ cells relative to K8+ cells increase in RSK2-KO mice in response to inhibition of protein turnover. (Bar, median ± quartile, n=3 mice/genotype and condition). (C) ERα protein levels increase in response to oophorectomy (Bar, median ± quartile, n ≥2 mice/genotype and procedure).

*Zach Sandusky contributed panels B and C.

Figure 25

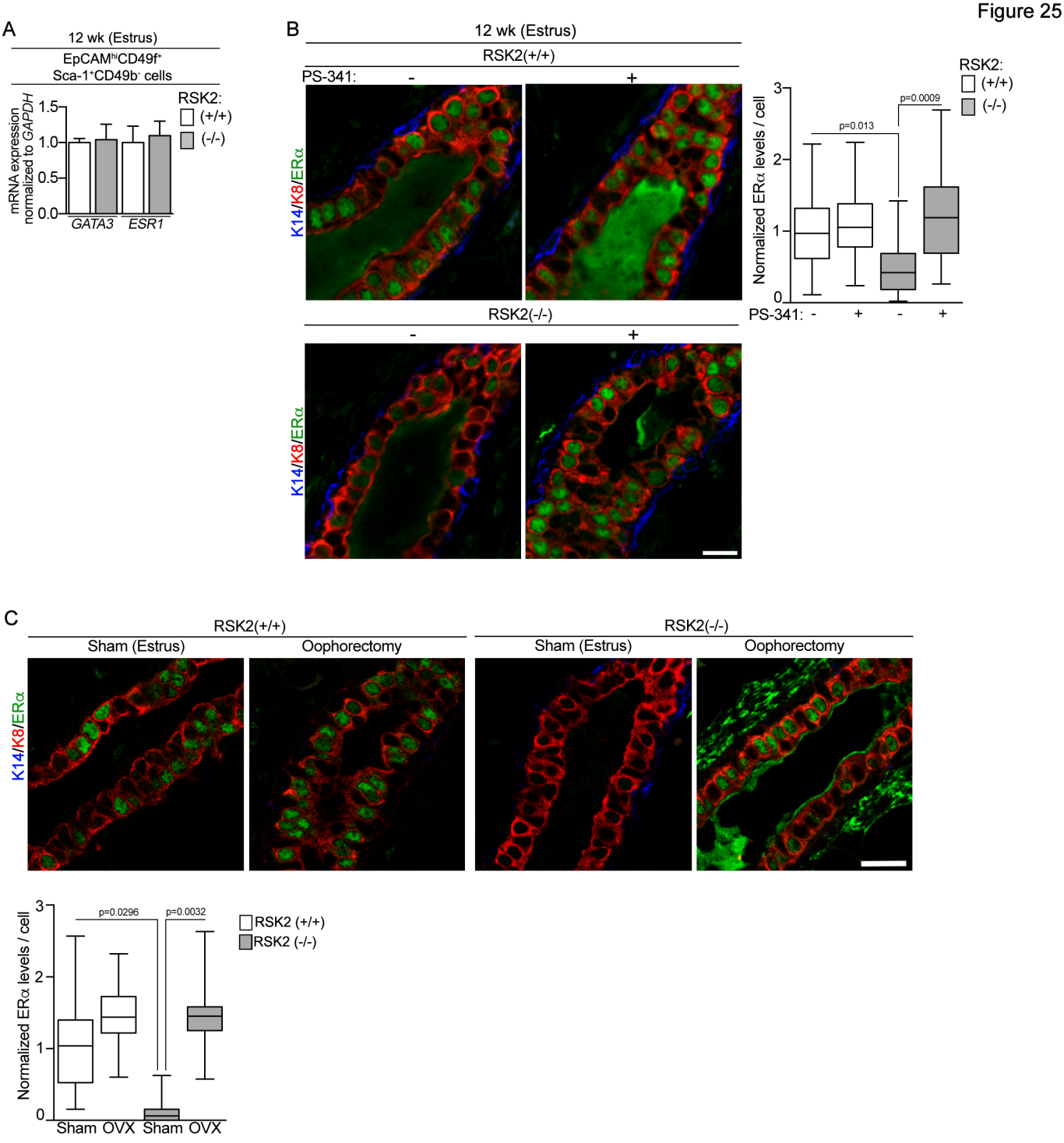
A
12 wk (Estrus)
EpCAM^hiCD49f^+
Sca-1^+CD49b^- cells
mRNA expression normalized to GAPDH
RSK2:
(+/+)
(-/-)
GATA3
ESR1
B
12 wk (Estrus)
RSK2(+/+)
PS-341:
K14/K8/ERα
RSK2(-/-)
Normalized ERα levels / cell
p=0.013
p=0.0009
C
RSK2(+/+)
RSK2(-/-)
Sham (Estrus)
Oophorectomy
p=0.0296
p=0.0032
RSK2 (+/+)
RSK2 (-/-)
Sham OVX Sham OVX

RSK2 is necessary for the maintenance of mammary gland homeostasis

According to the literature RSK2 positively regulates various aspects of translation [6, 228-230]. Therefore, it was unexpected that numerous gene signatures associated with various aspects of protein biogenesis were enriched in the RSK2-KO compared to WT during estrus (Fig. 26A). This gene enrichment was driven by E_2 as the gene signatures for various aspects of protein biogenesis were enriched in the RSK2-KO at estrus compared to diestrus. Additional gene signatures associated with oxidative phosphorylation were also enriched in the RSK2-KO during estrus when comparing to WT or RSK2-KO during diestrus, which is most likely explained by the increased translational demands dictated by enhanced ERα-mediated transcription (Fig. 26B, Table 6).

Gene signatures associated with cell cycle genes were found to be enriched at estrus in RSK2-KO mice compared to WT (Fig. 26C, Table 6). These results were puzzling, as we did not detect any evidence of hyperplasia in the RSK2-KO glands. To investigate these cell cycle signatures we measured proliferation in regenerated glands in which MECs from WT and RSK2-KO mice were separately introduced into a WT recipient. Incorporation of 5-ethynyl-2'-deoxyuridine (EdU) was measured over a single estrous cycle (Fig. 26D). An ~ 2.5 fold reduction in the ability of the NCL population to proliferate was observed in the RSK2-KO regenerated gland compared to its counterpart (Fig. 26E, F). Statistically significant changes were not observed in other cell populations (Fig. 26G). Thus despite the increase in cell proliferation genes in the RSK2-KO NCL cells this population was unable to proliferate. The reduced ability of the RSK2-KO mammary gland to proliferate also explains the reduced alveolar expansion observed during lactation.

Figure 26 Analysis of gene expression in RSK2-KO mice

Heat maps illustrating that the NCL cells isolated from RSK2-KO mice in estrus are enriched for genes associated with: (A) ribosomal biogenesis [231]; (B) oxidative phosphorylation [164]; and (C) cell cycle [232]. (D) Fluorescence minus one strategy for determining the gates for EdU labeling. (E) RSK2-KO NCL cells show a decrease in proliferation as compared to the WT. RSK2-KO or WT MECs were used to regenerate the mammary gland in a WT mouse. These mice were staged in proestrus and administered EdU throughout one estrus cycle. The mammary glands were isolated and analyzed by FACS. (n=3 glands/genotype; two-tailed paired t-test). (F) Loss of RSK2 does not alter the proliferation of the luminal progenitor or undefined populations in mammary glands from (E). (G) Loss of RSK2 reduces proliferation of the luminal cells at the onset of pregnancy. RSK2-KO or WT MECs were used to regenerate the mammary gland in a WT mouse. The EdU was administered on pregnancy day 2 and the mammary glands were isolated and analyzed by FACS on pregnancy day 5. (n≥3 glands/genotype; Student t-test).

*Zach Sandusky assisted with panels B and C.

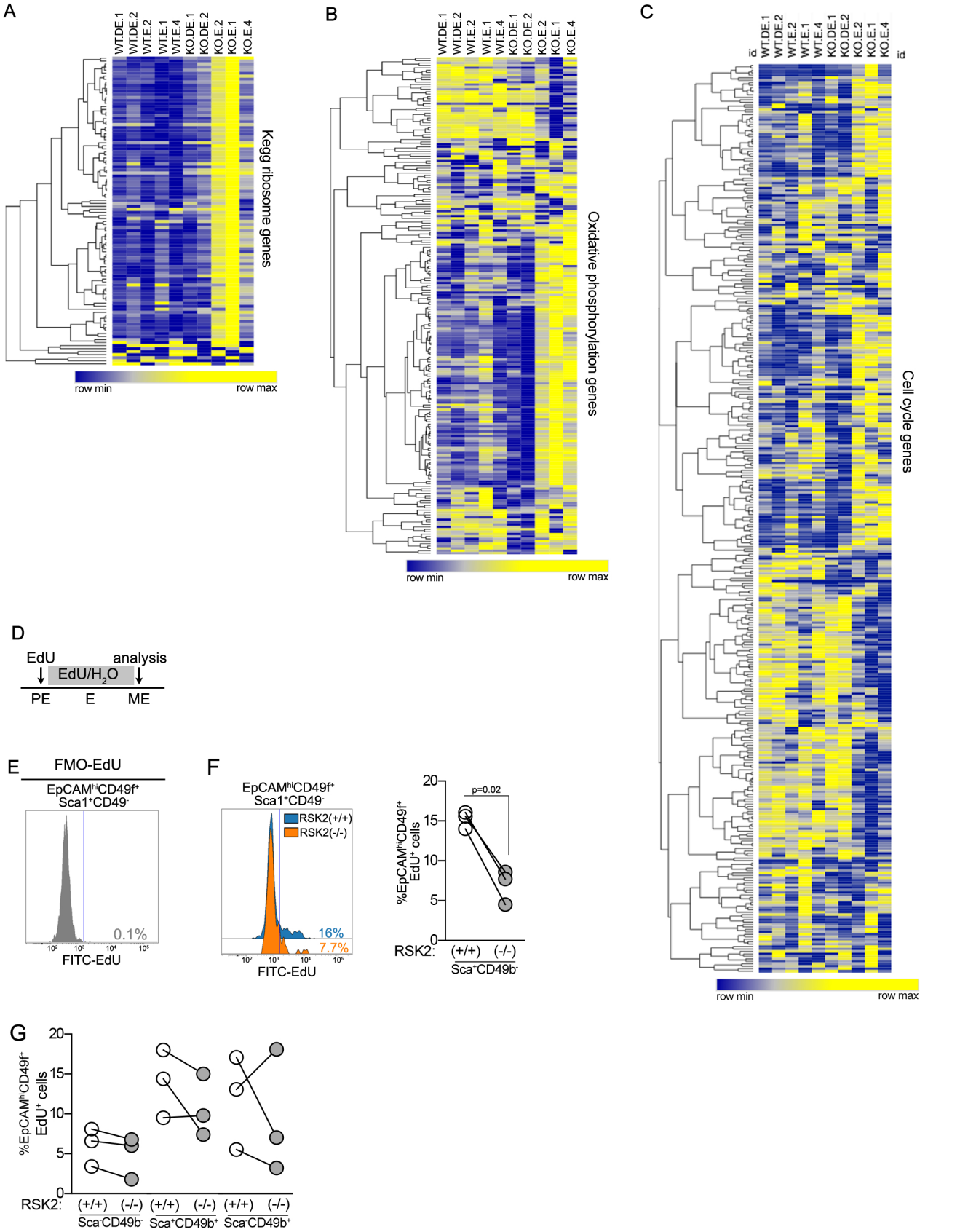
A
WT.DE.1
WT.DE.2
WT.E.2
WT.E.1
WT.E.4
KO.DE.1
KO.DE.2
KO.E.2
KO.E.1
KO.E.4
Kegg ribosome genes
row min
row max
B
Oxidative phosphorylation genes
C
Cell cycle genes
D
EdU
analysis
EdU/H2O
PE
E
ME
E
FMO-EdU
EpCAMhiCD49f+
Sca1+CD49-
0.1%
FITC-EdU
F
RSK2(+/+)
RSK2(-/-)
16%
7.7%
p=0.02
%EpCAMhiCD49f+ EdU+ cells
RSK2:
(+/+)
(-/-)
Sca+CD49b-
G
Sca-CD49b-
Sca+CD49b+
Sca-CD49b+

Table 6 Gene set overlap analysis

Gene sets in overlap		Fisher's exact test for overlap
Genes UP in R2KO-E vs R2KO-DE	E2_24h_UP	0.00001
Genes DOWN in R2KO-E vs R2KO-DE	E2_24h_DOWN	0.00001
Genes UP in R2KO-E vs R2KO-DE	REACTOME_CELL_CYCLE	0.0007
Genes UP in R2KO-E vs R2KO-DE	KEGG_RIBOSOME	0.00001
Genes UP in R2KO-E vs R2KO-DE	HALLMARK_OXPHOS	0.00001

Discussion

All ER+ tissues respond to estrogen signaling and therefore, are subject to the normal fluctuations in the levels of estrogen that occur throughout the estrous cycle. Alterations in metabolic function, which occur during menopause, oophorectomy or anti-estrogen therapy in women, highlight the importance of estrogen signaling in maintaining homeostasis [197]. Here, we provide the first evidence of the importance of growth factor signaling through the ERK1/2-RSK2 pathway to maintain estrogen homeostasis *in vivo* by regulating the turnover and transcriptional activity of ERα. The physiological importance of this regulation is demonstrated by the reduced pup size and decreased fertility in the RSK2-KO females. RSK2 regulation of ERα-mediated transcription was dependent on estrogen, as very few differences were observed in the gene expression profiles in the mammary gland between the WT and RSK2-KO during diestrus. Furthermore, oophorectomy prevented activation of the ERK1/2 pathway and resulted in increased ERα protein levels. ERK1/2 activity was essential for RSK2 regulation of ERα protein levels, as demonstrated in the uterus in which only the epithelial cells, which contained active ERK1/2, showed reduced ERα protein levels in the RSK2-KO. The ability of the ERK1/2-RSK2 pathway to dampen ERα-mediated transcription was unexpected, as the contributions of growth factor signaling to breast cancer are well established [[233]].

We observed that ERK1/2-RSK2 signaling was not active in the juvenile gland but is temporally regulated throughout the estrous cycle in the adult. The necessity for this switch is unclear but ERK signaling is activated in the adult *C. elegans* and not in the larvae and is responsible for regulating protein homeostasis by preventing the accumulation of oxidized proteins [234]. Temporal activation of ERK1/2 in response to the circadian clock occurs in adult hepatocytes [235] but alteration of ERK1/2 throughout the estrous cycle has not been reported previously. The gene signature of RSK2-KO glands isolated at estrus was substantially

enriched for estrogen-responsive genes expressed in the human ER+ breast cancer line, MCF-7 [184]. In contrast to the <3500 DE genes observed between estrus and diestrus in the RSK2-KO we observed only 40 DE genes in the WT. As degradation is linked to the rate of transcription, the gene expression data are consistent with our observations that no change was observed in ERα levels in response to proteasome inhibition in the WT compared to the five-fold change observed in the RSK2-KO. Also in agreement with our data prior transcriptomic analysis of the entire mammary gland isolated at estrus or diestrus in C57BL/6 mice showed very few DE genes even though there are major morphological differences in the mammary gland at these stages [236].

ERα turnover has been primarily studied in ER+ breast cancer and endometrial cancer lines [209, 237-239]. Many of the identified regulators that stimulate ERα degradation simultaneously act as ERα co-activators [209]. Phosphorylation is a common mechanism for targeting proteins for degradation [240]. In fact ERK1/2 induces oncogene-induced senescence by increasing the degradation rate of a subset of proteins required for proliferation and transformation [241]. In contrast, we have identified that the ERK1/2-RSK2 pathway inhibits ERα degradation in the normal mammary gland. The possible mechanisms by which RSK2 could inhibit ERα turnover include direct or indirect phosphorylation of ERα and its co-regulators or through physical association with ERα [36, 55, 154]. Previously, we found that RSK2 association with ERα rather than the phosphorylation of ERα acts as a driver in ER+ breast cancer, as the levels of the RSK2- ERα complex correlate with tumor formation and result in high grade ductal carcinoma in situ [154].

Chapter 4 Development of a RSK Inhibitor as a Novel Therapy for Triple Negative Breast Cancer

Adapted from [144]: Ludwik K.A., Campbell J.P., Li M., Li Y., Sandusky Z.M., Pasic L., Sowder M.E., Brenin D.R., Pietenpol J.A., O'Doherty G.A., Lannigan D.A. (2016) Development of a RSK Inhibitor as a Novel Therapy for Triple-Negative Breast Cancer. Mol Cancer Ther. 15(11):2598-2608

Summary

Metastatic breast cancer is an incurable disease and identification of novel therapeutic opportunities is vital. Triple negative breast cancer (TNBC) frequently metastasizes and high levels of activated RSK, a downstream MEK-ERK1/2 effector, are found in TNBC. We demonstrate using direct pharmacological and genetic inhibition of RSK1/2 that these kinases contribute to the TNBC metastatic process *in vivo*. Kinase profiling demonstrated that RSK1 and RSK2 are the predominant kinases targeted by the new inhibitor, which is based on the natural product, SL0101. Further evidence for selectivity was provided by the observations that silencing RSK1 and RSK2 eliminated the ability of the analogue to further inhibit survival or proliferation of a TNBC cell line. *In vivo,* the new derivative was as effective as the FDA-approved MEK inhibitor, trametinib, in reducing the establishment of metastatic foci. Importantly, inhibition of RSK1/2 did not result in activation of AKT, which is known to limit the efficacy of MEK inhibitors in the clinic. Our results demonstrate that RSK is a major contributor to the TNBC metastatic program and provide preclinical proof-of-concept for the efficacy of the novel SL0101 analogue *in vivo*.

Introduction

Metastatic breast cancer remains incurable, with therapy limited to slowing disease progression [242]. In particular, triple negative breast cancer (TNBC) patients have increased probability of death due to metastasis compared with other breast cancer subtypes [243]. TNBC is characterized by its lack of currently available targeted markers [244]. However, the MEK-ERK1/2 cascade is now considered as a viable drug target for TNBC [245-248]. In genetic analysis of basal-like breast cancers, which includes ~ 70% of TNBCs, activated MEK-ERK1/2 signaling is thought to occur in ~ 80% of the tumors [245, 249, 250]. Additionally, numerous TNBC cell lines possess an activated RAS-transcriptional program and enhanced sensitivity to MEK inhibition [251, 252]. In support of these pre-clinical observations, a complete response was observed in a phase Ib trial using a combination of trametinib, a MEK inhibitor, and gemcitabine, a nucleotide analogue, in a TNBC patient who had failed multiple therapies [246]. Based on these data various MEK inhibitors are being tested in clinical trials, which include TNBC patients [253].

However, treating patients with drugs that inhibit “global regulators” such as MEK causes a number of side effects that result in limited efficacy [253]. We postulate that inhibiting downstream effectors of MEK like the Ser/Thr protein kinase, p90RSK (RSK), will have fewer side effects because it controls a more limited set of targets. RSK phosphorylates various substrates that control diverse cellular processes, including metastasis [73, 156, 157, 254-256]. Approximately, 85% of TNBC patient samples have activated RSK, which is identified by the presence of phosphorylated residues critical for its activity [54]. Taken together, these observations suggest that RSK is a viable target for TNBC.

RSK contains two non-identical functional kinase domains referred to as the N-terminal (NTKD) and C-terminal (CTKD) [254]. The CTKD functions to regulate RSK activation whereas the NTKD, which belongs to the AGC kinase family, is responsible for substrate phosphorylation

[254]. In a screen of botanical extracts we identified the first RSK inhibitor, SL0101 (**1a**), which was isolated from *Forsteronia refracta* [59]. SL0101 is an extremely specific allosteric inhibitor for the NTKD [59, 135, 137, 156].

In addition to SL0101, other RSK inhibitors have been described. However, the currently available NTKD inhibitors are not RSK specific [103, 128, 135, 257, 258] or demonstrate poor pharmacokinetics [147, 148]. Covalent inhibitors of the RSK CTKD [21, 132, 259], targeting autoactivation, are also available and have limited off-target effects. However, CTKD inhibitors do not inhibit an activated kinase and the autoactivation mechanism can be bypassed [21], suggesting that the clinical utility of CTKD inhibitors is limited.

Because of the selectivity of SL0101 for RSK we continue to improve its drug-like properties through extensive structure-activity-relationship (SAR) analysis. We have now identified a SL0101 analogue, *C6"-n-propyl* cyclitol SL0101 (**1b**), which retains specificity for RSK1/2 and is more potent in *in vitro* and cell-based assays than the parent compound. This improved analogue inhibits proliferation, survival in a non-adherent environment, and migration of TNBC lines but, unlike MEK inhibitors, does not activate the AKT pathway. Inhibition of RSK1/2 using (**1b**) or silencing RSK1 or RSK2 inhibited TNBC metastatic colonization *in vivo*. Moreover, (**1b**) was as effective as the FDA-approved MEK inhibitor, trametinib. Taken together, these results indicate that RSK1/2 are viable drug targets for TNBC metastasis.

Materials and Methods

Animals

Animal procedures had approval of the Vanderbilt University Institutional Animal Care and Use Committee. For in vivo metastatic models, NOD-SCID-IL2Rγ_c (NSG) mice (6-8 weeks) (Jackson Laboratory) were injected in the left cardiac ventricle with 1x10^5 cells/100 μL PBS. Mice injected with MCF-7 cells received a 17β-estradiol pellet (0.36-mg 60-day release; Innovative Research of America). Mice bearing MCF-7 metastasis were injected IP with vehicle (10% (2-hydroxypropyl)-β-cyclodextrin (HPBCD) in 10% DMSO) or (**1b**) (40 mg/kg) 2h prior to euthanasia (day 50). Mice injected with HDQ-P1-Luc were randomized and at 2 h after injection were treated for 5d with HPBCD, (**1b**) (40 mg/kg) IP Q12h or trametinib (2 mg/kg, Santa Cruz Biotechnology, Inc) IP Q24 h. For bioluminescence imaging, mice were injected IP with RediJect D-Luciferin (1.5 mg) (PerkinElmer, Inc.) and imaged with a Xenogen IVIS using Living Image acquisition software (Xenogen Corp.). For ex vivo imaging, organs were placed in D-Luciferin (150 mg/mL PBS). After imaging tissue was fixed in 4% buffered formalin and paraffin-embedded.

Antibodies

Primary antibodies used for immunofluorescence: chicken anti-keratin-14 (Abcam plc); rat anti-keratin 8 (University of Iowa); anti-phospho-S6 (Cell Signaling Technology, Inc.); rabbit anti-p-Thr359/Ser363-RSK (EMD Milipore). Secondary antibodies for immunofluorescence: AlexaFluor goat anti-rat 546 IgG (H+L), goat anti-chicken IgG 488 (H+L), goat anti-rabbit 647 IgG (H+L) (Thermo Fisher Scientific, Inc.). Antibodies used for immunoblotting: rabbit anti-pSer167-ERα, rabbit anti-pSer51-eEF2, rabbit anti-eEF2, mouse anti-cyclin D1, rabbit anti-pSer235/236-S6, rabbit anti-S6, rabbit anti-pSer473-AKT, rabbit anti- AKT, rabbit anti-pThr359/Ser363-RSK, rabbit anti-pSer380-RSK, rabbit anti-caspase3, rabbit anti-cleaved caspase-3 (Asp175), rabbit

anti-PARP (Cell Signaling Technology, Inc.); rabbit anti- ERα (Thermo Fisher Scientific Inc.); rabbit anti-Ran (provided by I.G. Macara, Vanderbilt University); mouse anti-RSK2, and rabbit anti-RSK1 (Santa Cruz Biotechnology, Inc.). Secondary antibodies used were HRP- conjugated donkey antirabbit and goat anti-mouse (Jackson ImmunoResearch Laboratories, Inc.).

Immunostaining

Human breast cancer tissue removed during breast reduction or breast cancer surgery was collected as waste tissue with institutional review board approval. A list of the age and race for each of the patient samples used in this study is provided (Table 7).

For detection of pS6, mouse tibiae were fixed in 4% buffered formalin for 3 d and decalcified in 20% EDTA pH 7.4 at r.t. for 3-4 d. Decalcified samples were then placed in 70% ethanol, paraffin-embedded, and 5-μm sections were cut. MCF-7 cells plated on poly-lysine coated coverslips were fixed with 4% paraformaldehyde, washed with PBS, permeabilized with 0.5% Triton X, and blocked in 10% bovine serum albumin (BSA) in PBS. For detection of pRSK, human breast tissue was fixed in buffered 10% formalin for 2 d and placed in 70% ethanol, paraffin-embedded, and 5-μm sections were cut. The sections were deparaffinized and blocked in 10% BSA in PBS. Sections and fixed cells were incubated with primary antibody in 3% BSA/PBS overnight at 4°C, washed with 3% BSA/PBS, and incubated with secondary antibody for 1 h at r.t. The sections and cells were washed and DNA stained with Hoechst for 10 min. The coverslips were mounted using Fluoro-Gel (EMS).

Fluorescent images were obtained with a laser-scanning microscope (510/Meta/FCS Carl Zeiss, Inc.). Objectives were: mouse tissue 40× Plan-Neofluar oil NA 1.3 (zoom 0.7×); human tissue 20× NA 0.8. Images were acquired using LSM-FCS software (Carl Zeiss, Inc.), quantitated using Openlab 5.5.0 (PerkinElmer, Inc.) and processed in Photoshop version CS6 version 13.0 (Adobe).

In vitro cell assays

Cell lines were obtained and cultured as directed by American Type Culture Collection or by German Collection of Microorganisms and Cell Culture. Stocks were prepared within one to two passages after receipt and new stocks thawed frequently and passaged < 6 months. Authentication was based on growth rate, morphology and absence of mycoplasma. Serum-starved cells were pre-treated for 2h with vehicle or inhibitor. MCF-7 cells were treated with phorbol 12-myristate 13-acetate (PMA, Sigma) for 20 min. Cells were lysed as described [141].

For motility assays $2.5x10^5$ cells were plated on fibronectin-coated (5 μg/mL, Corning) 2-chamber Lab Teks (Thermo Fisher Scientific). After 48 h cells were pre-treated with vehicle or inhibitors for 2h and scratched with a P200 pipette tip. After washing, HEPES (50 mM, Thermo Fisher Scientific)-buffered media with vehicle or inhibitor was added and images taken every 20 min using Nikon Eclipse Ti microscope and an Orca R2 digital CCD camera (Hamamatsu). Migration velocity was quantified using Volocity software (PerkinElmer, Inc.).

For 2D proliferation assays, $2x10^5$ cells/well in 24-well or 10^3 cells/well in 96-well were seeded. For 3D proliferation 1.5×10^3 cells/well in 96-well were plated in 2% matrigel (MG; Corning, Inc.) onto 100% MG. Inhibitor or vehicle was added and proliferation was measured at 48-72h using CellTiterGlo reagent (Promega Corp.) with a GloMax Discover luminometer (Promega Corp.).

For survival assays, cells were seeded at $1.5x10^3$ cells/well in 96-well poly-HEMA coated plates (Corning, Inc.) and vehicle or inhibitors added and bioluminescence measured at 48-72h.

The IC_{50} values for proliferation and survival were determined using non-linear regression analysis (GraphPad Prism version 6.0a).

In vitro kinase assays

RSK2 kinase assays performed as described [141]. The kinase screen was performed using the ZLYTE screen (Thermo Fisher Scientific, Inc.).

Statistical Analysis

Statistical analyses (GraphPad Prism 6.0a) using the Mann-Whitney test (two-sided) unless indicated. *$p<0.05$ was statistically significant.

Results

SL0101 analogue with improved in vitro and cell-based efficacy

In prior SAR studies of the flavonoid glycoside, SL0101 (**1a**), we determined that replacement of the C5-methyl group on the pyran with an *n*-propyl moiety (**1c**), improved the IC_{50} by > twenty-five -fold but that the compound had limited aqueous solubility [141]. Additionally, we determined that exchanging the rhamnose with a cyclitol (**1d**), improved the cell-based efficacy for inhibition of proliferation but this compound was not RSK specific [142]. We hypothesized that combining the modifications would improve the potency for RSK inhibition while maintaining specificity for RSK. Consistent with our hypothesis *C6"-n-propyl* cyclitol SL0101 (**1b**) has a six-fold improved IC_{50} in an *in vitro* kinase assay for RSK inhibition compared to SL0101 (**1a**) (Fig. 27A). Furthermore, (**1b**) inhibited the proliferation in 2D culture of the ER+ breast cancer line, MCF-7, with an IC_{50} of ~ 8 μM versus ~ 50 μM for SL0101 (Fig. 27B) [59]. Previously, we found that the proliferation of the immortalized but untransformed breast line, MCF-10A, is less dependent on RSK for proliferation than the MCF-7 line [142]. Consistent with these observations, only a slight decrease in MCF-10A proliferation occurred at the highest concentrations of (**1b**) (Fig. 32B). The efficacy of SL0101 diminishes after > 48h in *in vitro* culture [59]. One advantage in replacing the rhamnose with a cyclitol moiety is that the cyclitol should be resistant to acid catalyzed anomeric bond hydrolysis, which should increase stability. To test this possibility we incubated MCF-7 cells with (**1b**) (25 μM) for varying lengths of time. In agreement with our rationale, only a minor increase in proliferation over a 96h time course was observed when MCF-7 cells were incubated with (**1b**) (Fig. 27C). In contrast, there was a 100% increase in proliferation from 48-96h in the presence of SL0101 (100 μM). These data indicate that the modifications to generate the SL0101 analogue (**1b**) resulted in a more potent RSK inhibitor than the parent compound.

Figure 27 *C6"-n-propyl* cyclitol SL0101 (1b) shows improved potency compared to the parent compound

(A) Structure and IC_{50} for selected SL0101 analogues. (B) Efficacy of (**1a**) and (**1b**) in inhibiting proliferation of MCF-7 and MCF-10A cells. Symbol, mean ± S.D. ($n \geq 2$, triplicate; *$p < 0.01$ compared to vehicle). (C) The *in vitro* stability of (**1b**) (25 μM) is increased in comparison to (**1a**) (100 μM). Bar, mean (n=2, quadruplicate; *$p < 0.0001$). (D) Analysis of lysates from MCF-7 cells pre-treated with (**1a**), (**1b**) or DMSO for 2h and treated with or without 500 nM PMA (20 min). (E) Representative images of MCF-7 cells treated as in D. Scale bar = 10 μm. Bar graph showing the decrease in pS6. ($n \geq 30$ cells). (F) Representation of (**1b**) specificity in a kinase screen indicating % inhibition at 10 μM compared to RSK2. (G) Bioluminescence images of NSG mice at day 50 after IC injection with MCF-7-Luc cells. (H) Representative paraffin-embedded tibia sections from mice in (G) treated with (40 mg/kg) or vehicle 2h prior to euthanasia. Scale bar = 40 μm. Bar graph showing the decrease in pS6. (n= 6 sections/mouse).

*Dr. Preston Campbell assisted with Panel G.

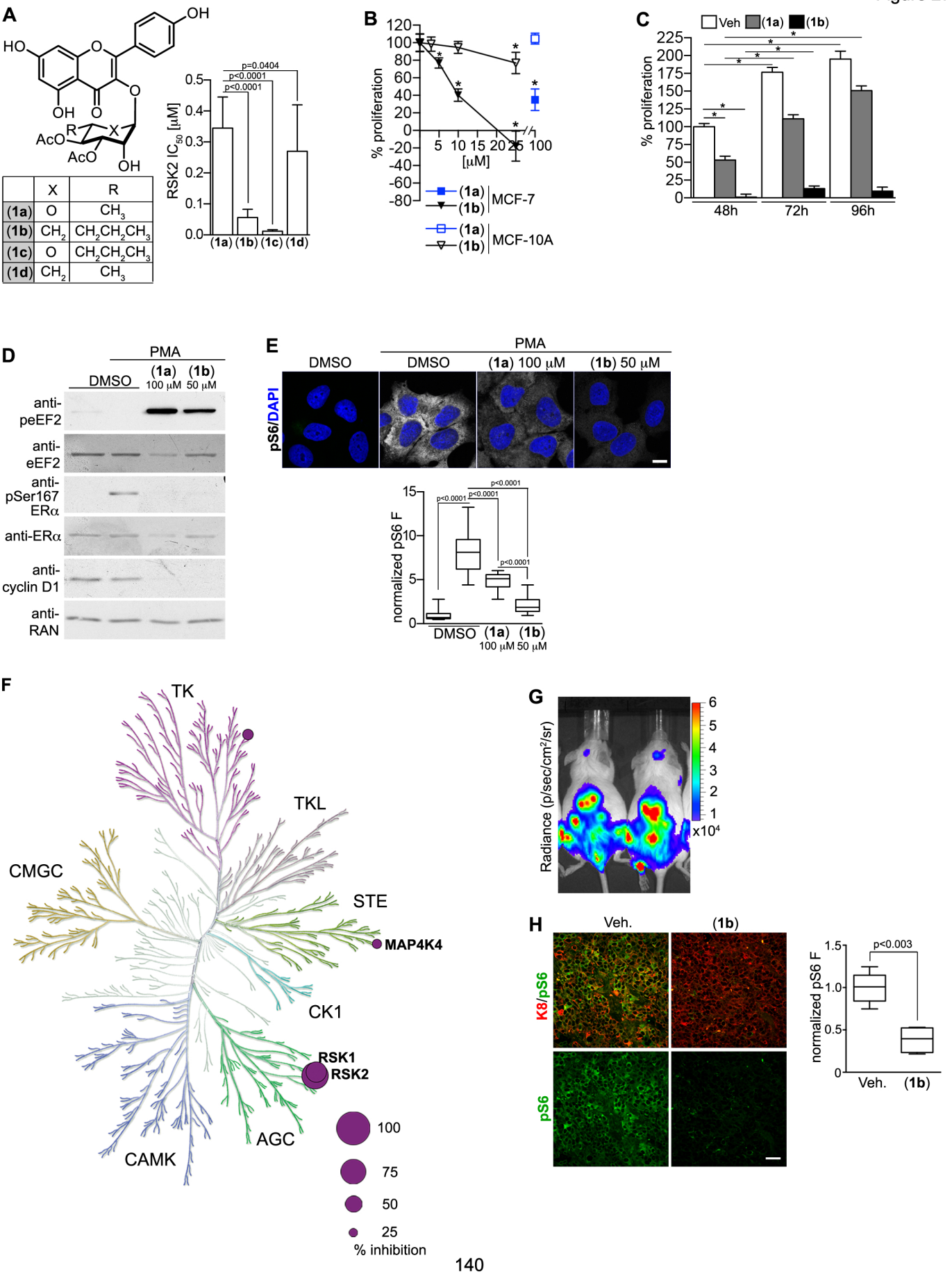

	X	R
(1a)	O	CH_3
(1b)	CH_2	$CH_2CH_2CH_3$
(1c)	O	$CH_2CH_2CH_3$
(1d)	CH_2	CH_3

*Specificity of C6"-n-propyl cyclitol SL0101 (**1b**) for RSK1/2*

SL0101 (**1a**) is highly selective for RSK [135, 156], which is most likely due to the fact that SL0101 inhibits RSK by an allosteric mechanism [137]. Therefore, to evaluate the specificity of (**1b**) we compared its ability to inhibit RSK substrates in comparison to SL0101 (**1a**). In agreement with previous results, SL0101 induces an increase in the phosphorylation of eukaryotic elongation factor 2 (p-eEF2) in MCF-7 cells, which also occurred with (**1b**) (Fig. 27D). This increase is due to the activation of eEF2 kinase, which is inhibited by RSK [229]. Furthermore, both RSK inhibitors decreased the phosphorylation of Ser167-ERα, an important marker for anti-estrogen responsiveness [55]. SL0101 and (**1b**) also decreased the phosphorylation of the ribosomal protein, S6 (pS6), a known RSK downstream effector (Fig. 27E) [6]. Previously, we identified that silencing RSK2 reduced cyclin D1 levels [24], and consistent with these results RSK inhibition decreased cyclin D1 levels. In a more global analysis, *in vitro* kinase assays were performed against a panel of 247 purified kinases, which contained representatives from all kinase families (Fig. 27F). At 10 μM of (**1b**), RSK1 and RSK2 were the top hits, with colony stimulating factor 1 receptor (CSF1R) and mitogen-activated protein kinase kinase kinase kinase (MAP4K4) being inhibited by ~ 37 % compared to RSK2 (Fig. 27F). CSF1R regulates macrophage function, and inhibitors are currently in development as cancer therapies [260]. MAP4K4 is an endothelial protein kinase, and inhibitors are being developed as anti-diabetic drugs [261]. Thus, the off target effects of (**1b**) are very limited. Neither of these off-target effects is viewed as problematic for further drug development. Taken together, these data demonstrate that (**1b**) is very specific for RSK1/2.

Figure 28 Active RSK in TNBC

(A) Activated RSK levels are increased in TNBC. Bar, median ± quartile (n ≥ 5 field/tissue sample). (B*) Representative paraffin-embedded sections of normal breast and TNBC tissue stained for the cytokeratins 8 (K8), 14 (K14) and phospho-Thr359/phospho-Ser363 RSK (pRSK). Scale bar = 20 μm. (C) Analysis of TNBC cell lysates normalized using the housekeeping protein, RAN. (D) Quantitation of the levels of pRSK normalized to RAN. (n=3) (E) Comparison of pRSK relative to total RSK1 and RSK2 for various TNBC lines. To control for antibody sensitivity the levels of RSK1 and RSK2 were determined using purified, recombinant protein.

*Lejla Pasic assisted with Panel B.

Figure 28

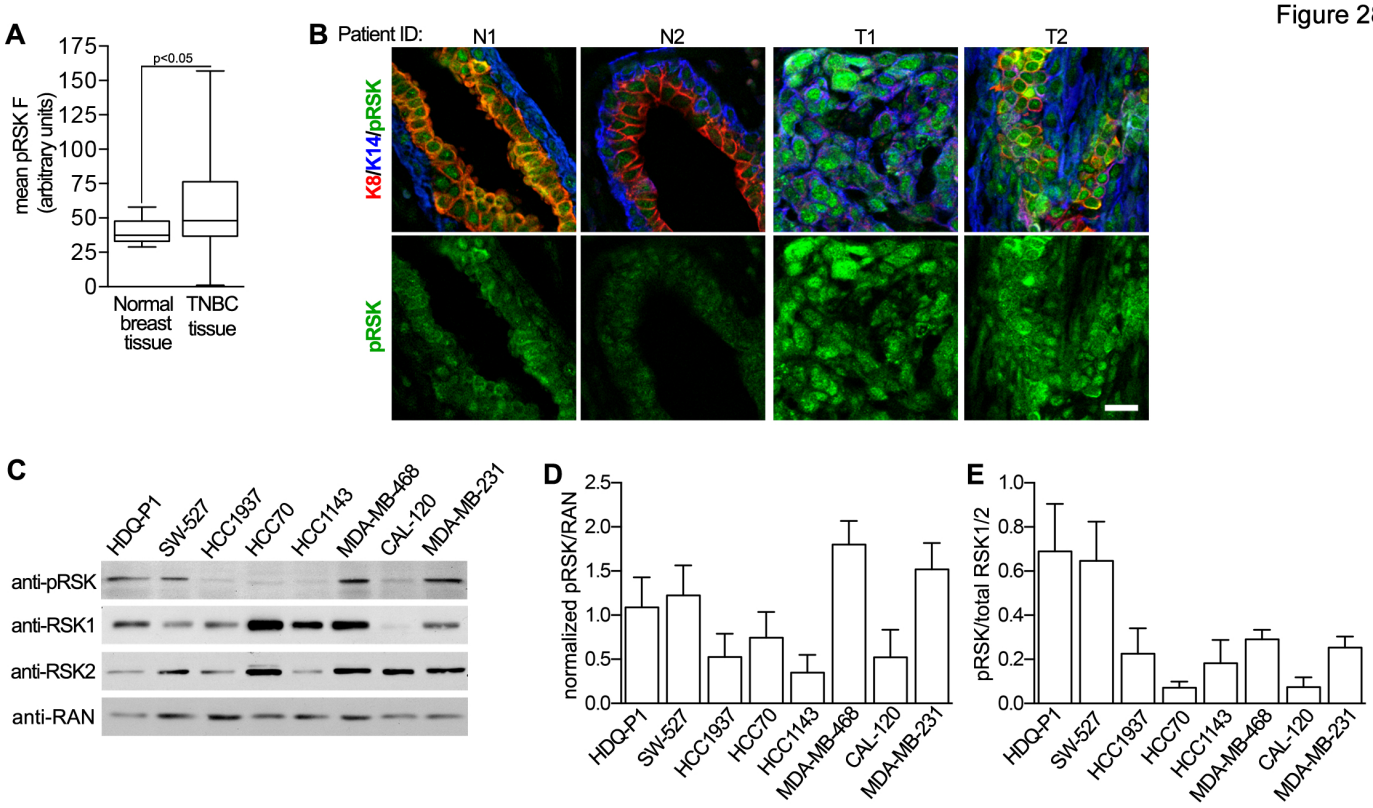
A
mean pRSK F (arbitrary units)
175
150
125
100
75
50
25
0
p<0.05
Normal breast tissue
TNBC tissue
B
Patient ID:
N1
N2
T1
T2
K8/K14/pRSK
pRSK
C
HDQ-P1
SW-527
HCC1937
HCC70
HCC1143
MDA-MB-468
CAL-120
MDA-MB-231
anti-pRSK
anti-RSK1
anti-RSK2
anti-RAN
D
normalized pRSK/RAN
2.5
2.0
1.5
1.0
0.5
0.0
HDQ-P1
SW-527
HCC1937
HCC70
HCC1143
MDA-MB-468
CAL-120
MDA-MB-231
E
pRSK/total RSK1/2
1.0
0.8
0.6
0.4
0.2
0.0
HDQ-P1
SW-527
HCC1937
HCC70
HCC1143
MDA-MB-468
CAL-120
MDA-MB-231

Table 7 Patient information

Patient ID	Race	Age
T1	Caucasian	64
T2	African-American	52
T3	Caucasian	28
T4	African-American	60
T5	Other	43
T6	African-American	56
T7	African-American	53
T8	Caucasian	55
N1	Caucasian	62
N2	Caucasian	39
N3	Caucasian	35

RSK Inhibition in vivo

The overall goal of our studies is to develop a RSK inhibitor for *in vivo* use. To evaluate the ability of (**1b**) to inhibit RSK1/2 *in vivo* we used an MCF-7 metastatic model because most of our prior characterization of SL0101 was performed using this line. MCF-7 cells that stably express luciferase (MCF7-Luc) were introduced by intracardiac (IC) injection into NSG mice, and metastasis were established for ~ 50 days. Before treatment we determined that the tumor burden between animals was equivalent (Fig. 27G). Two hours after treatment with (**1b**) or vehicle the animals were euthanized and the tibia isolated, as ER+ tumors frequently metastasize to the bone. Moreover, MCF-7 cells within the tibia were easily identified by their positive staining with cytokeratin 8 (K8) (Fig. 27H). The levels of the RSK target, pS6, were decreased by > 2.5-fold with (**1b**). These results demonstrate that (**1b**) is able to attain a sufficient concentration to induce pharmacodynamic changes *in vivo*.

RSK as a drug target for TNBC

RSK has been proposed as a drug target for TNBC based on observations that ~ 85% of TNBC tumors have activated RSK [54]. In agreement with these observations we found that the levels of activated RSK (pRSK) were higher in TNBC tumors than normal tissue (Fig. 28A, B and Table 7). The levels of activated RSK varied considerably within and between tumors. Moreover, in TNBC tumor tissue activated RSK could be present in the nucleus, cytoplasm or both whereas it was mainly cytoplasmic in normal breast cells. The differences in subcellular localization suggest that the substrates regulated by RSK differ between normal and TNBC tissue. Taken together, these results are consistent with RSK as a viable drug target for TNBC.

To investigate whether activated RSK was functionally important in TNBC we chose a panel of 8 cell lines representing 5 different TNBC subtypes [262]. We observed that activated RSK was present at different levels in these lines (Fig. 28C-E). In 2D culture the proliferation of

all the TNBC lines was inhibited at a lower concentration of (**1b**) than SL0101 (**1a**) (Fig. 29A). The lines from the mesenchymal subtype, CAL-120 and MDA-MB-231, were relatively resistant whereas the basal-like 2 (BL2), HDQ-P1 and HCC70 were among the most sensitive (Fig. 29B). The BL2 lines are of interest clinically because this subtype is correlated with the poorest response to neoadjuvant chemotherapy [263]. To better understand these observations we compared the levels of activated RSK normalized to total RSK1 and RSK2, which should reflect RSK1/2 specific activity (Fig. 29C-E). The anti-RSK2 antibody is less sensitive than the anti-RSK1 antibody and this difference was accounted for by normalizing to recombinant proteins. We observed an inverse relationship between the IC_{50} for (**1b**) and the specific activity of the combined isoforms (Fig. 29D), consistent with the hypothesis that higher RSK specific activity increases sensitivity to the inhibitor. In a separate analysis active RSK was normalized to RSK2 or RSK1 separately and a statistically significant inverse correlation was observed for RSK2 (Fig. 29C-E).

To evaluate specificity we investigated the efficacy of (**1b**) in the context of RSK1/2 silencing. As expected, loss of RSK1/2 decreased 2D proliferation by ~ 60% in MDA-MB-231 cells (Figs. 29F, G). Importantly, silencing RSK1/2 resulted in loss of sensitivity to (**1b**) (Fig. 29G). These results support the conclusion that (**1b**) is specific for RSK1/2 and also demonstrate that RSK1/2 are primarily responsible for regulating the proliferation of MDA-MB-231 cells.

Proliferation of the MDA-MB-231 line is reported to be more sensitive to RSK inhibition in 3D versus 2D [147]. In agreement we observed that the IC_{50} for (**1b**) is ~ 8 μM in 3D and ~ 50 μM in 2D (Fig. 29H). Surprisingly, HDQ-P1 and HCC70 were unable to proliferate in 3D, suggesting that these lines have more stringent requirements for proliferation than MDA-MB-231.

Figure 29 RSK is required for TNBC proliferation and survival

(A) IC_{50}s for (**1b**) in MCF-7 and TNBC lines. Bar, median ± range (n ≥ 2, ≥ quadruplicate). (B) Efficacy of (1a) and (1b) in inhibiting proliferation of various TNBC lines. Symbol, mean ± S.D. (n ≥ 2, triplicate). (C) Correlation of IC50 for inhibition of proliferation by (1b) versus activated RSK normalized to total RSK2 levels. (D) Correlation of IC50 for inhibition of proliferation by (1b) versus activated RSK normalized to total RSK1 and RSK2 levels. (E) Correlation of IC_{50} for inhibition of proliferation by (**1b**) of TNBC lines versus total RSK1 levels. (F) Analysis of lysates from MDA-MB-231 cells transduced with scramble (scrbl) or double transduced with RSK1/2 targeting shRNAs. Bar: non-relevant lanes removed. ns:nonspecific. (G) Efficacy of (**1b**) in inhibiting proliferation of MDA-MB-231 cells transduced as in (F). Symbol, mean ± S.D. (n ≥ 2, triplicate; *p < 0.03 compared to vehicle). (H) Bar graph showing (**1b**) IC_{50} for MDA-MB-231 proliferation in 2D and 3D. Bar,median ± range (n ≥ 2, ≥ quadruplicate). (I) IC_{50}s for (**1b**) for survival of TNBC lines. Bar, median ± range (n ≥ 2, triplicate). (J) Efficacy of (**1b**) in inhibiting survival of MDA-MB-231 cells transduced as in (F). Symbol, mean ± S.D (n ≥ 2, triplicate; *p < 0.01 compared to vehicle).

*Dr. Preston Campbell assisted with Panels F, G and J.

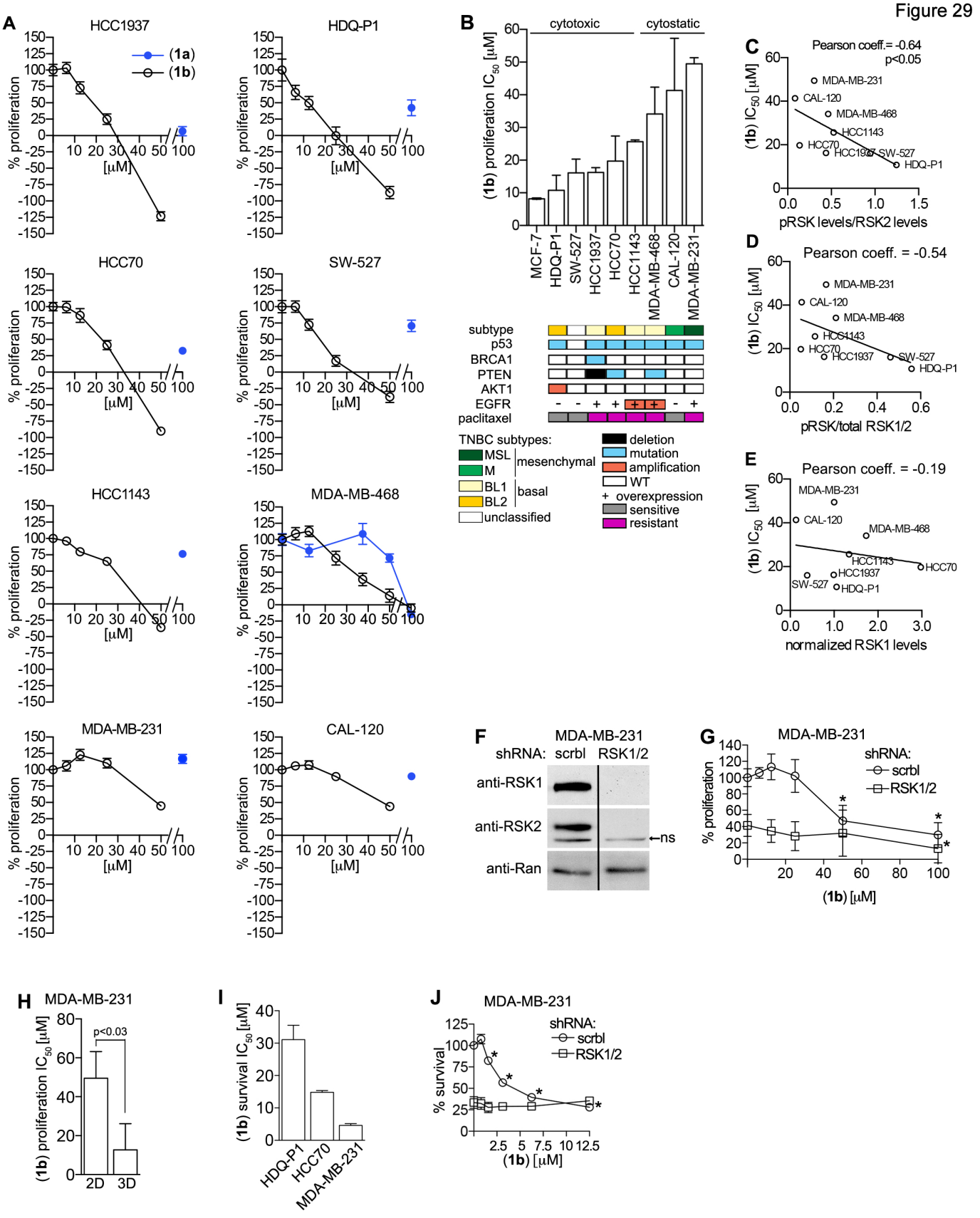
A
HCC1937
HDQ-P1
HCC70
SW-527
HCC1143
MDA-MB-468
MDA-MB-231
CAL-120
(1a)
(1b)
% proliferation
[μM]
B
cytotoxic
cytostatic
(1b) proliferation IC50 [μM]
MCF-7
HDQ-P1
SW-527
HCC1937
HCC70
HCC1143
MDA-MB-468
CAL-120
MDA-MB-231
subtype
p53
BRCA1
PTEN
AKT1
EGFR
paclitaxel
TNBC subtypes:
MSL
M
BL1
BL2
unclassified
mesenchymal
basal
deletion
mutation
amplification
WT
+ overexpression
sensitive
resistant
C
Pearson coeff.= -0.64
p<0.05
(1b) IC50 [μM]
pRSK levels/RSK2 levels
D
Pearson coeff. = -0.54
pRSK/total RSK1/2
E
Pearson coeff. = -0.19
normalized RSK1 levels
F
MDA-MB-231
shRNA: scrbl RSK1/2
anti-RSK1
anti-RSK2
anti-Ran
←ns
G
MDA-MB-231
shRNA:
scrbl
RSK1/2
% proliferation
(1b) [μM]
H
MDA-MB-231
p<0.03
(1b) proliferation IC50 [μM]
2D
3D
I
(1b) survival IC50 [μM]
HDQ-P1
HCC70
MDA-MB-231
J
MDA-MB-231
shRNA:
scrbl
RSK1/2
% survival
(1b) [μM]

The ability of cancer cells to survive in circulation is an important step in metastasis [264] and therefore, we analyzed survival in ultra-low adhesion plates. Survival of HDQ-P1, HCC70, and MDA-MB-231 was dependent on RSK and the IC_{50} for inhibition of survival by (**1b**) was ~ 30, 15 and 3 μM, respectively (Fig. 29I). Silencing RSK1/2 in MDA-MB-231 cells decreased survival by ~ 75% and was not further inhibited by (**1b**) (Fig. 29J). These results demonstrate that the survival of some TNBC lines depends on RSK and confirm that (**1b**) is a very specific RSK inhibitor.

RSK has been implicated in regulating motility [156] and we investigated this possibility using the scratch assay. In all lines tested, (**1b**) reduced cell velocity to the same extent as SL0101 but at lower concentrations (Fig. 30A-C). The motility of HCC70 was reduced by ~ 50%, and in MDA-MB-231 and HDQ-P1 cells motility was decreased by at least 75%. Apoptosis was not detected with the doses and time course used in the scratch assay (Fig. 30D). Taken together, our results demonstrate that inhibition of RSK by (**1b**) reduces proliferation, survival in a non-adherent environment and motility, which are essential components of the metastatic process.

Figure 30 RSK regulates TNBC cell motility

(A*) (1b) and (1a) inhibit motility of the indicated cell lines as measured by the scratch assay. The cells were plated as a confluent monolayer on fibronectin, pre-treated with vehicle or inhibitors for 2 h and a wound introduced into the monolayer. The movement of the cells was monitored over time. The velocity of individual cells was calculated from their distance traveled over the time and normalized to the vehicle control. Representative DIC images and cell traces (as shown by the colored lines) and scatter plots showing efficacy of (**1a**) and (**1b**) in inhibiting motility of of (A) MDA-MB-231, (B) HCC70 and (C) HDQ-P1 cells. Each circle represents a cell trace. Bar, median ($n \geq 2$, 30 cells/treatment). (D) Lysates were obtained from cells treated with vehicle or (1b) for a 10 h time period, which was the maximum length that the scratch assay was performed. Arrows indicate location of full length and cleaved products. The absence of cleaved products indicates that apoptosis was not occurring. MW markers are shown on the right. ns=nonspecific

*Zach Sandusky contributed Panels A, B and C.

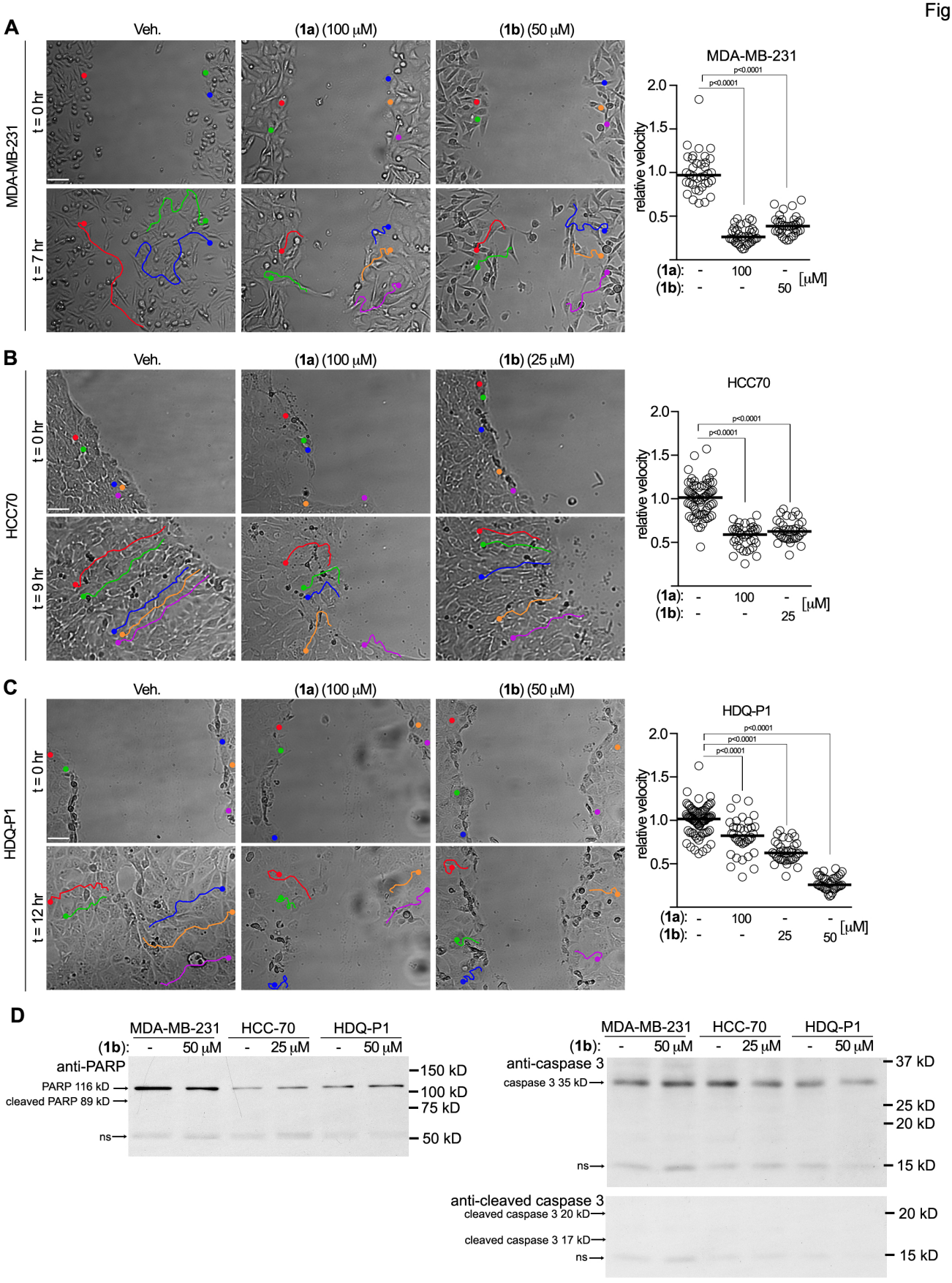
A
Veh.
(1a) (100 μM)
(1b) (50 μM)
MDA-MB-231
t = 0 hr
t = 7 hr
MDA-MB-231
p<0.0001
p<0.0001
relative velocity
2.0
1.5
1.0
0.5
(1a): - 100 - [μM]
(1b): - - 50
B
Veh.
(1a) (100 μM)
(1b) (25 μM)
HCC70
t = 0 hr
t = 9 hr
HCC70
p<0.0001
p<0.0001
relative velocity
2.0
1.5
1.0
0.5
(1a): - 100 - [μM]
(1b): - - 25
C
Veh.
(1a) (100 μM)
(1b) (50 μM)
HDQ-P1
t = 0 hr
t = 12 hr
HDQ-P1
p<0.0001
p<0.0001
p<0.0001
relative velocity
2.0
1.5
1.0
0.5
(1a): - 100 - - [μM]
(1b): - - 25 50
D
MDA-MB-231
HCC-70
HDQ-P1
(1b): - 50 μM - 25 μM - 50 μM
anti-PARP
PARP 116 kD
cleaved PARP 89 kD
ns
150 kD
100 kD
75 kD
50 kD
MDA-MB-231
HCC-70
HDQ-P1
(1b): - 50 μM - 25 μM - 50 μM
anti-caspase 3
caspase 3 35 kD
ns
37 kD
25 kD
20 kD
15 kD
anti-cleaved caspase 3
cleaved caspase 3 20 kD
cleaved caspase 3 17 kD
ns
20 kD
15 kD

Silencing RSK decreases TNBC metastasis in vivo

To identify the contributions of RSK1 and RSK2 to metastasis we used an *in vivo* metastatic MDA-MB-231 model in which luciferase was stably expressed (MDA-MB-231-Luc). MDA-MB-231-Luc cells were transduced with control, RSK1 or RSK2 specific shRNAs (Fig. 31A). The cells were quality controlled for their luciferase signal, and equal numbers of cells were introduced by IC injection into female NSG mice (Fig. 31B). This model will identify whether RSK1 or RSK2 contribute to the metastatic processes that includes metastatic colonization and proliferation at the metastatic site. At day 19 silencing RSK1 or RSK2 decreased the total metastatic burden, as determined by bioluminescence, by > three-fold (Fig. 31C, D). This decrease in metastatic burden is further supported by the observations that silencing RSK1 or RSK2 increased survival by ~ 40-60% (Fig. 31E). Silencing RSK1 or RSK2 reduced the number of metastatic foci by ~ half (Fig. 32A), and remained constant over the duration of the experiment. The number of bioluminescent foci was linearly correlated with the number of metastatic foci as determined by histology (Fig. 32B). Therefore, we conclude that the increased whole animal bioluminescence from day 5 onwards reflects proliferation at the metastatic sites (Fig. 32C). Thus, silencing RSK1 or RSK2 decreased proliferation from day twelve to day nineteen > three-fold compared to the control. We also conclude that the decrease in metastatic foci reflects that RSK1 or RSK2 is necessary for metastatic colonization. This decrease in metastatic foci was not organ dependent (Fig. 32D). *Ex vivo* analysis of bioluminescence was also performed as it improved the resolution for determining individual metastatic foci. These results of the *ex vivo* bioluminescence (Fig. 32E, F) and the histological analysis (Fig. 32G, H) were consistent. We conclude that RSK1/2 regulate numerous steps that comprise the metastatic process, which results in improved survival.

Figure 31 RSK1 and RSK2 contribute to TNBC metastasis*

(A) Analysis of lysates generated from MDA-MB-231 transduced with scramble (scrbl), RSK1 or RSK2-targeting shRNAs. (B) The luminescence signal correlates with the cell number of MDA-MB-231-Luc cells transduced with scramble (scrbl), RSK1- or RSK2- targeting shRNAs. (C) Bioluminescence images of NSG mice injected IC with MDA-MB-231-Luc cells transduced with scramble (scrbl), RSK1- or RSK2-targeting shRNAs (t=19 d). (D) RSK1 and RSK2 decreased the metastatic burden in mice from (A) (t=19 d). (n = 8 mice/group). (E) Kaplan-Meier curves from (A). (n= 8 mice/group; test = log-rank).

*Dr. Preston Campbell contributed Figure 31.

Figure 31

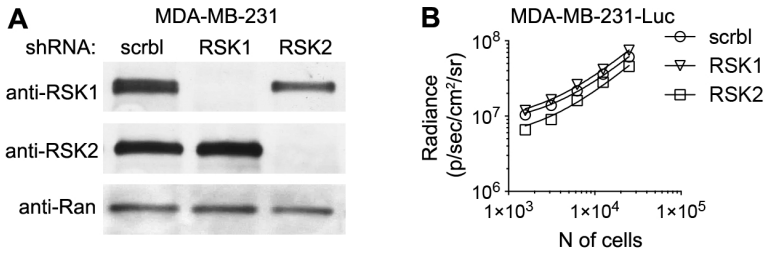
A
MDA-MB-231
shRNA: scrbl RSK1 RSK2
anti-RSK1
anti-RSK2
anti-Ran
B
MDA-MB-231-Luc
Radiance (p/sec/cm²/sr)
N of cells
scrbl
RSK1
RSK2

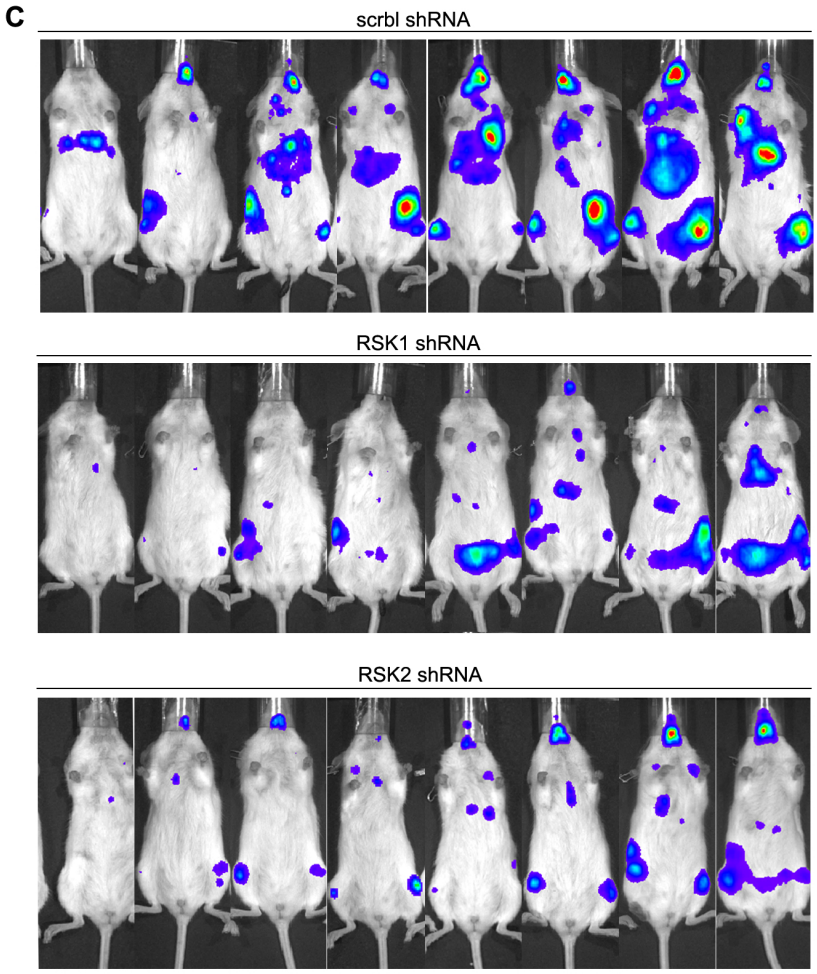
C
scrbl shRNA
RSK1 shRNA
RSK2 shRNA

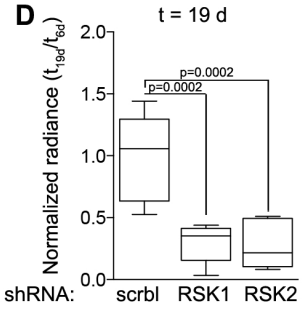
D
t = 19 d
Normalized radiance (t19d/t6d)
p=0.0002
p=0.0002
shRNA: scrbl RSK1 RSK2

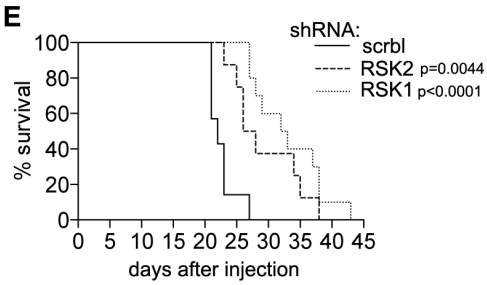
E
shRNA:
scrbl
RSK2 p=0.0044
RSK1 p<0.0001
% survival
days after injection

Figure 32 RSK1 and RSK2 contribute to the metastatic phenotype*

(A) The number of metastatic foci is constant in mice injected IC with MDA-MB-231-Luc cells transduced with scramble (scrbl), RSK1- or RSK2-targeting shRNAs. Symbol, mean. (B) The number of metastatic foci in livers in mice from (A) detected by histology correlates with the number of metastatic foci in livers detected by ex vivo bioluminescence imaging. (n= 8 mice/group, 4 sections/mouse). (C) Total bioluminescence in mice from (A) is decreased with RSK1 or RSK2 silencing. Each line represents a mouse; the data are fold change over day 6. (D) Loss of RSK1 or RSK2 decreased the number of metastatic foci in numerous organs in mice from (A) (t=19 d). Bar, mean ± SD (n = 8 mice/ group). (E) Representative *ex vivo* bioluminescence images of livers of mice from (A). (F) *Ex vivo* analysis confirms that silencing RSK1 or RSK2 decreased the number of metastatic foci in the livers from (A). Bar, median ± quartile (n=4 mice/group). (G) Representative paraffinembedded H&E sections of mouse livers from (A). Arrow heads indicate tumor foci. (H) Silencing RSK1 or RSK2 reduces the number of liver metastatic foci as detected by H&E. Bar, median + quartile (n = 8 mice/group, ≥4 sections/mouse).

*Dr. Preston Campbell contributed Panels A, D-H and assisted with Panels B and C.

Figure 32

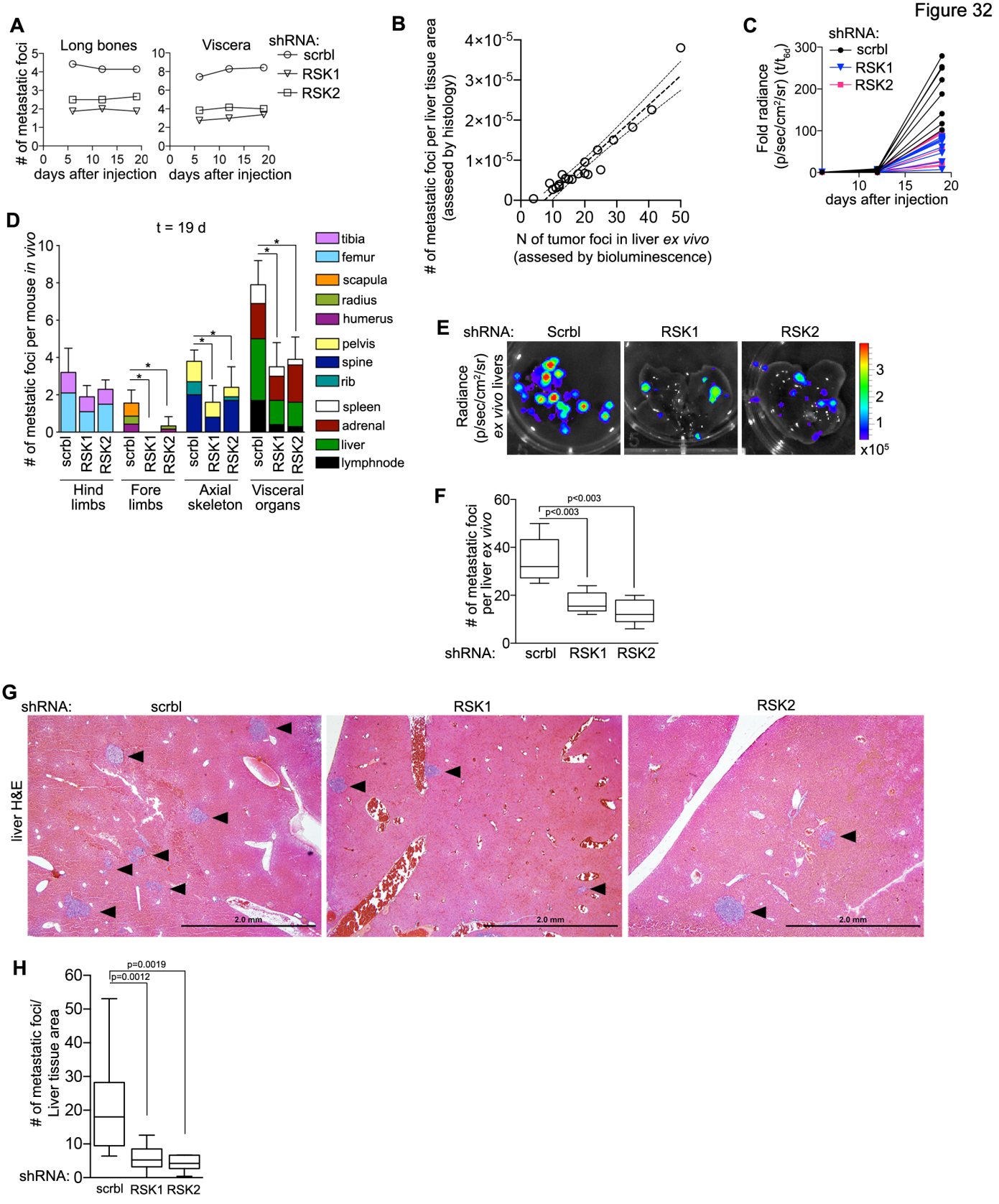
A
Long bones
Viscera
shRNA:
scrbl
RSK1
RSK2
# of metastatic foci
days after injection
B
# of metastatic foci per liver tissue area (assesed by histology)
N of tumor foci in liver ex vivo (assesed by bioluminescence)
C
shRNA:
scrbl
RSK1
RSK2
Fold radiance (p/sec/cm²/sr) (t/t8d)
days after injection
D
t = 19 d
# of metstatic foci per mouse in vivo
tibia
femur
scapula
radius
humerus
pelvis
spine
rib
spleen
adrenal
liver
lymphnode
Hind limbs
Fore limbs
Axial skeleton
Visceral organs
E
shRNA:
Scrbl
RSK1
RSK2
Radiance (p/sec/cm²/sr) ex vivo livers
x10⁵
F
# of metastatic foci per liver ex vivo
p<0.003
p<0.003
shRNA:
scrbl
RSK1
RSK2
G
shRNA:
scrbl
RSK1
RSK2
liver H&E
2.0 mm
H
# of metastatic foci/ Liver tissue area
p=0.0019
p=0.0012
shRNA:
scrbl
RSK1
RSK2

Inhibition of RSK decreases metastatic colonization

We investigated whether (**1b**) would be sufficiently efficacious to decrease metastatic colonization *in vivo*. For these experiments we used the HDQ-P1 model because of the clinical importance of the BL2 subtype. This model has not previously been used as an *in vivo* metastatic model. To validate the model, HDQ-P1 cells were transduced with luciferase (HDQ-P1-Luc) and introduced by IC injection into male NSG mice. At 24 h after injection, the cells were widespread through the animal, but by day five the cells were primarily localized to the liver, adrenal glands and testes (Fig. 33A, B). This model is in contrast to the widely used MDA-MB-231 IC metastatic model, in which the cells primarily metastasize to the bone. TNBC primarily metastasizes to lymph nodes and viscera more often than to the bone, and the HDQ-P1 model better recapitulates these clinical observations.

To evaluate the efficacy of (**1b**), we compared it to a drug that is in the same class as (**1b**) and therefore, would be expected to generate a similar phenotype. The MEK inhibitor, trametinib, is approved for melanoma and is currently in multiple clinical trials including those for breast cancer [265]. MEK inhibition will decrease ERK1/2 activity and reduce RSK activation [254]. HDQ-P1-Luc cells were introduced by IC injection into female NSG mice and treatment began 2 h after injection. The animals were imaged just before treatment to ensure viability and distribution of the cells *in vivo*. This approach recapitulates the clinical scenario of tumor cells within the circulation, which have been proposed to act as a negative prognostic marker and demonstrate similar therapeutic responsiveness as the metastatic tumor [242]. By 24 h both (**1b**) and trametinib decreased the total *in vivo* bioluminescence by three-fold (Fig. 33C, D). Moreover, the number of metastatic foci in both the skeleton and the viscera was reduced by drug treatment (Fig. 33E). Treatments were stopped on day 5 and on day 6 the total *in vivo* bioluminescence was reduced three-fold by drug treatment in comparison to the control (Fig. 33F). To confirm these findings we measured the bioluminescence of the liver and adrenal

glands *ex vivo* and observed a five-fold reduction in metastatic burden in mice treated with either drug (Fig.33G-J). We conclude that inhibition of RSK or its upstream activator, MEK, decreases metastatic colonization. Moreover, these observations with HDQ-P1 confirm those obtained with MDA-MB-231.

Inhibition of RSK does not activate AKT

Inhibiting "global regulators" such as MEK results in a number of side effects and their ability to induce an effective clinical response appears limited [253]. MEK inhibition can result in activation of AKT [266] and based on these results there are clinical trials underway combining MEK inhibitors with an AKT or PI3K inhibitor [267]. Consistent with the literature, we observed that treatment of MDA-MB-231 cells with trametinib enhanced the levels of phosphoSer 473 AKT (pAKT), which is necessary for AKT activity (Fig. 34A). In contrast, activation of AKT was not observed in response to (**1b**). In comparison to MDA-MB-231, HDQ-P1 have high basal levels of active AKT but consistent with the results observed in MDA-MB-231, (**1b**) did not increase AKT activity in contrast to trametinib (Fig. 34B). Taken together, these results indicate that RSK inhibition by itself will effectively target the TNBC metastatic process but not have the undesirable side effect of activating AKT.

Figure 33 Pharmacological inhibition of metastatic colonization by (1b)*

(A) Representative bioluminescence images at the indicated times of male NSG mice injected IC with HDQ-P1-Luc cells. (B) Total bioluminescence signal from HDQ-P1-Luc metastases stabilizes within the viscera in mice from (A). Symbol, mean ± S.D. (n= 4 mice). (C) Bioluminescence images of NSG mice injected IC with HDQ-P1-Luc cells at t=1h and 24h after injection. At 2h after injection mice were treated with vehicle, (**1b**) (40 mg/kg) IP Q12h or trametinib (tram) (2 mg/kg) IP Q24h. Inhibition of RSK or MEK decreases total metastatic burden (D) and the number of metastatic foci in individual organs (t=24h) (E). Bar, mean ± SD (n=4 mice/group, *p<0.05). (F) Inhibition of RSK or MEK decrease total metastatic burden (t=6d). (n=4 mice/group). Representative *ex vivo* bioluminescence images of livers (G) and adrenal glands (I) (t=6d). *Ex vivo* analysis confirms that inhibiting RSK or MEK activity decreased the metastatic burden in livers (H) and adrenals (J). (n=4 mice/group).

*Dr. Preston Campbell contributed Figure 33.

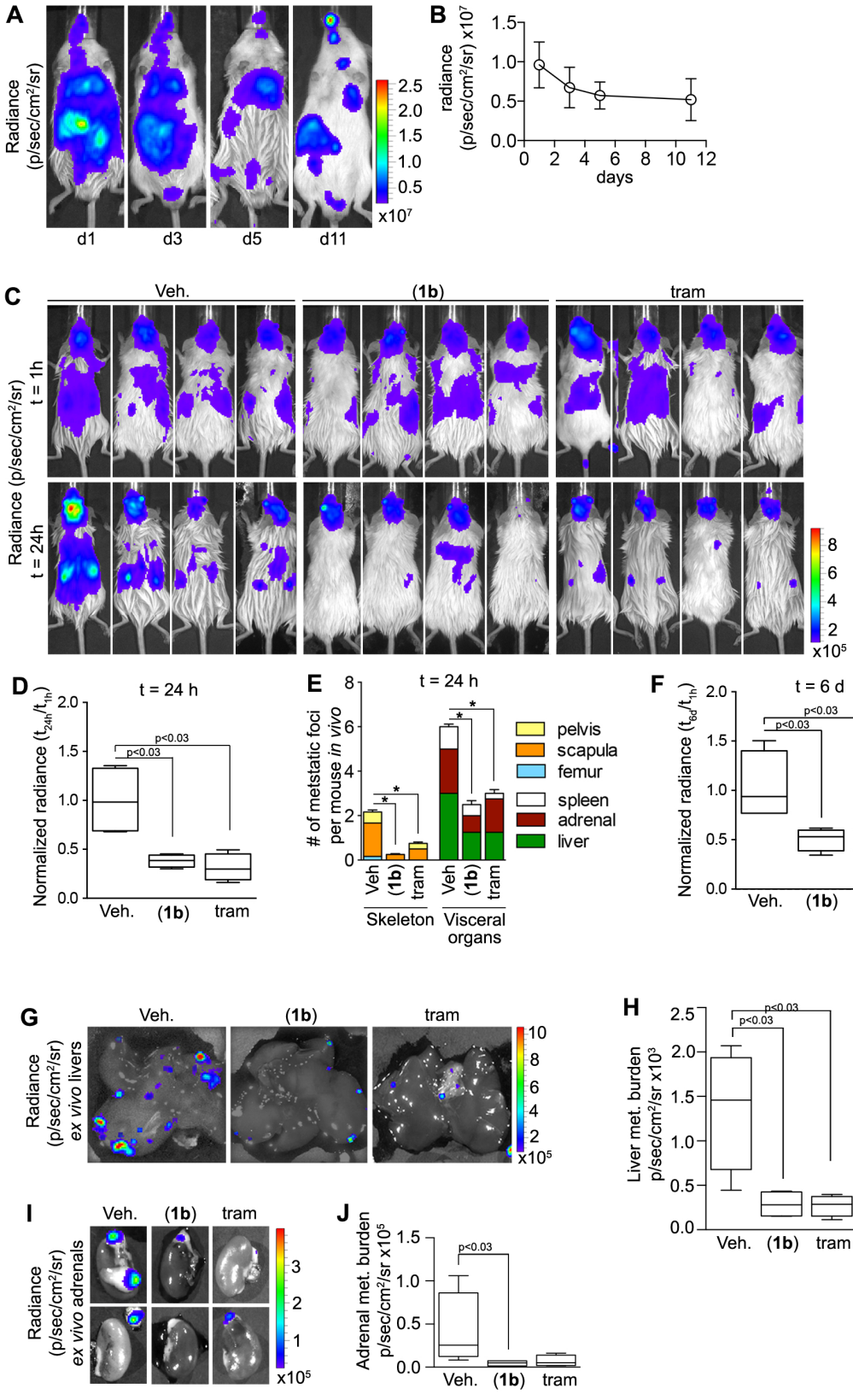
A
Radiance (p/sec/cm²/sr)
d1
d3
d5
d11
x10⁷
B
radiance (p/sec/cm²/sr) x10⁷
days
C
Veh.
(1b)
tram
t = 1h
t = 24h
Radiance (p/sec/cm²/sr)
x10⁵
D
t = 24 h
Normalized radiance (t24h/t1h)
p<0.03
Veh.
(1b)
tram
E
t = 24 h
# of metstatic foci per mouse in vivo
pelvis
scapula
femur
spleen
adrenal
liver
Skeleton
Visceral organs
F
t = 6 d
Normalized radiance (t6d/t1h)
G
Radiance (p/sec/cm²/sr) ex vivo livers
x10⁵
H
Liver met. burden p/sec/cm²/sr x10³
I
Radiance (p/sec/cm²/sr) ex vivo adrenals
x10⁵
J
Adrenal met. burden p/sec/cm²/sr x10⁵

Figure 34 (1b) does not activate AKT*

Analysis of lysates from (A) MDA-MB-231 and (B) HDQ-P1 cells treated with vehicle, trametinib (1 μM) or (**1b**) (25 μM) for 2h. Bar = separate gels.

*Dr. Preston Campbell contributed Figure 34.

Figure 34

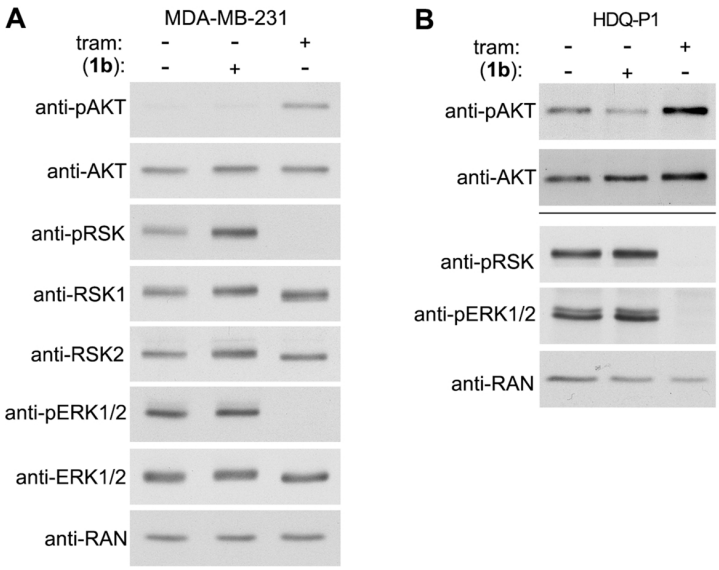
A
MDA-MB-231
tram: - - +
(1b): - + -
anti-pAKT
anti-AKT
anti-pRSK
anti-RSK1
anti-RSK2
anti-pERK1/2
anti-ERK1/2
anti-RAN
B
HDQ-P1
tram: - - +
(1b): - + -
anti-pAKT
anti-AKT
anti-pRSK
anti-pERK1/2
anti-RAN

Discussion

The importance of RSK in regulating metastasis *in vivo* has not been thoroughly investigated. Kang et al [69] reported that silencing RSK2 decreased metastatic colonization to the lymph nodes using a human head and neck squamous cell carcinoma line. They further followed up on these observations using the RSK CTKD inhibitor, FMK-MEA, which resulted in a modest decrease in metastatic tumor burden from 97% to 79% [70]. In a screen Lara et al [75] identified that loss of RSK1 increased motility in lung cancer lines but in contrast Zhou et al [76] found that inhibition of RSK activity was associated with decreased motility in lung cancer lines. It is possible that the discrepancy between these studies results from the ability of RSK1 to act as a scaffold and regulate other signaling pathways. RSK has also been proposed as a drug target for TNBC based on observations that it decreased the levels of the surface marker CD44, which is reported to be associated with cancer stem cells [54]. We demonstrated using genetic and pharmacological approaches *in vitro* and *in vivo* that reducing RSK1/2 activity or RSK1 or RSK2 levels inhibits multiple steps within the metastatic program. Furthermore, we confirmed that activated RSK is present in the majority of TNBCs. Our results strongly suggest that RSK is a viable drug target for TNBC metastasis.

We also report the generation and validation of a novel SL0101 analogue, *C6"-n-propyl* cyclitol SL0101 (**1b**) that is specific for RSK1/2. The specificity of the inhibitor for RSK1/2 is demonstrated by our observations that silencing RSK1/2 eliminates responsiveness to (**1b**) in MDA-MB-231 proliferation and survival assays. In *in vitro* assays using multiple TNBC cell lines the new analogue inhibits the major steps involved in the metastatic process, which include motility, proliferation and survival in a non-adherent environment. Additionally, (**1b**) was as effective at inhibiting metastatic colonization *in vivo* as the FDA-approved MEK inhibitor, trametinib. Activation of the AKT pathway is proposed as a mechanism to account for the lack of efficacy of selumetinib, a MEK inhibitor, in combination with the anti-estrogen, fulvestrant, in a

phase II clinical trial [268]. We propose that inhibitors of RSK will offer greater flexibility in designing combination cancer therapies than MEK inhibitors, as there will be no positive feedback loop that results in activation of AKT.

Chapter 5 A Breast Cancer Organoid System for Precision Medicine that Preserves Intra-Tumor Heterogeneity

Summary

Intra-tumor breast heterogeneity contributes to chemotherapy resistance and decreased patient survival. Therefore, to improve patient outcomes it is essential to develop a screening technology that will rapidly select the most efficacious therapy that targets the diverse phenotypes present within the tumor. We have developed robust organoid culture conditions for human breast cancer subtypes, based on empirical stromal growth factor analysis, that quantitatively recapitulate intra-tumor heterogeneity. The Jensen-Shannon divergence index demonstrated a high degree of similarity between the *in vitro* generated tumor organoids and starting tissue. HER1 drives intra-tumor heterogeneity to generate divergent cellular phenotypes that have differential sensitivities to chemotherapies. Our methodology, which focuses on quantifiable cellular phenotypes, provides a tractable system that complements genetic analysis to provide an unprecedented view of intra-tumor heterogeneity and will enhance the identification of novel therapies and facilitate personalized medicine.

Introduction

Breast cancer death rates have decreased during the last several decades but breast cancer is still the second leading cause of cancer deaths in women. In the clinic breast cancer is screened for the presence of estrogen receptor (ER), progesterone receptor (PR) and amplification of ERBB2/HER2 (HER2). Based on these assessments tumors are divided into ER+, HER2+ with or without ER+, and triple negative breast cancer (TNBC) subgroups, and the outcome of these analyses plays a major role in determining treatment options [269]. However, genomic and transcriptomic analysis reveals that breast cancer can be subdivided into at least five different subtypes [270] with associated gene mutations and signaling pathway activations [249]. Adding to this complexity is a substantial phenotypic and genetic intra-tumor heterogeneity [271-275], which, depending on the tumor region analyzed, can significantly impact the prognosis [152]. Importantly, the various cell types that comprise the tumor are likely to respond differentially to therapies, which could lead to chemotherapy resistance and treatment failure. This complexity is not unique to breast cancer and numerous efforts are underway to develop models that will provide clinically actionable insights into the development of intra-tumor heterogeneity and its contribution to treatment resistance, and to identify durable therapies that can overcome the diversity within a patient's tumor.

Patient-derived xenografts (PDX) have demonstrated an ability to predict patient response to treatment [153]. However, the establishment of PDX models takes many months, precluding their use for personalized medicine. Two-dimensional cultures of dissociated human tumors do not recapitulate the structural complexity, cellular phenotypes, or gene expression profiles of the intact tumor tissue [276]. Thus, the ability to use primary tissue in a 3D culture system that generates an organ or tumor with properties similar to the tissue of origin is an attractive alternative, which would greatly facilitate investigations of tumor progression, responses to therapy, and diagnostics. This type of organoid system has been particularly well

characterized for the normal human gastrointestinal tract [277] and the normal human breast [162]. More recently, organoid models were described for colorectal cancer [278], pancreatic ductal adenocarcinoma [279], prostate cancer [280, 281] and breast cancer [282]. However, in these reports the similarity of the starting tumor tissue to the organoids was based only on H&E staining, qualitative immunohistochemistry and DNA or gene expression analyses, which does not fully address the key issue of intra-tumor heterogeneity. Recently described organoid culture systems for breast cancer did not provide any comparison between the starting tumor tissue and the tumor organoid [283, 284]. Thus, it is entirely unknown whether these model systems effectively capture the multiple cellular phenotypes observed in the starting tumor tissue.

The overall goal of this study was to identify robust *in vitro* conditions that would recapitulate the *in situ*, inter- and intra- breast cancer phenotypes, using approaches that we pioneered for normal mammary organoids [162]. We analyzed stromal production of growth factors from different breast cancer subtypes as a starting point for developing our culture conditions. We also developed an identity score that allows quantitative comparison of the phenotype of the tumor organoid generated in culture with that of the starting tissue. Using this method we discovered that EGF is necessary for recapitulating the TNBC phenotype, whereas AREG is required for capturing the phenotype of ER+ and ER+/HER2+ breast cancers. Furthermore, intrinsic differences to HER1 signaling in the cells that comprise the tumor are sufficient to generate the diverse intra-tumor phenotypes observed *in situ*. We could identify differing responses to drug treatments between patient samples, and in most instances enrichment of a resistant cell phenotype was observed. The diverse phenotypes observed in the tumors survived cryopreservation and multiple passages of primary ER+ and ER+/HER2+ breast cancers. Therefore, this methodology will greatly facilitate our ability to study patient-

derived breast cancer tissue, to identify drivers of heterogeneity, and to improve breast cancer treatments.

Materials and Methods

Organoid and fibroblast isolation

Human breast tissue from reduction mammoplasty or breast cancer surgery was collected as waste tissue with institutional review board approval. A list of age, race, and diagnosis for each patient used in this study is provided (Table 8). Organoids were prepared as previously described [162]. Briefly, tissue was minced and digested in Collagenase A medium (DMEM/F12 (Thermo Fisher Scientific), 1 mg/mL Collagenase A (Roche Diagnostics), 1 µg/mL insulin (Sigma-Aldrich), 600 U/µL Nystatin (Sigma-Aldrich), 100 U/mL penicillin–100 µg/mL streptomycin (Thermo Fisher Scientific)) for 18-21h in a 37°C 5% CO_2 incubator. Digested material was pelleted at 180g for 5 min and the supernatant collected for fibroblast isolation. The remaining pellet was resuspended in DMEM/F12 with DNAse I (1000 U/ml) (Sigma-Aldrich) for 3-5 min in a 37°C 5% CO_2 incubator. Fetal bovine serum (FBS) (0.5 mL) was added and the digested tissue was pelleted at 180g for 10 min. The pellet was resuspened in 9 ml of DMEM/F12 and centrifuged at 350g for 15 sec. This wash was repeated 4-6 times. The pellet was resuspended in 1 ml of base medium (DMEM/F12, 1 µg/mL hydrocortisone (Sigma-Aldrich), 10 µg/mL insulin-5.5 µg/mL transferrin–6.7 ng/mL selenium-2 µg/mL ethanolamine (Thermo Fisher Scientific), 2.5 µg/mL Amphotericin B (Sigma-Aldrich), 50 µg/mL gentamicin (Thermo Fisher Scientific), 100 U/mL penicillin-100µg/mL streptomycin). A volume of 60µl of a 60% Matrigel in base media was added into the wells of an 8-well LabTek plate and solidified for 15 minutes in a 37°C 5% CO_2 incubator. Organoids were counted and resuspended in a 50% Matrigel in base media. A volume of 40 µl of Matrigel/organoid solution containing 30-40 medium sized organoids was plated onto the solidified Matrigel layer and allowed to solidify for 15 minutes at 37°C.

Table 8 Patient Information

Patient ID	Age	Race	Diagnosis	Treatment
494	64	Caucasian	Normal	
520	35	Caucasian	Normal	
552	42	Caucasian	Normal	
581	43	African-American	Normal	
586	32	African-American	Normal	
272	47	African-American	TNBC	chemo
275	28	Caucasian	TNBC	
287	56	African-American	TNBC	radiation/chemo
297	56	African-American	TNBC	
323	43	Caucasian	TNBC	chemo
396	40	African-American	TNBC	
435	58	Caucasian	ER+	
502	62	Caucasian	ER+	
549	54	Caucasian	ER+	
510	45	Caucasian	ER+/HER2+	
486	30	Caucasian	ER+	
461	50	Caucasian	ER+	

Organoid culture and drug treatment

For drug treatments organoids were treated with 4-hydroxy tamoxifen (Sigma-Aldrich), fulvestrant (Santa Cruz Biotechnology Inc.), palbocicilib (Selleckchem), or paclitaxel (R&D systems) starting at day 0. For all conditions, the medium was replaced every 2-3 days and drugs were added with fresh medium every 48 h. The organoids were cultured for 7-10 days.

Antibodies

Primary antibodies used were rat anti-Keratin 8 (University of Iowa), chicken anti-Keratin 14 (BioLegend), mouse anti-ZO1 (Thermo Fisher Scientific), rabbit anti-Ki-67 (Thermo Fisher Scientific), rabbit anti-cleaved caspase 3 (Cell Signaling Technology), rabbit anti-ERα (Thermo Fisher Scientific), and rabbit anti-EGFR (Cell Signaling Technology). DNA was stained using Hoeschst 33342 dye (Invitrogen). Secondary antibodies were goat anti-mouse AlexaFluor 488 IgG (H+L) *highly cross-adsorbed*, goat anti-chicken AlexaFluor 546 IgY (H+L), goat anti-rat AlexaFluor 647 IgG (H+L), donkey antirabbit AlexaFluor 488 IgG (H+L) (Invitrogen).

Immunostaining

Organoids were fixed and immunostained as previously described [162]. Detailed methods for immunostaining, imaging, and analysis are provided in the supplementary experimental procedures. Briefly, organoids were washed twice with room-temperature (RT) PBS, fixe0d in 4% paraformaldehyde (PFA, 500ul) for 1 h at RT and incubated in 0.4% PFA at 4oC overnight. The PFA was removed and 120 mL of 1.5% agarose in PBS was added. The solidified agar block was transferred into a cell-safe mesh biopsy capsule (Cancer Diagnostics, Inc.), paraffin-embedded, and cut into 5-µm sections. The sections were deparaffinized, rehydrated, and blocked in 10% bovine serum albumin (BSA) in PBS, and incubated with primary antibody for 16-21 h at 4°C. The sections were incubated with secondary antibody in 3% BSA in PBS for 1 h at RT. After three washes with PBS, the sections were incubated with

Hoechst 33342 in PBS for 10 min at RT and washed three times with PBS. The coverslips were mounted using Fluoro-Gel (Electron Microscopy Sciences). A list of the primary and secondary antibodies used in this study is provided.

Image analysis

DIC images were obtained using a Nikon Ti-E microscope with a 10X CFI Plan Fluor objective NA 0.30 (Nikon). Immunostained sections were imaged using a laser-scanning microscope (510/Meta/FCS Carl Zeiss, Inc.) with a 40x Plan-Neofluar oil objective NA 1.3 using 0.7x zoom. Images were acquired using Volocity software (PerkinElmer) or LSMFCS software (Carl Zeiss, Inc.) and quantified using ImageJ software version 1.49v (National Institutes of Health) or OpenLab (PerkinElmer). Images were processed in Photoshop version CS6 version 13.0 (Adobe Systems).

RNA-sequencing

RNA samples were prepared using the TruSeq mRNA library method (poly-A selected). Sequencing was done using the Illumina HiSeq 3000 at 2X75 paired-end reads by Vanderbilt Technologies for Advanced Genomics with a mean of 30e6 reads per library. TopHat (v2.0.9) spliced aligner software was used to align reads to hg19, using refseq transcripts as a guide [285]. Transcripts were assembled and quantified using refseq transcripts as a guide with cufflinks, and normalized FPKMs generated using cuffnorm [286]. Normalized FPKM expression levels were analyzed in R/Bioconductor. Principle Component Analysis was performed using pcaMethods [287].

Statistical Analysis

Statistical analyses were performed using GraphPad Prism 6. Statistical significance was determined using the Mann-Whitney test (two-sided) and all p-values <0.05 are reported.

Results

Breast Tumor Heterogeneity

The normal mammary duct consists of two layers, with cytokeratin 8 (K8) expressed in epithelial cells of the luminal layer and cytokeratin 14 (K14) expressed primarily in the surrounding basal layer of myoepithelial cells [288]. We observed previously that the proportions of the different cell types within normal breast tissue are highly consistent within and between patients [162]. However, for breast cancers we observed substantial heterogeneity within and between tumors regardless of their subtype. Therefore, a first major hurdle was to develop robust methodologies for the visualization and quantitative discrimination of this heterogeneity.

Tumor subtypes were based on clinical assessment (Table 8) and a pathologist independently evaluated the tissue used in this study (Fig. 35). The levels of ERα and EGF receptor (HER1), as appropriate for the tumor type, were also evaluated as a complement to the H&E sections. The data set contained tumors from thirteen different breast cancer patients and five samples from breast surgery reduction (normal). To analyze heterogeneity we used immunofluorescence immunostaining, which allows preservation of tissue architecture and thus provides high morphologic resolution at the subcellular level. The cytokeratin markers 8 (K8) and 14 (K14) are expressed in the normal breast and to varying extents in different types of breast cancers [289] and therefore, we initially focused on these markers. Initially, the $\log_{10}$ of the ratio of K8+ to K14+ area for each section was graphed separately for the normal breast tissue and the various breast cancer types and a probability density function generated (Fig. 36A). The normal tissue is highly uniform and as expected TNBC generated a distribution that was skewed to the left of the normal reflecting the high K14+ content whereas ER+ breast cancer was skewed to the right indicative of the high K8+ content (Fig. 36A, B).

Figure 35 Representative H&E stained sections of patients

Figure 35

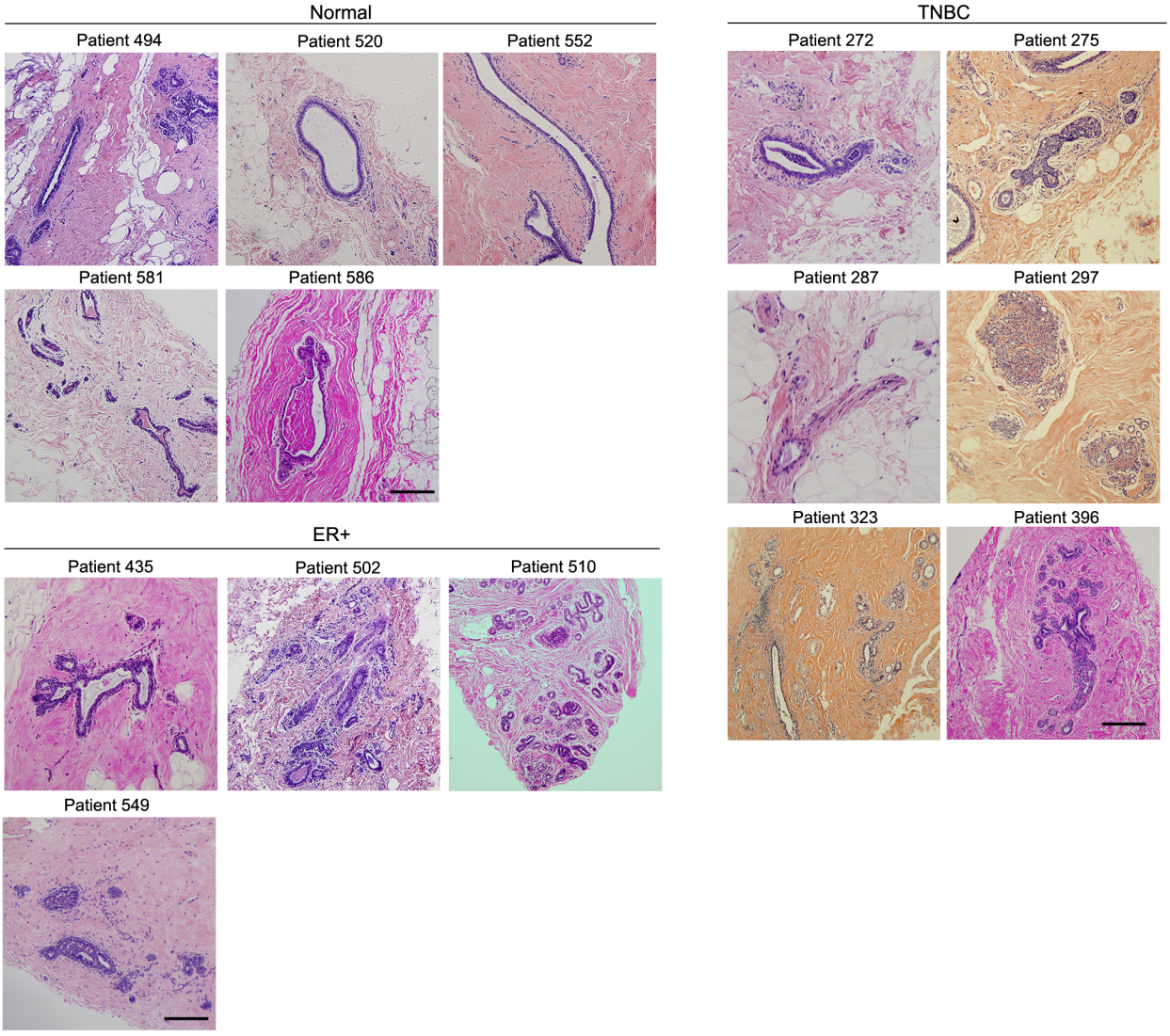
Normal
Patient 494
Patient 520
Patient 552
Patient 581
Patient 586
ER+
Patient 435
Patient 502
Patient 510
Patient 549
TNBC
Patient 272
Patient 275
Patient 287
Patient 297
Patient 323
Patient 396

To facilitate analysis the distribution obtained from the normal tissue was divided into equal groups and these quartiles were used to bin the data. Additionally, sections in the tumor types that fell outside the normal tissue distribution to the extreme left or right generated additional bins. The percentage of sections present in each bin was used to generate heat maps, and the difference between TNBC, ER+ and normal breast tissue is easily visualized (Fig. 36C).

Comparison of tissue phenotypes using JSI

Section distribution across the bins provided the basis of our statistical approach using the Jensen-Shannon divergence analysis to quantitatively evaluate our ability to distinguish between TNBC, ER+ and normal tissue using only K8 and K14 as markers. We measured the similarity between the probability distributions of TNBC, ER+ and normal tissue among bins using Jensen-Shannon divergence index (JSI):

$$JSI(P||Q) = 0.5(\sum P(logP - logM) + \sum Q(logQ - logM))$$

in which M = 0.5(P+Q), P = probability distribution of the sections obtained from starting tissue (ST) obtained from an individual patient X (X = patient identifier), Q = probability distribution of the sections randomly selected from the total number of ST for all tissue. The more similar two distributions are the closer the JSI will be to zero. To provide context for the JSI we used a bootstrap method in which we compared a random subset of the ST available for a particular patient X to a randomly selected subset from the total number of ST. We calculated the JSI and repeated the randomization process 10^3 times to generate an average JSI, which will be equal to 0.246. The average JSI ($JSI_{ave)}$ is used as a cutoff to determine whether distributions are similar. Thus when the JSI between two patient distributions is $<JSI_{ave}$ then the two distributions are more similar than when $>JSI_{ave}$. To facilitate comparisons a JSI matrix was generated, which compares all patient ST to each other (Table 9). The matrix illustrates that

Figure 36 Probability density distribution as a method to visualize intra- and inter-tumor heterogeneity.

(A) The $\log_{10}$ ratio of K8+ to K14+ cells was plotted as a probability density distribution for normal tissue, TNBC, and ER+. The dashed lines indicate the quartiles associated with the normal tissue distribution. (B) Heat map showing inter-tumor heterogeneity of all the starting tissue analyzed, which was based on the percentage of sections that fall within a defined bin. (C) Representative images from the bins associated with a particular phenotype are shown. (D) Heat map showing intra-tumor heterogeneity of all the starting tissue analyzed, which was based on the percentage of sections that fall within a defined bin. (E) The $\log_{10}$ ratio of K8+ to K14+ cells was plotted as a probability density distribution for individual patients based on the indicated diagnosis. The dashed lines indicate the quartiles associated with the normal tissue distribution

*Lejla Pasic and Frances Greathouse assisted with Figure 36.

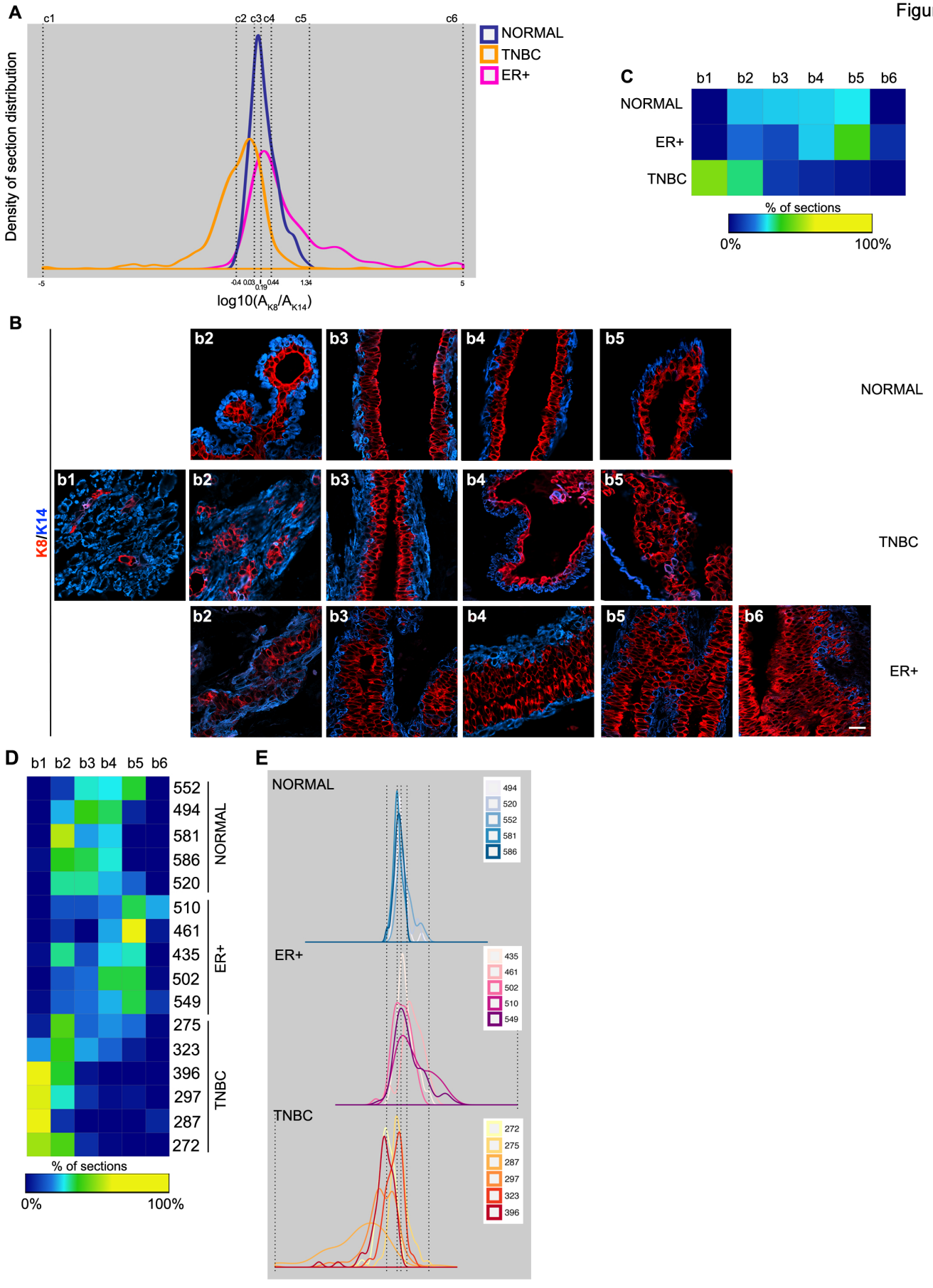
A
c1
c2 c3 c4
c5
c6
NORMAL
TNBC
ER+
Density of section distribution
-5
-04 0.03
0.19
0.44
1.34
5
log10(A_K8/A_K14)
C
b1 b2 b3 b4 b5 b6
NORMAL
ER+
TNBC
% of sections
0%
100%
B
K8/K14
b1
b2
b3
b4
b5
b6
NORMAL
TNBC
ER+
D
b1 b2 b3 b4 b5 b6
552
494
581
586
520
510
461
435
502
549
275
323
396
297
287
272
NORMAL
ER+
TNBC
% of sections
0%
100%
E
NORMAL
494
520
552
581
586
ER+
435
461
502
510
549
TNBC
272
275
287
297
323
396

Table 9 JSI values for each patient to patient comparison.

Thick lines delineate within subtype comparisons

Table 9

Pat.ID	272	275	287	297	323	396	435	461	549	502	510	520	494	552	581	586
272	0.000	0.337	0.191	0.027	0.154	0.016	0.645	0.813	0.574	0.458	0.666	0.486	0.528	0.666	0.388	0.388
275	0.337	0.000	0.691	0.312	0.074	0.430	0.116	0.318	0.106	0.028	0.198	0.051	0.110	0.146	0.121	0.120
287	0.191	0.691	0.000	0.159	0.469	0.128	0.877	0.873	0.759	0.787	0.797	0.859	0.874	0.914	0.831	0.783
297	0.027	0.312	0.159	0.000	0.139	0.036	0.565	0.718	0.498	0.411	0.591	0.451	0.496	0.578	0.442	0.418
323	0.154	0.074	0.469	0.139	0.000	0.233	0.277	0.545	0.249	0.157	0.362	0.141	0.158	0.281	0.144	0.110
396	0.016	0.430	0.128	0.036	0.233	0.000	0.732	0.850	0.658	0.546	0.743	0.596	0.641	0.761	0.502	0.503
435	0.645	0.116	0.877	0.565	0.277	0.732	0.000	0.141	0.043	0.052	0.103	0.082	0.124	0.022	0.279	0.251
461	0.813	0.318	0.873	0.718	0.545	0.850	0.141	0.000	0.148	0.199	0.157	0.348	0.455	0.199	0.594	0.602
549	0.574	0.106	0.759	0.498	0.249	0.658	0.043	0.148	0.000	0.071	0.034	0.114	0.173	0.069	0.310	0.270
502	0.458	0.028	0.787	0.411	0.157	0.546	0.052	0.199	0.071	0.000	0.154	0.055	0.127	0.080	0.186	0.185
510	0.666	0.198	0.797	0.591	0.362	0.743	0.103	0.157	0.034	0.154	0.000	0.193	0.259	0.140	0.388	0.373
520	0.486	0.051	0.859	0.451	0.141	0.596	0.082	0.348	0.114	0.055	0.193	0.000	0.029	0.073	0.106	0.091
494	0.528	0.110	0.874	0.496	0.158	0.641	0.124	0.455	0.173	0.127	0.259	0.029	0.000	0.109	0.098	0.054
552	0.666	0.146	0.914	0.578	0.281	0.761	0.022	0.199	0.069	0.080	0.140	0.073	0.109	0.000	0.302	0.247
581	0.388	0.121	0.831	0.442	0.144	0.502	0.279	0.594	0.310	0.186	0.388	0.106	0.098	0.302	0.000	0.033
586	0.388	0.120	0.783	0.418	0.110	0.503	0.251	0.602	0.270	0.185	0.373	0.091	0.054	0.247	0.033	0.000

sections derived from a particular ST of an individual were highly similar to those obtained from the ST of a different individual who had a similar diagnosis. The similarities and differences are visualized by using the matrix to generate a heat map. These data demonstrate that the JSI can be used to identify similarities between patients with a similar diagnosis.

The distribution across the bins also reflects the extent of intra-tumor heterogeneity, which is observed by the varying distributions of sections obtained from an individual (Fig. 36D, E). The JSI matrix also provides an indication of the amount of intra-tumor heterogeneity in a particular patient sample compared to other samples with a similar diagnosis (Table 9). Based on this analysis the ER+ tissues appear more homogenous to each other than the TNBC tissue. As an example, the TNBC patient 275 is similar to 323 but differs from the other TNBC using the JSI_{ave} as a cutoff as described. In contrast the ER+ patient 435 is similar to all other ER+ patient samples.

We next investigated whether additional markers would aid in further characterizing intra- tumor heterogeneity. For TNBC the markers cluster of differentiation 10 (CD10) and smooth muscle actin (SMA) were used in combination with K8 and K14. The distribution of CD10 or SMA compared to that of K14 showed a positive linear correlation, which was significant (Fig. 37A) and indicates that the CD10 and SMA markers are redundant to K14. We also investigated the use of the markers K18 or ERα in ER+ breast cancer in combination with K8 and K14 (Fig. 37B). The distribution of K18 generated a strong positive correlation with K8 but ERα weakly positively correlated with K8 and therefore, we decided to include ERα as an additional marker in our analysis.

To demonstrate that the *JSI* is sensitive to treatment-induced changes in marker distribution we cultured isolated epithelial fragments from normal breast tissue in either AREG/FGF7, or EGF/FG7, or a system based on intestinal organoid culture, referred to as the

Figure 37 Identification of the minimal marker set to identify heterogeneity in breast cancer

(A) Positive linear correlation was observed with CD10 and SMA with K14 area in TNBC. Representative images are shown. (B) ERα provides non-redundant information to K8 in contrast to K18 in ER+ breast cancer. Representative images are shown.

*Lejla Pasic and Frances Greathouse assisted with Figure 37.

Figure 37

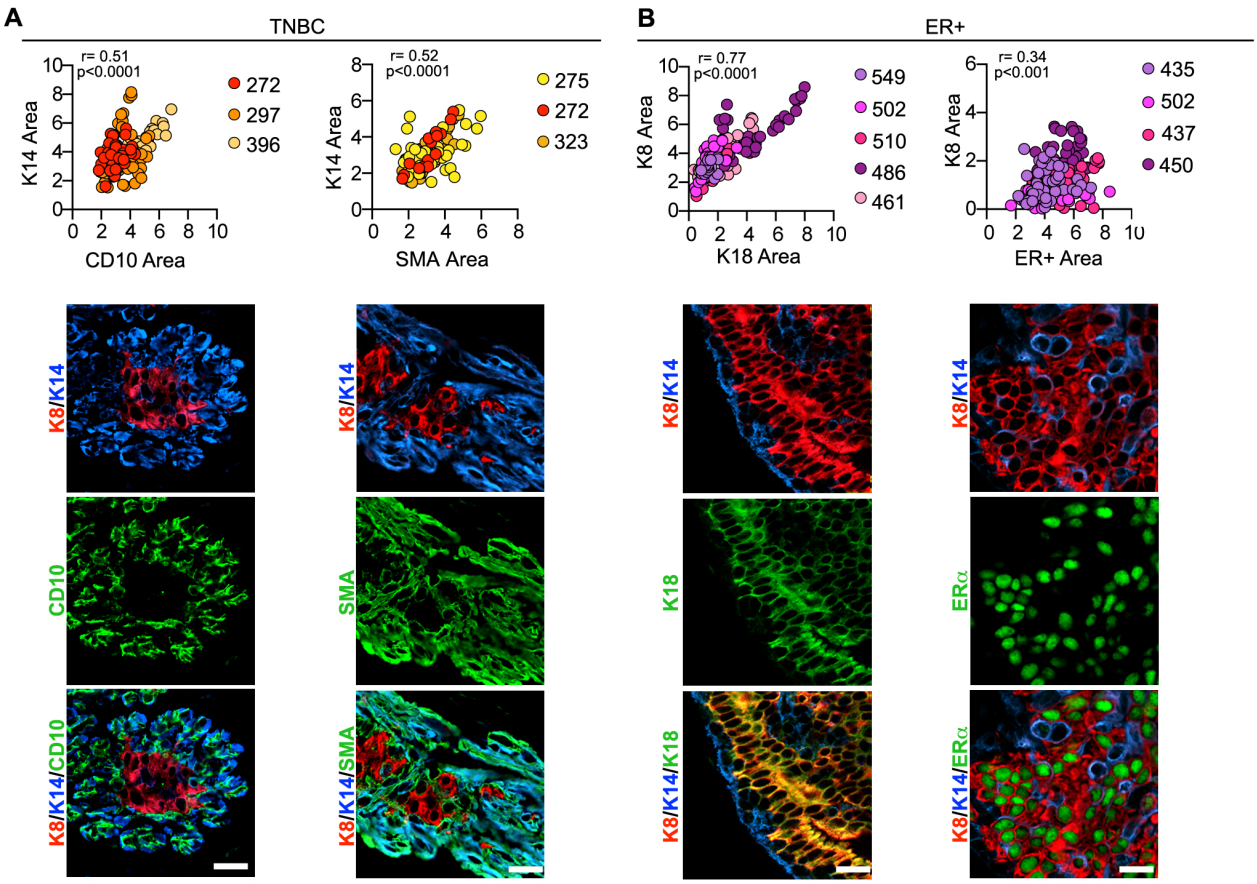
A
TNBC
r= 0.51
p<0.0001
K14 Area
CD10 Area
272
297
396
r= 0.52
p<0.0001
K14 Area
SMA Area
275
272
323
B
ER+
r= 0.77
p<0.0001
K8 Area
K18 Area
549
502
510
486
461
r= 0.34
p<0.001
K8 Area
ER+ Area
435
502
437
450
K8/K14
CD10
K8/K14/CD10
K8/K14
SMA
K8/K14/SMA
K8/K14
K18
K8/K14/K18
K8/K14
ERα
K8/K14/ERα

R-spondin culture method [290]. AREG/FGF7 was chosen because this growth factor mixture quantitatively recapitulates the normal ductal architecture *in situ* [162]. We also showed that EGF/FGF7 caused abnormal expansion of the dual-positive population and that prolonged treatment resulted in an increase in K14+ cells. The R-spondin method comprises a complex mixture that includes EGF. Therefore, based on our previous observations using normal breast tissue we replaced EGF with AREG in the R-spondin method (AREG/R-spondin). In these experiments JSI was calculated similar to above except that Q is defined as the probability distribution of organoid sections generated from an individual patient X. The probability density distributions illustrate that treatment of tissue with EGF/FGF-7 or R-spondin results in a left ward switch indicating that the organoids are more K14+ than the ST (Fig. 38A, B). Confirming this analysis the JSI (AREG/FGF-7) < JSI_{ave} and JSI (EGF/FGF-7) or JSI (R-spondin) >JSI_{ave}. These data demonstrate that we can detect alterations in the phenotypes within organoids.

Organoid culture methodology

To develop an organoid culture system that would recapitulate the tumor microenvironment we performed growth factor and cytokine analysis from the isolated normal and tumor epithelial or stromal fibroblasts. Interestingly, fibroblasts isolated from TNBC secreted significantly higher levels of EGFR and FGF ligands than normal tissue or other breast cancer subtypes. These ligands are of physiological relevance because EGFR is overexpressed in ~ half of TNBC and amplification of FGFR1 or FGFR2 occurs in ~ 10% of TNBC patients [249, 291].

Figure 38 Probability density distribution is able to identify treatment-induced phenotypic changes within the tissue.

(A) The probability density distribution for starting tissue obtained from patients with a normal diagnosis and the resulting organoids cultured under various conditions. The dashed lines indicate the quartiles associated with the normal tissue distribution. (B) Representative images from the bins relevant to the phenotype are shown.

*Lejla Pasic and Frances Greathouse assisted with Figure 38.

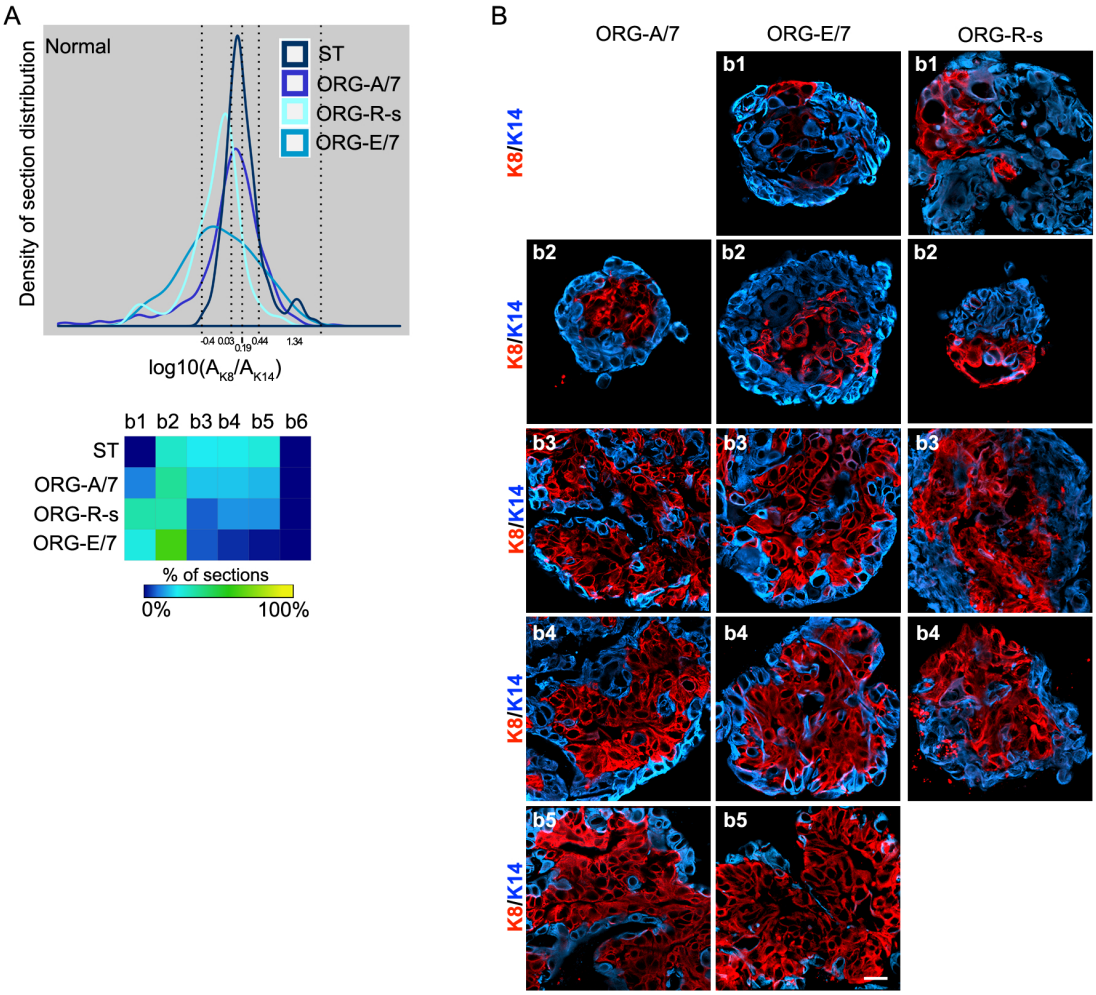
A
Normal
ST
ORG-A/7
ORG-R-s
ORG-E/7
Density of section distribution
-0.4 0.03 0.19 0.44 1.34
log10(A_K8/A_K14)
b1 b2 b3 b4 b5 b6
ST
ORG-A/7
ORG-R-s
ORG-E/7
% of sections
0%
100%
B
ORG-A/7
ORG-E/7
ORG-R-s
K8/K14
b1
b2
b3
b4
b5

TNBC tumor organoids and chemotherapy responses

Tissues from 6 different patients were obtained; of these one had undergone chemotherapy (patient 272), and one had been treated with both radiation and chemotherapy (patient 287). Epithelial tumor fragments were isolated from the patient samples and cultured in 3D. According to the probability density distribution and the JSI analysis we were able to recapitulate the starting tissue with the only exception being patient 275 (Fig. 39A, B, Table 10). We also analyzed the starting tissue and tumor organoids for HER1 levels, as HER1 is overexpressed in ~ 50% of TNBC patients [292]. Consistent with this, HER1 levels were higher in the starting tumor tissue than in normal tissue, and this difference was maintained in the tumor organoids (Fig. 39C). Taken together these results demonstrate that TNBC tumor organoids remain similar to their starting tissue.

To further evaluate this similarity, we performed gene expression analysis using RNAseq on TNBC and normal breast tissue, and on their respective organoids. The strongest differential between the samples was due to the proliferation signal in the organoids, and the next strongest was the variance between patient samples. Such differences were expected and we removed these batch effects from the analysis. We observed that the TNBC tissue and the corresponding organoids segregated from the normal tissue with its corresponding organoids (Fig. 39D). These results indicate that our organoid culture conditions successfully capture the gene expression profile of the starting tissue. Furthermore, these data demonstrate that using cellular phenotypes allows for analysis of intra-tumor heterogeneity, which cannot be easily captured by genetic approaches.

A primary goal of recapitulating tumor heterogeneity *in vitro* is to develop a tractable system for the analysis of drug responses, as tumor recurrence is likely to arise from cells that are unresponsive to the therapy. Paclitaxel was selected for organoids generated from TNBC

Table 10 JSI values for TNBC organoids

Pat.ID	Type of comp.	JSI
272	STvsORG	0.0187
275	STvsORG	0.3176
287	STvsORG	0.0758
297	STvsORG	0.0827
323	STvsORG	0.1124
396	STvsORG	0.0214
272	ORGvsORG-PAC	0.3242
396	ORGvsORG-PAC	0.1579

tissue because it is frequently used as an initial therapy for patients with TNBC [293]. In response to paclitaxel, tumor tissue obtained from patient 272 demonstrated ~3-fold decrease in total proliferation, as measured by Ki67, and an ~8-fold increase in apoptosis – as measured by cleaved caspase-3 staining (Fig. 39E). Analysis of proliferation responses in K8+ versus K14+ cells showed that only the proliferation of the K14+ cells was decreased with paclitaxel. Similar responses were observed with patient 396. In the probability density analysis for patient 272 the distribution of sections skews to the right. This enrichment in K8+ cells is most likely due to the decreased proliferation in the K14+ cells. The paclitaxel-induced phenotypic changes within the tissue compared to the untreated sample are confirmed by JSI analysis (Fig 39F, Table 10). However, for patient 396 the probability density distribution and the JSI analysis indicate that the phenotype of the tissue did not alter in response to paclitaxel most likely as the effect on K14+ cells was only two-fold as compared to ten-fold for patient 272. As an independent measure of drug response, the area of the organoids was measured from differential interference contrast (DIC) images using multiple fields for each patient and normalized to that obtained with the vehicle control (Fig. 39G). Paclitaxel decreased the overall size of the tumor organoids for patient 272 but the size was unaffected for patient 396. Importantly, differential responses to drug treatment can be observed for TNBC tumor tissue from different patients, as enrichment for a particular phenotype may reveal potential resistance to the treatment.

Figure 39 TNBC tissue intra-tumor heterogeneity and drug responses.

(A) The probability density distribution for TNBC starting tissue and the resulting organoids. Inset- the heat map indicates the percentage of sections within a bin with a particular phenotype. (B) Representative images from the bins associated with a particular phenotype are shown. (C) TNBC tumor organoids recapitulate the expression of HER1 observed in the starting tumor tissue. (D) Analysis of RNAseq data shows that TNBC tumor tissue and its respective organoids segregate from normal breast tissue and its respective organoids. (E) Probability density distribution and heat map analysis of starting tissue from patients 272 and 396 and their organoids treated with or without paclitaxel (Pac; 1μM). (F) Tumor organoids identify differing intra-tumor proliferation and apoptotic responses to paclitaxel. (G) Inhibition of tumor organoid proliferation in response to paclitaxel as measured by DIC.

*Lejla Pasic and Frances Greathouse assisted with Figure 39.

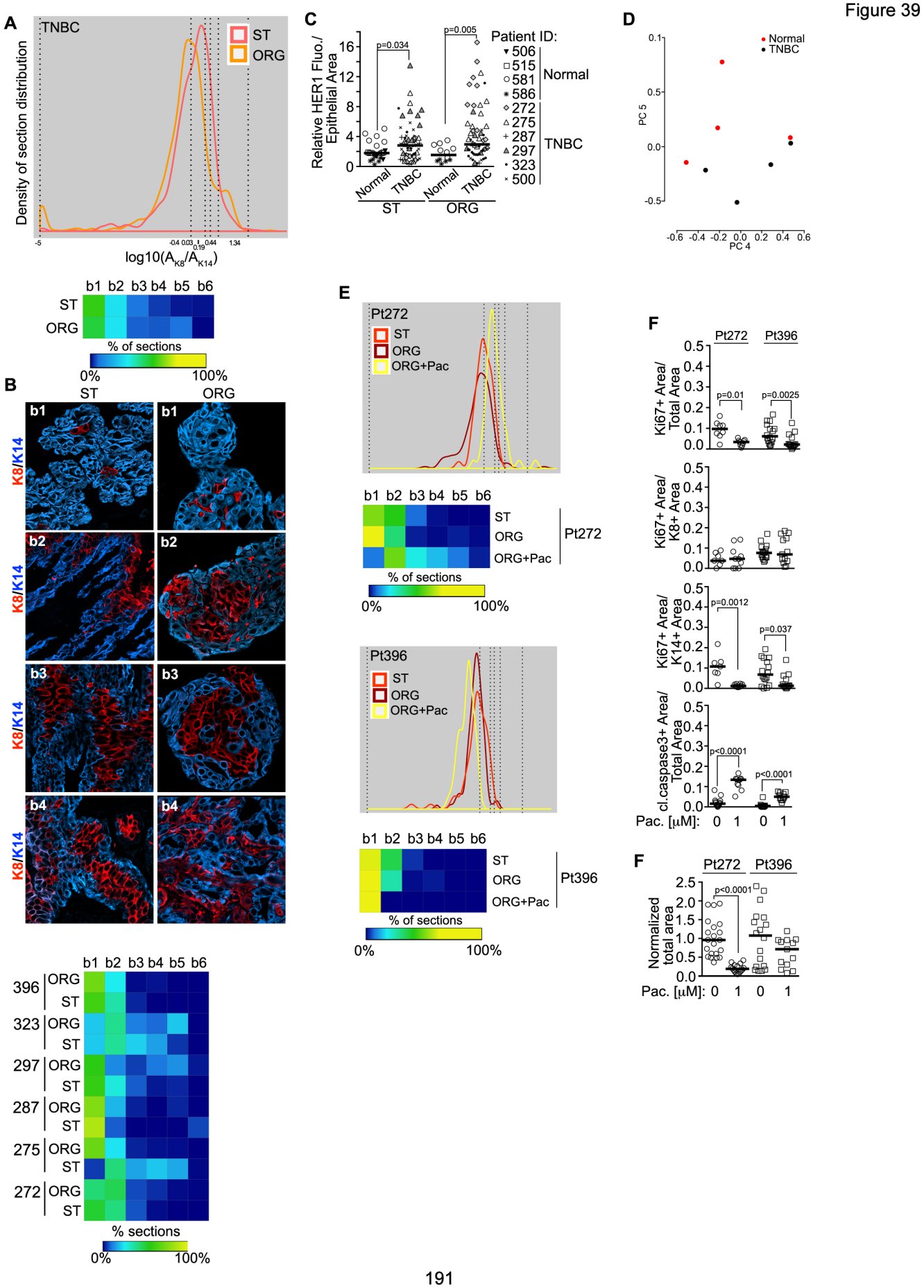
A
TNBC
ST
ORG
Density of section distribution
log10(A_K8/A_K14)
b1 b2 b3 b4 b5 b6
ST
ORG
% of sections
0%
100%
B
ST
ORG
K8/K14
b1
b2
b3
b4
396 ORG ST
323 ORG ST
297 ORG ST
287 ORG ST
275 ORG ST
272 ORG ST
% sections
0%
100%
C
Relative HER1 Fluo./ Epithelial Area
p=0.034
p=0.005
Patient ID:
506
515
581
586
272
275
287
297
323
500
Normal
TNBC
ST
ORG
D
Normal
TNBC
PC 5
PC 4
E
Pt272
ST
ORG
ORG+Pac
b1 b2 b3 b4 b5 b6
% of sections
0%
100%
Pt396
F
Pt272
Pt396
Ki67+ Area/ Total Area
Ki67+ Area/ K8+ Area
Ki67+ Area/ K14+ Area
cl.caspase3+ Area/ Total Area
p=0.01
p=0.0025
p=0.0012
p=0.037
p<0.0001
Pac. [μM]: 0 1 0 1
Normalized total area

ER+ breast cancer tumor organoids

Tissue from five different ER+ breast cancers were obtained and epithelial fragments from these tumors cultured. Based on the probability density distribution and JSI analysis we were able to recapitulate the starting tissue (Fig. 40A, B, Table 11). Breast cancers are classified as ER+ when > 1% of the cells within the tumor tissue stains for ERα [294]. In analyzing the starting ER+ breast tumor tissue in our cohort we found that ~40% of the K8+ cells expressed ERα as compared to ~15% in normal tissue (Fig. 40B). The % of K8+ cells expressing ERα did not change significantly with culture conditions.

For ER+ tumor organoids we evaluated drug responses to the selective estrogen receptor modulator 4-hydroxy tamoxifen (4-OHT), the estrogen receptor degrader, fulvestrant, and the CDK4/6 inhibitor, palbociclib [295, 296]. 4-OHT is an active metabolite of tamoxifen, which is used to treat ER+ breast cancer patients. In response to fulvestrant, tumor tissue obtained from patient 549 was unaffected, in agreement with the probability density distribution and JSI analysis (Fig. 40D, Table 11). Treatment with 4-OHT resulted in decreased proliferation of K14+ cells and overall increased apoptosis without altering the tissue phenotype. Palbociclib decreased proliferation primarily in K8+ and K14+ cells but unexpectedly, a rightward shift in the probability distribution was observed. An increase in the JSI was observed in the treated compared to the untreated tissue but did not reach significance. In response to 4-OHT, tumor tissue obtained from patient 461 was unaffected (Fig. 40E, Table 11). Together, these data demonstrate that we can observe differential vulnerabilities between patients to various drug treatments, and can monitor effects of chemotherapy.

Figure 40 ER+ tissue intra-tumor heterogeneity and drug responses

(A) ER+ tumor organoids recapitulate the ER+ content of the starting tissue. (B) Representative images from the bins associated with a particular phenotype are shown. (C) ER+ tumor organoids recapitulate the expression of ERα observed in the starting tumor tissue. (D) Probability density distribution and heat map analysis of starting tissue from patients 549 and 461 and their organoids treated with or without 4-hydroxtamoxifen (4OHT), Fulvestrant (Fulv), or Palbocyclib (Palb). (E) Tumor organoids identify differing intra-tumor proliferation and apoptotic responses to endocrine therapies

*Lejla Pasic and Frances Greathouse assisted with Figure 40.

Figure 40

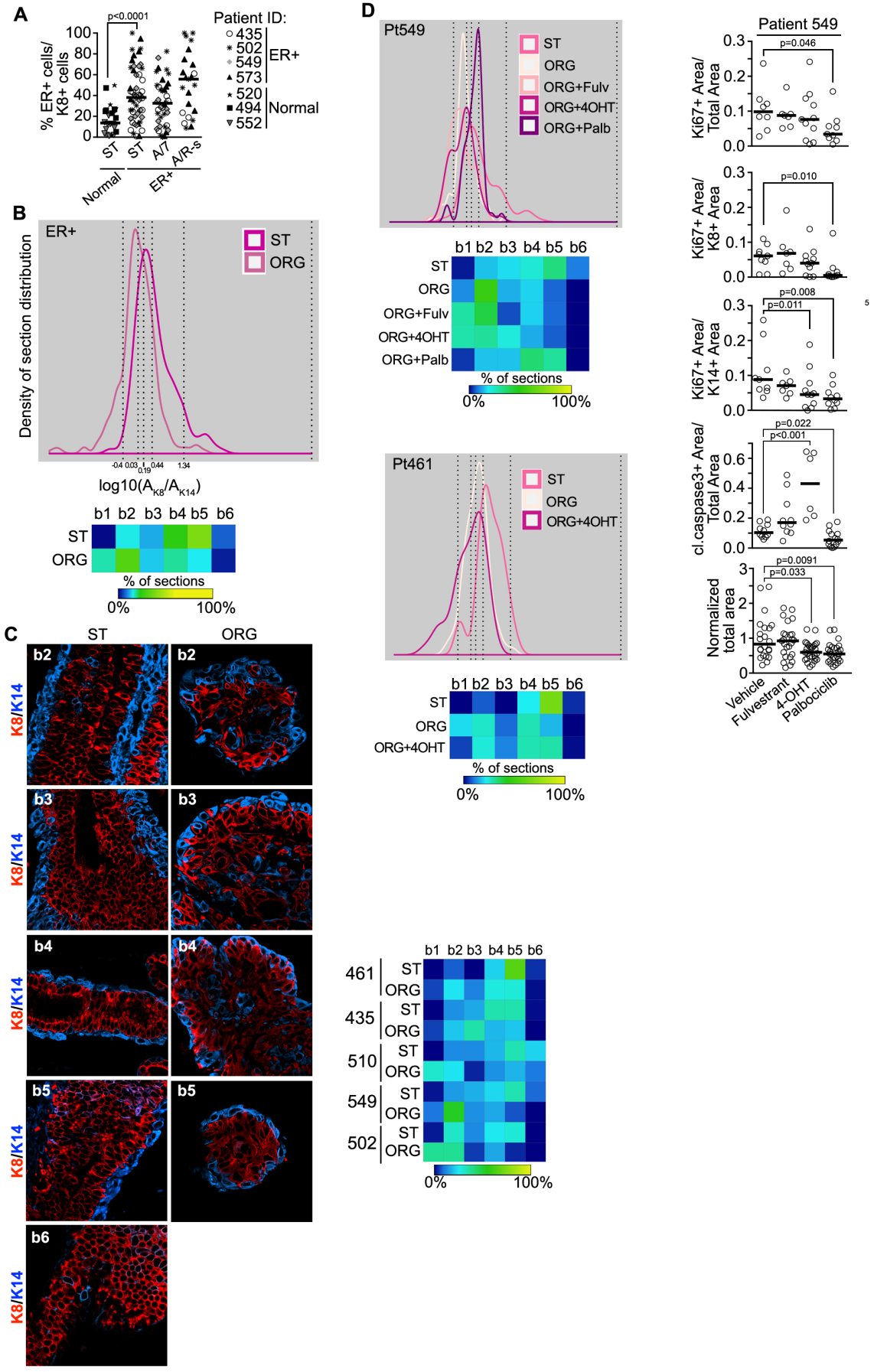
A
p<0.0001
% ER+ cells/ K8+ cells
Patient ID:
435
502
549
573
520
494
552
ER+
Normal
ST
ST
A/7
A/R-s
Normal
ER+
B
ER+
ST
ORG
Density of section distribution
log10(A_K8/A_K14)
b1 b2 b3 b4 b5 b6
ST
ORG
% of sections
0%
100%
C
ST
ORG
K8/K14
b2
b3
b4
b5
b6
D
Pt549
ST
ORG
ORG+Fulv
ORG+4OHT
ORG+Palb
b1 b2 b3 b4 b5 b6
ST
ORG
ORG+Fulv
ORG+4OHT
ORG+Palb
% of sections
0%
100%
Pt461
ST
ORG
ORG+4OHT
b1 b2 b3 b4 b5 b6
ST
ORG
ORG+4OHT
% of sections
0%
100%
b1 b2 b3 b4 b5 b6
461
435
510
549
502
ST
ORG
0%
100%
Patient 549
Ki67+ Area/ Total Area
p=0.046
Ki67+ Area/ K8+ Area
p=0.010
Ki67+ Area/ K14+ Area
p=0.008
p=0.011
cl.caspase3+ Area/ Total Area
p=0.022
p<0.001
Normalized total area
p=0.0091
p=0.033
Vehicle
Fulvestrant
4-OHT
Palbociclib

Table 11 JSI values for ER+ organoids

Pat.ID	Type of comp.	JSI
435	STvsORG	0.0937
461	STvsORG	0.1802
502	STvsORG	0.2465
510	STvsORG	0.2225
549	STvsORG	0.2241
461	ORGvsORG-OHT	0.0501
549	ORGvsORG-OHT	0.0623
549	ORGvsORG-Palb	0.1732
549	ORGvsORG-ICI	0.0509

Discussion

Here we have established human breast cancer organoids of different subtypes as a tractable and robust methodology amenable to interrogation of chemotherapy sensitivities, gene expression profiling, and micro-environmental characteristics. Additionally, we describe a statistical approach that can quantify tumor heterogeneity, enabling objective analysis of the similarities and differences between organoids and the source tissue, and between different growth conditions. Importantly, we identified conditions for each subtype of breast cancer that recapitulate the tumor heterogeneity present in the original tumors, and can propagate the organoids while maintaining heterogeneity. Therefore, this approach will provide a powerful tool with which to investigate the human cancer "stem cell" hypothesis using primary human breast cancer tissue, and to analyze chemo-resistance mechanisms.

We demonstrated that HER1 ligands contribute to the phenotype of normal and breast cancer tissues. This ability to recapitulate intra-tumor heterogeneity with a single growth factor suggests that there are intrinsic differences in HER1 signaling between the various phenotypes that comprise the tumor. This observation may partially explain the lack of success of HER1 inhibitors in breast cancer, as those cells that are less dependent on HER1 are responsible for the observed resistance [297].

In addition to identifying the growth factors secreted by normal and cancer-associated fibroblasts we observed that there were breast cancer subtype differences in cytokine secretion by cancer-associated fibroblasts. Specifically cancer-associated fibroblasts from ER+ breast cancer secreted higher levels of CXCL1, which has been associated with poor prognosis in breast cancer patients [298]. CXCL1 directly altered the phenotype distribution in normal breast tissue, and it is possible that this effect, in addition to the ability of CXCL1 to recruit a subset of myeloid cells, promotes tumorigenesis [299]. In TNBC-associated fibroblasts we observed

higher levels of secreted leptin, which is consistent with observations of increased leptin levels in TNBC and its association with obesity and metabolic syndrome [300, 301]. CXCL5 is one of several cytokines, which includes CXCL1-8, that are located in the 4qp21 region, that are reported to be expressed at higher levels as a result of amplification or increased gene transcription in breast cancer [302, 303]. However, our results show that in ER+/HER2+-associate fibroblasts CXCL5 is specifically secreted at higher levels compared to the levels produced by fibroblasts from other breast cancer types. The importance of CXCL5 to breast cancer has not been well studied. In ER+ and ER+/HER2+ breast cancer a decrease in IL-6 was observed, which is associated with progression and metastasis in breast cancer [304]

Intra-tumor heterogeneity resulting from genetic and phenotypic differences within the patient tumor is a major obstacle to reducing breast cancer patient mortality. The cellular context of an oncogenic genetic change influences the tumor types that arise [305, 306]. Therefore, it is important to obtain not only genomic characterization of tumor-derived organoids but also to identify the cellular phenotypes within the tumor. Based on these observations it is reasonable to propose that differing cell types within the tumor will respond differentially to therapy. Our data clearly validate this hypothesis as paclitaxel resulted in an enrichment of K8+ cells in TNBC tissue. The ease with which different primary breast cancers can now be grown as in vitro organoids opens many exciting opportunities for future research.

Chapter 6 General discussion

In normal tissues, all members of the RSK family are expressed ubiquitously and little is known about functions of specific isoforms [307]. However, despite the high degree of sequence homology RSK isoforms are thought to perform distinct cellular functions [8, 308]. These functional differences can be more easily discerned in the context of cancer. The evidence suggests, that expression and functions of RSK1 and RSK2 promote tumorigenesis, whereas RSK3 and RSK4 are thought to act as tumor suppressors [81]. Yet, specific RSK-dependent processes underlying these observations remain poorly understood. In multiple *in vitro* approaches, RSK1 and RSK2 have been shown to contribute to cancer by regulation of proliferation, survival and motility. However, only a limited number of studies have confirmed these findings *in vivo* [70]. RSK2 knock-out mice exist, but their use was limited to discerning RSK2 functions in bone and brain development, and in immune system [45, 309]. Therefore, to this end, there has been no cohesive approach to integrate *in vitro* and *in vivo* models to investigate RSK role in the etiology of cancer.

Breast cancer is one of several human pathologies in which RSK has been implicated [1, 307, 310]. Levels of active RSK are reported to be increased in 70% of locally advanced ER+ breast cancers and ~85% of TNBC have active RSK [53, 54]. Therefore, the goal of my work has been to elucidate molecular mechanisms of RSK2-mediated processes in normal and cancerous mammary epithelial cells using multiple *in vitro* and *in vivo* approaches.

RSK2: an obligate partner in ERα-driven tumorigenesis

While investigating RSK2 functions in ER+ breast cancer, we found that RSK2 is sequestered in the nucleus by ERα and that RSK2 nuclear accumulation is required for ER+ breast cancer growth. ER+ xenograft tumor growth was strongly dependent on nuclear RSK2 and mammary-restricted forced expression of RSK2 in the nucleus resulted in development of

high grade ductal carcinoma *in situ*. These findings are consistent with previous observations that silencing or inhibition of RSK2 decreases proliferation of ER+ breast cancer cell lines and that nuclear RSK2 is necessary for the expression of oncogenic cyclin D1 [24, 59]. Further, we have found that RSK2 promotes tumorigenic transformation by activation of pro-neoplastic transcriptional network critical for the ER+ lineage in the mammary gland. These results are in agreement with observations that RSK2 enhances ERα -mediated transcription by direct interaction and/or phosphorylation of ERα [36, 62]. These observations are also consistent with numerous studies indicating that RSK2 can modulate activity of transcription factors like ATF4 [45], YB-1 [54] and c-Fos by phosphorylation [311]. We also found that RSK2-regulated a gene signature correlated with invasive ER+ breast cancer. We identified 529 genes differentially expressed in RSK2-KO cells as compared to WT. Gene set enrichment analysis demonstrated that genes up-regulated in invasive ductal breast cancer versus ductal carcinoma *in situ* (DCIS) were significantly enriched in WT versus RSK-KO. Furthermore, analysis of Z-scores from ER+ breast cancer patients from RSK2-high compared to RSK2-low cohort demonstrated concordance with directionality of gene expression in RSK2-KO. These results suggested that RSK2 regulates a subset of ERα associated transcriptome and are consistent with previous work from our laboratory showing that RSK2 regulates transcriptional activity of ERα [36, 55]. Taken together, these findings suggest that localization of RSK2 in the nucleus allows for RSK2-mediated regulation of transcription factors. Therefore, we investigated how RSK2 localization was regulated.

We have partially elucidated the mechanism of RSK2 nuclear accumulation. We have found that RSK2 nuclear localization was dependent on the activation of the upstream signaling cascade, as inhibition of ERK1/2 decreased RSK2 nuclear signal. These results are in agreement with early observations of RSK2 nuclear translocation in response to mitogens [24, 312]. Our findings are also supported by observations from other groups that active RSK is

predominantly nuclear [25, 53]. Additionally, we found that RSK2 was sequestered in the nucleus by ERα, as silencing of ERα or anti-estrogen treatments strongly inhibited the ability of RSK2 to accumulate. These results agree with previous reports from our lab showing that RSK2 binds ERα and that this interaction is disrupted by 4-OHT [55]. Taken together, we showed that ERK1/2 activation is necessary for RSK2 nuclear entry and ERα sequesters RSK2 in the nucleus.

The specific mechanism of RSK2 nuclear entry remains elusive. As RSK2 is too large (90kD) to freely diffuse into the nucleus, we sought to identify an amino acid sequence that controls RSK2 nuclear targeting. Based on the differential ability of RSK2 and RSK1 to accumulate in the nucleus and by focusing on the most divergent sequences within the two isoforms, we mapped the sequence from 1 to 67 amino acids in the RSK2 N-terminus to be essential for RSK2 nuclear accumulation. The inability of RSK1 to accumulate in the nucleus was in contrast to previous reports that RSK1 was nuclear in response to growth factors [25]. A likely cause underlying these discrepancies is the lack of reliable RSK1 antibodies. Our studies, as well as work presented by Gao et al., were limited to the use of ectopic expression systems. In contrast, the nuclear accumulation of RSK2 was confirmed by immunodetection of the endogenous protein, both in cell lines and primary tissue, visualization of ectopic, GFP-tagged protein, and CRISPR directed GFP-tagging of endogenous RSK2 (data not shown). Furthermore, RSK1 localization could be context dependent, as different cell types were used to obtain these conflicting observations. Gao et al. identified a putative nuclear localization sequence (NLS) within RSK1 (RSK1 316-332aa). This region is conserved between RSK1 and RSK2 but we found it does not promote RSK2 nuclear localization. Therefore, further studies are necessary to fully elucidate the differences between RSK1 and RSK2 subcellular localization. The N-terminal 1 to 67 residues of RSK2 were necessary for RSK2 nuclear accumulation, but they were not sufficient and to this end we were unable to identify canonical

nuclear localization signal within RSK2. In an alternative hypothesis, RSK2 could bind a piggy-back factor to be carried into the nucleus. The most obvious candidate for such a protein is ERα, as it contains multiple strong NLS and interacts with RSK2. ERα -silencing and inhibition reduced RSK2-nuclear accumulation, yet it did not result in complete exclusion of RSK2 from the nucleus. Therefore, although necessary for RSK2 accumulation, ERα is unlikely to bring RSK2 into the nucleus. Thus, the specific mechanism by which RSK2 enters the nuclear compartment remains unknown.

We further sought to investigate the physiological consequences of RSK2 nuclear accumulation. In a transgenic mouse model with mammary specific expression of NLS-RSK2 we found that nuclear RSK2 was sufficient to drive development of high grade ER+ carcinoma *in situ*. Importantly, these lesions required 16 months to develop and in younger, 6 month old, animals only hyperplasia was observed. Besides advanced DCIS, we did not detect invasive tumors, likely due to a need for additional time or requirement for additional genetic alteration that would allow the cells to undergo invasion. Such long latency and limited metastatic potential are frequently observed in models of ER+ breast cancer [193]. For example, in a mouse model of ERα overexpression (CERM), hyperplasia is frequently observed but only 3% of mice develop DCIS. Introduction of heterozygous deletion of tumor suppressor, p53, in these mice increases the incidence of DCIS [313], but additional genetic perturbations are necessary to allow for invasive cancer to development. For example, excision of BRCA1 combined with p53 haploinsufficiency in CERM mice was necessary to allow for tumor development, but only 50% were ER+ [314]. Therefore, similarly, additional genetic perturbation might be necessary for NSL-RSK2 mice to develop metastasis. Together, we our observations suggest that nuclear accumulation of RSK2 is physiologically relevant as it promotes ER+ DCIS formation.

In clinical samples of ER+ breast cancer, increased levels of ERα phospho-Ser167 and active RSK were correlated with disease-free survival and response to endocrine-based

therapies [56-58]. Importantly, RSK2-mediated phosphorylation of ERα at Ser167, but also RSK2 physical association with ERα can activate ERα -mediated transcription. Notably, we have found that 4-OHT disrupted the interaction between RSK2 and ERα without altering the phospho-Ser-167 levels. Furthermore, in a xenograft model tumor growth was absolutely dependent on the ability of RSK2 to localize to the nucleus, while levels of phospho-Ser167 were not. Together these findings suggest that physical interaction of RSK2 with ERα, rather than phosphorylation is the mechanism by which RSK2 contributes to tumor formation. Consequently, elevated levels of phospho-Ser167 are likely an indirect biomarker for active RSK, but are not causally related to ER+ breast cancer.

Taken together, my studies of the RSK2 function in ER+ breast cancer show that RSK2 is a key tumorigenic factor in this malignancy. My work indicates that RSK2 subcellular localization is an important modulator of RSK2 function and that RSK2 physical interaction with its binding partners regulates RSK-dependent processes. Therefore, I propose that regulation of RSK2-dependent cellular functions is achieved by integrating subcellular localization, physical interaction and phosphorylation of substrates.

RSK2: regulator of ER+ cell homeostasis

Cancer arises as a result of an accumulation of somatic mutations. An altered genetic landscape provides survival fitness and ultimately leads to activation of uncontrolled proliferation. However, transformed cells frequently rely on the repertoire of pre-existing normal pathways to satisfy their altered needs. Therefore, a comprehensive understanding of processes underlying basic biological functions remains critical to deciphering cancer vulnerabilities. To better understand the function of RSK2 in breast cancer we investigated RSK2-regulated processes in normal mammary epithelium.

The mammary gland undergoes changes in response to fluctuations in reproductive hormones' levels. In adult mammal females the hormonal milieu is dynamically changing in specific intervals, defined as estrous cycle. During a proestrus stage of the cycle, estrogen levels increase, leading to ovulation during estrus stage [201]. Then, in the absence of pregnancy, the estrogen levels decrease through metestrus and diestrus stages [201]. ERα is degraded in response to estrogen by the 26S proteasome pathway, and consistently with changes in estrogen levels throughout estrous cycle, we observed that ERα protein levels fluctuated in the adult. They were at the lowest in proestrus and estrus, increased throughout metestrus, and reached the highest levels in diestrus stage. These findings also confirm previous reports of ERα levels across estrous stages [205]. Importantly, despite the relative decrease in estrogen levels in metestrus and diestrus, the hormone levels remain higher in the reproductive years than during prepubertal and postmenopausal periods [315]. Therefore, it is surprising that ERα-protein levels are maintained prior to menopause, despite the constant presence of estrogen.

ERα positively regulates expression of multiple growth factors, and, therefore, we hypothesized that ERK1/2-RSK2 signaling pathway provides feedback to regulate ERα protein levels. Using the RSK2 knock out mouse model (RSK2-KO), we found that loss of RSK2 resulted in decreased number of ER+ cells in the mammary gland as well as decreased ERα levels across all stages of the estrous cycle. Consistently, while examining the cellular composition of RSK2-KO mammary glands by FACS, we found that non-clonogenic luminal cell (NCL) subpopulation was diminished, and the undefined population was concomitantly increased in RSK2-KO mammary glands as compared to WT at all estrus stages. This observation is in agreement with previous reports showing that NCL population contains majority of ER+ population [316]. Furthermore, in agreement with the reports that multiple growth factors are expressed in response to ERα ligand-dependent activation [210], we found

that active ERK was higher in mice during estrus compared to diestrus stage. ERK1/2 was also phosphorylated in adult mice but not in juvenile mice, in agreement with the reports of E2 being increased upon reaching sexual maturity [317-319]. We found that ERK1/2-RSK2 activation during estrus stage was critical for protection of ERα from proteosomal degradation, as decrease in ERα levels in RSK2-KO mice could be rescued by inhibition of 26S proteasome. Consistently, as ERα-transcriptional activity is intimately linked with its transcriptional activity, we discovered that ERα -associated gene expression profile was enhanced in the absence of RSK2, when the ERα turnover was the highest. These findings agree with studies showing that proteolysis of ERα occurs exclusively through ubiquitin mediated pathway [237] and that ERα-mediated transcription upon exposure to estrogens is dependent on rapid degradation through this pathway [203, 204] [205] [206, 207]. Taken together, we discovered a novel negative feedback mechanism between ERK1/2-RSK2 signaling cascade and estrogen signaling that is critical for maintenance of ERα protein levels in response to estrogen.

We then sought to investigate the physiological consequences of increased ERα protein turnover in the RSK2-KO mammary glands. Pubertal mammary gland development is absolutely dependent on ERα, as mammary specific ERα -knock out results in complete inhibition of ductal development [149]. Interestingly, we found that pubertal mammary gland development was unaffected in RSK2-KO mice. Consistently we found that number of ERα+ cells was unaffected in prepubertal RSK2-KO mice. These results are in agreement with our observations that ERK1/2 was not active until adulthood, indicating that the estrogen-ERK1/2-RSK2 feedback loop is not important in juvenile mice. These findings are especially interesting in the context of previous studies showing that growth factors and their receptors, including amphiregulin (AREG), fibroblast growth factor 7(FGF7) and insulin-like growth factor 1 (IGF1), are critical for mammary gland development during puberty [220]. Growth factors are known activators of the ERK1/2 signaling cascade, and therefore these studies suggest that ERK1/2

participates in pubertal mammary gland development. Importantly, signaling downstream of the growth factor receptors in these studies was only examined in a transgenic model in which IGF-1 was overexpressed in the mammary gland [320]. Consistent with our observations that ERK1/2 is not activated in juvenile mice, Tian et al. observed that in response to IGF-1 there was a switch from PI3/AKT activation in the juvenile to ERK1/2 activation in the adult. Thus, we conclude that pathways alternative to ERK1/2 downstream of growth factor receptors contribute to pubertal mammary gland development and ERK1/2-RSK2 cascade is responsible for mammary homeostasis in the adult.

To this end we have not identified the growth factor responsible for activation of ERK1/2 pathway in the adult. Intriguingly, the analysis of differentially expressed genes between diestrus and estrus stages revealed that chemokine C-X-C motif ligand 1 (CXCL1, GROα) is the only gene up-regulated in estrus in both genotypes. CXCL1 is a ligand for a C-X-C chemokine receptor type 2 (CXCR2) receptor and can activate ERK1/2 and RSK2 [154]. CXCL1 is a neutrophil and basophil attractant and activator and has been indicated as a pro-angiogenic chemokine in melanoma, but there is no known function for CXCL1 in mammary epithelium [321] [322]. Therefore, the identification of upstream activator of ERK1/2 in the adult mammary gland remains an open question.

In addition to functions during pubertal development, ER+ cells in the mammary gland act as sensor cells to respond to changes in the hormonal milieu and are crucial for proper lactation [150]. In agreement with these observations, we found that reduced ERα levels due to the loss of RSK2 resulted in defective mammary gland expansion on the onset of lactation. Furthermore, it has been reported that mammary-specific silencing of ERα during gestation leads to in insufficient lactation resulting in reduced pup size [150]. Consistent with these observations, we found that pups fed by RSK2-KO dams were smaller. This phenotype could be rescued by fostering the RSK2-KO pups to a wild type dam, indicating that the reduced size

was due to lactation defect. This is an important observation, as previous reports have indicated that RSK2 pups are smaller compared to WT, but credited this observation to defects in skeletal development in pups [46] rather than insufficient lactation in dams.

To understand how loss of RSK2 affected estrogen responsiveness in the mammary gland we analyzed the transcriptomic changes in the NCL populations between estrus and diestrus in RSK2-KO and WT. There were over 2700 differentially expressed genes between diestrus and esrus RSK2-KO mice as compared to only 40 genes in WT, indicating, that remodeling of the transcriptome architecture is occurring in the RSK2-KO mice in response to estrogen. In agreement with these observations, we found that the directionality of ERα-regulated gene signature expression was concordant in the RSK2-KO between diestrus and estrus stages, but not observed in WT. Increased estrogen-responsiveness is consistent with our hypothesis that the decrease in ERα-levels in the RSK2-KO mammary gland is due to the transcription-linked degradation through 26S proteasome. Functional enrichment analysis revealed that genes regulating various aspects of protein biogenesis were upregulated in RSK2-KO compared to WT at estrous. Furthermore, increased transcriptional and translational demands dictated by the enhanced estrogen response, manifested in up-regulation of oxidative phosphorylation gene signature. We also found that cell-cycle associated genes were enriched in RSK2-KO glands as compared to WT. Surprisingly, examination of NCL proliferation by EdU incorporation revealed that RSK2-KO have reduced proliferation compared to WT. Many of the cell-cycle genes up-regulated in RSK2-KO mice at estrus are DNA remodeling genes involved in replication. Therefore, we hypothesize that inhibition of proliferation results from a stress response triggered by the collisions of transcription and replication machinery [323].

The importance of ERα is not limited to the mammary gland, for example, estrogen signaling in the uterus is critical for reproductive functions. We found that ERK1/2-RSK2 had a similar protective effect on the levels of ERα in the uteri as in the mammary gland. In uteri from

RSK2-KO mice, ERα levels were decreased specifically in the epithelium, but not in the stroma, consistently with our observations that RSK2 function is intrinsic to the epithelium. In agreement with these findings, we observed that active ERK1/2 was present only in the epithelial regions and not the stroma. Reduced ERα-levels in the epithelium manifested in reduced fertility and smaller litter sizes of RSK2-KO mice, in agreement with reports that the secretion from glandular epithelium is necessary for implantation [225].

Taken together, our findings demonstrate that ERK1/2-RSK2 signaling is a critical regulator of mammary gland homeostasis, through regulation of ERα stability. Our findings are may not be limited to the mammary gland and reproductive track. ERα-mediated signaling has been shown to be associated with metabolic syndrome and type 2 diabetes and therefore, we hypothesize that ERK1/2-RSK2 pathway could also play a role in these malignancies.

RSK2: a double edge sword

Loss of RSK2 increases ERα protein turnover in response to systemic estrogens. Unchecked, degradation-coupled transcriptional activation of ERα triggers expression of proliferation and translation-related genes, yet, no evidence of increased proliferation is observed. Therefore, we hypothesize that ER+ cells do not complete the proliferation program in RSK2-KO mammary glands due to a stress response triggered by collisions of replication and transcription forks and unmet needs for nutrients due to an accelerated pro-proliferative response. Therefore, in normal mammary epithelium, RSK2 acts as 'breaks' on the estrogen responsiveness to regulate the homeostasis of ER+ cells. On the other hand, we found that in ER+ breast cancer cells RSK2 is an obligate partner in ER+-driven tumorigenesis and promotes a pro-neoplastic transcriptional network. These results are seemingly in contrast with our observations that in normal mammary gland loss of RSK2 enhances ERα-mediated transcription. According to TCGA and METABRIC databases, ~70-80% of ER+ (luminal) breast

cancer patients are postmenopausal [324, 325]. As systemic estrogen levels gradually decrease after menopause [315], we would expect that estrogen-mediated expression of growth factors is also suppressed after menopause. As activating mutations in ERK1/2 pathway rarely occur in luminal breast cancer, one could expect that ERK1/2 pathway is likely not activated in the ER+ breast cancer. However, surprisingly, it was recently reported that increased ERK1/2 phosphorylation is associated with hotspot mutations in phosphatidylinositol-4,5-bisphosphate 3-kinase catalytic subunit alpha (*PIK3CA*), the most frequently detected genetic alteration in ER+ breast cancer [326]. These observations are unexpected, because, although studies have indicated that feedback exists between these two pathways [327], the exact mechanism of ERK1/2 activation in these tumors remains unknown. Importantly, increased activity of ERK1/2-RSK2 pathway in the environment where estrogen levels are low could serve as a double-edged sword. Although necessary in a maintenance of normal homeostasis, in the context of low-estrogen, elevated activation of ERK1/2-RSK2 pathway could result in 'protection' of ERα against a threat that no longer exist. Therefore, in such milieu the unnecessary safeguard could result in inappropriate stabilization of ERα protein levels and combined with genetic alterations provide the survival advantage to the cancer cells.

RSK2: a drug target in breast cancer

My work illuminated the role of RSK2 in ER+ breast cancer, yet RSK functions are not limited to this particular breast cancer subtype. Active RSK is known to contribute to tumorigenesis independently of ERα, by phosphorylation of substrates that control processes important for cancer cell survival and metastasis [307, 310]. For instance, in models of triple negative breast cancer (TNBC) RSK has been shown to promote the prometastatic gene program by phosphorylating and hence activating YB-1 transcription factor [54] [151]. Importantly, isoform specificity is not delineated in TNBC, and both RSK1 and RSK2 are thought

to contribute to the disease etiology. In support of the *in vitro* studies, investigation of TNBC tissue samples revealed that ~85% of these tumors have activated RSK [54] and in agreement with these reports, we found that levels of activated RSK were higher in TNBC tumors than in normal tissue. As there are no targeted therapies for TNBC and these patients have increased probability of death due to metastasis compared to patients with other breast cancer subtypes, we considered RSK as a therapeutic target for metastatic TNBC.

In previous work from our laboratory we identified a RSK inhibitor, SL0101 [136]. The initial compound, despite its remarkable specificity for RSK1 and RSK2, had poor stability and *in vivo* pharmacokinetics [141]. Therefore, a series of structure-activity relationship-guided medicinal chemistry efforts were undertaken to improve SL0101 drug-like properties (Introduction: RSK inhibitors) [143]. A resulting inhibitor, a n-substituted-cyclitol-SL0101 (1b) was six times more effective in *in vitro* kinase assays than SL0101 and had eight times lower IC50 in proliferation assay, while retaining specificity for RSK1/2. The efficacy of (1b) for RSK was also maintained *in vivo*, as treatment with (1b) resulted in decreased phosphorylation of S6 protein, a known RSK target, in bone metastasis of ER+ cancer in a xenograft model.

While identifying contributions of RSK1 and RSK2 to TNBC metastasis, we found that both isoforms sustained metastatic tumor growth. Silencing of either of the isoforms resulted in a four-fold decrease in metastatic burden and prolonged survival by ~50%. Consistently, inhibition of RSK in *in vivo* models of metastatic TNBC decreased metastatic colonization and growth of the metastatic loci. These results are in agreement with our *in vitro* findings that silencing of RSK1 and RSK2 decreases anchorage independent growth and motility of TNBC cell lines and with our observations that inhibition of RSK reduces motility and proliferation of TNBC cell lines. These findings are also in agreement with studies showing that silencing RSK2 decreased metastatic colonization to the lymph node of HNCC cell and observations that inhibition of RSK activity was associated with decreased motility in lung cancer lines [76].

Evaluation of (1b) efficacy revealed that it was as effective as the MEK inhibitor, trametinib, in inhibiting metastatic colonization in an *in vivo* model. Trametinib is currently approved for melanoma and is in multiple clinical trials including those for breast cancer [265]. The MEK-ERK1/2 cascade is now considered as a viable drug target for TNBC. Yet, inhibiting "global regulators" such as MEK results in a number of side effects [253]. For example, inhibition of MEK can result in activation of AKT, a pathway shown to promote tumor growth. Importantly, treatment with (1b), unlike trametinib, did not result in increased activation of AKT in TNBC cell lines, suggesting that targeting RSK could be as effective as targeting MEK but would not have undesirable side effects.

Our study was a first report showing efficacy of an RSK inhibitor in reducing TNBC metastasis. We showed that RSK is a viable target for otherwise non-targetable disease. Although (1b) showed promising results in the mouse model, its *in vivo* half-life is still limited (t1/2=40min) and it is not suitable for large scale pre-clinical studies. However, there is an ongoing effort to further improve the biological availability of SL0101 analogues.

Organoids: the next frontier in drug development

We developed a 3D in vitro system for recapitulation of breast tumor heterogeneity. In order to detect differences between phenotypes of normal, TNBC and ER+ tissue, we used imaging-driven quantitative approach and combined it with Jensen-Shannon divergence, a statistical method that compares probability distributions. Using this methodology, we were able to identify similarities between patients within each of the above subtypes, but also identify specific differences between individual patients. Additionally, our approach has sufficient sensitivity to identify treatment-induced changes in phenotypes. Importantly, we were able to show that organoids generated form a given patient tissue mimic in situ phenotypes. We successfully reconstituted variable populations comprising normal, ER+ and TNBC tissues.

Furthermore, our approach allowed us to monitor changes in phenotypes occurring in response to treatment with chemotherapeutic agents. In developing a minimal growth media that allowed for maintenance of diverse cellular population, we demonstrated that HER1-ligands contribute to the phenotypes of normal and breast cancer tissue.

Future directions

Intracellular compartmentalization is an important mechanism for regulation of cellular functions. Proper localization within the cell ensures existence of specific micro-environments for spatial-temporal separation of biological processes [328]. To facilitate delivery of crucial factors into these microenvironments the subcellular 'address' frequently changes in response to stimulation or stress. In this body of work, we found that RSK2 nuclear accumulation was necessary for ER+ tumor growth. In the previous studies from our laboratory we have shown that RSK2 localized to stress granules in response to stress [24]. However, little is known about localization of the other RSK isoforms. Work from our laboratory indicated that RSK1 localizes to mitochondria and preliminary data suggests that RSK4 is mostly localized to the plasma membrane (data not shown). Yet, mechanisms governing these distinct localizations remain largely unknown. Taking into account how important localization is for regulation of RSK2 cellular functions, this gap in our knowledge is worth addressing.

RSK2-regulation of transcription factors activity is thought to occur mostly through phosphorylation, yet we found that RSK2 modulates ERα predominantly through physical interaction. Furthermore, ERα serves as an anchor for RSK2 in the nucleus. From these findings emerge questions whether other transcription factors could exhibit similar behaviors and partake in sequestering of RSK2 in the nucleus. We have identified 5 amino acids (RSK2(27-32)) in the N-terminus of RSK2 to interact with ERα, as deletion of these residues

prevented co-immunoprecipitation of ERα from MCF7 lysates by recombinant RSK2 N-terminal fragments. However, due to the use of whole cell lysates in this approach it remains unknown whether the interaction between RSK2 and ERα is direct or facilitated by additional biding partners. As nuclear receptors frequently share coregulators [329], identification of proteins that facilitate and/or are the limiting factors of RSK2- ERα complex formation could aid an understanding whether that other receptors/transcription factors could recruit RSK2. Furthermore, our findings indicate that RSK2 can modulate ERα-dependent transcription, but we have not uncovered the specific mechanism. ERα binding to chromatin regulatory elements has been shown to be extremely context dependent and relies on engagement of multiple co-factors [190]. Therefore, identification of RSK2 binding partners would shed light onto the mechanism through which RSK2 regulates ERα-mediated transcription and allow us to explore whether RSK2 nuclear accumulation is a general process that can be used by multiple nuclear receptors. In previous work from our laboratory we used a mass spectrometry approach to identify RSK2-associated proteins [24]. However, these results were obtained using cells under serum starvation conditions, and, therefore, to explore RSK2 partners in the nuclear compartment a new approach is necessary.

We partially deciphered a mechanism of RSK2 nuclear accumulation but did not formally test the contribution of RSK2 kinase activity to ER+ tumorigenesis in our models. In previous work, we showed that inhibition of RSK2 activity with SL0101 impairs proliferation of ER+ cells [59, 144]. However, it is not possible to attribute this effect to RSK2 alone as SL0101 targets both RSK2 and RSK1. To further explore the contribution of kinase activity, a kinase-dead RSK2 mutant could be used, preferably introduced by CRISPR mutation at the endogenous locus to avoid artifacts of overexpression. Yet, it is difficult to predict to what extent the mutations in the kinase domain would alter overall protein structure which in turn could result in alterations in the binding partners. Understanding how inhibition of RSK2 kinase activity would

affect its interaction with binding partners and whether it would consequently affect their functions remains an important area of investigation.

In recent years, ERα mutations have been identified to arise secondary to anti-estrogen treatments specifically in the metastatic cancer [330-332]. The most frequent mutations, Y537S and D538G, were shown to confer resistance to the inhibition by selective ERα modulators, but also stimulate ligand-independent transcriptional activity [333]. Ligand-independent activation has also been linked with increased ability of ERα mutant proteins to interact with cofactors [332]. Consistent with these findings, in preliminary data we have found that RSK2 remains nuclear in the presence of 4-OHT in cells expressing mutant form of ERα as compared to the WT (data not shown). These findings suggest that RSK2 could be involved in regulation of mutant ERα activity and partake in modulating endocrine therapy resistance. Therefore, further exploration of RSK2-ERα complex is of clinical importance, as targeting RSK2 could be an avenue for therapeutic intervention.

It is well established that estrogen signaling is critical for homeostasis and cancer of reproductive tissues, but it is also now appreciated that ERα plays an important role in metabolic syndrome and type 2 diabetes [197-199]. Therefore, our discovery of a feedback loop between estrogen signaling and ERK1/2-RSK2 pathway suggests that RSK2 could also have unexpected functions in etiologies of these diseases. This hypothesis is supported by observations that ERα-levels are increased [334] and RSK is overexpressed and activated in hepatic fibrosis [120]. Therefore, as there are no available treatments for liver cirrhosis, understanding the relationship between RSK2 and ERα in liver and other tissues outside of reproductive organs is of clinical interest.

Many questions regarding ‘druggability’ of RSK in various pathologies emerge from this and previous work from our laboratory. There is substantial evidence that RSK regulates a wide variety of pathologies that are major contributors to human disease and morbidity and,

therefore, it seems surprising that there are no RSK inhibitors that have good pharmacokinetic properties and there appears to be only a few groups working on developing inhibitors for this kinase family. The most likely explanation is that the pharmaceutical industry has focused on developing inhibitors to the upstream RSK activator, MEK1/2. MEK1/2 inhibitors are currently used clinically, but it was observed that MEK1/2 inhibition can lead to undesirable side effects. We hypothesize that RSK has an untapped potential as a drug target and that further improved understanding of RSK functions is necessary for bring RSK inhibitors to the clinic.

REFERENCES

1. Ludwik, K.A. and D.A. Lannigan, *Ribosomal S6 kinase (RSK) modulators: a patent review.* Expert Opin Ther Pat, 2016. **26**(9): p. 1061-78.

2. Sturgill, T.W., et al., *Insulin-stimulated MAP-2 kinase phosphorylates and activates ribosomal protein S6 kinase II.* Nature, 1988. **334**(6184): p. 715-8.

3. Erikson, E. and J.L. Maller, *A protein kinase from Xenopus eggs specific for ribosomal protein S6.* Proc Natl Acad Sci U S A, 1985. **82**(3): p. 742-6.

4. Jones, S.W., et al., *A Xenopus ribosomal protein S6 kinase has two apparent kinase domains that are each similar to distinct protein kinases.* Proc Natl Acad Sci U S A, 1988. **85**(10): p. 3377-81.

5. Fingar, D.C. and J. Blenis, *Target of rapamycin (TOR): an integrator of nutrient and growth factor signals and coordinator of cell growth and cell cycle progression.* Oncogene, 2004. **23**(18): p. 3151-71.

6. Roux, P.P., et al., *RAS/ERK signaling promotes site-specific ribosomal protein S6 phosphorylation via RSK and stimulates cap-dependent translation.* J Biol Chem, 2007. **282**(19): p. 14056-64.

7. Zeniou, M., et al., *Expression analysis of RSK gene family members: the RSK2 gene, mutated in Coffin-Lowry syndrome, is prominently expressed in brain structures essential for cognitive function and learning.* Hum Mol Genet, 2002. **11**(23): p. 2929-40.

8. Romeo, Y., X. Zhang, and P.P. Roux, *Regulation and function of the RSK family of protein kinases.* Biochem J, 2012. **441**(2): p. 553-69.

9. Ohno, S., *Evolution by gene duplication*. 1970, Berlin, New York,: Springer-Verlag. xv, 160 p.

10. Dehal, P. and J.L. Boore, *Two rounds of whole genome duplication in the ancestral vertebrate.* PLoS Biol, 2005. **3**(10): p. e314.

11. Fisher, T.L. and J. Blenis, *Evidence for two catalytically active kinase domains in pp90rsk.* Mol Cell Biol, 1996. **16**(3): p. 1212-9.

12. Dummler, B.A., et al., *Functional characterization of human RSK4, a new 90-kDa ribosomal S6 kinase, reveals constitutive activation in most cell types.* J Biol Chem, 2005. **280**(14): p. 13304-14.

13. Dalby, K.N., et al., *Identification of regulatory phosphorylation sites in mitogen-activated protein kinase (MAPK)-activated protein kinase-1a/p90rsk that are inducible by MAPK.* J Biol Chem, 1998. **273**(3): p. 1496-505.

14. Smith, J.A., et al., *Identification of an extracellular signal-regulated kinase (ERK) docking site in ribosomal S6 kinase, a sequence critical for activation by ERK in vivo.* J Biol Chem, 1999. **274**(5): p. 2893-8.

15. Kang, S., et al., *FGFR3 activates RSK2 to mediate hematopoietic transformation through tyrosine phosphorylation of RSK2 and activation of the MEK/ERK pathway.* Cancer Cell, 2007. **12**(3): p. 201-14.

16. Kang, S., et al., *Epidermal growth factor stimulates RSK2 activation through activation of the MEK/ERK pathway and src-dependent tyrosine phosphorylation of RSK2 at Tyr-529.* J Biol Chem, 2008. **283**(8): p. 4652-7.

17. Vaidyanathan, H. and J.W. Ramos, *RSK2 activity is regulated by its interaction with PEA-15.* J Biol Chem, 2003. **278**(34): p. 32367-72.

18. Roux, P.P., S.A. Richards, and J. Blenis, *Phosphorylation of p90 ribosomal S6 kinase (RSK) regulates extracellular signal-regulated kinase docking and RSK activity.* Mol Cell Biol, 2003. **23**(14): p. 4796-804.

19. Jensen, C.J., et al., *90-kDa ribosomal S6 kinase is phosphorylated and activated by 3-phosphoinositide-dependent protein kinase-1.* J Biol Chem, 1999. **274**(38): p. 27168-76.

20. Gogl, G., et al., *Dynamic control of RSK complexes by phosphoswitch-based regulation.* FEBS J, 2018. **285**(1): p. 46-71.

21. Cohen, M.S., H. Hadjivassiliou, and J. Taunton, *A clickable inhibitor reveals context-dependent autoactivation of p90 RSK.* Nat Chem Biol, 2007. **3**(3): p. 156-60.

22. Zaru, R., et al., *The MAPK-activated kinase Rsk controls an acute Toll-like receptor signaling response in dendritic cells and is activated through two distinct pathways.* Nat Immunol, 2007. **8**(11): p. 1227-35.

23. Zaru, R., et al., *Structural and functional basis for p38-MK2-activated Rsk signaling in toll-like receptor-stimulated dendritic cells.* Mol Cell Biol, 2015. **35**(1): p. 132-40.

24. Eisinger-Mathason, T.S., et al., *Codependent functions of RSK2 and the apoptosis-promoting factor TIA-1 in stress granule assembly and cell survival.* Mol Cell, 2008. **31**(5): p. 722-36.

25. Gao, X., D. Chaturvedi, and T.B. Patel, *Localization and retention of p90 ribosomal S6 kinase 1 in the nucleus: implications for its function.* Mol Biol Cell, 2012. **23**(3): p. 503-15.

26. Zhao, Y., et al., *RSK3 encodes a novel pp90rsk isoform with a unique N-terminal sequence: growth factor-stimulated kinase function and nuclear translocation.* Mol Cell Biol, 1995. **15**(8): p. 4353-63.

27. Chaturvedi, D., et al., *Subcellular localization and biological actions of activated RSK1 are determined by its interactions with subunits of cyclic AMP-dependent protein kinase.* Mol Cell Biol, 2006. **26**(12): p. 4586-600.

28. Gao, X., D. Chaturvedi, and T.B. Patel, *p90 ribosomal S6 kinase 1 (RSK1) and the catalytic subunit of protein kinase A (PKA) compete for binding the pseudosubstrate region of PKAR1alpha: role in the regulation of PKA and RSK1 activities.* J Biol Chem, 2010. **285**(10): p. 6970-9.

29. Leighton, I.A., et al., *Comparison of the specificities of p70 S6 kinase and MAPKAP kinase-1 identifies a relatively specific substrate for p70 S6 kinase: the N-terminal kinase domain of MAPKAP kinase-1 is essential for peptide phosphorylation.* FEBS Lett, 1995. **375**(3): p. 289-93.

30. Bonni, A., et al., *Cell survival promoted by the Ras-MAPK signaling pathway by transcription-dependent and -independent mechanisms.* Science, 1999. **286**(5443): p. 1358-62.

31. Buck, M., et al., *C/EBPbeta phosphorylation by RSK creates a functional XEXD caspase inhibitory box critical for cell survival.* Mol Cell, 2001. **8**(4): p. 807-16.

32. Bruning, J.C., et al., *Ribosomal subunit kinase-2 is required for growth factor-stimulated transcription of the c-Fos gene.* Proc Natl Acad Sci U S A, 2000. **97**(6): p. 2462-7.

33. Rivera, V.M., et al., *A growth factor-induced kinase phosphorylates the serum response factor at a site that regulates its DNA-binding activity.* Mol Cell Biol, 1993. **13**(10): p. 6260-73.

34. Nakajima, T., et al., *The signal-dependent coactivator CBP is a nuclear target for pp90RSK.* Cell, 1996. **86**(3): p. 465-74.

35. Wang, Z., et al., *Persistent ERK phosphorylation negatively regulates cAMP response element-binding protein (CREB) activity via recruitment of CREB-binding protein to pp90RSK.* J Biol Chem, 2003. **278**(13): p. 11138-44.

36. Joel, P.B., et al., *pp90rsk1 regulates estrogen receptor-mediated transcription through phosphorylation of Ser-167.* Mol Cell Biol, 1998. **18**(4): p. 1978-84.

37. Wang, H., et al., *Proteinase-activated receptors induce interleukin-8 expression by intestinal epithelial cells through ERK/RSK90 activation and histone acetylation.* FASEB J, 2010. **24**(6): p. 1971-80.

38. Fujita, N., S. Sato, and T. Tsuruo, *Phosphorylation of p27Kip1 at threonine 198 by p90 ribosomal protein S6 kinases promotes its binding to 14-3-3 and cytoplasmic localization.* J Biol Chem, 2003. **278**(49): p. 49254-60.

39. Vigneron, S., et al., *RSK2 is a kinetochore-associated protein that participates in the spindle assembly checkpoint.* Oncogene, 2010. **29**(24): p. 3566-74.

40. Sulzmaier, F.J. and J.W. Ramos, *RSK isoforms in cancer cell invasion and metastasis.* Cancer Res, 2013. **73**(20): p. 6099-105.

41. Pereira, P.M., et al., *Coffin-Lowry syndrome.* Eur J Hum Genet, 2010. **18**(6): p. 627-33.

42. Facher, J.J., et al., *Cardiomyopathy in Coffin-Lowry syndrome.* Am J Med Genet A, 2004. **128A**(2): p. 176-8.

43. Schneider, A., et al., *Altered ERK/MAPK signaling in the hippocampus of the mrsk2_KO mouse model of Coffin-Lowry syndrome.* J Neurochem, 2011. **119**(3): p. 447-59.

44. Poirier, R., et al., *Deletion of the Coffin-Lowry syndrome gene Rsk2 in mice is associated with impaired spatial learning and reduced control of exploratory behavior.* Behav Genet, 2007. **37**(1): p. 31-50.

45. Yang, X., et al., *ATF4 is a substrate of RSK2 and an essential regulator of osteoblast biology; implication for Coffin-Lowry Syndrome.* Cell, 2004. **117**(3): p. 387-98.

46. Laugel-Haushalter, V., et al., *RSK2 is a modulator of craniofacial development.* PLoS One, 2014. **9**(1): p. e84343.

47. Dugani, C.B., et al., *Coffin-Lowry syndrome: A role for RSK2 in mammalian neurogenesis.* Dev Biol, 2010.

48. Putz, G., et al., *The S6KII (rsk) gene of Drosophila melanogaster differentially affects an operant and a classical learning task.* J Neurosci, 2004. **24**(44): p. 9745-51.

49. Dumont, J., et al., *p90Rsk is not involved in cytostatic factor arrest in mouse oocytes.* J Cell Biol, 2005. **169**(2): p. 227-31.

50. David, J.P., et al., *Essential role of RSK2 in c-Fos-dependent osteosarcoma development.* J Clin Invest, 2005. **115**(3): p. 664-72.

51. Elf, S., et al., *p90RSK2 is essential for FLT3-ITD- but dispensable for BCR-ABL-induced myeloid leukemia.* Blood, 2011. **117**(25): p. 6885-94.

52. Lin, J.X., R. Spolski, and W.J. Leonard, *Critical role for Rsk2 in T-lymphocyte activation.* Blood, 2008. **111**(2): p. 525-33.

53. Moon, H.G., et al., *Phosphorylation of p90RSK is associated with increased response to neoadjuvant chemotherapy in ER-positive breast cancer.* BMC Cancer, 2012. **12**: p. 585.

54. Stratford, A.L., et al., *Targeting p90 ribosomal S6 kinase eliminates tumor-initiating cells by inactivating Y-box binding protein-1 in triple-negative breast cancers.* Stem Cells, 2012. **30**(7): p. 1338-48.

55. Clark, D.E., et al., *Rsk2 allosterically activates estrogen receptor alpha by docking to the hormone-binding domain.* EMBO J, 2001. **20**(13): p. 3484-94.

56. Yamashita, H., et al., *Phosphorylation of estrogen receptor alpha serine 167 is predictive of response to endocrine therapy and increases postrelapse survival in metastatic breast cancer.* Breast Cancer Res, 2005. **7**(5): p. R753-64.

57. Yamashita, H., et al., *Low phosphorylation of estrogen receptor alpha (ERalpha) serine 118 and high phosphorylation of ERalpha serine 167 improve survival in ER-positive breast cancer.* Endocr Relat Cancer, 2008. **15**(3): p. 755-63.

58. Jiang, J., et al., *Phosphorylation of estrogen receptor-alpha at Ser167 is indicative of longer disease-free and overall survival in breast cancer patients.* Clin Cancer Res, 2007. **13**(19): p. 5769-76.

59. Smith, J.A., et al., *Identification of the first specific inhibitor of p90 ribosomal S6 kinase (RSK) reveals an unexpected role for RSK in cancer cell proliferation.* Cancer Res, 2005. **65**(3): p. 1027-34.

60. Berman-Booty, L.D. and K.E. Knudsen, *Models of neuroendocrine prostate cancer.* Endocr Relat Cancer, 2015. **22**(1): p. R33-49.

61. Beltran, H., et al., *Divergent clonal evolution of castration-resistant neuroendocrine prostate cancer.* Nat Med, 2016. **22**(3): p. 298-305.

62. Clark, D.E., et al., *The serine/threonine protein kinase, p90 ribosomal S6 kinase, is an important regulator of prostate cancer cell proliferation.* Cancer Res, 2005. **65**(8): p. 3108-16.

63. Marzuka, A., et al., *Melanoma Treatments: Advances and Mechanisms.* J Cell Physiol, 2015. **230**(11): p. 2626-33.

64. Cho, Y.Y., et al., *RSK2 as a key regulator in human skin cancer.* Carcinogenesis, 2012. **33**(12): p. 2529-37.

65. Cho, Y.Y., et al., *A regulatory mechanism for RSK2 NH(2)-terminal kinase activity.* Cancer Res, 2009. **69**(10): p. 4398-406.

66. Zhu, Z., W. Liu, and V. Gotlieb, *The rapidly evolving therapies for advanced melanoma-Towards immunotherapy, molecular targeted therapy, and beyond.* Crit Rev Oncol Hematol, 2016. **99**: p. 91-9.

67. Theodosakis, N., et al., *p90RSK Blockade Inhibits Dual BRAF and MEK Inhibitor-Resistant Melanoma by Targeting Protein Synthesis.* J Invest Dermatol, 2017. **137**(10): p. 2187-2196.

68. Sacco, A.G. and E.E. Cohen, *Current Treatment Options for Recurrent or Metastatic Head and Neck Squamous Cell Carcinoma.* J Clin Oncol, 2015. **33**(29): p. 3305-13.

69. Kang, S., et al., *p90 ribosomal S6 kinase 2 promotes invasion and metastasis of human head and neck squamous cell carcinoma cells.* J Clin Invest, 2010. **120**(4): p. 1165-77.

70. Li, D., et al., *The prometastatic ribosomal S6 kinase 2-cAMP response element-binding protein (RSK2-CREB) signaling pathway up-regulates the actin-binding protein fascin-1 to promote tumor metastasis.* J Biol Chem, 2013. **288**(45): p. 32528-38.

71. Ostrom, Q.T., et al., *CBTRUS Statistical Report: Primary Brain and Other Central Nervous System Tumors Diagnosed in the United States in 2009-2013.* Neuro Oncol, 2016. **18**(suppl_5): p. v1-v75.

72. Hamaoka, Y., M. Negishi, and H. Katoh, *EphA2 is a key effector of the MEK/ERK/RSK pathway regulating glioblastoma cell proliferation.* Cell Signal, 2016. **28**(8): p. 937-45.

73. Gawecka, J.E., et al., *RSK2 protein suppresses integrin activation and fibronectin matrix assembly and promotes cell migration.* J Biol Chem, 2012. **287**(52): p. 43424-37.

74. Shi, G.X., et al., *RSK2 drives cell motility by serine phosphorylation of LARG and activation of Rho GTPases.* Proc Natl Acad Sci U S A, 2018. **115**(2): p. E190-E199.

75. Lara, R., et al., *An siRNA screen identifies RSK1 as a key modulator of lung cancer metastasis.* Oncogene, 2011. **30**(32): p. 3513-21.

76. Zhou, Y., et al., *Crucial roles of RSK in cell motility by catalysing serine phosphorylation of EphA2.* Nat Commun, 2015. **6**: p. 7679.

77. Graves, P.R., et al., *Ionizing radiation induces EphA2 S897 phosphorylation in a MEK/ERK/RSK-dependent manner.* Int J Radiat Biol, 2017. **93**(9): p. 929-936.

78. Yao, K., et al., *RSK2 phosphorylates T-bet to attenuate colon cancer metastasis and growth.* Proc Natl Acad Sci U S A, 2017. **114**(48): p. 12791-12796.

79. Calvo, N., et al., *RSK activation via ERK modulates human colon cancer cells response to PTHrP.* J Mol Endocrinol, 2017. **59**(1): p. 13-27.

80. Katayama, K., et al., *Inhibition of the mitogen-activated protein kinase pathway results in the down-regulation of P-glycoprotein.* Mol Cancer Ther, 2007. **6**(7): p. 2092-102.

81. Bignone, P.A., et al., *RPS6KA2, a putative tumour suppressor gene at 6q27 in sporadic epithelial ovarian cancer.* Oncogene, 2007. **26**(5): p. 683-700.

82. Milosevic, N., et al., *Synthetic lethality screen identifies RPS6KA2 as modifier of epidermal growth factor receptor activity in pancreatic cancer.* Neoplasia, 2013. **15**(12): p. 1354-62.

83. Arechavaleta-Velasco, F., et al., *Ribosomal S6 kinase 4 (RSK4) expression in ovarian tumors and its regulation by antineoplastic drugs in ovarian cancer cell lines.* Med Oncol, 2016. **33**(2): p. 11.

84. Lopez-Vicente, L., et al., *Regulation of replicative and stress-induced senescence by RSK4, which is down-regulated in human tumors.* Clin Cancer Res, 2009. **15**(14): p. 4546-53.

85. Cai, J., et al., *Low expression of RSK4 predicts poor prognosis in patients with colorectal cancer.* Int J Clin Exp Pathol, 2014. **7**(8): p. 4959-70.

86. Dewdney, S.B., et al., *Aberrant methylation of the X-linked ribosomal S6 kinase RPS6KA6 (RSK4) in endometrial cancers.* Clin Cancer Res, 2011. **17**(8): p. 2120-9.

87. Li, Q., et al., *Frequent epigenetic inactivation of RSK4 by promoter methylation in cancerous and non-cancerous tissues of breast cancer.* Med Oncol, 2014. **31**(1): p. 793.

88. Thakur, A., et al., *Aberrant expression of X-linked genes RbAp46, Rsk4, and Cldn2 in breast cancer.* Mol Cancer Res, 2007. **5**(2): p. 171-81.

89. Serra, V., et al., *RSK3/4 mediate resistance to PI3K pathway inhibitors in breast cancer.* J Clin Invest, 2013.

90. Fan, L., et al., *Ribosomal s6 protein kinase 4: a prognostic factor for renal cell carcinoma.* Br J Cancer, 2013. **109**(5): p. 1137-46.

91. Takeishi, Y., et al., *Activation of mitogen-activated protein kinases and p90 ribosomal S6 kinase in failing human hearts with dilated cardiomyopathy.* Cardiovasc Res, 2002. **53**(1): p. 131-7.

92. Takahashi, E., J. Abe, and B.C. Berk, *Angiotensin II stimulates p90rsk in vascular smooth muscle cells. A potential Na(+)-H+ exchanger kinase.* Circ Res, 1997. **81**(2): p. 268-73.

93. Takeishi, Y., et al., *Differential regulation of p90 ribosomal S6 kinase and big mitogen-activated protein kinase 1 by ischemia/reperfusion and oxidative stress in perfused guinea pig hearts.* Circ Res, 1999. **85**(12): p. 1164-72.

94. Garciarena, C.D., et al., *Myocardial reperfusion injury: reactive oxygen species vs. NHE-1 reactivation.* Cell Physiol Biochem, 2011. **27**(1): p. 13-22.

95. Itoh, S., et al., *Role of p90 ribosomal S6 kinase-mediated prorenin-converting enzyme in ischemic and diabetic myocardium.* Circulation, 2006. **113**(14): p. 1787-98.

96. Cheng, W.H., et al., *Angiotensin II inhibits neuronal nitric oxide synthase activation through the ERK1/2-RSK signaling pathway to modulate central control of blood pressure.* Circ Res, 2010. **106**(4): p. 788-95.

97. Doyon, P. and M.J. Servant, *Tumor necrosis factor receptor-associated factor-6 and ribosomal S6 kinase intracellular pathways link the angiotensin II AT1 receptor to the phosphorylation and activation of the IkappaB kinase complex in vascular smooth muscle cells.* J Biol Chem, 2010. **285**(40): p. 30708-18.

98. Le, N.T., et al., *A crucial role for p90RSK-mediated reduction of ERK5 transcriptional activity in endothelial dysfunction and atherosclerosis.* Circulation, 2013. **127**(4): p. 486-99.

99. Heo, K.S., et al., *Disturbed flow-activated p90RSK kinase accelerates atherosclerosis by inhibiting SENP2 function.* J Clin Invest, 2015. **125**(3): p. 1299-310.

100. Maekawa, N., et al., *Inhibiting p90 ribosomal S6 kinase prevents (Na+)-H+ exchanger-mediated cardiac ischemia-reperfusion injury.* Circulation, 2006. **113**(21): p. 2516-23.

101. Le, N.T., et al., *p90RSK targets the ERK5-CHIP ubiquitin E3 ligase activity in diabetic hearts and promotes cardiac apoptosis and dysfunction.* Circ Res, 2012. **110**(4): p. 536-50.

102. Shi, X., et al., *The RSK Inhibitor BIX02565 Limits Cardiac Ischemia/Reperfusion Injury.* J Cardiovasc Pharmacol Ther, 2016. **21**(2): p. 177-86.

103. Fryer, R.M., et al., *Mitigation of off-target adrenergic binding and effects on cardiovascular function in the discovery of novel ribosomal S6 kinase 2 inhibitors.* J Pharmacol Exp Ther, 2012. **340**(3): p. 492-500.

104. Moor, A.N., et al., *Activation of Na+/H+ exchanger-directed protein kinases in the ischemic and ischemic-reperfused rat myocardium.* J Biol Chem, 2001. **276**(19): p. 16113-22.

105. Cuello, F., et al., *Evidence for direct regulation of myocardial Na+/H+ exchanger isoform 1 phosphorylation and activity by 90-kDa ribosomal S6 kinase (RSK): effects of the novel and specific RSK inhibitor fmk on responses to alpha1-adrenergic stimulation.* Mol Pharmacol, 2007. **71**(3): p. 799-806.

106. Karmazyn, M., *NHE-1: still a viable therapeutic target.* J Mol Cell Cardiol, 2013. **61**: p. 77-82.

107. Murphy, E. and D.G. Allen, *Why did the NHE inhibitor clinical trials fail?* J Mol Cell Cardiol, 2009. **46**(2): p. 137-41.

108. Artamonov, M., et al., *The p90 ribosomal S6 kinase (RSK) is a mediator of smooth muscle contractility.* PLoS One, 2013. **8**(3): p. e58703.

109. Uehata, M., et al., *Calcium sensitization of smooth muscle mediated by a Rho-associated protein kinase in hypertension.* Nature, 1997. **389**(6654): p. 990-4.

110. Murthy, S.N., B.D. Nossaman, and P.J. Kadowitz, *New approaches to the treatment of pulmonary hypertension: from bench to bedside.* Cardiol Rev, 2010. **18**(2): p. 76-84.

111. Li, J., et al., *Anchored p90 ribosomal S6 kinase 3 is required for cardiac myocyte hypertrophy.* Circ Res, 2013. **112**(1): p. 128-39.

112. Passariello, C.L., et al., *p90 ribosomal S6 kinase 3 contributes to cardiac insufficiency in alpha-tropomyosin Glu180Gly transgenic mice.* Am J Physiol Heart Circ Physiol, 2013. **305**(7): p. H1010-9.

113. Fu, B., et al., *Activation of p90 ribosomal S6 kinases by ORF45 of Kaposi's sarcoma-associated herpesvirus is critical for optimal production of infectious viruses.* J Virol, 2015. **89**(1): p. 195-207.

114. Kuang, E., et al., *Activation of p90 ribosomal S6 kinase by ORF45 of Kaposi's sarcoma-associated herpesvirus and its role in viral lytic replication.* J Virol, 2008. **82**(4): p. 1838-50.

115. Karijolich, J., et al., *Kaposi's sarcoma-associated herpesvirus ORF45 mediates transcriptional activation of the HIV-1 long terminal repeat via RSK2.* J Virol, 2014. **88**(12): p. 7024-35.

116. Avey, D., et al., *Phosphoproteomic Analysis of KSHV-Infected Cells Reveals Roles of ORF45-Activated RSK during Lytic Replication.* PLoS Pathog, 2015. **11**(7): p. e1004993.

117. McCoy, M.W., et al., *The C-terminal tail of Yersinia pseudotuberculosis YopM is critical for interacting with RSK1 and for virulence.* Infect Immun, 2010. **78**(6): p. 2584-98.

118. Nusrat, S., et al., *Cirrhosis and its complications: evidence based treatment.* World J Gastroenterol, 2014. **20**(18): p. 5442-60.

119. Buck, M. and M. Chojkier, *A ribosomal S-6 kinase-mediated signal to C/EBP-beta is critical for the development of liver fibrosis.* PLoS One, 2007. **2**(12): p. e1372.

120. Morales-Ibanez, O., et al., *Kinase analysis in alcoholic hepatitis identifies p90RSK as a potential mediator of liver fibrogenesis.* Gut, 2015.

121. Buck, M., et al., *Phosphorylation of rat serine 105 or mouse threonine 217 in C/EBP beta is required for hepatocyte proliferation induced by TGF alpha.* Mol Cell, 1999. **4**(6): p. 1087-92.

122. Yang, M.F., et al., *Involvement of 90-kuD ribosomal S6 kinase in collagen type I expression in rat hepatic fibrosis.* World J Gastroenterol, 2009. **15**(17): p. 2109-15.

123. Buck, M. and M. Chojkier, *C/EBPbeta-Thr217 phosphorylation signaling contributes to the development of lung injury and fibrosis in mice.* PLoS One, 2011. **6**(10): p. e25497.

124. Hutchinson, J., et al., *Global incidence and mortality of idiopathic pulmonary fibrosis: a systematic review.* Eur Respir J, 2015. **46**(3): p. 795-806.

125. Falconer, J. and C.D. Buckley, *Rheumatoid arthritis. The two faces of Rsk2 in hyperplastic disease.* Nat Rev Rheumatol, 2015. **11**(4): p. 203-5.

126. Derer, A., et al., *Rsk2 controls synovial fibroblast hyperplasia and the course of arthritis.* Ann Rheum Dis, 2016. **75**(2): p. 413-21.

127. De Cesare, D., et al., *Rsk-2 activity is necessary for epidermal growth factor-induced phosphorylation of CREB protein and transcription of c-fos gene.* Proc Natl Acad Sci U S A, 1998. **95**(21): p. 12202-7.

128. Kirrane, T.M., et al., *Indole RSK inhibitors. Part 2: optimization of cell potency and kinase selectivity.* Bioorg Med Chem Lett, 2012. **22**(1): p. 738-42.

129. Najafi, A., et al., *beta-adrenergic receptor signalling and its functional consequences in the diseased heart.* Eur J Clin Invest, 2016.

130. Endicott, J.A., M.E. Noble, and L.N. Johnson, *The structural basis for control of eukaryotic protein kinases.* Annu Rev Biochem, 2012. **81**: p. 587-613.

131. Zuccotto, F., et al., *Through the "gatekeeper door": exploiting the active kinase conformation.* J Med Chem, 2010. **53**(7): p. 2681-94.

132. Cohen, M.S., et al., *Structural bioinformatics-based design of selective, irreversible kinase inhibitors.* Science, 2005. **308**(5726): p. 1318-21.

133. Noble, M.E., J.A. Endicott, and L.N. Johnson, *Protein kinase inhibitors: insights into drug design from structure.* Science, 2004. **303**(5665): p. 1800-5.

134. Taunton, J., et al., *Selective Serine/Threonine kinase inhibitors*. 2010, The Regents of the University of California, Oakland, CA (US).

135. Bain, J., et al., *The selectivity of protein kinase inhibitors: a further update.* Biochem J, 2007. **408**(3): p. 297-315.

136. Smith, J.A., et al., *Structural basis for the activity of the RSK-specific inhibitor, SL0101.* Bioorg Med Chem, 2007. **15**(14): p. 5018-34.

137. Utepbergenov, D., et al., *Insights into the Inhibition of the p90 Ribosomal S6 Kinase (RSK) by the Flavonol Glycoside SL0101 from the 1.5 A Crystal Structure of the N-Terminal Domain of RSK2 with Bound Inhibitor.* Biochemistry, 2012. **51**(33): p. 6499-510.

138. Derewenda, U., et al., *Identification of quercitrin as an inhibitor of the p90 S6 ribosomal kinase (RSK): structure of its complex with the N-terminal domain of RSK2 at 1.8 A resolution.* Acta Crystallogr D Biol Crystallogr, 2013. **69**(Pt 2): p. 266-75.

139. Smith, J.A., et al., *Rhamnose substituents of SL0101 and therapeutic use of thereof*. 2013, Univeristy of Virginia Patent Foundation, Charlottesville, VA (US).

140. Smith, J.A., et al., *Influence of rhamnose substituents on the potency of SL0101, an inhibitor of the Ser/Thr kinase, RSK.* Bioorg Med Chem, 2006. **14**(17): p. 6034-42.

141. Mrozowski, R.M., et al., *Improving the affinity of SL0101 for RSK using structure-based design.* ACS Med Chem Lett, 2012. **4**(2): p. 175-179.

142. Li, M., et al., *Synthesis and Structure-Activity Relationship Study of 5a-Carbasugar Analogues of SL0101.* ACS Med Chem Lett, 2015. **6**(1): p. 95-9.

143. Li, M., et al., *Stereoselective Synthesis and Evaluation of C6''-Substituted 5a-Carbasugar Analogues of SL0101 as Inhibitors of RSK1/2.* Org Lett, 2017. **19**(9): p. 2410-2413.

144. Ludwik, K.A., et al., *Development of a RSK Inhibitor as a Novel Therapy for Triple-Negative Breast Cancer.* Mol Cancer Ther, 2016. **15**(11): p. 2598-2608.

145. Sapkota, G.P., et al., *BI-D1870 is a specific inhibitor of the p90 RSK (ribosomal S6 kinase) isoforms in vitro and in vivo.* Biochem J, 2007. **401**(1): p. 29-38.

146. Takada, I., Y. Yogiashi, and M. Makishima, *The ribosomal S6 kinase inhibitor BI-D1870 ameliorated experimental autoimmune encephalomyelitis in mice.* Immunobiology, 2016. **221**(2): p. 188-92.

147. Aronchik, I., et al., *Novel potent and selective inhibitors of p90 ribosomal S6 kinase reveal the heterogeneity of RSK function in MAPK-driven cancers.* Mol Cancer Res, 2014. **12**(5): p. 803-12.

148. Jain, R., et al., *Discovery of Potent and Selective RSK Inhibitors as Biological Probes.* J Med Chem, 2015. **58**(17): p. 6766-83.

149. Mehta, R.G., et al., *Differential roles of ERalpha and ERbeta in normal and neoplastic development in the mouse mammary gland.* PLoS One, 2014. **9**(11): p. e113175.

150. Feng, Y., et al., *Estrogen receptor-alpha expression in the mammary epithelium is required for ductal and alveolar morphogenesis in mice.* Proc Natl Acad Sci U S A, 2007. **104**(37): p. 14718-23.

151. Cuesta, R. and M.K. Holz, *RSK-mediated down-regulation of PDCD4 is required for proliferation, survival, and migration in a model of triple-negative breast cancer.* Oncotarget, 2016. **7**(19): p. 27567-83.

152. Gerlinger, M., et al., *Intratumor heterogeneity and branched evolution revealed by multiregion sequencing.* N Engl J Med, 2012. **366**(10): p. 883-92.

153. Whittle, J.R., et al., *Patient-derived xenograft models of breast cancer and their predictive power.* Breast Cancer Res, 2015. **17**: p. 17.

154. Ludwik, K.A., et al., *ERalpha-mediated nuclear sequestration of RSK2 is required for ER+ breast cancer tumorigenesis.* Cancer Res, 2018.

155. Clarke, R., J.J. Tyson, and J.M. Dixon, *Endocrine resistance in breast cancer--An overview and update.* Mol Cell Endocrinol, 2015. **418 Pt 3**: p. 220-34.

156. Doehn, U., et al., *RSK is a principal effector of the RAS-ERK pathway for eliciting a coordinate promotile/invasive gene program and phenotype in epithelial cells.* Mol Cell, 2009. **35**(4): p. 511-22.

157. Smolen, G.A., et al., *A genome-wide RNAi screen identifies multiple RSK-dependent regulators of cell migration.* Genes Dev, 2010. **24**(23): p. 2654-65.

158. Frech, M.S., et al., *Deregulated estrogen receptor alpha expression in mammary epithelial cells of transgenic mice results in the development of ductal carcinoma in situ.* Cancer Res, 2005. **65**(3): p. 681-5.

159. Archibald, A., et al., *Oncogenic suppression of apoptosis uncovers a Rac1/JNK proliferation pathway activated by loss of Par3.* Oncogene, 2015. **34**(24): p. 3199-206.

160. Hammond, M.E., et al., *American society of clinical oncology/college of american pathologists guideline recommendations for immunohistochemical testing of estrogen and progesterone receptors in breast cancer.* J Oncol Pract, 2010. **6**(4): p. 195-7.

161. Wolff, A.C., et al., *American Society of Clinical Oncology/College of American Pathologists guideline recommendations for human epidermal growth factor receptor 2 testing in breast cancer.* Arch Pathol Lab Med, 2007. **131**(1): p. 18-43.

162. Pasic, L., et al., *Sustained activation of the HER1-ERK1/2-RSK signaling pathway controls myoepithelial cell fate in human mammary tissue.* GEnes & Dev, 2011. **25**: p. 1641-1653.

163. Groehler, A.L. and D.A. Lannigan, *A chromatin-bound kinase, ERK8, protects genomic integrity by inhibiting HDM2-mediated degradation of the DNA clamp PCNA.* J Cell Biol, 2010. **190**(4): p. 575-86.

164. Liberzon, A., et al., *The Molecular Signatures Database (MSigDB) hallmark gene set collection.* Cell Syst, 2015. **1**(6): p. 417-425.

165. Zufferey, R., et al., *Multiply attenuated lentiviral vector achieves efficient gene delivery in vivo.* Nat Biotechnol, 1997. **15**(9): p. 871-5.

166. McCaffrey, L.M. and I.G. Macara, *The Par3/aPKC interaction is essential for end bud remodeling and progenitor differentiation during mammary gland morphogenesis.* Genes Dev, 2009. **23**(12): p. 1450-60.

167. Malliri, A., et al., *The Rac exchange factor Tiam1 is required for the establishment and maintenance of cadherin-based adhesions.* J Biol Chem, 2004. **279**(29): p. 30092-8.

168. Cong, L., et al., *Multiplex genome engineering using CRISPR/Cas systems.* Science, 2013. **339**(6121): p. 819-23.

169. Shannon, P., et al., *Cytoscape: a software environment for integrated models of biomolecular interaction networks.* Genome Res, 2003. **13**(11): p. 2498-504.

170. Janky, R., et al., *iRegulon: from a gene list to a gene regulatory network using large motif and track collections.* PLoS Comput Biol, 2014. **10**(7): p. e1003731.

171. Szklarczyk, D., et al., *The STRING database in 2017: quality-controlled protein-protein association networks, made broadly accessible.* Nucleic Acids Res, 2017. **45**(D1): p. D362-D368.

172. Gene Ontology, C., *Gene Ontology Consortium: going forward.* Nucleic Acids Res, 2015. **43**(Database issue): p. D1049-56.

173. Finn, R.S., A. Aleshin, and D.J. Slamon, *Targeting the cyclin-dependent kinases (CDK) 4/6 in estrogen receptor-positive breast cancers.* Breast Cancer Res, 2016. **18**(1): p. 17.

174. Subramanian, A., et al., *Gene set enrichment analysis: a knowledge-based approach for interpreting genome-wide expression profiles.* Proc Natl Acad Sci U S A, 2005. **102**(43): p. 15545-50.

175. Mootha, V.K., et al., *PGC-1alpha-responsive genes involved in oxidative phosphorylation are coordinately downregulated in human diabetes.* Nat Genet, 2003. **34**(3): p. 267-73.

176. Schuetz, C.S., et al., *Progression-specific genes identified by expression profiling of matched ductal carcinomas in situ and invasive breast tumors, combining laser capture microdissection and oligonucleotide microarray analysis.* Cancer Res, 2006. **66**(10): p. 5278-86.

177. Kaddi, C.D., R.M. Parry, and M.D. Wang, *Multivariate hypergeometric similarity measure.* IEEE/ACM Trans Comput Biol Bioinform, 2013. **10**(6): p. 1505-16.

178. Parker, J.S., et al., *Supervised risk predictor of breast cancer based on intrinsic subtypes.* J Clin Oncol, 2009. **27**(8): p. 1160-7.

179. Charafe-Jauffret, E., et al., *Gene expression profiling of breast cell lines identifies potential new basal markers.* Oncogene, 2006. **25**(15): p. 2273-84.

180. Ashburner, M., et al., *Gene ontology: tool for the unification of biology. The Gene Ontology Consortium.* Nat Genet, 2000. **25**(1): p. 25-9.

181. The Gene Ontology, C., *Expansion of the Gene Ontology knowledgebase and resources.* Nucleic Acids Res, 2017. **45**(D1): p. D331-D338.

182. Turashvili, G., et al., *Novel markers for differentiation of lobular and ductal invasive breast carcinomas by laser microdissection and microarray analysis.* BMC Cancer, 2007. **7**: p. 55.

183. Stein, R.A., et al., *Estrogen-related receptor alpha is critical for the growth of estrogen receptor-negative breast cancer.* Cancer Res, 2008. **68**(21): p. 8805-12.

184. Dutertre, M., et al., *Estrogen regulation and physiopathologic significance of alternative promoters in breast cancer.* Cancer Res, 2010. **70**(9): p. 3760-70.

185. Bernardo, G.M., et al., *FOXA1 is an essential determinant of ERalpha expression and mammary ductal morphogenesis.* Development, 2010. **137**(12): p. 2045-54.

186. Asselin-Labat, M.L., et al., *Gata-3 is an essential regulator of mammary-gland morphogenesis and luminal-cell differentiation.* Nat Cell Biol, 2007. **9**(2): p. 201-9.

187. Kouros-Mehr, H., et al., *GATA-3 maintains the differentiation of the luminal cell fate in the mammary gland.* Cell, 2006. **127**(5): p. 1041-55.

188. Yi, P., et al., *Structure of a biologically active estrogen receptor-coactivator complex on DNA.* Mol Cell, 2015. **57**(6): p. 1047-58.

189. Metivier, R., et al., *Estrogen receptor-alpha directs ordered, cyclical, and combinatorial recruitment of cofactors on a natural target promoter.* Cell, 2003. **115**(6): p. 751-63.

190. Shang, Y., et al., *Cofactor dynamics and sufficiency in estrogen receptor-regulated transcription.* Cell, 2000. **103**(6): p. 843-52.

191. Cancer Genome Atlas, N., *Comprehensive molecular portraits of human breast tumours.* Nature, 2012. **490**(7418): p. 61-70.

192. Chuderland, D., A. Konson, and R. Seger, *Identification and characterization of a general nuclear translocation signal in signaling proteins.* Mol Cell, 2008. **31**(6): p. 850-61.

193. Dabydeen, S.A. and P.A. Furth, *Genetically engineered ERalpha-positive breast cancer mouse models.* Endocr Relat Cancer, 2014. **21**(3): p. R195-208.

194. Murakami, S., A. Nagari, and W.L. Kraus, *Dynamic assembly and activation of estrogen receptor alpha enhancers through coregulator switching.* Genes Dev, 2017. **31**(15): p. 1535-1548.

195. Motomura, K., et al., *Expression of estrogen receptor beta and phosphorylation of estrogen receptor alpha serine 167 correlate with progression-free survival in patients with metastatic breast cancer treated with aromatase inhibitors.* Oncology, 2010. **79**(1-2): p. 55-61.

196. St-Hilaire, S., et al., *Estrogen receptor positive breast cancers and their association with environmental factors.* Int J Health Geogr, 2011. **10**: p. 32.

197. Barros, R.P. and J.A. Gustafsson, *Estrogen receptors and the metabolic network.* Cell Metab, 2011. **14**(3): p. 289-99.

198. Mauvais-Jarvis, F., D.J. Clegg, and A.L. Hevener, *The role of estrogens in control of energy balance and glucose homeostasis.* Endocr Rev, 2013. **34**(3): p. 309-38.

199. Chuffa, L.G., et al., *The role of sex hormones and steroid receptors on female reproductive cancers.* Steroids, 2017. **118**: p. 93-108.

200. Xu, B., D. Lovre, and F. Mauvais-Jarvis, *The effect of selective estrogen receptor modulators on type 2 diabetes onset in women: Basic and clinical insights.* J Diabetes Complications, 2017. **31**(4): p. 773-779.

201. Fata, J.E., V. Chaudhary, and R. Khokha, *Cellular turnover in the mammary gland is correlated with systemic levels of progesterone and not 17beta-estradiol during the estrous cycle.* Biol Reprod, 2001. **65**(3): p. 680-8.

202. Wood, G.A., et al., *Circulating hormones and estrous stage predict cellular and stromal remodeling in murine uterus.* Reproduction, 2007. **133**(5): p. 1035-44.

203. Nawaz, Z., et al., *Proteasome-dependent degradation of the human estrogen receptor.* Proc Natl Acad Sci U S A, 1999. **96**(5): p. 1858-62.

204. Lonard, D.M., et al., *The 26S proteasome is required for estrogen receptor-alpha and coactivator turnover and for efficient estrogen receptor-alpha transactivation.* Mol Cell, 2000. **5**(6): p. 939-48.

205. Silberstein, G.B., et al., *Estrogen-triggered delays in mammary gland gene expression during the estrous cycle: evidence for a novel timing system.* J Endocrinol, 2006. **190**(2): p. 225-39.

206. Reid, G., et al., *Cyclic, proteasome-mediated turnover of unliganded and liganded ERalpha on responsive promoters is an integral feature of estrogen signaling.* Mol Cell, 2003. **11**(3): p. 695-707.

207. Zhang, H., et al., *The catalytic subunit of the proteasome is engaged in the entire process of estrogen receptor-regulated transcription.* EMBO J, 2006. **25**(18): p. 4223-33.

208. Valley, C.C., et al., *Temporal variation in estrogen receptor-alpha protein turnover in the presence of estrogen.* J Mol Endocrinol, 2008. **40**(1): p. 23-34.

209. Zhou, W. and J.M. Slingerland, *Links between oestrogen receptor activation and proteolysis: relevance to hormone-regulated cancer therapy.* Nat Rev Cancer, 2014. **14**(1): p. 26-38.

210. Brisken, C. and D. Ataca, *Endocrine hormones and local signals during the development of the mouse mammary gland.* Wiley Interdiscip Rev Dev Biol, 2015. **4**(3): p. 181-95.

211. Bruce, M.C., D. McAllister, and L.C. Murphy, *The kinome associated with estrogen receptor-positive status in human breast cancer.* Endocr Relat Cancer, 2014. **21**(5): p. R357-70.

212. Pawar, S., et al., *Minireview: Steroid-regulated paracrine mechanisms controlling implantation.* Mol Endocrinol, 2014. **28**(9): p. 1408-22.

213. Joshi, P.A., et al., *Progesterone induces adult mammary stem cell expansion.* Nature, 2010. **465**(7299): p. 803-7.

214. Byers, S.L., et al., *Mouse estrous cycle identification tool and images.* PLoS One, 2012. **7**(4): p. e35538.

215. Brill, B., et al., *A sparing procedure to clear the mouse mammary fat pad of epithelial components for transplantation analysis.* Lab Anim, 2008. **42**(1): p. 104-10.

216. Giraddi, R.R., et al., *Stem and progenitor cell division kinetics during postnatal mouse mammary gland development.* Nat Commun, 2015. **6**: p. 8487.

217. De Silva, D., et al., *Transcriptome analysis of the hormone-sensing cells in mammary epithelial reveals dynamic changes in early pregnancy.* BMC Dev Biol, 2015. **15**: p. 7.

218. Watson, C.J., *Involution: apoptosis and tissue remodelling that convert the mammary gland from milk factory to a quiescent organ.* Breast Cancer Res, 2006. **8**(2): p. 203.

219. Shehata, M., et al., *Phenotypic and functional characterization of the luminal cell hierarchy of the mammary gland.* Breast Cancer Res, 2012. **14**(5): p. R134.

220. Hynes, N.E. and C.J. Watson, *Mammary gland growth factors: roles in normal development and in cancer.* Cold Spring Harb Perspect Biol, 2010. **2**(8): p. a003186.

221. Pinter, O., et al., *Differences in the onset of puberty in selected inbred mouse strains.* Endocrine Abstracts, 2007. **14**: p. P617.

222. Saito, T., et al., *Estrogen contributes to gender differences in mouse ventricular repolarization.* Circ Res, 2009. **105**(4): p. 343-52.

223. Robertshaw, I., F. Bian, and S.K. Das, *Mechanisms of uterine estrogen signaling during early pregnancy in mice: an update.* J Mol Endocrinol, 2016. **56**(3): p. R127-38.

224. Winuthayanon, W., S.C. Hewitt, and K.S. Korach, *Uterine epithelial cell estrogen receptor alpha-dependent and -independent genomic profiles that underlie estrogen responses in mice.* Biol Reprod, 2014. **91**(5): p. 110.

225. Kelleher, A.M., et al., *Uterine glands impact uterine receptivity, luminal fluid homeostasis and blastocyst implantation.* Sci Rep, 2016. **6**: p. 38078.

226. Eeckhoute, J., et al., *Positive cross-regulatory loop ties GATA-3 to estrogen receptor alpha expression in breast cancer.* Cancer Res, 2007. **67**(13): p. 6477-83.

227. Uhlen, M., et al., *A pathology atlas of the human cancer transcriptome.* Science, 2017. **357**(6352).

228. Shahbazian, D., et al., *The mTOR/PI3K and MAPK pathways converge on eIF4B to control its phosphorylation and activity.* EMBO J, 2006. **25**(12): p. 2781-91.

229. Wang, X., et al., *Regulation of elongation factor 2 kinase by p90(RSK1) and p70 S6 kinase.* EMBO J, 2001. **20**(16): p. 4370-9.

230. Roux, P.P., et al., *Tumor-promoting phorbol esters and activated Ras inactivate the tuberous sclerosis tumor suppressor complex via p90 ribosomal S6 kinase.* Proc Natl Acad Sci U S A, 2004. **101**(37): p. 13489-94.

231. Kanehisa, M., et al., *KEGG: new perspectives on genomes, pathways, diseases and drugs.* Nucleic Acids Res, 2017. **45**(D1): p. D353-D361.

232. Fabregat, A., et al., *The Reactome Pathway Knowledgebase.* Nucleic Acids Res, 2018. **46**(D1): p. D649-D655.

233. Britten, C.D., *PI3K and MEK inhibitor combinations: examining the evidence in selected tumor types.* Cancer Chemother Pharmacol, 2013. **71**(6): p. 1395-409.

234. Rongo, C., *Epidermal growth factor and aging: a signaling molecule reveals a new eye opening function.* Aging (Albany NY), 2011. **3**(9): p. 896-905.

235. Chao, H.W., et al., *Circadian clock regulates hepatic polyploidy by modulating Mkp1-Erk1/2 signaling pathway.* Nat Commun, 2017. **8**(1): p. 2238.

236. Snijders, A.M., et al., *An interferon signature identified by RNA-sequencing of mammary tissues varies across the estrous cycle and is predictive of metastasis-free survival.* Oncotarget, 2014. **5**(12): p. 4011-25.

237. Tecalco-Cruz, A.C. and J.O. Ramirez-Jarquin, *Mechanisms that Increase Stability of Estrogen Receptor Alpha in Breast Cancer.* Clin Breast Cancer, 2017. **17**(1): p. 1-10.

238. Zhang, P., et al., *Endometrial cancer-associated mutants of SPOP are defective in regulating estrogen receptor-alpha protein turnover.* Cell Death Dis, 2015. **6**: p. e1687.

239. Fukuda, T., et al., *HAND2-mediated proteolysis negatively regulates the function of estrogen receptor alpha.* Mol Med Rep, 2015. **12**(4): p. 5538-44.

240. Hunter, T., *The age of crosstalk: phosphorylation, ubiquitination, and beyond.* Mol Cell, 2007. **28**(5): p. 730-8.

241. Deschenes-Simard, X., et al., *Tumor suppressor activity of the ERK/MAPK pathway by promoting selective protein degradation.* Genes Dev, 2013. **27**(8): p. 900-15.

242. Banys-Paluchowski, M., et al., *Circulating tumor cells in breast cancer-current status and perspectives.* Crit Rev Oncol Hematol, 2016. **97**: p. 22-9.

243. Dent, R., et al., *Triple-negative breast cancer: clinical features and patterns of recurrence.* Clin Cancer Res, 2007. **13**(15 Pt 1): p. 4429-34.

244. Badve, S., et al., *Basal-like and triple-negative breast cancers: a critical review with an emphasis on the implications for pathologists and oncologists.* Mod Pathol, 2011. **24**(2): p. 157-67.

245. Craig, D.W., et al., *Genome and transcriptome sequencing in prospective metastatic triple-negative breast cancer uncovers therapeutic vulnerabilities.* Mol Cancer Ther, 2013. **12**(1): p. 104-16.

246. Infante, J.R., et al., *A phase 1b study of trametinib, an oral Mitogen-activated protein kinase kinase (MEK) inhibitor, in combination with gemcitabine in advanced solid tumours.* Eur J Cancer, 2013. **49**(9): p. 2077-85.

247. Duncan, J.S., et al., *Dynamic reprogramming of the kinome in response to targeted MEK inhibition in triple-negative breast cancer.* Cell, 2012. **149**(2): p. 307-21.

248. Giltnane, J.M. and J.M. Balko, *Rationale for targeting the Ras/MAPK pathway in triple-negative breast cancer.* Discov Med, 2014. **17**(95): p. 275-83.

249. Network, T.C.G.A., *Comprehensive molecular portraits of human breast tumors.* Nature, 2012. **490**: p. 61-70.

250. Cossu-Rocca, P., et al., *Analysis of PIK3CA Mutations and Activation Pathways in Triple Negative Breast Cancer.* PLoS One, 2015. **10**(11): p. e0141763.

251. Hoeflich, K.P., et al., *In vivo antitumor activity of MEK and phosphatidylinositol 3-kinase inhibitors in basal-like breast cancer models.* Clin Cancer Res, 2009. **15**(14): p. 4649-64.

252. Jing, J., et al., *Comprehensive predictive biomarker analysis for MEK inhibitor GSK1120212.* Mol Cancer Ther, 2012. **11**(3): p. 720-9.

253. Samatar, A.A. and P.I. Poulikakos, *Targeting RAS-ERK signalling in cancer: promises and challenges.* Nat Rev Drug Discov, 2014. **13**(12): p. 928-42.

254. Eisinger-Mathason, T.S., J. Andrade, and D.A. Lannigan, *RSK in tumorigenesis: connections to steroid signaling.* Steroids, 2010. **75**(3): p. 191-202.

255. Larrea, M.D., et al., *RSK1 drives p27Kip1 phosphorylation at T198 to promote RhoA inhibition and increase cell motility.* Proc Natl Acad Sci U S A, 2009. **106**(23): p. 9268-73.

256. Vial, D. and P.J. McKeown-Longo, *Epidermal growth factor (EGF) regulates alpha5beta1 integrin activation state in human cancer cell lines through the p90RSK-dependent phosphorylation of filamin A.* J Biol Chem, 2012. **287**(48): p. 40371-80.

257. Sapkota, G.P., et al., *Phosphorylation of the protein kinase mutated in Peutz-Jeghers cancer syndrome, LKB1/STK11, at Ser431 by p90(RSK) and cAMP-dependent protein kinase, but not its farnesylation at Cys(433), is essential for LKB1 to suppress cell vrowth.* J Biol Chem, 2001. **276**(22): p. 19469-82.

258. Edgar, A.J., et al., *A combination of SILAC and nucleotide acyl phosphate labelling reveals unexpected targets of the Rsk inhibitor BI-D1870.* Biosci Rep, 2014. **34**: p. e00091.

259. Serafimova, I.M., et al., *Reversible targeting of noncatalytic cysteines with chemically tuned electrophiles.* Nat Chem Biol, 2012. **8**(5): p. 471-6.

260. Ries, C.H., et al., *CSF-1/CSF-1R targeting agents in clinical development for cancer therapy.* Curr Opin Pharmacol, 2015. **23**: p. 45-51.

261. Ammirati, M., et al., *Discovery of an in Vivo Tool to Establish Proof-of-Concept for MAP4K4-Based Antidiabetic Treatment.* ACS Med Chem Lett, 2015. **6**(11): p. 1128-33.

262. Lehmann, B.D., et al., *Identification of human triple-negative breast cancer subtypes and preclinical models for selection of targeted therapies.* J Clin Invest, 2011. **121**(7): p. 2750-67.

263. Lehmann, B.D. and J.A. Pietenpol, *Identification and use of biomarkers in treatment strategies for triple-negative breast cancer subtypes.* J Pathol, 2014. **232**(2): p. 142-50.

264. Pantel, K. and M.R. Speicher, *The biology of circulating tumor cells.* Oncogene, 2015.

265. Neuzillet, C., et al., *MEK in cancer and cancer therapy.* Pharmacol Ther, 2014. **141**(2): p. 160-71.

266. Turke, A.B., et al., *MEK inhibition leads to PI3K/AKT activation by relieving a negative feedback on ERBB receptors.* Cancer Res, 2012. **72**(13): p. 3228-37.

267. Jokinen, E. and J.P. Koivunen, *MEK and PI3K inhibition in solid tumors: rationale and evidence to date.* Ther Adv Med Oncol, 2015. **7**(3): p. 170-80.

268. Zaman, K., et al., *Fulvestrant with or without selumetinib, a MEK 1/2 inhibitor, in breast cancer progressing after aromatase inhibitor therapy: A multicentre randomised placebo-controlled double-blind phase II trial, SAKK 21/08.* Eur J Cancer, 2015. **51**(10): p. 1212-20.

269. Untch, M., et al., *13th st. Gallen international breast cancer conference 2013: primary therapy of early breast cancer evidence, controversies, consensus - opinion of a german team of experts (zurich 2013).* Breast Care (Basel), 2013. **8**(3): p. 221-9.

270. Sorlie, T., et al., *Repeated observation of breast tumor subtypes in independent gene expression data sets.* Proc Natl Acad Sci U S A, 2003. **100**(14): p. 8418-23.

271. Wang, Y., et al., *Clonal evolution in breast cancer revealed by single nucleus genome sequencing.* Nature, 2014. **512**(7513): p. 155-60.

272. Park, S.Y., et al., *Cellular and genetic diversity in the progression of in situ human breast carcinomas to an invasive phenotype.* J Clin Invest, 2010. **120**(2): p. 636-44.

273. Navin, N., et al., *Tumour evolution inferred by single-cell sequencing.* Nature, 2011. **472**(7341): p. 90-4.

274. Nik-Zainal, S., et al., *Mutational processes molding the genomes of 21 breast cancers.* Cell, 2012. **149**(5): p. 979-93.

275. Yates, L.R., et al., *Subclonal diversification of primary breast cancer revealed by multiregion sequencing.* Nat Med, 2015. **21**(7): p. 751-9.

276. Ridky, T.W., et al., *Invasive three-dimensional organotypic neoplasia from multiple normal human epithelia.* Nat Med, 2010. **16**(12): p. 1450-5.

277. Sato, T., et al., *Single Lgr5 stem cells build crypt-villus structures in vitro without a mesenchymal niche.* Nature, 2009. **459**(7244): p. 262-5.

278. van de Wetering, M., et al., *Prospective derivation of a living organoid biobank of colorectal cancer patients.* Cell, 2015. **161**(4): p. 933-45.

279. Boj, S.F., et al., *Organoid models of human and mouse ductal pancreatic cancer.* Cell, 2015. **160**(1-2): p. 324-38.

280. Drost, J., et al., *Organoid culture systems for prostate epithelial and cancer tissue.* Nat Protoc, 2016. **11**(2): p. 347-58.

281. Gao, D., et al., *Organoid cultures derived from patients with advanced prostate cancer.* Cell, 2014. **159**(1): p. 176-87.

282. Sachs, N., et al., *A Living Biobank of Breast Cancer Organoids Captures Disease Heterogeneity.* Cell, 2018. **172**(1-2): p. 373-386 e10.

283. Walsh, A.J., et al., *Drug response in organoids generated from frozen primary tumor tissues.* Sci Rep, 2016. **6**: p. 18889.

284. Walsh, A.J., et al., *Quantitative optical imaging of primary tumor organoid metabolism predicts drug response in breast cancer.* Cancer Res, 2014. **74**(18): p. 5184-94.

285. Kim, D., et al., *TopHat2: accurate alignment of transcriptomes in the presence of insertions, deletions and gene fusions.* Genome Biol, 2013. **14**(4): p. R36.

286. Trapnell, C., et al., *Transcript assembly and quantification by RNA-Seq reveals unannotated transcripts and isoform switching during cell differentiation.* Nat Biotechnol, 2010. **28**(5): p. 511-5.

287. Stacklies, W., et al., *pcaMethods--a bioconductor package providing PCA methods for incomplete data.* Bioinformatics, 2007. **23**(9): p. 1164-7.

288. Visvader, J.E. and J. Stingl, *Mammary stem cells and the differentiation hierarchy: current status and perspectives.* Genes Dev, 2014. **28**(11): p. 1143-58.

289. Santagata, S. and T.A. Ince, *Normal cell phenotypes of breast epithelial cells provide the foundation of a breast cancer taxonomy.* Expert Rev Anticancer Ther, 2014. **14**(12): p. 1385-9.

290. Fatehullah, A., S.H. Tan, and N. Barker, *Organoids as an in vitro model of human development and disease.* Nat Cell Biol, 2016. **18**(3): p. 246-54.

291. Turner, N., et al., *Integrative molecular profiling of triple negative breast cancers identifies amplicon drivers and potential therapeutic targets.* Oncogene, 2010. **29**(14): p. 2013-23.

292. Williams, C.B., et al., *Perspectives on Epidermal Growth Factor Receptor Regulation in Triple-Negative Breast Cancer: Ligand-Mediated Mechanisms of Receptor Regulation and Potential for Clinical Targeting.* Adv Cancer Res, 2015. **127**: p. 253-81.

293. O'Reilly, E.A., et al., *The fate of chemoresistance in triple negative breast cancer (TNBC).* BBA Clin, 2015. **3**: p. 257-75.

294. Calhoun, B.C. and L.C. Collins, *Predictive markers in breast cancer: An update on ER and HER2 testing and reporting.* Semin Diagn Pathol, 2015. **32**(5): p. 362-9.

295. Orlando, L., et al., *Molecularly targeted endocrine therapies for breast cancer.* Cancer Treat Rev, 2010. **36 Suppl 3**: p. S67-71.

296. Vidula, N. and H.S. Rugo, *Cyclin-Dependent Kinase 4/6 Inhibitors for the Treatment of Breast Cancer: A Review of Preclinical and Clinical Data.* Clin Breast Cancer, 2016. **16**(1): p. 8-17.

297. Lluch, A., P. Eroles, and J.A. Perez-Fidalgo, *Emerging EGFR antagonists for breast cancer.* Expert Opin Emerg Drugs, 2014. **19**(2): p. 165-81.

298. Zou, A., et al., *Elevated CXCL1 expression in breast cancer stroma predicts poor prognosis and is inversely associated with expression of TGF-beta signaling proteins.* BMC Cancer, 2014. **14**: p. 781.

299. Acharyya, S., et al., *A CXCL1 paracrine network links cancer chemoresistance and metastasis.* Cell, 2012. **150**(1): p. 165-78.

300. Garofalo, C., et al., *Increased expression of leptin and the leptin receptor as a marker of breast cancer progression: possible role of obesity-related stimuli.* Clin Cancer Res, 2006. **12**(5): p. 1447-53.

301. Hauner, D. and H. Hauner, *Metabolic syndrome and breast cancer: is there a link?* Breast Care (Basel), 2014. **9**(4): p. 277-81.

302. Bieche, I., et al., *CXC chemokines located in the 4q21 region are up-regulated in breast cancer.* Endocr Relat Cancer, 2007. **14**(4): p. 1039-52.

303. Beroukhim, R., et al., *The landscape of somatic copy-number alteration across human cancers.* Nature, 2010. **463**(7283): p. 899-905.

304. Taniguchi, K. and M. Karin, *IL-6 and related cytokines as the critical lynchpins between inflammation and cancer.* Semin Immunol, 2014. **26**(1): p. 54-74.

305. Koren, S., et al., *PIK3CA(H1047R) induces multipotency and multi-lineage mammary tumours.* Nature, 2015. **525**(7567): p. 114-8.

306. Van Keymeulen, A., et al., *Reactivation of multipotency by oncogenic PIK3CA induces breast tumour heterogeneity.* Nature, 2015. **525**(7567): p. 119-23.

307. Casalvieri, K.A., et al., *Selective Targeting of RSK Isoforms in Cancer.* Trends Cancer, 2017. **3**(4): p. 302-312.

308. Carriere, A., et al., *The RSK factors of activating the Ras/MAPK signaling cascade.* Front Biosci, 2008. **13**: p. 4258-75.

309. Zaru, R., et al., *The PDK1-Rsk Signaling Pathway Controls Langerhans Cell Proliferation and Patterning.* J Immunol, 2015. **195**(9): p. 4264-72.

310. Houles, T. and P.P. Roux, *Defining the role of the RSK isoforms in cancer.* Semin Cancer Biol, 2017.

311. Chen, R.H., C. Abate, and J. Blenis, *Phosphorylation of the c-Fos transrepression domain by mitogen-activated protein kinase and 90-kDa ribosomal S6 kinase.* Proc Natl Acad Sci U S A, 1993. **90**(23): p. 10952-6.

312. Chen, R.H., C. Sarnecki, and J. Blenis, *Nuclear localization and regulation of erk- and rsk-encoded protein kinases.* Mol Cell Biol, 1992. **12**(3): p. 915-27.

313. Diaz-Cruz, E.S. and P.A. Furth, *Deregulated estrogen receptor alpha and p53 heterozygosity collaborate in the development of mammary hyperplasia.* Cancer Res, 2010. **70**(10): p. 3965-74.

314. Jones, L.P., et al., *Activation of estrogen signaling pathways collaborates with loss of Brca1 to promote development of ERalpha-negative and ERalpha-positive mammary preneoplasia and cancer.* Oncogene, 2008. **27**(6): p. 794-802.

315. Davis, S.R., et al., *Menopause.* Nat Rev Dis Primers, 2015. **1**: p. 15004.

316. Shehata, M., et al., *Phenotypic and functional characterisation of the luminal cell hierarchy of the mammary gland.* Breast Cancer Res, 2012. **14**(5): p. R134.

317. Bidlingmaier, F., et al., *Plasma estrogens in childhood and puberty under physiologic and pathologic conditions.* Pediatr Res, 1973. **7**(11): p. 901-7.

318. Janfaza, M., et al., *Estradiol levels and secretory dynamics in normal girls and boys as determined by an ultrasensitive bioassay: a 10 year experience.* J Pediatr Endocrinol Metab, 2006. **19**(7): p. 901-9.

319. Vetter-O'Hagen, C.S. and L.P. Spear, *Hormonal and physical markers of puberty and their relationship to adolescent-typical novelty-directed behavior.* Dev Psychobiol, 2012. **54**(5): p. 523-35.

320. Tian, J., et al., *Transgenic insulin-like growth factor-1 stimulates activation of COX-2 signaling in mammary glands.* Mol Carcinog, 2012. **51**(12): p. 973-83.

321. Sawant, K.V., et al., *Chemokine CXCL1 mediated neutrophil recruitment: Role of glycosaminoglycan interactions.* Sci Rep, 2016. **6**: p. 33123.

322. Dhawan, P. and A. Richmond, *Role of CXCL1 in tumorigenesis of melanoma.* J Leukoc Biol, 2002. **72**(1): p. 9-18.

323. Brambati, A., et al., *Replication and transcription on a collision course: eukaryotic regulation mechanisms and implications for DNA stability.* Front Genet, 2015. **6**: p. 166.

324. Pereira, B., et al., *The somatic mutation profiles of 2,433 breast cancers refines their genomic and transcriptomic landscapes.* Nat Commun, 2016. **7**: p. 11479.

325. Ciriello, G., et al., *Comprehensive Molecular Portraits of Invasive Lobular Breast Cancer.* Cell, 2015. **163**(2): p. 506-19.

326. Ramirez-Ardila, D., et al., *Increased MAPK1/3 Phosphorylation in Luminal Breast Cancer Related with PIK3CA Hotspot Mutations and Prognosis.* Transl Oncol, 2017. **10**(5): p. 854-866.

327. Mendoza, M.C., E.E. Er, and J. Blenis, *The Ras-ERK and PI3K-mTOR pathways: cross-talk and compensation.* Trends Biochem Sci, 2011. **36**(6): p. 320-8.

328. Scott, M.S., et al., *Refining protein subcellular localization.* PLoS Comput Biol, 2005. **1**(6): p. e66.

329. Groner, A.C. and M. Brown, *Role of steroid receptor and coregulator mutations in hormone-dependent cancers.* J Clin Invest, 2017. **127**(4): p. 1126-1135.

330. Alluri, P.G., C. Speers, and A.M. Chinnaiyan, *Estrogen receptor mutations and their role in breast cancer progression.* Breast Cancer Res, 2014. **16**(6): p. 494.

331. Thomas, C. and J.A. Gustafsson, *Estrogen receptor mutations and functional consequences for breast cancer.* Trends Endocrinol Metab, 2015. **26**(9): p. 467-76.

332. Jeselsohn, R., et al., *ESR1 mutations-a mechanism for acquired endocrine resistance in breast cancer.* Nat Rev Clin Oncol, 2015. **12**(10): p. 573-83.

333. Reinert, T., et al., *Clinical Implications of ESR1 Mutations in Hormone Receptor-Positive Advanced Breast Cancer.* Front Oncol, 2017. **7**: p. 26.

334. Cengiz, M., S. Ozenirler, and G. Yilmaz, *Estrogen receptor alpha expression and liver fibrosis in chronic hepatitis C virus genotype 1b: a clinicopathological study.* Hepat Mon, 2014. **14**(9): p. e21885.